TECHNISCHE UNIVERSITÄT WIEN

PhD-Thesis

Dissertation

Color-stable formulations and novel photoinitiators for dental materials

ausgeführt zum Zwecke der Erlangung
des akademischen Grades eines Doktors der technischen Wissenschaften

unter der Leitung von
Univ. Prof. Dipl.-Ing. Dr. techn. Robert Liska
and
Univ.Ass. Dipl.-Ing. Dr.techn. Patrick Knaack

Institut für Angewandte Synthesechemie

IAS

Institute of Applied Synthetic Chemistry

eingereicht an der Technischen Universität Wien
Fakultät für Technische Chemie

von
Dipl.-Ing. David Bassenheim, BSc

Danksagung

An erster Stelle möchte ich **Prof. Robert Liska** danken. Einerseits dafür, dass du es mir ermöglicht an einem so spannenden Thema zu forschen, aber auch dafür, dass deine Türe immer offensteht und du jederzeit eine gute Idee parat hast, wenn es einmal knifflig wird. Dir ist es nicht nur gelungen so viele großartige Menschen um dich zu versammeln, sondern auch ein Umfeld zu schaffen, in dem man gerne arbeitet und sich wohl fühlt.

Ein riesengroßes Dankeschön auch an dich, **Patrick Knaack**. Du hast dir bei jedem akuten Problem Zeit genommen und mich mit Rat und Tat unterstützt, wo du nur konntest. Deine unglaubliche Hilfsbereitschaft und dein „Out of the box" – Denken haben nicht nur mich in vielen Situationen vorangebracht.

Ich möchte mich auch bei unseren Kooperationspartnern von Ivoclar ganz herzlich bedanken. Vielen Dank, **Yohann Catel** und **Prof. Norbert Moszner,** für die guten Ratschläge, Ideen und euer Fachwissen, und dir, **Kai Rist**, für deine Expertise und auch die praktische Unterstützung. Zusätzlich möchte ich **Prof. Georg Gescheidt**, **Konstantin Knaipp** und **Max Schmallegger** von der TU Graz für die gute Zusammenarbeit danken. Vielen Dank, **Stefan B.**, **Davide** und **Kathi**, aber auch **Dagmar**, **Jürgen**, **Walter** und **Heinz**, dass ihr alle unterstützt und dafür sorgt, dass der Arbeitsalltag reibungslos abläuft. Ich möchte auch meiner Bachelorstudentin **Stefanie** danken, die ebenfalls einen Beitrag zu dieser Arbeit geleistet hat.

Danke auch an all die lieben Menschen, die für das tolle Arbeitsklima gesorgt und mich in dieser guten Zeit begleitet haben. Hier möchte ich neben den längeren Weggefährten **Tina**, **Miriam**, **Roli**, **Betti**, **Carola**, **Klaus**, **Philip**, **Flo**, **Dani**, **Jakob**, **Sarah**, **Pontus**, **Viola** und **Jo** auch unsere Nachwuchstalente **Jelena**, **Selina**, **Björn**, **Edma**, **Kaja**, **Olja** und **Theresa** erwähnen. Doch auch den „Oldies" **Yazgan**, **Gernot**, **Nico**, **AD**, **Hofi**, **Hansi**, **Kury**, **Sebi**, **Patzi**, **Elise**, **Sascha**, **Schnölli**, **Moritz**, **Lunzer**, **Paul** und **Raffi** möchte ich an dieser Stelle Danke sagen. Und natürlich dir, **Stefan H.**, dass du mir nicht nur das Studium, sondern auch die Arbeitsgruppe nähergebracht hast und mich bis heute begleitest.

Ein besonderer Dank geht an **Flocki**, **Toni**, **Michi**, **Fitzi**, **Oskar**, **Baumi** und **Ricky**. Mit euch gingen die Gespräche weit über das Fachliche hinaus, woraus sich viele wunderbare Stunden ergeben haben, welche ich nicht missen möchte.

Larissa und **Lisa**, ihr beiden seid mir in unserer gemeinsamen Zeit in und außerhalb der Uni, besonders ans Herz gewachsen. Danke für diese schönen Jahre und für eure ganze Unterstützung währenddessen.

Und dann gibt es da noch die Kochcrew mit **Babsi**, **Anna** und **Ralle**. Ihr seid die letzten Jahre so viel mehr als nur Arbeitskollegen gewesen und ich hoffe, dass wir uns auch in Zukunft erhalten bleiben und uns nie aus den Augen verlieren. So gute Freunde zu finden, ist von unschätzbarem Wert. Danke für all die schönen Tage und Abende, die wir gemeinsam verbracht haben. **Ralle**, dich möchte ich hier nochmal erwähnen, da wir in den Jahren so sehr zusammengewachsen sind, dass es niemandem entgehen konnte. Unsere Kontinuität mit Kaffee am Morgen, dem gemeinsamen Mittagessen, dem sofortigen Mitteilen wichtigster Neuigkeiten, aber auch das Fachsimpeln, oder einfach über Gott und die Welt zu plaudern, hat uns unzertrennlich zusammengeschweißt. Danke dafür!

An dieser Stelle möchte ich auch meinen **Eltern** von tiefstem Herzen danken, für eure uneingeschränkte Unterstützung, die Tatsache, dass ihr mich bis heute begleitet und dass ihr stets darum bemüht wart, mir alles zu ermöglichen, um meinen Weg zu gehen. Und auch meinen beiden **Schwestern** möchte ich danken, dafür, dass ihr immer da wart und mich stets aufgebaut und unterstützt habt.

Zu guter Letzt möchte ich dir, **Natalie**, danken. Du begleitest mich schon länger als mein halbes Leben, durch alle Höhen und Tiefen und hast mich in allen Situationen stets unterstützt und motiviert. Und auch das Glück zu haben, mit dir gemeinsam, unsere Kinder aufwachsen zu sehen und immer wieder zu staunen, wie sie sich entwickeln, ist unvorstellbar wertvoll. Ich freue mich schon auf alles, was uns das Leben noch bringen wird und die schöne Zeit mit dir.

Danke!

Abstract

To satisfy requirements for aesthetics and health safety, photopolymerizable composites have emerged as replacements for materials like amalgam in dental applications. Despite the superiority of these materials, there is still room for improvement, as the photopolymers used tend to discolor to a greater or lesser extent over time, depending on the composition. Particularly due to the time-dependent nature of this discoloration, it poses challenges in achieving perfect color matching of the composite and the patients' tooth. This work identified the substances responsible and developed strategies to effectively reduce or completely suppress the intrinsic discoloration of such photopolymers.

The employed photoinitiators were identified as a primary contributor to discoloration. As these are indispensable for the photopolymers, an improved discoloration behavior was achieved by the modification of the photoinitiators. Additionally, the incorporation of additives such as stabilizers exhibited positive effects on the discoloration behavior. However, the introduction of the oxidizing agent cumene hydroperoxide (**CHP**) proved most effective in producing color-stable polymers.

The second part of the work addresses the replacement of the commonly used monoacylphosphine oxide (**MAPO**) photoinitiator (2,4,6-trimethylbenzoyl)diphenylphosphine oxide (**TPO**), which is increasingly being criticized with regard to health concerns. Finding an alternative for this photoinitiator proves challenging, given its exceptional reactivity, excellent absorption properties in the suitable wavelength range, and favorable photobleaching characteristics and applicable color stability. Since MAPOs, in particular, meet these high requirements, the objective is to synthesize and evaluate new derivatives within this substance class. In this context it was demonstrated that by incorporating sterically demanding substituents into the benzoyl moiety, photoinitiators with remarkably high color stability could be synthesized. Exploration extended to derivatives modified at the phosphorus atom of **TPO** with heteroatom substituents, similar to ethyl (2,4,6-trimethylbenzoyl) phenylphosphinate (**TPO-L**). It was assumed that this could improve the toxicological properties compared

to **TPO**. Although these derivatives exhibited improved absorption properties compared to **TPO-L**, they did not show any notable enhancements in reactivity over **TPO-L**. The modification of the phosphorus with alkyl or phenyl substituents, on the other hand, has demonstrated remarkable effectiveness. Through the incorporation of sterically demanding groups, it was possible to develop photoinitiators exhibiting a bathochromic shift in λ_{max} of up to 10 nm relative to **TPO**. Moreover, this approach has yielded substances with enhanced reactivity or superior color stability compared to **TPO**. This research not only introduces photoinitiators with exceptional properties, but also elucidates the modifications capable of generating desired properties, thus providing valuable information for future research.

Kurzfassung

Um den Anforderungen an Ästhetik und Gesundheitssicherheit gerecht zu werden, haben sich photopolymerisierbare Verbundwerkstoffe als Alternative für Materialien wie Amalgam in der Zahnmedizin etabliert. Trotz ihrer Überlegenheit besteht jedoch noch Verbesserungspotential, da die verwendeten Photopolymere je nach Zusammensetzung dazu neigen, sich im Laufe der Zeit mehr oder weniger stark zu verfärben. Insbesondere die zeitliche Abhängigkeit dieser Verfärbung stellt eine Herausforderung dar, wenn es darum geht, eine perfekte Farbübereinstimmung zwischen dem Komposit und dem Zahn des Patienten zu erzielen. In dieser Studie wurden die verantwortlichen Substanzen identifiziert und Strategien entwickelt, um die Eigenverfärbung solcher Photopolymere wirksam zu reduzieren oder gänzlich zu unterdrücken.

Die eingesetzten Photoinitiatorn wurden als hauptsächliche Auslöser der Verfärbungen identifiziert. Da diese unerlässlich für die Photopolymere sind, wurden an den Photoinitiatoren Modifikationen vorgenommen, um eine verbesserte Farbstabilität zu erreichen. Zusätzlich zeigte die Zugabe von Additiven wie Stabilisatoren einen positiven Einfluss auf das Verfärbungsverhalten. Vor allem der Einsatz des Oxidationsmittels Cumolhydroperoxid (**CHP**) erwies sich als eine der effektivsten Methode zur Herstellung von farbstabilen Polymeren.

Der zweite Teil dieser Arbeit widmet sich dem Ersatz des weit verbreiteten Monoacylphosphinoxid (**MAPO**) Photoinitiators (2,4,6-Trimethylbenzoyl)diphenylphosphinoxid (**TPO**), der aufgrund gesundheitlicher Bedenken zunehmend in die Kritik gerät. Die Suche nach einer Alternative gestaltet sich herausfordernd, da dieser Photoinitiator herausragende Reaktivität, exzellente Absorptionseigenschaften im geeigneten Wellenlängenbereich und günstige Bleicheigenschaften und akzeptable Farbstabilität aufweist. Da insbesondere MAPOs diese hohen Anforderungen erfüllen, besteht das Ziel darin, neue Derivate dieser Substanzklasse zu synthetisieren und zu evaluieren. In diesem Zusammenhang wurde gezeigt, dass durch die Einbringung sterisch anspruchsvoller Substituenten am Benzoylteil, Photoinitiatoren mit bemerkenswert hoher Farbstabilität hergestellt werden

können. Die Untersuchungen wurden auch auf Derivate ausgedehnt, die am Phosphoratom mit Heteroatomsubstituenten modifiziert wurden, ähnlich wie Ethyl-(2,4,6-trimethylbenzoyl)-phenylphosphinat (**TPO-L**). Hierbei bestand die Vermutung, dass dadurch Verbesserungen der toxikologischen Eigenschaften gegenüber **TPO** erzielt werden könnten. Obwohl diese Derivate im Vergleich zu **TPO-L** verbesserte Absorptionseigenschaften aufwiesen, zeigten sie keine nennenswerten Verbesserungen der Reaktivität gegenüber **TPO-L**. Die Modifikation des Phosphors durch Alkyl- oder Phenylsubstituenten erwies sich dagegen als ausgesprochen zielführend. Durch das Einbringen sterisch anspruchsvoller Gruppen konnten Photoinitiatoren entwickelt werden, die eine bathochrome Verschiebung von λ_{max} um bis zu 10 nm im Vergleich zu **TPO** aufweisen. Darüber hinaus führte dieser Ansatz zu Substanzen mit erhöhter Reaktivität oder verbesserter Farbstabilität im Vergleich zu **TPO**. Diese Forschungsarbeit stellt nicht nur Photoinitiatoren mit außergewöhnlichen Eigenschaften vor, sondern bietet auch Einblicke darüber welche Modifikationen, die die gewünschten Eigenschaften hervorrufen können, und liefert somit wertvolle Informationen für zukünftige Forschungsarbeiten.

Table of Contents

Introduction

Dental materials play a crucial role in modern dentistry and are indispensable for the treatment and care of teeth. They are used to improve and maintain the functionality, esthetics and durability of dental restorations. Due to their exceptional ability to withstand a diverse array of stresses, natural teeth represent a remarkable high-performance material. Consequently, dental restorative materials must meet extraordinarily high demands. An ideal material would therefore fulfill the following criteria:[1, 2]

- Match the mechanical properties of natural teeth
- Long term durability and abrasion resistance
- Strong adhesion to tooth structure or bone
- Biocompatible
- Jointless filling of gap to prevent bacteria contamination
- Visual resemblance to natural teeth
- Efficient processability
- Inexpensive

Since amalgam fulfills a large part of these properties, it has long been one of the most widely used materials in the dental sector. One drawback of amalgam is its metallic appearance, which is prominently visible on the teeth. But most importantly, there is a significant demand for alternatives, due to the health concerns associated with the mercury content of amalgam.[3] Another class of materials for dental applications are ceramics. These are characterized by their, excellent strength, durability, biocompatibility and the ability to imitate the natural tooth coloration. However, the high costs and the difficult processing are decisive disadvantages.[4] In recent decades the polymer-based composites have become one of the most commonly used restorative materials. These materials offer a wide range of applications, fulfill high esthetic requirements, while remaining cost-efficient and easy to use. Composite materials consist of an organic matrix and inorganic fillers. Depending on the size of the fillers they are categorized as follows: Microfills contain particles with an average size of around 0.04 µm, minifills with

0.6 – 1.0 µm and midifills with 1 – 5 µm.[5] The most frequently used fillers are different oxides (silica, alumina, titania, zirconia), alkaline silicate glasses (barium, strontium), biomimetic fillers (hydroxyapatite) and organic–inorganic hybrids.[6] The organic matrix comprises a polymerizable monomer and an initiator system, which triggers the polymerization process. In dentistry, multifunctional methacrylates are generally used as monomers, undergoing polymerization via free radicals. These free radicals are generated either thermally, by redox reactions or photochemically. Photopolymerization offers certain advantages, such as a wide range of possible applications, fast curing, storage stability and easy applicability.

Free radical photopolymerization

Photopolymerization requires photochemically active substances that generate reactive species by irradiation, the so-called photoinitiators. In the case of free radical photopolymerization, radicals act as reactive species that cause the polymerization of monomers. This process can be divided into three steps:

- Initiation

A photoinitiator (**PI**) absorbs light, leading to its transition to an excited state. Subsequently, the excited molecule can generate radicals, which initiate the polymerization reaction.

$$PI \xrightarrow{h\nu} |PI|^* \longrightarrow R_I \cdot$$
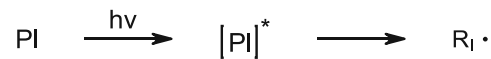
Figure 1: Initiation step – Light excitation of a photoinitiator and subsequent radical formation.

- Propagation

In the next step, the free radicals add to the double bonds of vinyl monomers, forming monomer radicals. These new radicals, can subsequently add to another monomer to facilitate the propagation of the chain growth reaction.
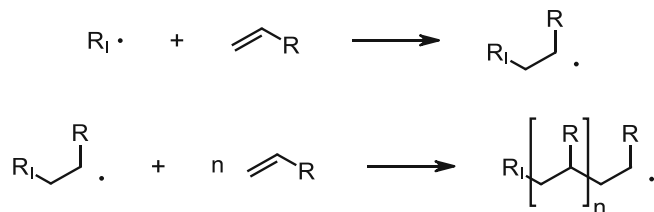
Figure 2: Propagation step – Radicals add to double bonds to propagate chain growth.

- Termination

The termination can occur in two different ways, either by recombination or disproportionation of two radicals. Which mechanism predominates influences the final molecular weight and depends on several factors, such as the reaction conditions, steric effects and polar factors.[7]
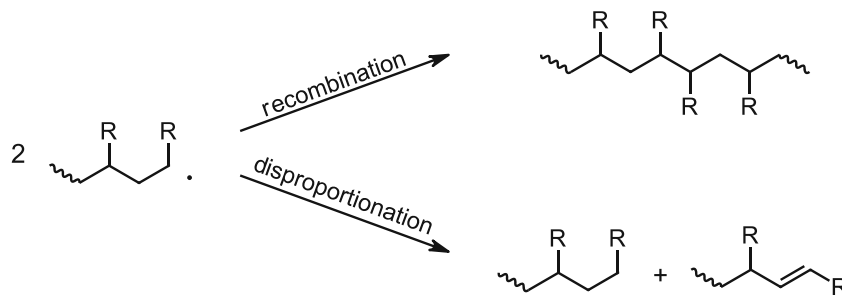
Figure 3: Termination – Recombination and disproportionation of two radicals.

Monomers

Particularly, methacrylate-based monomers are favored in dental materials, due to their relatively high reactivity and good biocompatibility. The choice of monomer is decisive for the material properties, the reactivity, the viscosity and also the volumetric shrinkage that occurs during curing. Specifically, the difunctional urethane dimethacrylate (**UDMA**) and bisphenol A-glycidyl dimethacrylate (**Bis-GMA**) hold significant importance (Figure 4). Their high intermolecular forces contribute to the formation of tough materials with high moduli. Despite offering excellent mechanical properties, these monomers exhibit high viscosity at room temperature, potentially impacting conversion and processability adversely. Therefore, reactive diluents like 1,10-decanediol dimethacrylate (**D₃MA**) or triethylenglycol dimethacrylate (**TEGDMA**) are commonly employed (Figure 4).[8-10]
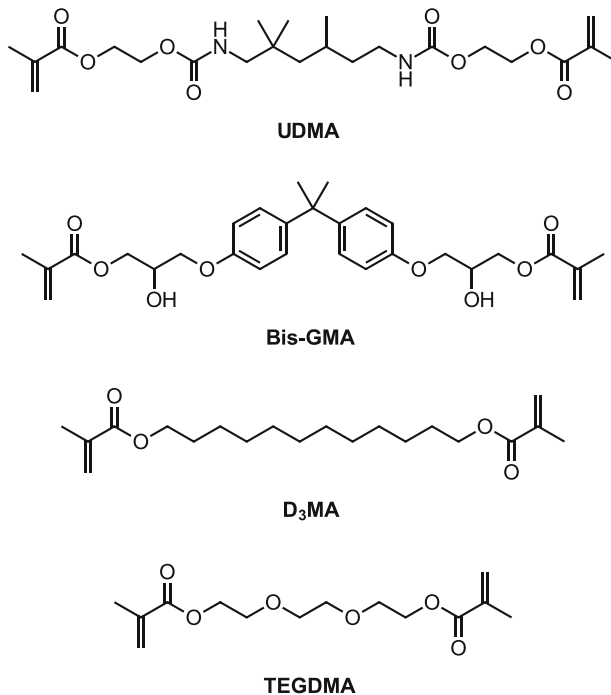
Figure 4: Commonly used difunctional methacrylate monomers for dental applications.

Radical photoinitiators

Photoinitiators represent a pivotal component in the photopolymerization process, serving as the catalyst for the conversion of monomers into polymers upon exposure to light. These molecules are characterized by their ability to absorb distinct wavelengths of light to transition into higher energy states and thus the formation of radicals. In order to absorb the radiation energy and thereby transition from the ground state (**S$_0$**) to an excited state (S$_1$, S$_2$, …), the molecules need a chromophore. In this transition, an electron is raised from an occupied orbital to an unoccupied one. When using the concept of molecular orbital (**MO**) theory, two orbitals are of particular importance: The highest occupied molecular orbital (**HOMO**) is the MO in the ground state of highest energy with electrons in it and the lowest unoccupied molecular orbital (**LUMO**) is the lowest energy MO, that is not populated by electrons. Therefore, the transition that requires the least energy is the one from HOMO to LUMO. Of all the possible transitions, the n→π* and the π→π* transitions are particularly important in photochemistry.[11-13] Figure 5 illustrates the n→π* and the π→π* transition of methanal in the MO scheme.[11]
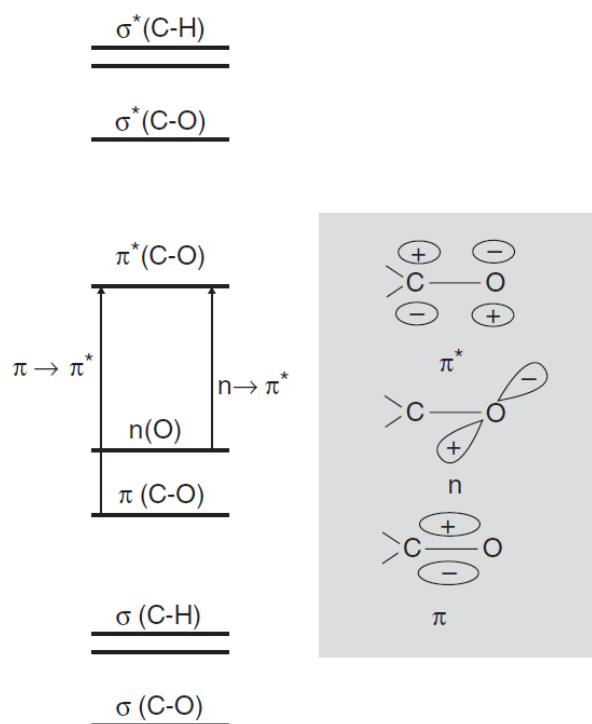
Figure 5: Molecule orbital scheme of methanal with the n→π* and π→π* transitions and the corresponding molecular orbitals.[11]

The energy gap between these transitions defines the wavelengths at which light must be absorbed in order to cause the respective transition. The excitation of an electron from the π- to the π*-orbital requires more energy than that from a n- to the π*-orbital (Figure 5). Therefore, this excitation occurs at comparatively shorter wavelengths (Figure 6). This gap from the π→π* transition can be reduced by forming conjugated systems, as this raises the energy of the π-orbital and lowers that of the π*-orbital.[11]

The molar absorption coefficient (ε) is highest when the electron transition from one orbital to the other is more likely. The π→π* transition is both spin allowed and symmetry allowed and the two orbitals exhibit a large overlap, which facilitates a transition and thus leads to high absorption coefficients. The n→π* transition, on the other hand, is spin allowed but symmetry forbidden, as it occurs between symmetrically different orbitals. Consequently, it results in significantly lower absorbance compared to the π→π* transition (Figure 6).[12]
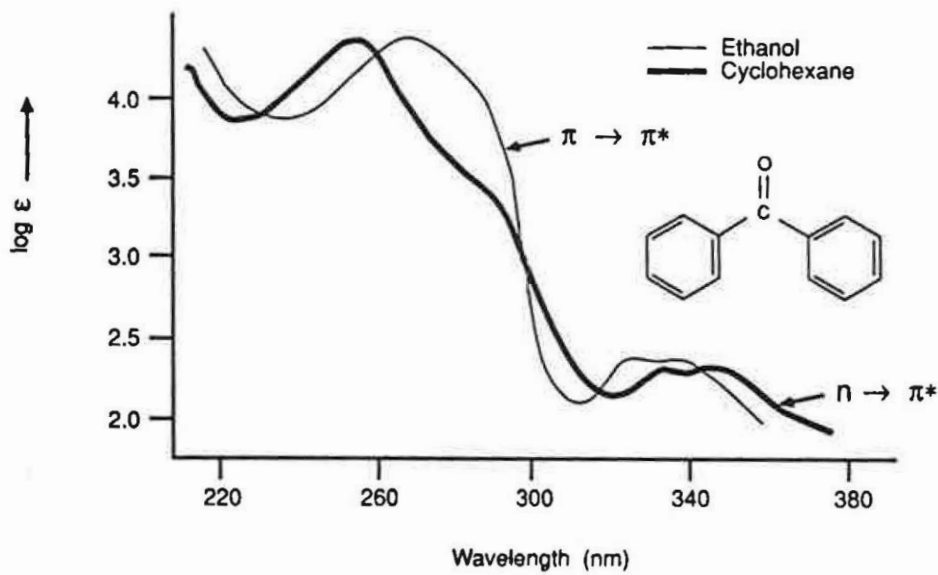
Figure 6: Absorption spectra of benzophenone in ethanol and cyclohexane.[12]

After the excitation of a photoinitiator molecule from the ground state (S_0) into an excited singlet state (S_1, S_2, …) upon light absorption, the subsequent relaxation pathway is critical. The Jablonski diagram (Figure 7) shows how this could take place. Via vibrational relaxation (VR) and internal conversion (**IC**) rapid relaxation to the lowest level of the excited singlet state (**S_1**) occurs without photon emission. The return to the ground state (**S_0**) can then occur via non-radiative deactivation or fluorescence emission. Alternatively, the excited electrons can be transferred to a longer-lasting excited triplet state (T_1) via intersystem crossing (**ISC**). Notably, aromatic ketones exhibit highly efficient intersystem crossing, so that their photochemistry is dominated by the triplet - state processes. From this triplet state (**T_1**) radical formation can be induced to initiate the polymerization. This process directly competes with non-radiative deactivation, emission of photons (phosphorescence), or bimolecular quenching.[11-13]

Introduction
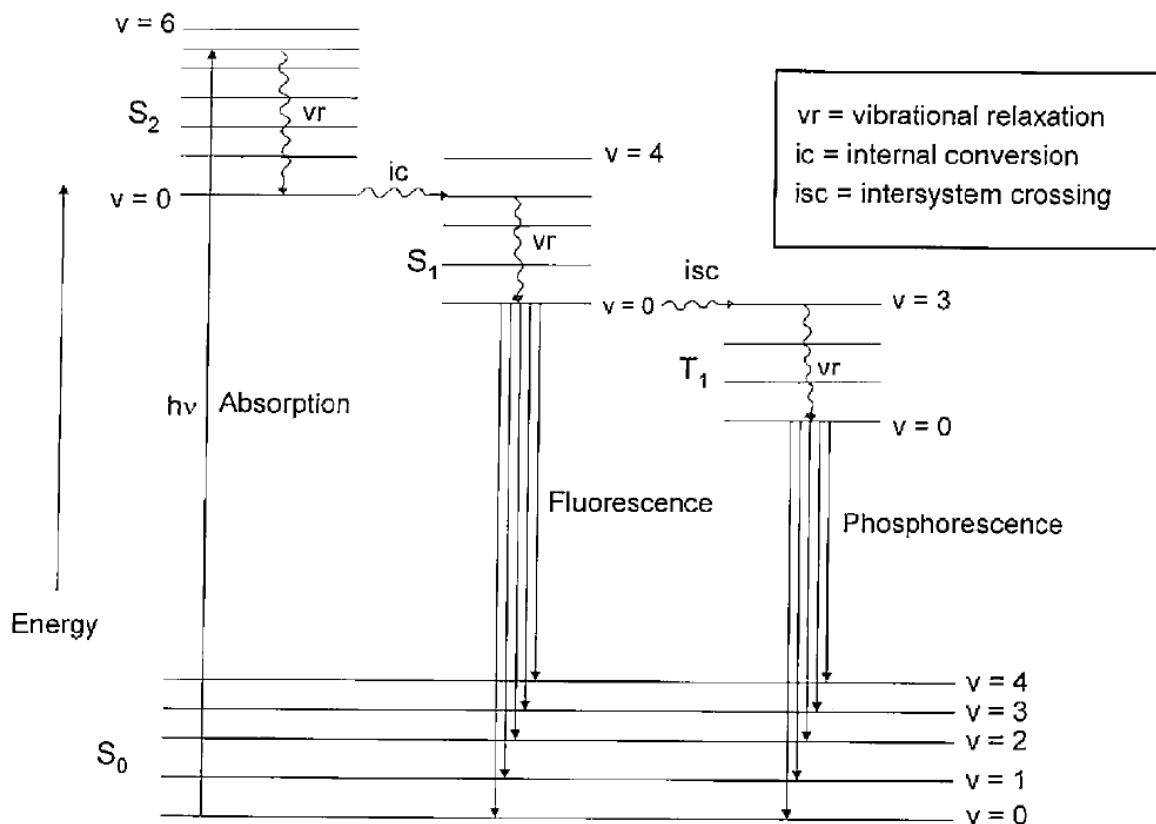
Figure 7: Jablonski diagram – Illustrates excitation and relaxation processes of organic molecules.[11]

Depending on how the initiating radical is formed, two types of photoinitiators are distinguished (Figure 8). Norrish Type I photoinitiators decompose in a unimolecular process, whereby a homolytic bond cleavage (α-scission) takes place to generate radicals. In Norrish Type II initiators, on the other hand, radicals are generated in a bimolecular mechanism, requiring a coinitiator (**CoI**).[12, 14]
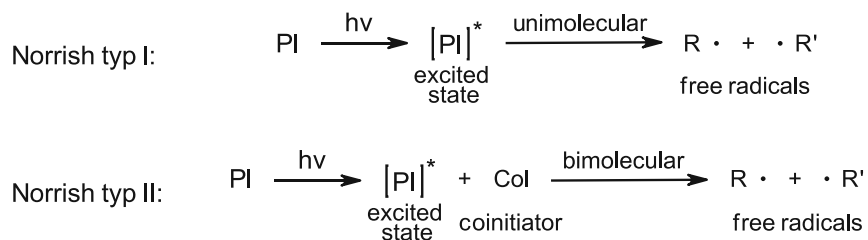
Figure 8: Radical generation mechanism for Norrish Type I and Norrish Type II photoinitiators.

Norrish Type II photoinitiators

In these bimolecular systems (Norrish Type II) radicals are formed by two different reaction pathways:[12-15]

- Direct hydrogen abstraction from hydrogen donating compounds, such as ethers or alcohols, by the excited ketone (Figure 9). This process takes place from the long-lasting n-π* excited triplet state.

- Electron transfer from suitable electron donors, such as tertiary amines, to the excited ketone, to form a charge transfer complex (**CTC**). This is followed by a proton transfer from the α-carbon on the donor to the photoinitiator (Figure 10). In this mechanism the π-π* triplet state is equally as effective as the n-π* triplet state.
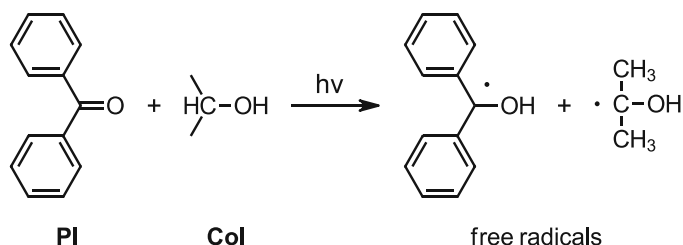
Figure 9: Direct hydrogen abstraction mechanism for Norrish Type II photoinitiator systems illustrated by the photoinitiator benzophenone and the coinitiator isopropanol.
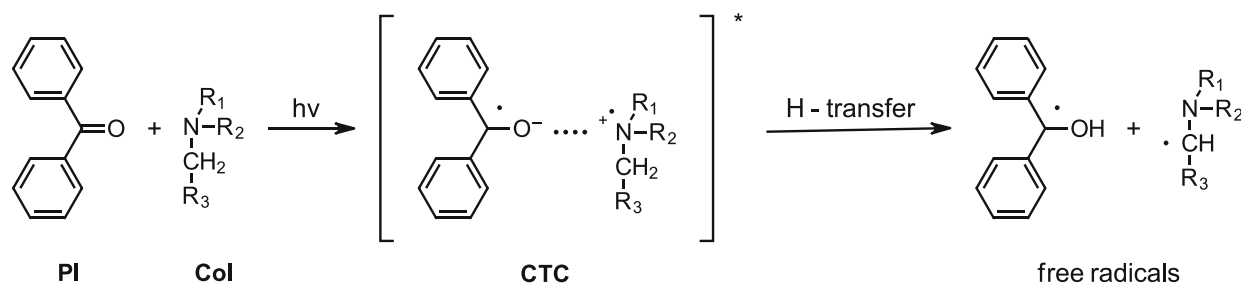
Figure 10: Electron transfer and proton transfer mechanism for Norrish Type II photoinitiator systems illustrated by the photoinitiator benzophenone and a tertiary amine coinitiator.

Commonly used Type II photoinitiators are benzophenones, xanthones, thioxanthones, benzils, α-ketocoumarins, anthraquinones, fluorenones and camphorquinone.[16] Whereby the most important Type II photoinitiator system for dental composites is camphorquinone (**CQ**) in combination with tertiary amine coinitiators (Figure 11).[17, 18] The most significant advantage of this system is its capacity to absorb visible light with λ_{max} = 472 nm. This enables the use of long-wavelength irradiation for curing, which avoids damage to surrounding tissue.[19, 20] In any case, the amines utilized in these systems present a

challenge due to concerns regarding biocompatibility and the potential for discoloration.[21, 22] Due to the necessity of Norrish Type II initiators to interact with their co-initiators, these bimolecular systems inherently exhibit lower reactivity compared to Norrish Type I systems.[12, 13] Therefore, they are hardly suitable for certain dental applications such as 3D printing.
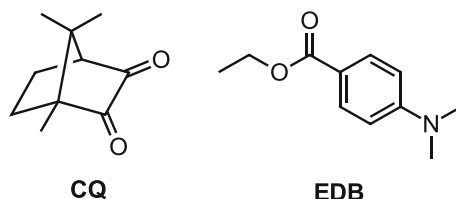
*Figure 11: Commonly used Type II photoinitiator system, consisting of camphorquinone (**CQ**) and the tertiary amine ethyl 4-(dimethylamino)benzoate (**EDB**).*

Norrish Type I photoinitiators

Radical photoinitiators which decompose via α-cleavage (Norrish Type I) typically feature a benzoyl moiety in their molecular structure, serving as a chromophore.[12, 16, 23] The radical formation usually occurs from the lowest n-π* triplet state, which is achieved by excitation with light of the appropriate wavelength. From this state the α-scission is much more likely than from an excited singlet state.[12] In most cases, the homolytic bond cleavage takes place adjacent to the carbonyl, producing two free radicals. The formed benzoyl radicals are known to trigger polymerization of various unsaturated species efficiently.[24] The simultaneously generated counter radical can also contribute directly or indirectly to the initiation of polymerization, depending on the nature of the formed radical. The efficiency of α-cleavage depends mainly on two factors: The configuration of the excited state and the type of substituents in α-position.[12] In this context it is important that the bond dissociation energy is lower than the excitation energy of the reactive excited state, but sufficiently high to be thermally stable.[12]

There is a large market with a large number of compounds that act as Type I initiators encompassing derivatives of benzoin ethers, hydroxyalkylacetophenones, dialkoxyacetophenones, and others. For dental applications, acylphosphine oxides hold paramount significance.

The following properties are particularly important for the application of photoinitiators:[16]

- High absorption in the region of activation
- High quantum yield for free radical formation
- Adequate solubility in the resin system used
- High storage stability
- Odorless and non-yellowing
- Non-toxic, cheap and easy to handle

Acylphosphine oxides

The notable importance of acylphosphine oxides not only attributed to their high reactivity and their ability to absorb light at high wavelengths, but also due to their excellent photobleaching.[25] The long-wavelength absorption is attributed to the n→π* transition. The strong bathochromic shift of this transition can be explained by two phenomena. Firstly, the overlap of the π*-orbital of carbonyl C with the empty d-orbital on phosphorus can be considered.[12] Secondly, the interaction of the filled nonbonding orbital of the phosphonyl oxygen with the π-orbital of the carbonyl C is postulated.[26, 27] Irradiation of these acylphosphine oxides results in a homolytic bond break between carbonyl and phosphorus to form radicals. This bond cleavage also destroys the chromophore which is responsible for the long-wavelength absorption, which in turn explains the remarkable photobleaching behavior of this substances.[12] Apart from the already highly reactive benzoyl radicals, phosphorus radicals are generated, exhibiting even higher addition rate constants, leading to the exceptionally high reactivity of acylphosphine oxides.[28] This contributes to the exceptional reactivity of acylphosphine oxides. An important structural element of acylphosphine oxides are the methyl groups, in ortho position on the benzoyl part. The steric demand of these substituents prevents the C-P bond from being cleaved by nucleophiles (such as water, alcohols or amines) and is therefore essential to ensure storage stability.[12] Three typical and widely used, commercial acylphosphine oxides are depicted in Figure 12.
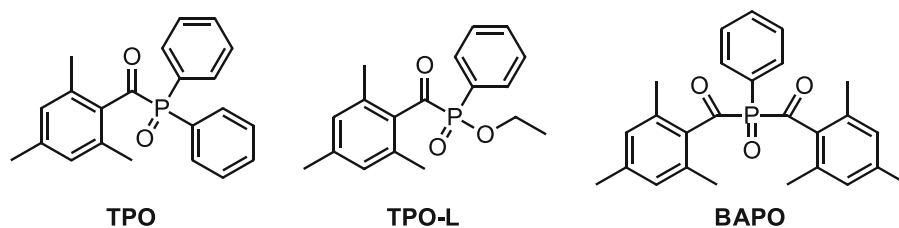
Figure 12: Commonly used, commercial acylphosphine oxide photoinitiators.

These three structures also represent two classes of acylphosphine oxides. **TPO** and **TPO-L** are monoacylphosphine oxides (**MAPO**), which releases 2 radicals during cleavage. In comparison, bisacylphosphine oxides (**BAPO**) are able to release up to 4 radicals, making them even more reactive. In addition, **BAPOs** absorb light at higher wavelengths due to the strong carbonyl-phosphonyl-carbonyl conjugation. Even if these properties are clear arguments in favor of using **BAPO**, it has decisive disadvantages compared to **TPO** and **TPO-L**, especially for use in dental applications. One is the low color stability that **BAPO**-based polymers exhibit.[29-31] The other drawback concerns the toxicological properties. **BAPO** appears not only to be more cytotoxic than **TPO**, but also potentially genotoxic.[31-33] Although **TPO** displays lower cytotoxicity than **BAPO**, this remains a cause for concern.[31, 33, 34] Apart from its cytotoxic properties, **TPO** is suspected of damaging fertility and is therefore classified as category 2 for reproductive toxicity according to Regulation (EC) No 1272/2008.[35] Nevertheless, the use of **TPO** in dental composites has already been extensively studied, yet its significance extends to dental 3D printing as well.[31, 36-40] In terms of toxicological properties, **TPO-L** represents a promising alternative.[33] However, due to its lower reactivity compared to **TPO**, **TPO-L** has a considerable disadvantage, which is a significant problem, especially in 3D printing.[41]

Additive manufacturing for dental applications

The ability to create complex structures while minimizing waste and costs renders additive manufacturing immensely significant within the dental industry.[40, 42-46] The wide range of potential applications is outlined in numerous publications.[47-50] Apart from stereolithography (**SLA**), digital light processing (**DLP**) is one of the most important technologies for photopolymerization-based 3D printing in dentistry.[40, 46, 51, 52] In this technique, a photoresist is employed to manufacture 3D objects through a layer-by-layer

building process. The curing occurs by exposing the photoresist to irradiation from a projector, allowing an entire layer to be cured simultaneously. Most projection systems used predominantly emit light with a wavelength of 385 nm or 405 nm.[52] Within this wavelength range, acylphosphine oxides demonstrate their outstanding performance, underscoring their significance as photoinitiators.[39, 40, 52, 53]

Considering 3D printed dental materials from an aesthetic point of view, some works show that there are issues with their color stability.[39, 54-56] If only the intrinsic causes are considered, the literature shows that particularly the monomers and photoinitiators used have a significant influence on the discoloration behavior.[10, 29, 30, 57-65] Regarding the monomers, unreacted double bonds are considered to be responsible for discoloration, but correlations have also been found between water absorption and water solubility of the monomer and the discoloration behavior.[10, 58] With respect to photoinitiators, higher initiator concentrations can result in incomplete bleaching, leading to discoloration caused by the remaining photoinitiator.[62-64] Furthermore, different photoinitiators seem to cause different discolorations, whereby the photolysis products formed are suspected of causing them.[65, 66]

Consequently, dental 3D printing is confronted with two primary challenges. Firstly, there is a need to enhance color stability to align with the aesthetic standards of the dental field. Secondly, the replacement of the important photoinitiator **TPO**, which is coming under increasing criticism due to health concerns, is necessary. However, an alternative photoinitiator must match the reactivity of **TPO** to guarantee its efficacy in 3D printing.

Introduction

Objectiv

This work aims to improve dental materials in two key aspects. Firstly, it focuses on addressing the time-dependent discoloration of polymer materials caused by intrinsic factors. Particularly within dentistry, achieving color-stability in dental materials tailored to each patient's teeth is paramount. To address this concern the development of a method for qualitative and quantitative analysis of these discolorations is essential. For exploring the underlying reasons behind these discolorations, polymer samples are prepared, subjected to diverse storage conditions, to determine factors exhibiting positive or negative influences. Following this, polymer samples of varied compositions will be examined and compared to identify the specific substances responsible for discoloration. In addition, strategies for substituting or modifying these substances will be explored and additives that can mitigate the discoloration will be identified. The initial focus of these investigations will be the combination of the photoinitiator (2,4,6-trimethylbenzoyl)diphenylphosphinoxide (**TPO**) and the monomer urethane dimethacrylate (**UDMA**).

In the second part of the study, alternative options to **TPO** as a photoinitiator will be explored due to concerns regarding potential health hazards. As **TPO** finds application in 3D printing of dental materials, any potential substitute must fulfill a multitude of criteria beyond improved biocompatibility. These include high reactivity, effective absorption at the wavelength of the printing device (385 nm), excellent photobleaching properties and high color-stability of the resulting polymers. Furthermore, good solubility in the monomer, high stability and low production costs are desirable. The class of monoacylphosphine oxides appears to be the most promising for meeting these requirements, due to their excellent reactivity and effective photobleaching within the desired absorption range. Consequently, novel monoacylphosphine oxide photoinitiators will be developed, synthesized, and characterized. This characterization will include the absorption properties using UV-Vis spectroscopy, the evaluation of photoreactivity via photo-DSC, and the assessment of discoloration tendencies of prepared polymer samples.

General part

1 Color-stability of light cured dental materials

1.1 State of the art

In addition to mechanical properties, one of the main requirements for resin-based materials in dentistry is color stability. It is crucial for adapting the color of dental restorative materials to the individual patient. The causes of discoloration of these materials are diverse. In addition to extrinsic factors, numerous intrinsic parameters seem to have an influence. For instance, the discoloration could be attributed to unreacted double bonds of the monomer, as these might form colored peroxides.[58, 67] This connection between discoloration and double bond conversion (**DBC**) was also observed in the work of Imazato et al.[68] However, it should be noted that in these experiments the monomer composition was altered, resulting in a modified polymer matrix. Conversely, in the research by Fonseca et al., this relationship was disproved.[10] Instead, a correlation was found between water absorption, water solubility and color stability. Therefore, the physical and chemical characteristics of the polymer matrix seem to be of primary importance. These in turn depend directly on the type of monomers used. Further studies also validate the relationship between discoloration and the choice of monomers.[57, 60, 69] Other components of photoactive formulations have also been identified as potential contributors to discoloration. These include, for example, stabilizers and coinitiators for Norrish typ II initiator systems.[70] Stabilizers can undergo a transformation into colored substances through their stabilization mechanism. For instance, quinone methide (Figure 13) structures may form, along with even higher conjugated systems, resulting in significant discoloration.[71-73]
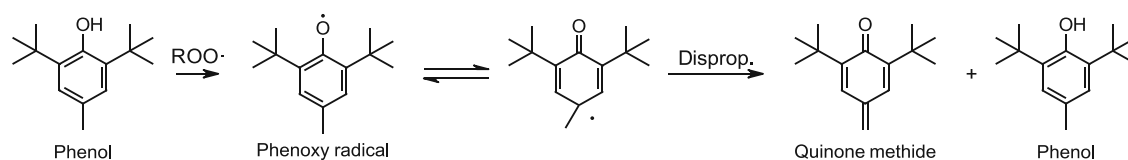

Figure 13: Stabilization mechanism of a phenolic stabilizer with quinone methide formation .[73]

Regarding the coinitiators, tertiary amines were identified as responsible structures for discoloration, with aliphatic amines generally causing less intense discoloration

compared to aromatic ones.[70, 74] In addition, a higher ratio of amine coinitiator to initiator adversely affects the discoloration behavior as unreacted amine residues persist.[22, 69] These residues possess significant discoloration potential due to oxidation reactions.[21, 22, 69]

Further, the photoinitiators themselves were recognized as another origin of discoloration. For instance, remaining photoinitiator may persist in the material, leading to discoloration.[63, 74, 75] This can arise from high initiator concentrations, the use of inappropriate light sources, or incomplete decomposition due to shielding effects. In addition to residual photoinitiator, other causes of photoinitiator-induced discoloration are described in literature. In the work of Segurola et al., a wide range of commercial Typ I and Typ II photoinitiators were investigated with regard to the yellowing they cause.[65] It has been shown that even substances of the same substance class differ in their discoloration behavior. Such occurrences could be attributed to photolysis products and bimolecular radical reactions. Apart from the creation of benzaldehyde, the recombination of radicals leading to the generation of benzil, benzoin and quinoidal structures has been described as the underlying cause of yellowing in certain industrial photoinitiators (Figure 14).[66, 76]
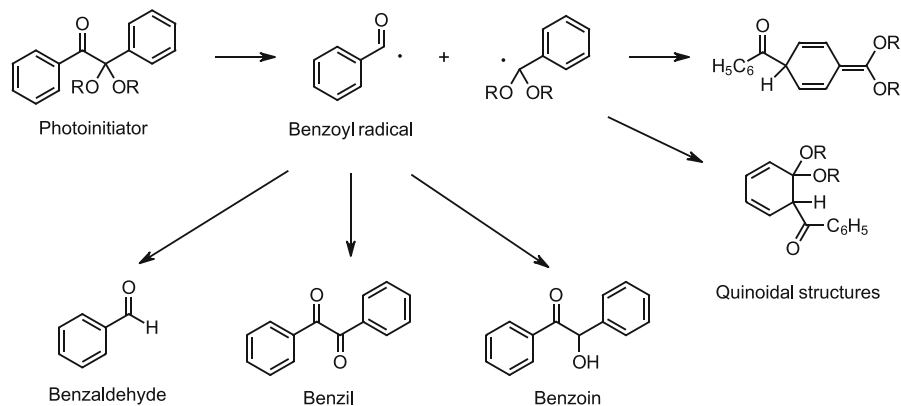

Figure 14: Possible photolysis products causing yellowing.[66]

Depending on the photoinitiator used, the possible photolysis products would differ in their structure. In the case of acylphosphine oxides the benzoyl moiety is usually modified with three methyl substituents. Therefore, possible photolysis products causing discoloration could be mesitaldehyde, mestil or mesitoin (Figure 15).
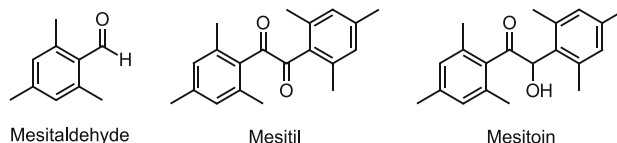
Figure 15: Structures of possible acylphosphine oxide photolysis products.

In the work of Griesser et al., the formation of mesitaldehyde and mesitil was actually demonstrated in the case of a bisacylphosphine oxide photoinitiator.[77]

This work is concerned with the discoloration of polymer samples based on the acylphosphine oxide photoinitiator **TPO**. The aim is to investigate the causes of discoloration and to develop technologies to produce formulations with improved color-stability. Parts of the results presented in the following will be published in our work "Color-stable formulations for 3D-photoprintable dental materials".[i]

1.2 Determination of the color change

This study aims to investigate color changes and the discoloration behavior of cured polymer samples. To achieve this, it is imperative to establish a suitable method for measuring parameters, which offer insights into the intensity of these discolorations as well as their underlying causes. In the dental field, measurements of the CIELAB parameters are commonly used to assess colors. While these measurements are excellent for quantifying colors and accurately determining changes, they do not provide any chemical information that could be used to investigate potential causes. UV-Vis absorption measurements appear to be better suited for this purpose, as they offer precise information regarding the wavelengths at which absorption occurs or diminishes. Therefore, these measurements also provide a certain degree of chemical information, as various substances absorb light at distinct wavelengths owing to their respective chromophores.

1.2.1 UV-Vis Spectroscopy

This analytical method is employed to assess the absorption characteristics of light-cured polymer thin film samples. Ensuring a uniform layer thickness is crucial for accurately quantifying absorption changes. To achieve this precision, all samples were prepared using a photorheometer, providing an exact gap width.[78] A layer thickness of 1200 μm was found to be suitable to ensure complete curing of the polymer samples and to be able to assess sufficiently strong changes in the absorption spectrum within a reasonable period of time. Unless otherwise stated, the samples were therefore produced with this layer thickness. Depending on the composition of the sample, a suitable light source was selected for the curing process, which is mentioned in the experimental part for the respective sample preparation. The obtained polymer samples were then post-cured in a suitable light oven, whereby the used device and the respective conditions are also listed in the experimental section.

The standard formulation for these measurements consists of a homogeneous mixture of the monomer urethane dimethacrylate (**UDMA**, stabilized with 100 ppm MeHQ) and 1.07 mol% of the photoinitiator **TPO**. **UDMA** is an important monomer for dental materials which is capable of producing suitable thin films samples and exhibits time-dependent discoloration in first tests. **TPO** is a commonly utilized photoinitiator that holds significant importance for 3D printing applications in the dental field, where challenges with discoloration are most pronounced. Unless otherwise stated, the samples are stored under standard storage conditions, which is dry (in air atmosphere without the addition of water) at 37°C and in the absence of light. Under these conditions, the discoloration behavior can be easily assessed and monitored. The temperature of 37°C was selected because it corresponds to the human body temperature, ensuring realistic results. The thin film samples are measured at regular intervals using a spectrophotometer.

To investigate the discoloration behavior and to gain new insights, these samples undergo alterations in their composition or are subjected to varying storage conditions. For a direct quantitative comparison of different samples, these are produced and evaluated simultaneously and in one series of measurements.

Evaluation of UV-Vis measurements

The spectra from measurements of a sample at different times can be overlaid to observe how absorption changes in relation to storage duration (Figure 16a). To emphasize only the temporal changes of the absorption, difference spectra can be created (Figure 16b). Here, the absorption spectrum of day 0 is subtracted from the measurements of the other points in time. Whether this operation was performed or not can be recognized by the labeling of the y-axis ($A_t - A_{t=o}$).

Another way of displaying the discoloration behavior is to show the change in absorbance at a certain wavelength against time (Figure 16c). This illustration is particularly suitable for comparing multiple samples in one diagram, whose absorbances arise at the same wavelengths. Generally, a wavelength is selected where the changes are significant and can therefore be easily quantified. The y-axis of these diagrams is labeled with ΔAbs and the subscript of the wavelength (e.g. ΔAbs_{350nm}).
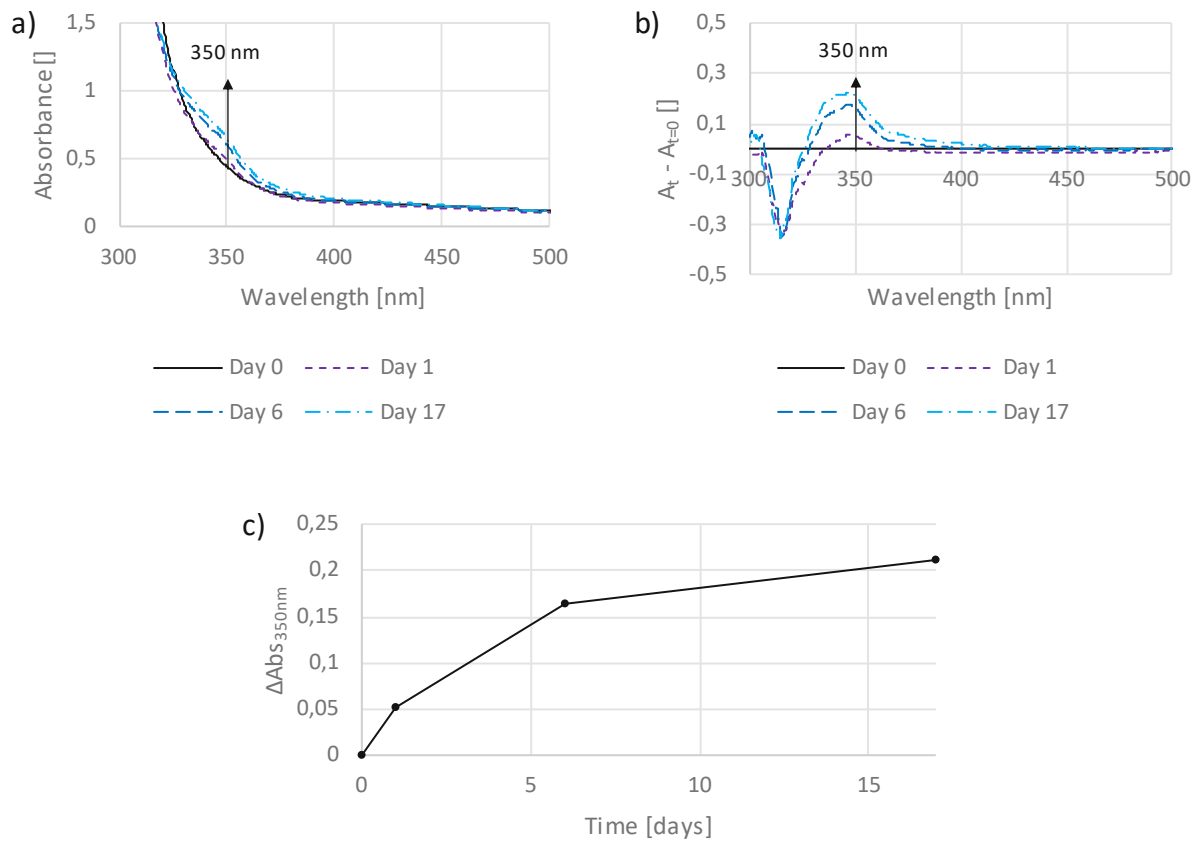
Figure 16: Absorption spectra of a standard thin film sample at different times (a), the corresponding illustration as difference spectra (b) and the change in absorbance at 350 nm (c).

1.2.2 CIELAB

For the exact quantification and determination of absolute values of the discolorations, samples were prepared which were measured in the CIELAB color space (Figure 17).

Figure 17: Schematic illustration of the coordinates in the CIELAB color space.[79]

General part

This method can also be used to better compare samples that produce absorbances at different wavelengths, by the determination of the total color change (ΔE). The CIELAB color space represents colors through 3 axes: The L*-axis specifies t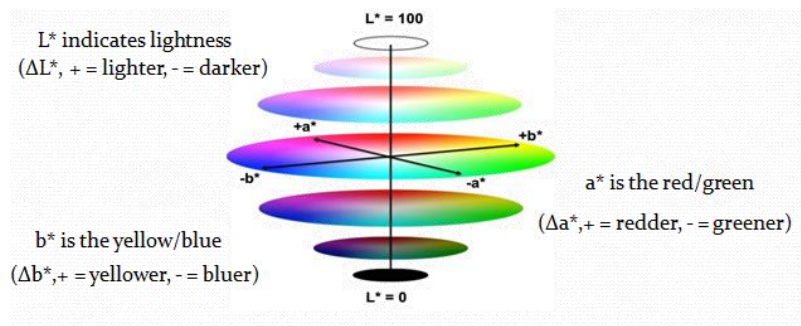he lightness from 0 (black) to 100 (white), a* describes the green-red error (-a: green, +a: red) and b* indicates the blue-yellow axis (-a: blue, +a: yellow). The color change (ΔE) is evaluated by the following formula:

$$\Delta E = \sqrt{\Delta L^2 + \Delta a^2 + \Delta b^2}$$

For these measurements, circular specimens with a height of 2 mm are produced and measured against a black and a white reference surface using a spectrophotometer. The used sample compositions are indicated with the respective measurements. The storage of the samples takes place at 50°C immersed in water.
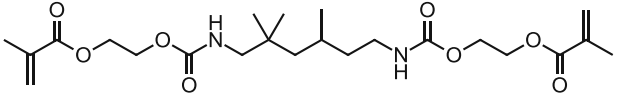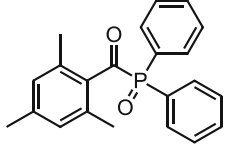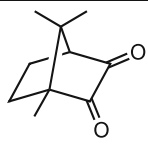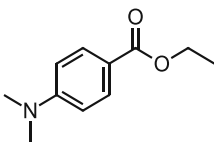
1.3 Studies on the discoloration of polymers

1.3.1 Preliminary tests

The initial phase of this study involved a formulation comprising the monomer **UDMA** and the photoinitiator system **TPO**, **CQ** and **EDB** (Table 1), prompted by issues concerning the discoloration behavior of this formulation. First, it was necessary to determine an appropriate layer thickness and storage conditions in order to evaluate samples using UV-Vis spectroscopy. Experiments with various film thicknesses ranging from 200 – 1600 µm have revealed that thicknesses of 1000 µm and 1200 µm are most suitable. These thicknesses allow the detection of discoloration within a reasonable period of time and good processability. Higher layer thicknesses can lead to problems with incomplete curing, subsequent processing or the production of samples based on low-viscosity monomers. Only initial tests that explicitly stated this were carried out with a layer thickness of 1000 µm, later all samples were uniformly prepared with 1200 µm.

Table 1: Composition of the starting formulation for discoloration experiments.

UDMA	98.75 wt% ≜ 97.79 mol%	
TPO	0.8 wt% ≜ 1.07 mol%	
CQ	0.15 wt% ≜ 0.42 mol%	
EDB	0.3 wt% ≜ 0.72 mol%	

The initial formulation (Table 1) was employed to create thin film samples, which were utilized to investigate the fundamental discoloration behavior over an extended duration. The samples were stored under standard conditions (37°C, dry) and absorption spectra were measured regularly. The results for the period day 0 – day 35 are shown in Figure 18a and for day 35 – day 100 in Figure 18b. In addition to the regular measurements, a spectrum was recorded before post-curing (Figure 18a).

*Figure 18: UV-Vis absorption spectra of a 1000 µm thin film sample consisting of **UDMA**, **TPO** (0.8 wt% ≙ 1.07 mol%), **CQ** (0.15 wt% ≙ 0.42 mol%) and **EDB** (0.3 wt% ≙ 0.72 mol%). **a)**: Day 0 – Day 35; **b)**: Day 35 – Day 100.*

Figure 18a shows that from day 0 to day 35 several absorbances form at different wavelengths, which increase in intensity over time. With even longer storage (Figure 18b), these absorbances gradually decrease again until they have vanished. Comparing the curve before post-curing with that after (Day 0), it is apparent that a significant absorbance disappeared completely. This absorbance is attributed to the remaining **TPO** photoinitiator, which is cleaved by the post-treatment. The absorbance is congruent in shape and shift with that of **TPO** when measured in solution (Figure 19).
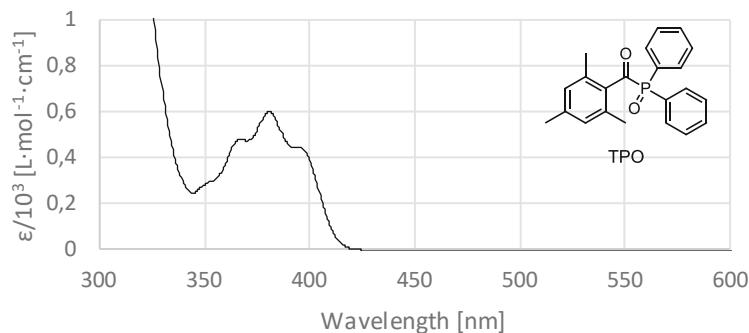
*Figure 19: UV-Vis absorption spectrum of the photoinitiator **TPO** in acetonitrile solution.*

Figure 20 shows the same measurements as in Figure 18a as difference spectra. The comparison of the two illustrates the relevance of this visualization method. Absorbances are effectively highlighted in terms of shape and intensity, enabling the identification of specific changes, such as those at 345 nm, which become visible for the first time.
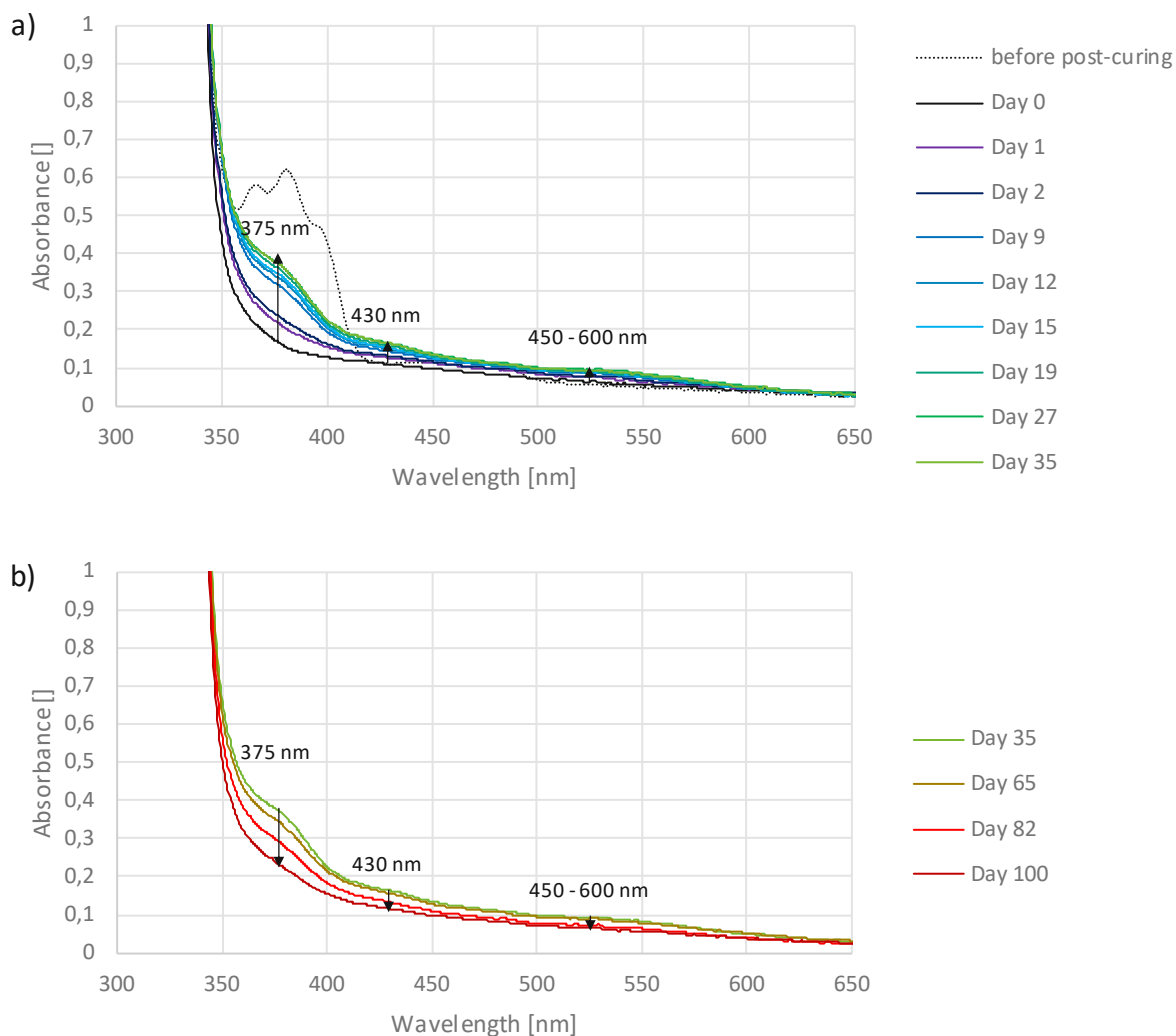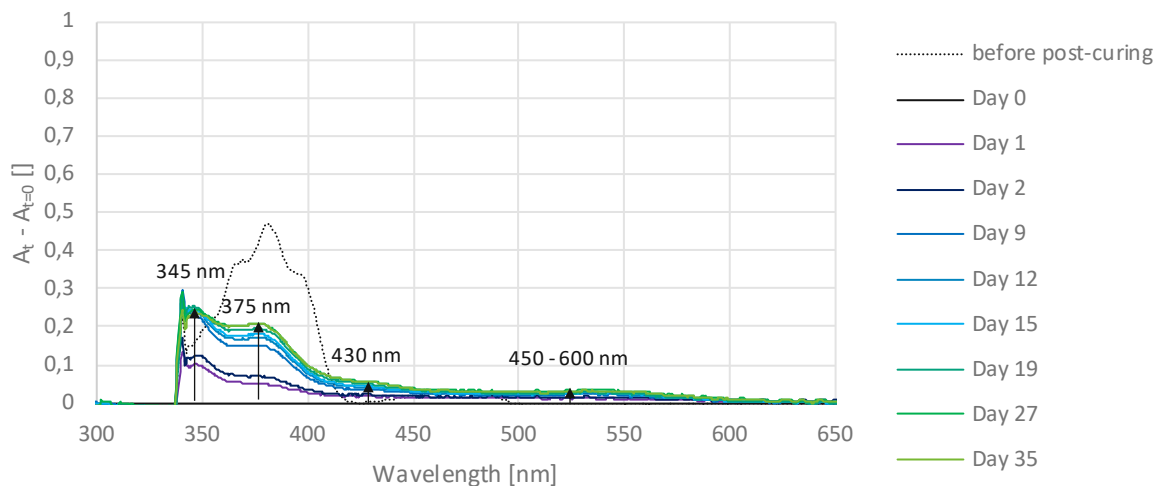

*Figure 20: UV-Vis difference spectra of a 1000 µm thin film sample consisting of **UDMA**, **TPO** (0.8 wt% ≙ 1.07 mol%), **CQ** (0.15 wt% ≙ 0.42 mol%) and **EDB** (0.3 wt% ≙ 0.72 mol%).*

Subsequently, individual components of the formulation were examined to investigate how each of them affects the discoloration process. To demonstrate the influence of the polymer matrix, **UDMA** and **D3MA** were compared with each other. For this purpose, the mixture was simplified, with only **TPO** being utilized as photoinitiator. Figure 21 shows the results of the corresponding UV-Vis absorption measurements.
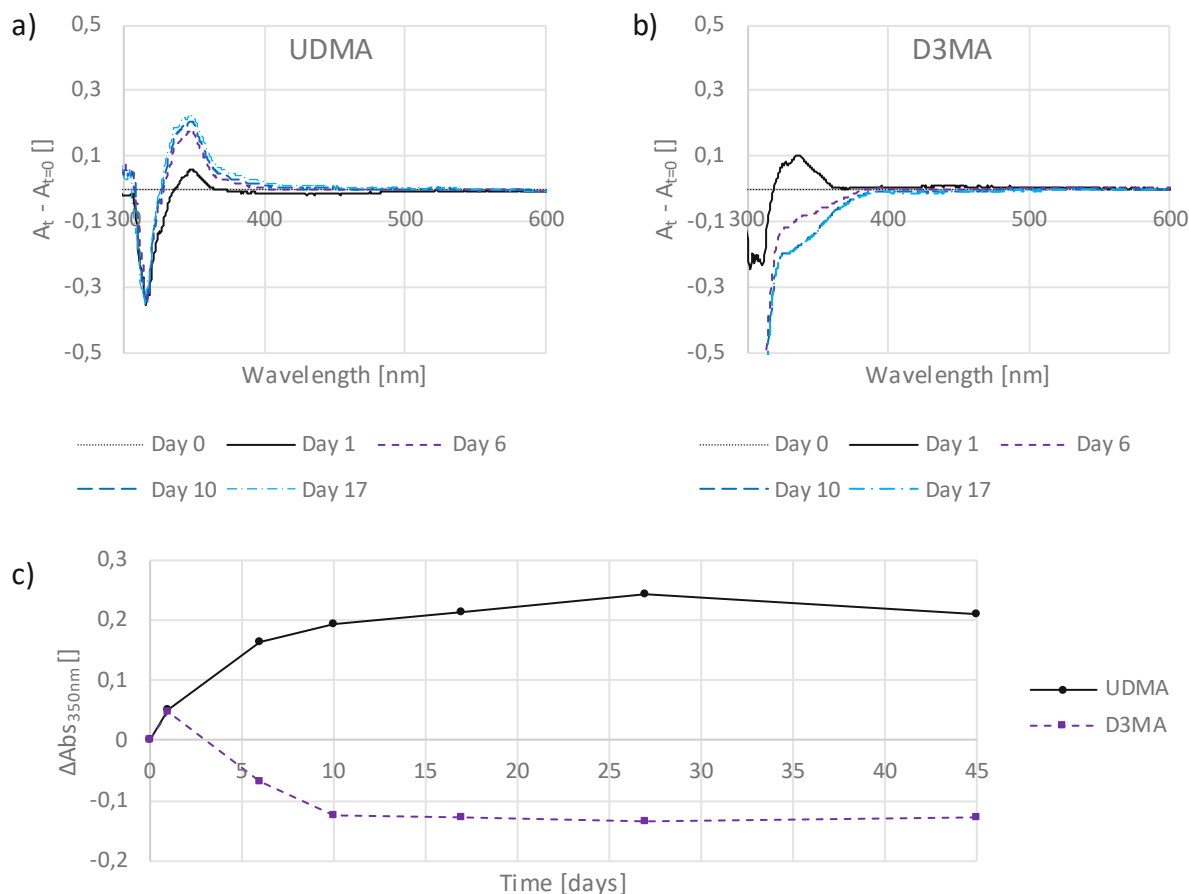
*Figure 21: UV-Vis difference spectra of thin film samples prepared with **TPO** (1.07 mol%) and the monomers **UDMA** (a) and **D3MA** (b). The change in absorbance at 350 nm of these two samples is shown in (c).*

Considering the two measurements from day 1 (Figure 21) the curves appear to be almost equal, with an absorbance growing in a similar wavelength range. The significant difference caused by the respective polymer matrix only becomes apparent on further storage. Here a rapid decolorization of the **D3MA**-based sample can be seen, while the absorbance of the **UDMA**-based one continues to increase. Therefore, the cause of the discoloration appears to be the same, but the temporal behavior depends on the monomer used.

Next, the individual components of the photoinitiator system were examined in the less strongly discoloring **D3MA** matrix (Figure 22).

a) D3MA/TPO

b) D3MA/TPO/CQ

c) D3MA/TPO/EDB

d) D3MA/TPO/CQ/EDB
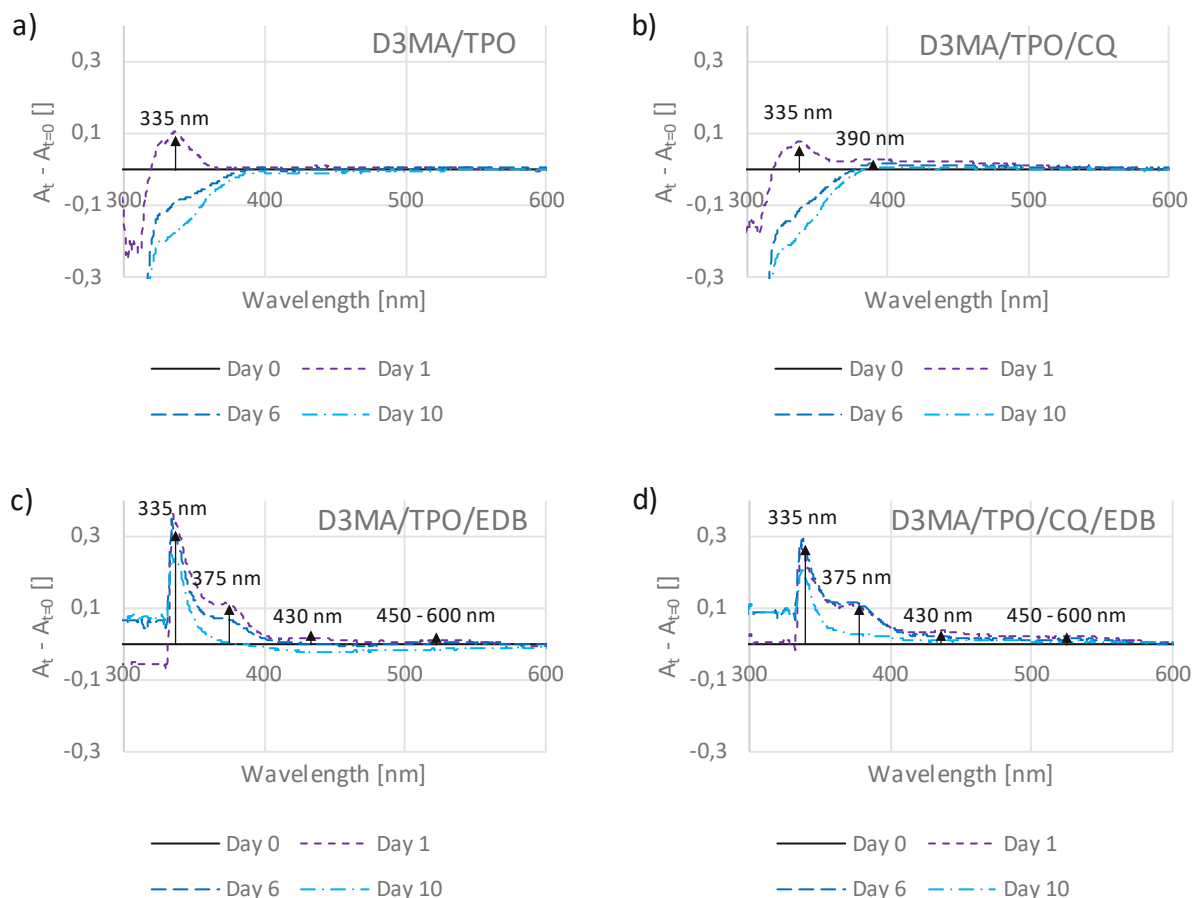
*Figure 22: UV-Vis difference spectra of thin film samples prepared with **D3MA** and **a)**: TPO (0.8 wt% ≙ 1.07 mol%); **b)**: TPO (0.8 wt% ≙ 1.07 mol%) / CQ(0.15 wt% ≙ 0.42 mol%); **c)**: TPO (0.8 wt% ≙ 1.07 mol%) / EDB (0.3 wt% ≙ 0.72 mol%; **d)**: TPO (0.8 wt% ≙ 1.07 mol%) / CQ(0.15 wt% ≙ 0.42 mol% / EDB (0.3 wt% ≙ 0.72 mol%)*

If **D3MA** is cured only with the photoinitiator **TPO**, a developing absorbance around 335 nm can be observed, which is already completely faded after 6 days (Figure 22a). If **CQ** is added (Figure 22b), a further weaker absorbance can be observed at higher wavelengths. Significant and long-lasting absorptions in the visible range of light are only observed with the addition of the co-initiator **EDB** (Figure 22c and d). These absorbances lead to strong discoloration of the samples, which are also clearly visible. The phenomenon of strong discoloration of amine-based coinitiators is already described in literature and is attributed to their oxidation.[21, 22, 69, 70, 74] Since the Type II initiator system, comprising **CQ** and **EDB**, is not strictly essential and tends to pronounced discoloration, subsequent efforts primarily focused on the photoinitiator **TPO**. The monomer **UDMA**, on

the other hand, is almost indispensable in dental materials, therefore the combination with **TPO** was investigated in more detail.

Figure 23 illustrates the long-term discoloration behavior of a thin film sample consisting of **UDMA** and **TPO** (1.07 mol%), stored at 37°C under standard storage conditions, using the difference spectra.
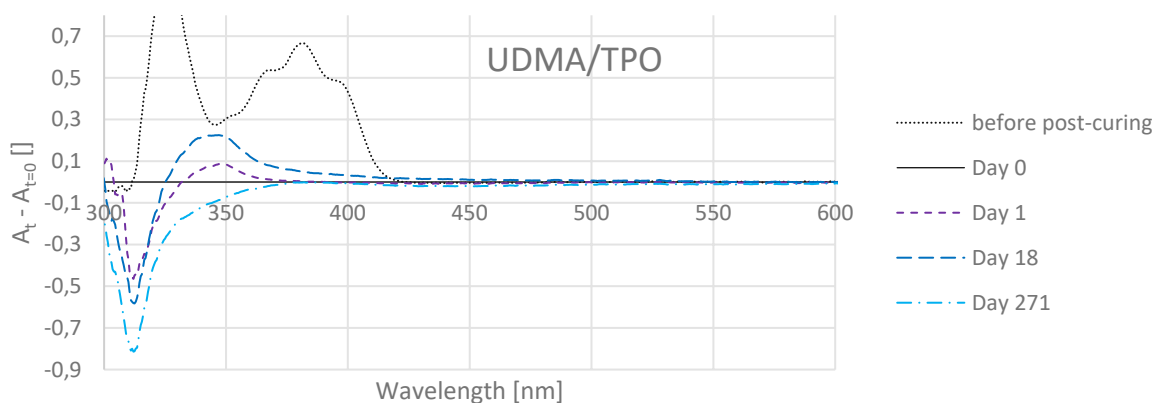
Figure 23: Difference absorption spectra of a standard thin film sample at different times.

Similar to the very first sample (Figure 20), the **TPO** absorbance can be observed in Figure 23 before post-curing. Another similarity is the temporal behavior. A growing absorbance can be observed initially (Day 1 – Day 18), followed by the disappearance of the absorbance over a longer period of time (Day 271). The absorption increases predominantly in the region around 345 nm, but tails out into the visible, resulting in a yellow discoloration. Due to the suspicion that an impurity of the monomer **UDMA** could cause the long-lasting discoloration, a thin film sample was prepared for which the monomer **UDMA** was purified by column chromatography beforehand. Figure 24 shows the comparison of the absorbance behavior of samples produced in the same way with conventional **UDMA** and purified **UDMA**.
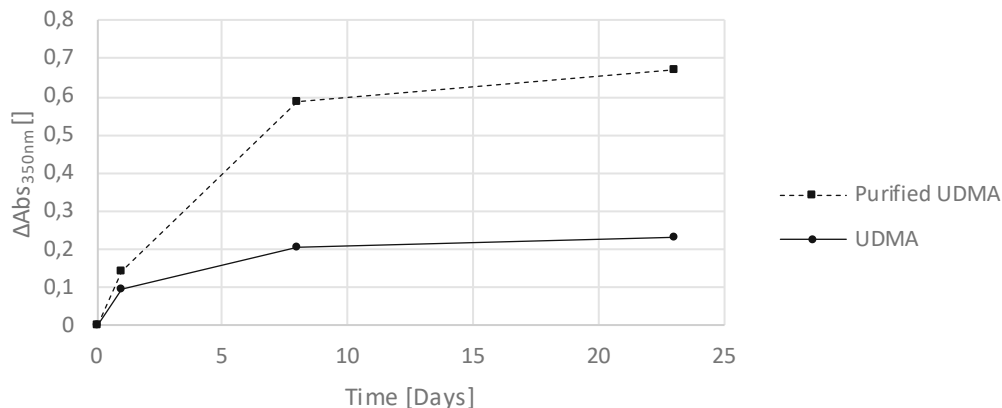
*Figure 24: Temporal change in absorbance at 350 nm of thin film samples consisting of **TPO** (1.07 mol%) and untreated or purified **UDMA** monomer.*

The results from Figure 24 show that contrary to expectations contaminants do not cause or intensify discoloration, but instead significantly suppresses it. The most notable "impurity" removed from **UDMA** by column chromatography is the stabilizer **MeHQ**, which was present in the amount of 100 ppm. To confirm if **MeHQ** is indeed accountable for the enhanced color stability, another sample was prepared with conventional **UDMA** (stabilized with 100 ppm **MeHQ**), supplemented with additional 300 ppm of **MeHQ** (Figure 25).
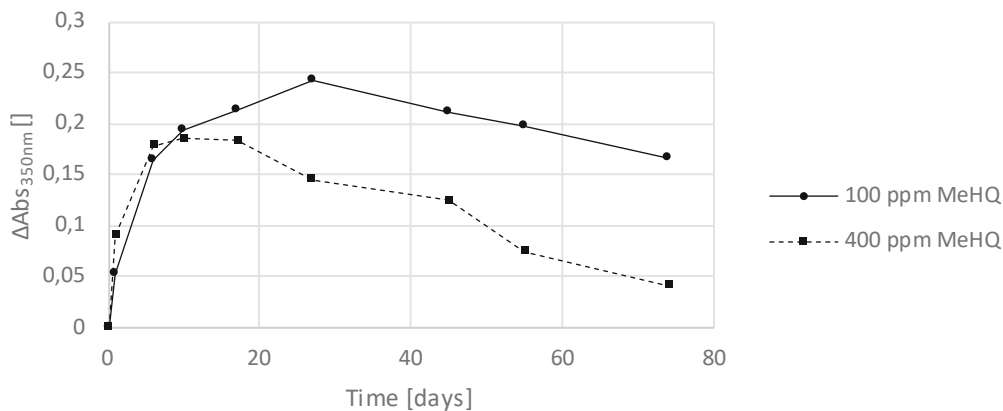
*Figure 25: Temporal change in absorbance at 350 nm of thin film samples consisting of **TPO** (1.07 mol%) and **UDMA** (stabilized with 100 ppm **MeHQ**) (100 ppm **MeHQ**) and additional 300 ppm of **MeHQ** (400 ppm **MeHQ**).*

Figure 25 illustrates that the inclusion of another 300 ppm **MeHQ** can further reduce discoloration, which confirms that **MeHQ** actually has a positive effect on color stability. Quantitatively, the initial 100 ppm of **MeHQ** (Figure 24) appears to have a significantly

greater impact on ΔAbs_{350nm} than the additional 300 ppm (Figure 25). It is assumed that the stabilizer scavenges residual free radicals that would otherwise lead to discoloration. This discoloration could result directly from the formation of colored radicals, the oxidation of other constituents by residual free radicals, their recombination, or their conversion into colored substances through subsequent reactions. Further investigations regarding these radicals were conducted in chapter "1.3.5 Persistent radicals – EPR". Additional studies on different stabilizers were performed in section "1.4.2 Stabilizers".

1.3.2 Storage conditions

Next the influence of the storage conditions on the discoloration was examined. Dental materials are often preserved in a wet environment to simulate the humid conditions in the mouth. Therefore, a comparison was made between samples stored under standard storage conditions and samples immersed in water (Figure 26a). Furthermore, the influence of temperature was investigated at 37°C, 60°C and 90°C (Figure 26b). Since **EDB** is known to cause discoloration due to oxidation, the effects of the presence and absence of oxygen were investigated (Figure 26c). For this purpose, the samples were stored sealed under pure oxygen or pure argon atmosphere at 37°C, 60°C and 110°C (for 110°C see exp. part: Figure 87).
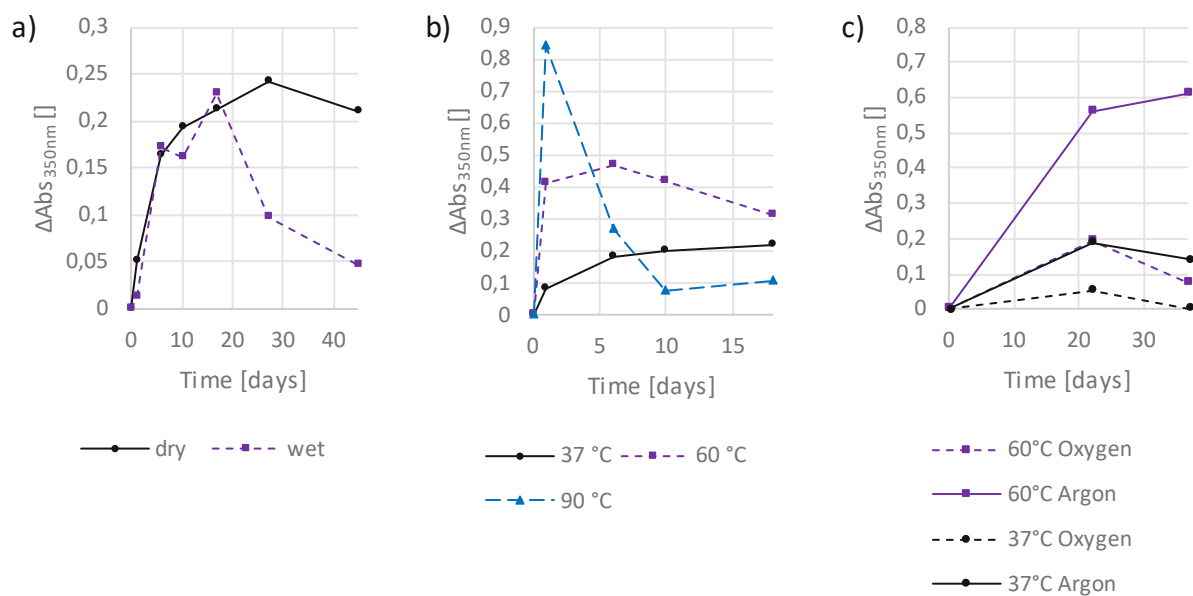
*Figure 26: Temporal change in absorbance at 350 nm of **TPO**-based thin film samples under different storage conditions. a): Dry and wet storage at 37°C; b): Dry storage at 37°C, 60°C and 90°C; c): Dry storage in the oxygen and argon atmosphere at 37°C and 60°C.*

Figure 26a illustrates that there is no difference in the discoloration behavior of dry and wet stored samples at the beginning. However, after 17 days, a trend reversal can be observed in the wet stored sample, followed by a relatively rapid bleaching. In the case of dry storage, this reversal occurs only by day 27 and is less pronounced. Figure 26b reveals that at lower temperatures the increase in absorbance is slower and less steep. At high temperatures, on the other hand, the discoloration, is strong and apparent after a short time, but also vanishes quickly. Higher temperatures appear to accelerate both the discoloration and the subsequent bleaching process. However, the absorbances do not appear to be affected in terms of shape and shift (Exp. part: Figure 86). The results of the investigations regarding the influence of oxygen were unexpected (Figure 26c). Samples stored in oxygen did not discolor more strongly due to oxidation reactions, but rather less strongly than those stored in an argon atmosphere. Since the subsequent bleaching process is also accelerated by the presence of oxygen, oxygen seems to be a crucial part of the decolorization process. These trends can be seen at 37°C, 60°C and also 110°C (Exp. part: Figure 87).

1.3.3 Photoinitiator

Initial tests (Figure 22) have shown that photoinitiators play a significant role in causing discoloration. In this section their influence will be investigated in more detail. Firstly, thin film samples consisting of different concentrations of **TPO** in **UDMA** are examined (Figure 27).
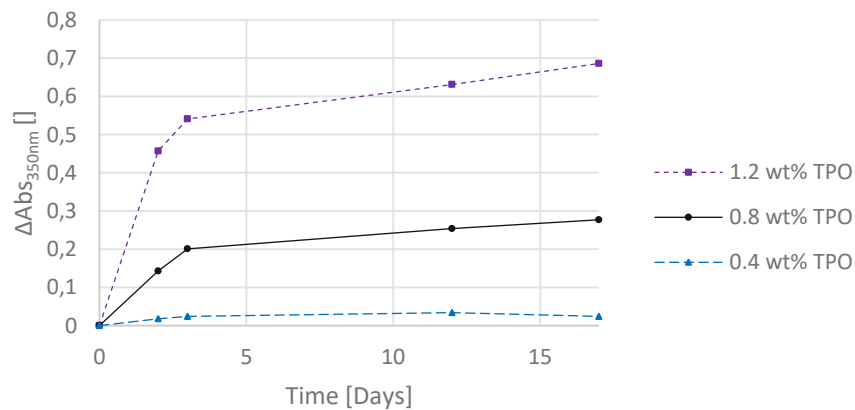
*Figure 27: Temporal change in absorbance at 350 nm of thin film samples consisting of **UDMA** and different concentrations of **TPO** (0.4 wt% ≙ 0.54 mol%; 0.8 wt% ≙ 1.1 mol%; 1.2 wt% ≙ 1.62 mol%)*

The measurements reveal that, the intensity of the absorbances increases with higher initiator concentration. But once again, the shape and shift of the absorbances are not affected, as can be seen in the experimental part in Figure 88.

As described in section 1.1 State of the art, photolysis products of photoinitiators could be responsible for discoloration. This would mean that different photoinitiators would provoke different absorbances. By the evaluation of thin film samples consisting of different photoinitiators this was investigated. The selected substances differ considerably in terms of structure, absorption behavior and the radicals formed. The currently used phosphorus-based photoinitiator **TPO** is being compared to Darocur 1173 (**D1173**), a carbon-based photoinitiator that absorbs shorter wavelength light, and Ivocerin®, a germanium-based photoinitiator that absorbs longer wavelength light. The results for the thin film samples, which were produced with 1.07 mol% of the respective photoinitiator, are depicted in Figure 28.

General part
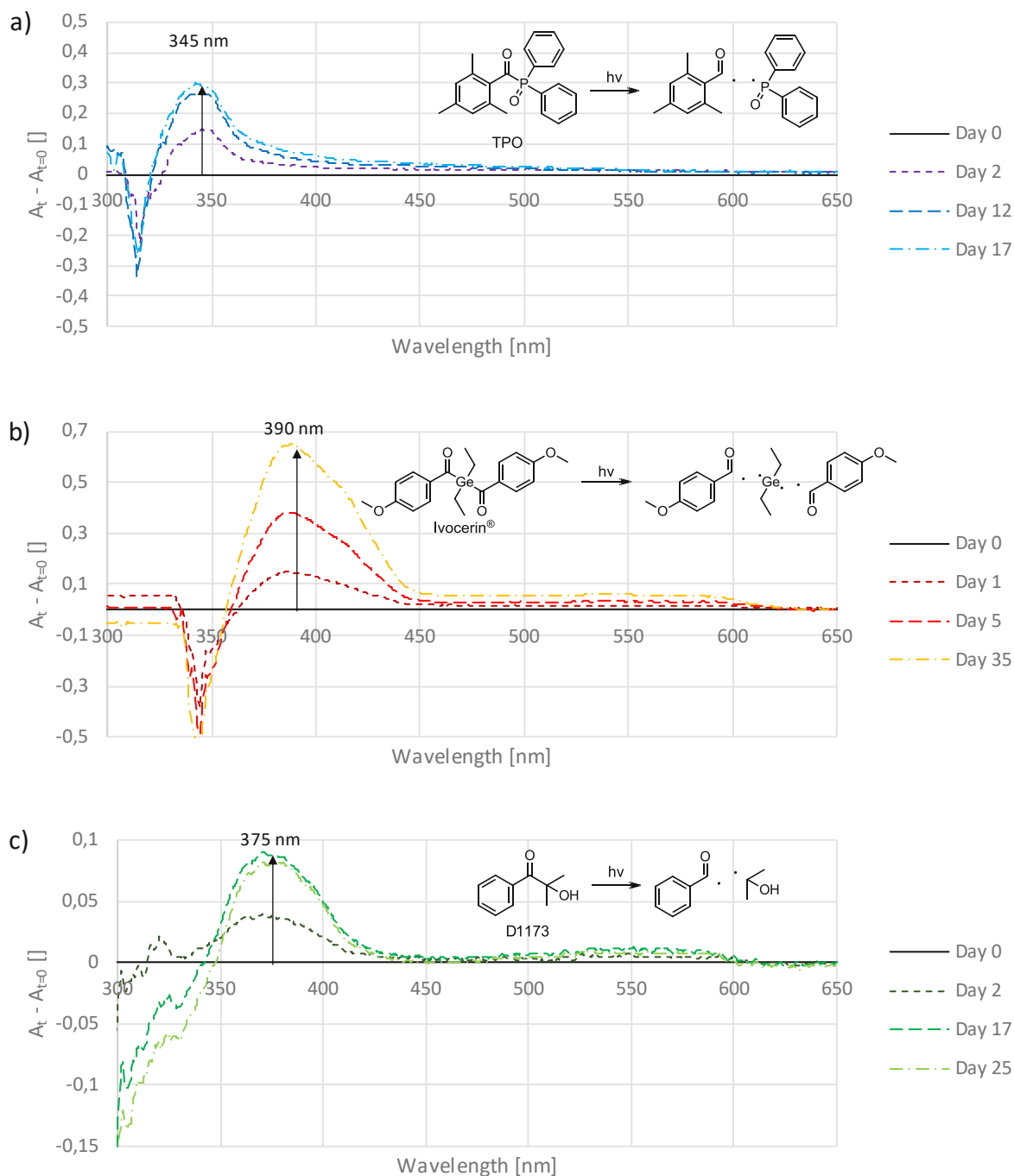
*Figure 28: Time-dependent difference absorption spectra of thin film samples consisting of **UDMA** and 1.07 mol% of the photoinitiator **TPO** (a), Ivocerin® (b) or **D1173** (c).*

In fact, the use of different photoinitiators results in differently shifted absorbances with varying shapes and intensities, as can be seen in Figure 28. **TPO** causes an increasing absorbance predominantly around 345 nm (Figure 28a). For Ivocerin® this is localized at

around 390 nm (Figure 28b) and is therefore at higher wavelengths than for **TPO**. This could lead to the assumption that photoinitiators that cleave at higher wavelengths also cause discoloration at longer wavelengths. However, this assumption is refuted when considering **D1173** (Figure 28c), whose discoloration absorbances increase in the area around 375 nm and are therefore higher than those of **TPO**, although **D1173** is excited at lower wavelengths. Furthermore, weaker absorptions can be observed in the long-wavelength range, which also differ depending on the initiator used. For **TPO**, those weak absorbances occur continuously from approximately 385 nm up to around 550 nm. In the case of Ivocerin® they range between 450 – 625 nm and for **D1173** they are located in the region of 450 – 600 nm. In any case, these experiments show that the choice of photoinitiator influences the wavelengths at which discoloration occurs, which indicates that the photoinitiator is directly related to the substances causing discoloration. On this basis, further investigations were carried out on the benzoyl chromophore of the photoinitiators. Thin film samples were prepared with photoinitiators containing the same benzoyl moieties as the previously tested ones. Thus, **TPO** (Figure 29a) was compared with **BAPO** (Figure 29b), Ivocerin® (Figure 29c) with Irgacure 2959 (**I2959**) (2.2 mol%) (Figure 29d) and **D1173** (Figure 29e) with Irgacure 184 (**I184**) (Figure 29f).
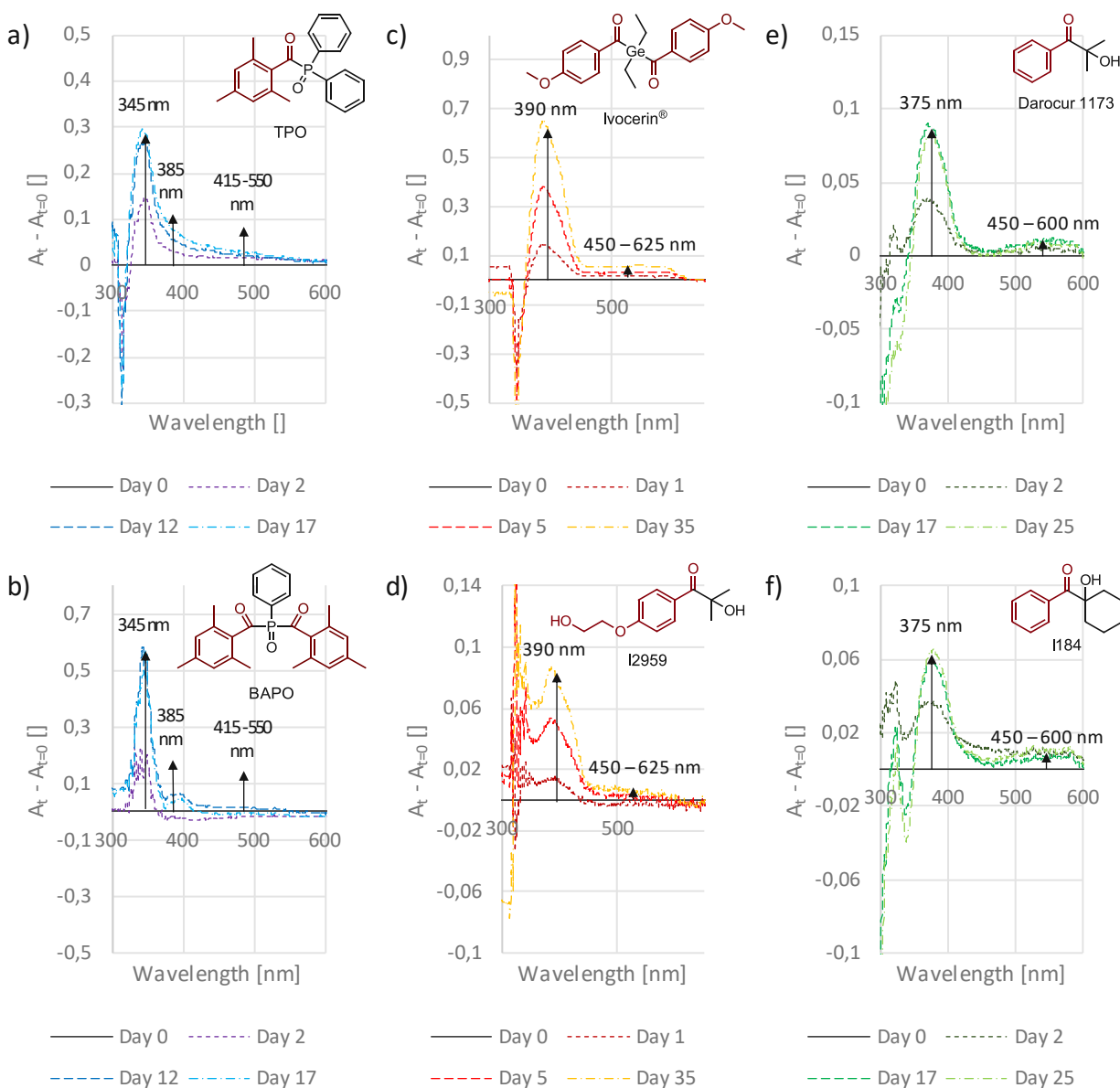
*Figure 29: Time-dependent difference absorption spectra of thin film samples consisting of **UDMA** and different photoinitiators: a): **TPO** (1.07 mol%); b): **BAPO** (1.07 mol%); c): Ivocerin® (1.07 mol%); d): **I2959** (2.16 mol%); e): **D1173** (1.07 mol%); e): **I184** (1.07 mol%).*

The results in Figure 29 are remarkable conclusive. The photoinitiators **TPO** and **BAPO**, which both contain mesitoyl chromophores, provoke the same absorbances. In the same way the absorbance spectra of Ivocerin® and **I2959** based thin film samples resemble each other, whereby both initiators exhibit the same *p*-oxybenzoyl chromophore (*p*-methoxybenzoyl in the case of Ivocerin® and *p*-2-hydroxyethoxybenzoyl in the case of

I2959). The equal behavior was observed for the benzoyl chromophore containing initiators **D1173** and **I184**. This is a clear indication that, depending on the chromophore of the photoinitiator, discoloration is caused in a certain wavelength region. However, this does not seem to be related to the intensity of the discoloration. Considering Ivocerin® it is many times higher than with **I2959**, although **I2959** is used in twice the concentration and therefore has the same number of chromophoric groups as Ivocerin® (Figure 29c, d). As a control, a thin film sample consisting of the thermal initiator **AIBN** and **UDMA** was prepared and evaluated with regard to the discoloration. Unlike the samples containing a photoinitiator, this sample is not expected to discolor, as **AIBN** does not contain a chromophoric group. Figure 30 depicts the results of the measurements of this sample.
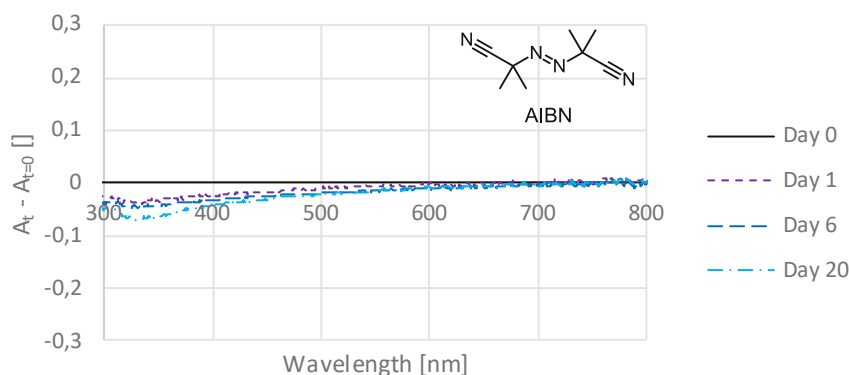
*Figure 30: Time-dependent difference absorption spectra of a thermally cured thin film sample consisting of **UDMA** and **AIBN** (1.07 mol%)*

As expected, the **AIBN**-based sample does not exhibit increasing absorbances leading to discoloration. Once more, this experiment illustrates that the benzoyl chromophores of the photoinitiators are accountable for the observed discolorations.

1.3.4 Photoreactor

Since the photoinitiator was identified as the primary source of the resulting discoloration, more comprehensive studies were conducted. For this purpose solutions of **TPO** were irradiated in photoreactor experiments to investigate the photobleaching behavior and to detect the formation of light-absorbing photolysis products. Figure 31 shows the UV-Vis spectra of photoreactor studies with two different concentrations of **TPO**.

General part

a) c = 0.005 M   b) c = 0.1 M
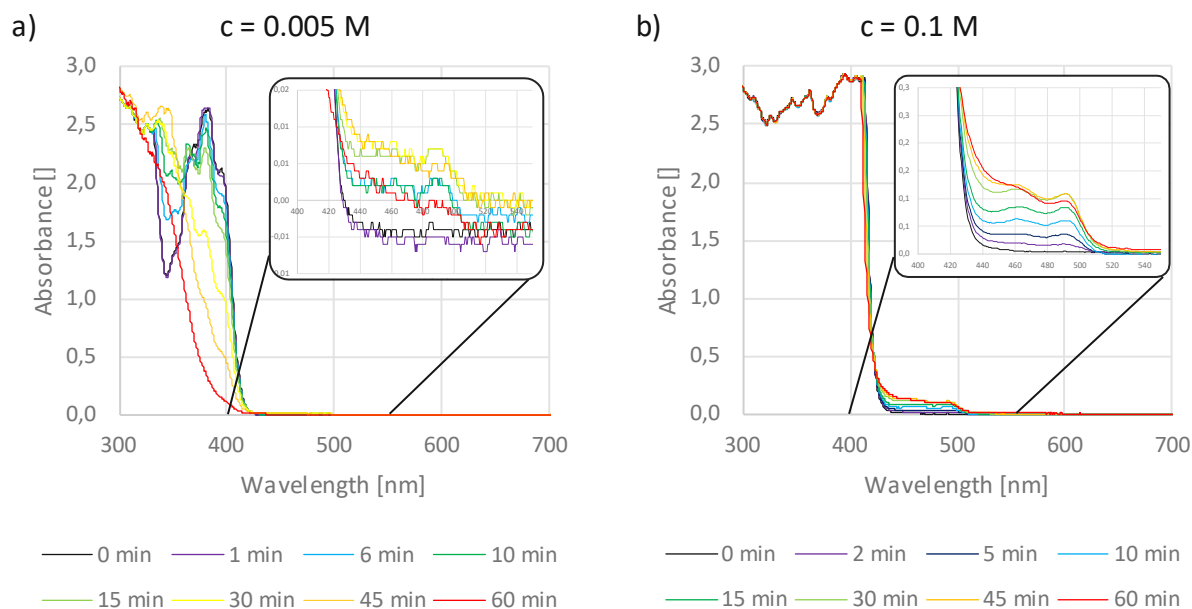
*Figure 31: Time-dependent UV-Vis spectra of photoreactors with 0.005 M (a) and 0.1 M (b) solutions of **TPO** in acetonitrile, degassed with argon and irradiated with 100 mW/cm² at 385 nm.*

The experiment Figure 31a shows the photobleaching of **TPO**, with the characteristic absorbance of the n→π* transition in the range of 355 – 420 nm. With zoom in the range of 400 – 550 nm, a weak emerging absorbance can be seen, which could cause discoloration. In order to be able to better observe this weak absorbance, a photoreactor with a higher **TPO** concentration was conducted (Figure 31b). In fact, the weak absorbance with two peaks at 463 nm and 491 nm becomes more apparent as a result. The origin of this absorbance is most likely the recombination product mesitil, which is formed from two mesitoyl radicals. This is apparent from the comparison with the literature absorption spectrum from the work of Wolf et al. (Figure 32).[80]
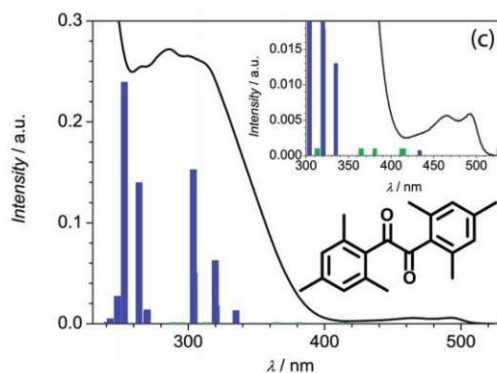
Figure 32: UV-Vis absorption spectrum of mesitil from the work of Wolf et al.[80]

To determine if mesitil could indeed be a contributing factor to the discoloration in thin film samples, the absorption spectra of the photoreactor were compared with those of a **TPO**-based thin film sample (Figure 33).
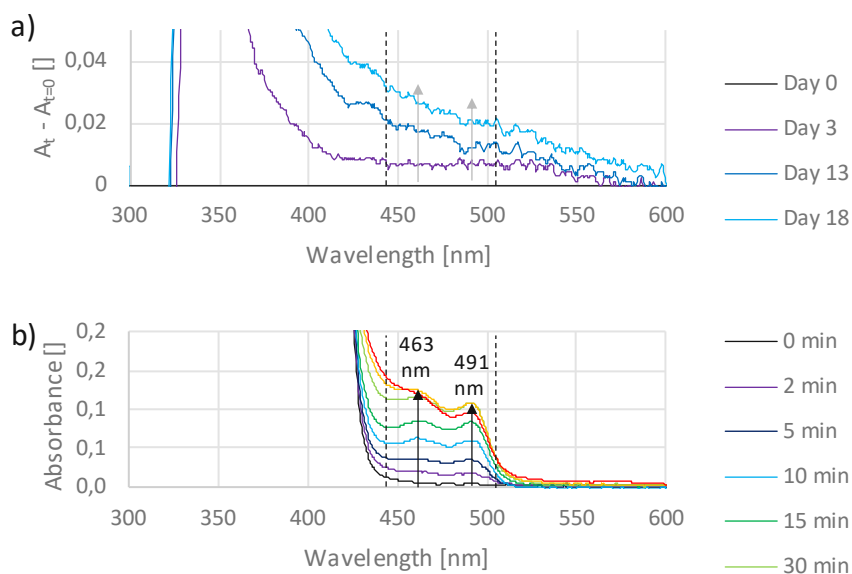
*Figure 33: UV-Vis spectra of a thin film sample consisting of **UDMA** and **TPO** (1.07 mol%) stored under standard storing conditions (a) and a photoreactor with **TPO** (c = 0.1 M) in acetonitrile (b).*

In Figure 33a and b the range from 400-550 nm is particularly displayed, to compare the emerging absorption bands. While in the photoreactor (Figure 33b) two distinct bands are clearly recognizable at 463 nm and 491 nm, for the thin film sample (Figure 33a) a more continuous absorption ranging from 400 nm to 550 nm is apparent. This undefined absorption pattern of the thin film sample suggests that either another substance or a combination of substances could be responsible for these absorbances. If mesitil is

indeed part of this absorption, this would mean that it would gradually form in the cured thin film sample. In the case of the photoreactor, mesitil is formed by the recombination of two mesitoyl radicals. Assuming that the same mechanism occurs in the thin film sample, this means that persistent mesitoyl radicals are trapped in the polymer matrix. If this is the case, they should be detectable by electron paramagnetic resonance (**EPR**) measurements.

1.3.5 Persistent radicals – EPR measurements

As previously demonstrated, the addition of stabilizers can notably diminish discoloration. Based on tests with different photoinitiators and photoreactor experiments, it is suspected that persistent photoinitiator radicals could be trapped in the polymer matrix, leading to colored follow up products. Another possibility is that discoloration is caused by long-lasting colored radicals. In order to detect possible trapped radicals and perhaps identify specific radicals, electron paramagnetic resonance (**EPR**) measurements were conducted. These measurements were performed by Max Schmallegger at the TU Graz in the working group of Georg Gescheidt. Two thin film samples with identical compositions were measured, each stored for varying durations. The first sample, stored for 22 days, exhibited a visible yellow coloration. In contrast, the second sample, stored for 271 days, had already completely bleached. The resulting EPR spectra are shown in Figure 34.
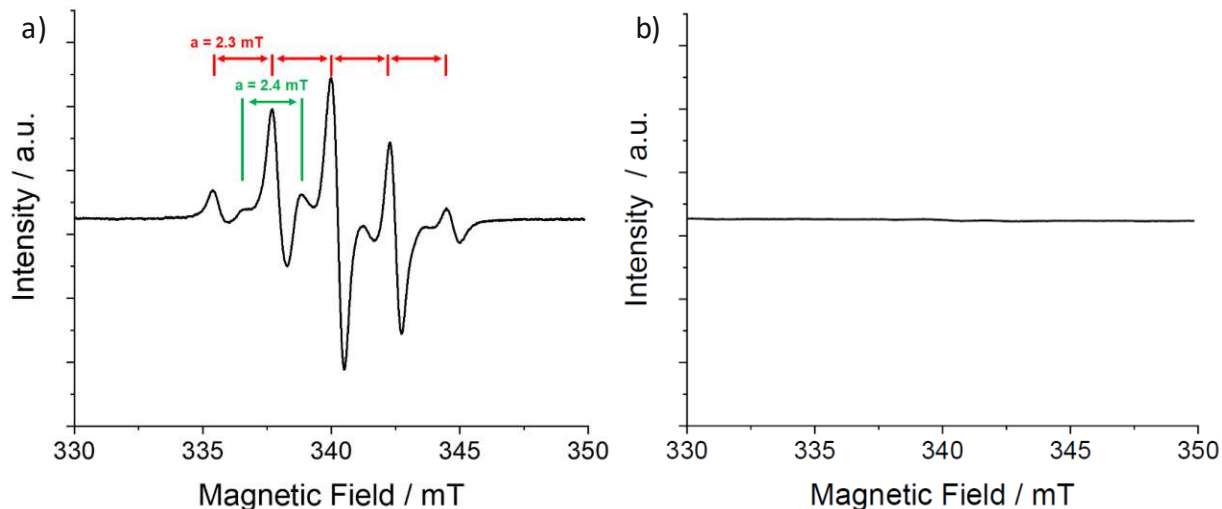
*Figure 34: EPR spectra of thin film samples consisting of **UDMA** and **TPO** (1.07 mol%) stored for 22 days (a) and 271 days (b) under standard storage conditions.*

The measurements show that long-lived radicals are detectable in the discolored thin film sample stored for 22 days. The one that has been stored for 271 days and completely bleached, on the other hand, does not give any signals. Next, two samples were prepared with the two different photoinitiators **TPO** and **D1173**, and measured after 15 minutes. The EPR spectra in these experiments (Exp. part: Figure 91) look identical to that shown in Figure 34a. This reveals that these radicals are present from the beginning, although the samples do not yet show any discoloration. Moreover, it is apparent that the observed radicals are independent from the photoinitiator used. This proves that colored radicals cannot be the cause of the discoloration. Furthermore, another experiment demonstrated that also the type of methacrylate monomer used does not change the resulting EPR spectrum (Exp. part: Figure 93).

The radicals detected are probably propagating chain radicals, radicals which are formed from remaining monomers or polymer chain breaks.[81, 82] In all cases the same radicals could be formed causing the EPR spectrum shown in Figure 34a. This is primarily characterized by 5 lines with a hyperfine coupling constant of 2.3 mT (red lable) and an intensity distribution of 1:4:6:4:1, indicating four equivalent protons. The second, weaker spectrum displays a coupling constant of 2.4 mT and an intensity distribution of 1:3:3:1 (green lable), indicating 3 equivalent protons. Figure 35 elucidates the reason for obtaining two spectra with varying intensities. Specifically, only the protons highlighted in

green contribute to the EPR spectrum. The presence of different conformations results in the generation of two spectra. Notably, the conformation depicted on the left is thermodynamically more stable, leading to a more intense EPR spectrum.
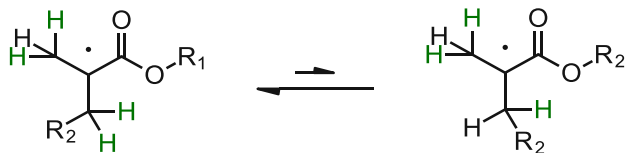

Figure 35: Structures of long-lived radicals leading to the EPR spectra.

These experiments have shown that neither colored radicals nor remaining photoinitiator radicals are trapped in the polymer. This indicates the absence of mesitoyl radicals, which could potentially induce discoloration via recombination. Nevertheless, these long-lived radicals could contribute to discoloration or subsequent bleaching, as radicals are highly reactive and could, for example, participate in redox reactions.

1.3.6 Leaching tests

As the substances responsible for discoloration have not yet been identified, leaching tests of discolored thin film samples are to be conducted. The extracted substances should then be separated from each other and analyzed with regard to absorption and identity. Initially, a thin film sample consisting of **UDMA** and **TPO** (1.07 mol%) was stored for 23 days under standard storing conditions. Afterwards the sample was stored dry at 110°C for 15 minutes before being ground to a powder and extracted for 14 days with DCM. The resulting UV-Vis absorption spectra are displayed in Figure 36. Heating of the sample to 110°C is required to generate sufficient discoloration, as preliminary tests have indicated that otherwise, the extract appears colorless in UV-Vis measurements.
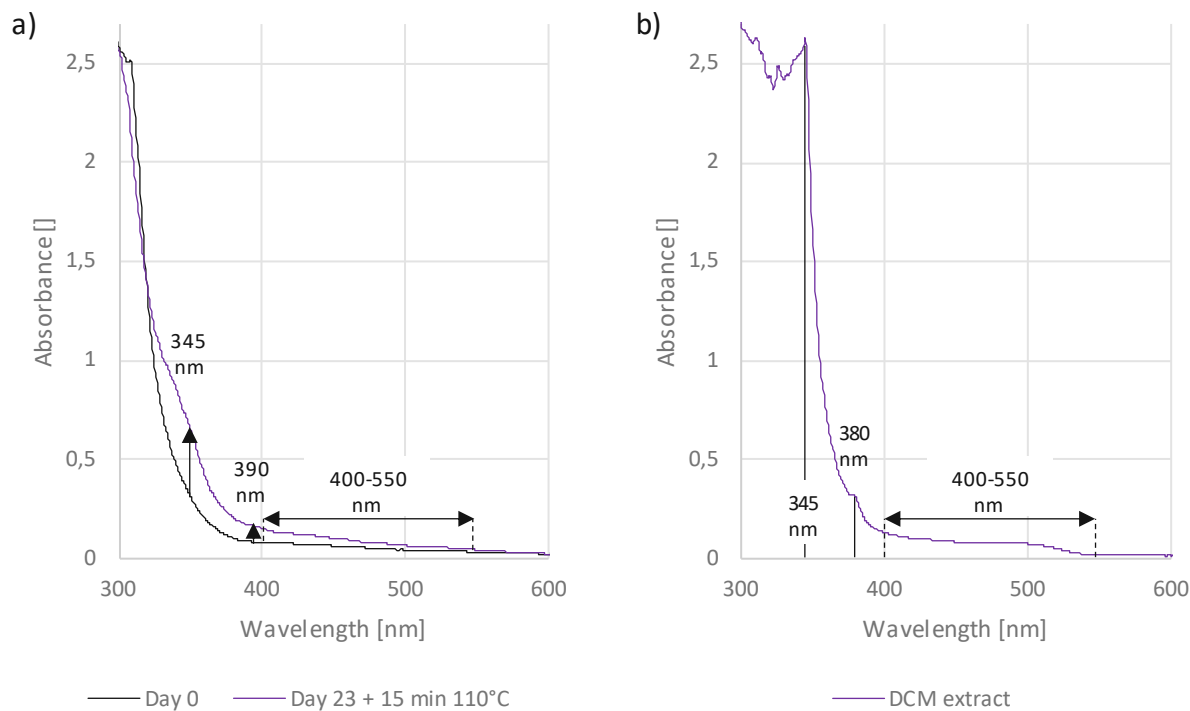
*Figure 36: UV-Vis absorption spectra of a thin film sample consisting of **UDMA** and **TPO** (1.07 mol%) (a) and the extract of this sample after extraction for 14 days with DCM (b).*

Figure 36 indicates that all substances contributing to the discoloration can be extracted from the polymer sample. The extract was then analyzed using UPLC-MS coupled with a PDA (photo diode array) detector. However, no signals above 350 nm could be recovered on the PDA detector. The signal at the highest wavelength exhibited a peak at 322 nm and a mass of 167 g/mol (Exp. part: Figure 95) and cannot be assigned to any of the signals observed in Figure 36. Therefore, the discoloration substances could not be characterized in terms of their mass with this method. A 2D TLC experiment indicates that the extract can be separated by column chromatography (Exp. part: Figure 96).

Thus, the alternative method to identify the substances causing the discoloration would involve extraction, isolation through column chromatography, and analysis using NMR spectroscopy. In order to obtain larger quantities of these substances, bulk samples were prepared, post-treated at 110°C, ground with a cryomill and extracted.

Several upscaled extraction experiments were conducted, but all extracts obtained were less colored than expected. Extraction tests were carried out with the solvents DCM, Et$_2$O, ACN, PE and Toluene, whereby only DCM and Et2O are suitable for obtaining colored

General part

extracts. Extraction tests using a Soxhlet apparatus, have produced completely colorless polymers and colorless extracts within one day, and are therefore inappropriate. Overall, there were issues regarding the reproducibility of these experiments, with yellow extracts obtained in certain instances but not in others. The reasons for these varying results are unclear. Nonetheless, a silica-based column chromatography of an extract consisting of a large number of substances was performed (Exp. part: 1.3.6 - 5th attempt). Several visible yellow fractions were obtained, but none of these fractions was pure although the separation looked promising at the UV detector of the preparative chromatography systems. 2D TLC experiments have shown that the substances collected are not stable under the chromatographic conditions. This could be due to the acidic silica on the one hand or exposure to atmosphere on the other. An UPLC-MS measurement under basic conditions resulted in a large number of substances being separated and detected. One of these shows an absorption behavior that could match the absorbance around 345 nm observed in **TPO** based thin film samples. To illustrate this, Figure 37 depicts the difference absorption spectrum of a **TPO**-based thin film sample (a) overlaid with the absorption spectrum of the substance from the UPLC-MS measurement (b) and the corresponding mass signal from this substance (c).
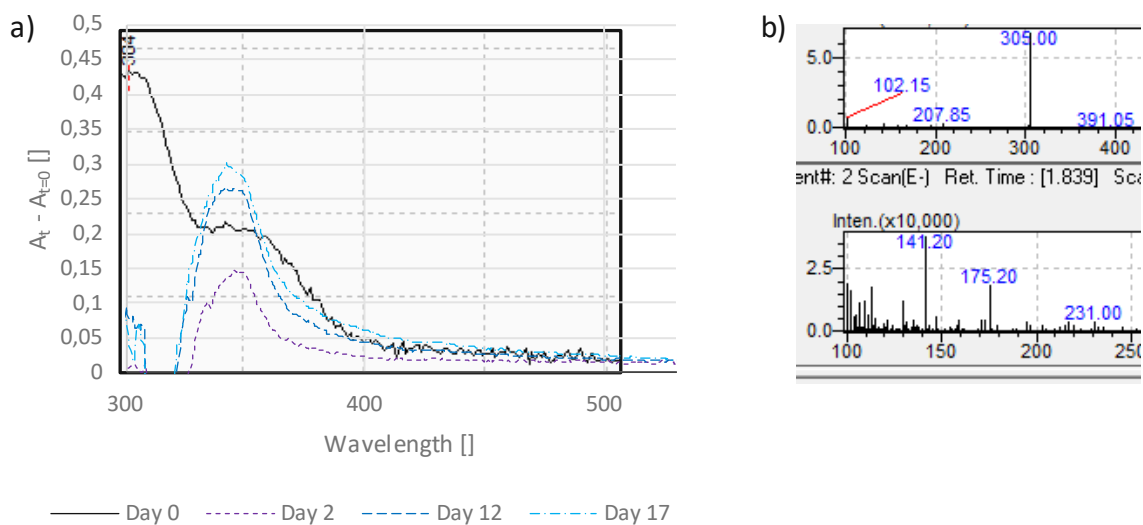

*Figure 37: a): Difference absorption spectra of a thin film sample consisting of **UDMA** and **TPO** (1.07 mol%), overlayed with the PDA-detector signal of a substance from a DCM extract of a discolored polymer sample separated by UPLC (black line). b): Corresponding mass signal from the separated substance (Top: positive mode; bottom: negative mode).*

Despite the fact that a possible discoloration substance was characterized, no clear molecular mass can be determined from the mass spectrum. From the positive mode (Figure 37c: top) a molar mass of 305 g/mol [M+H] would be likely, regarding the negative mode (Figure 37c: bottom) 141 g/mol [M-H] or 175 g/mol [M-H] are probable. As described later (1.5.2 Hypothesis 2), none of these masses match the postulated discoloration products.

Therefore, a further attempt to isolate the substances involved using neutral aluminum oxide as the stationary phase in column chromatography. Since the preparation of the extract used for this experiment yielded a rather weakly colored extract, the aluminum oxide-based column chromatography had to be carried out with a small initial quantity of discoloration. One yellow colored fraction was obtained. However, this was not a pure substance and has only been obtained in the amount of 6 mg. The NMR spectra of this fraction also showed a variety of signals that did not allow any interpretation. The effort to identity the substance or substances responsible for discoloration was consequently discontinued.

1.4 Approaches to enhance color-stability

1.4.1 Photoinitiators

While the causes of the observed discoloration have not been definitively determined, possibilities are being sought to reduce or even prevent it. It has been demonstrated that photoinitiators make a decisive contribution to the discoloration behavior and their benzoyl chromophore determine the wavelength range in which absorbances occur. One potential explanation for this could be the recombination of two benzoyl radicals to form benzil or its corresponding derivatives (Figure 38).
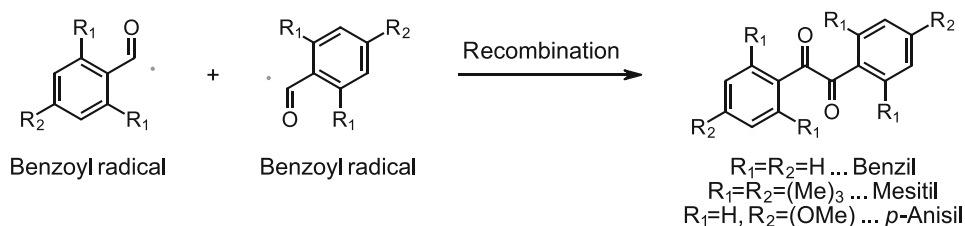

Figure 38: Recombination reaction of two benzoyl radicals.

If indeed the recombination product of two benzoyl radicals, or its secondary products (benzoin, mesitoin, *p*-anisoin), are responsible, the introduction of sterically demanding substituents on the benzoyl part in the ortho position (R_1) could impede recombination and therefore decrease discoloration. To investigate this, two literature known MAPO derivatives (Figure 39) with modifications on the benzoyl moiety were prepared by the company Ivoclar AG and compared with **TPO** in terms of their discoloration behavior.[83]

B1

B2

Figure 39: Literature known MAPO derivatives with increased steric demand on the benzoyl moiety.[83]

Figure 40 depicts the difference spectra of the absorption measurements of thin films produced with **B1** and **B2**.
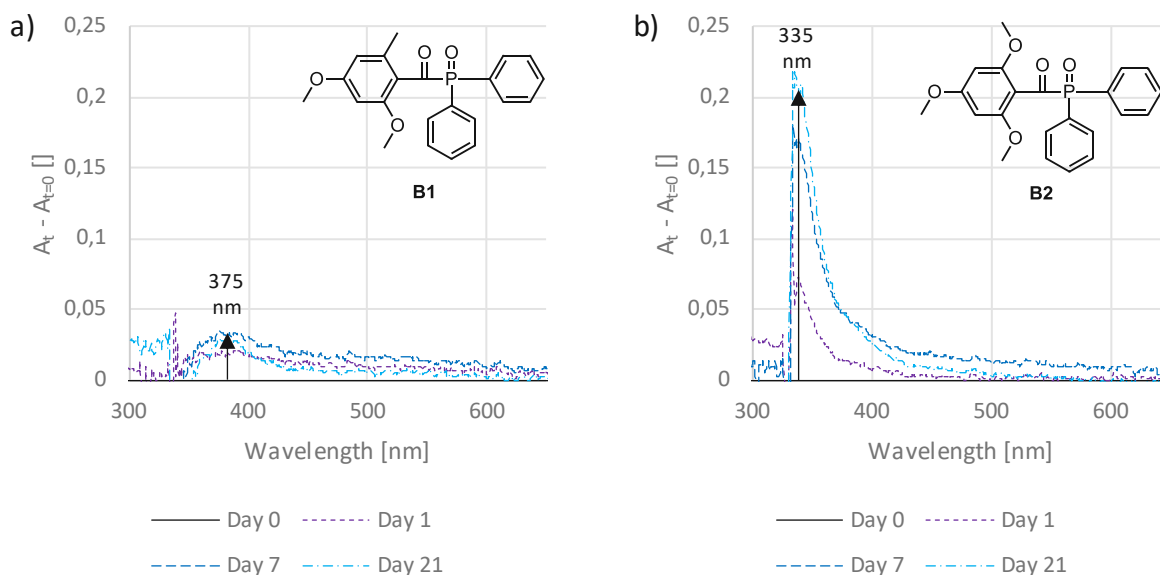
Figure 40: Time-dependent difference absorption spectra of thin film samples consisting of **UDMA** and **B1** (1.07 mol%) (a) or **B2** (1.07 mol%) (b).

As demonstrated in previous experiments, it can also be seen in this case that the variation of the benzoyl chromophore leads to absorption bands shifted to different wavelengths. For **B1** the maximum change in absorbance is around 375 nm, for **B2** it is around 335 nm. Due to these differences the discoloration behavior of these two

General part 43

substances cannot be compared with each other using this method. Therefore, measurements in the CIELAB color space are used to compare these two photoinitiators. Figure 41 displays the color change ΔE versus time for the sterically hindered photoinitiators **B1** and **B2** in contrast to **TPO**.
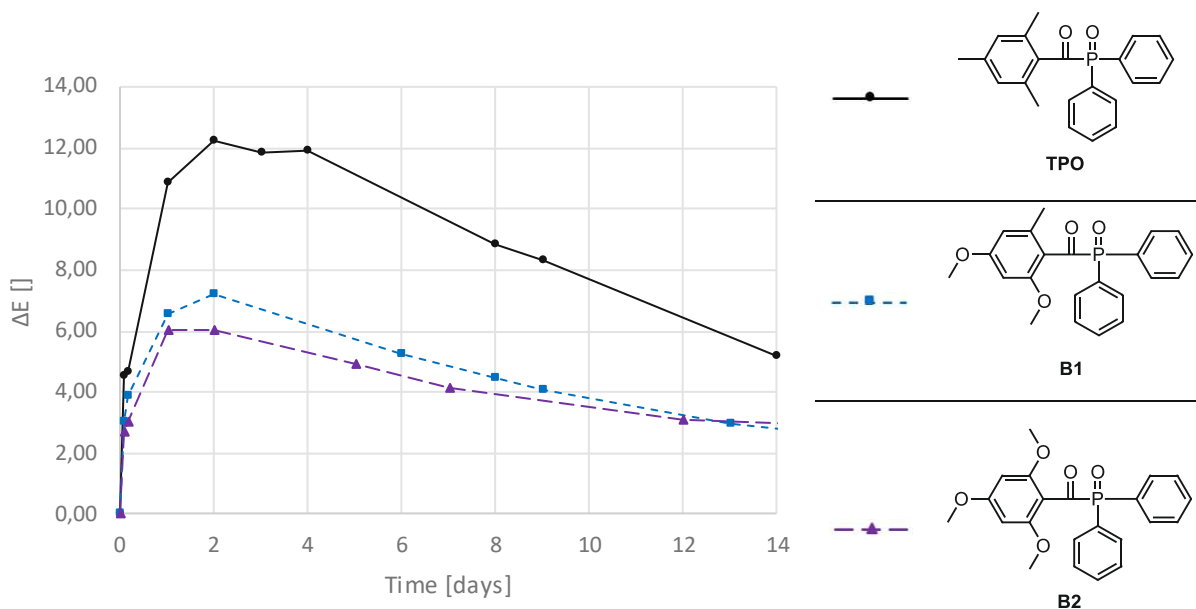
The measurements show how effectively the discoloration is reduced by the use of **B1** and **B2**, with **B2** being even slightly more efficient. This improved discoloration behavior, may be achieved by decreased recombination reactions of benzoyl radicals due to the steric hindrance. However, other factors could also account for the improvements. As has been shown in Figure 40, the resulting absorbances shift in terms of their wavelength. Concerning this, another suggestion would be that the improvements are achieved by a modified absorption behavior of the discolored species regarding wavelengths and extinction coefficients.

1.4.2 Stabilizers

As demonstrated in previous experiments (Figure 24 and Figure 25), the addition of stabilizers appears to diminish occurring discoloration. So far, this has only been investigated by the phenolic stabilizer **MeHQ**. Further investigations are intended to

discover whether there are other particularly effective substances to prevent discoloration. For this study, three series of measurements were conducted involving a wide array of substances known as stabilizers or antioxidants. Thin film samples were prepared comprising conventional **UDMA** (stabilized with 100 ppm **MeHQ**), **TPO** (1.07 mol%), and 1000 ppm of the respective stabilizer. These samples were then evaluated over time using UV-Vis absorption measurements. The evaluated compounds and their designations are depicted in Figure 42 and Figure 43. In certain experiments, it was observed that the substances used appear to generate colored by-products themselves. These stabilizers are summarized in Figure 43. Since this contradicts the aim of achieving color-stable formulations, they are not described in detail here. However, the results, along with the depiction of emerging absorbances, are shown in the experimental section (Table 19 – Table 21). It is assumed that these colored species are generated from the stabilizer during the stabilization process, forming quinone methide and other highly conjugated compounds, as described by Pospíšil et al.[71, 72] No additional absorbances were observed with the compounds shown in Figure 42. The complete designations of all structures shown in Figure 42 and Figure 43 are listed in the section Materials and Methods.
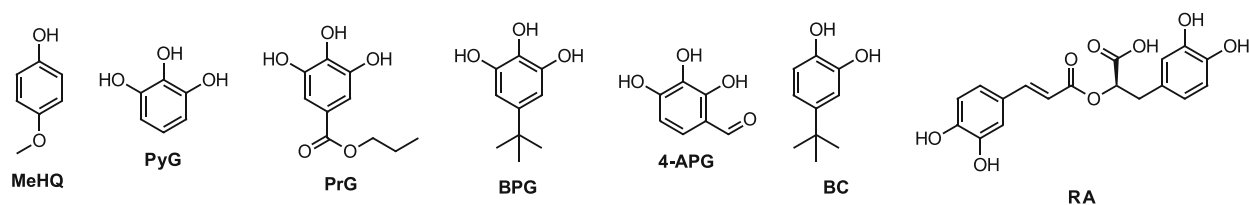

Figure 42: Tested stabilizers that did not induce additional absorbances in thin film samples.
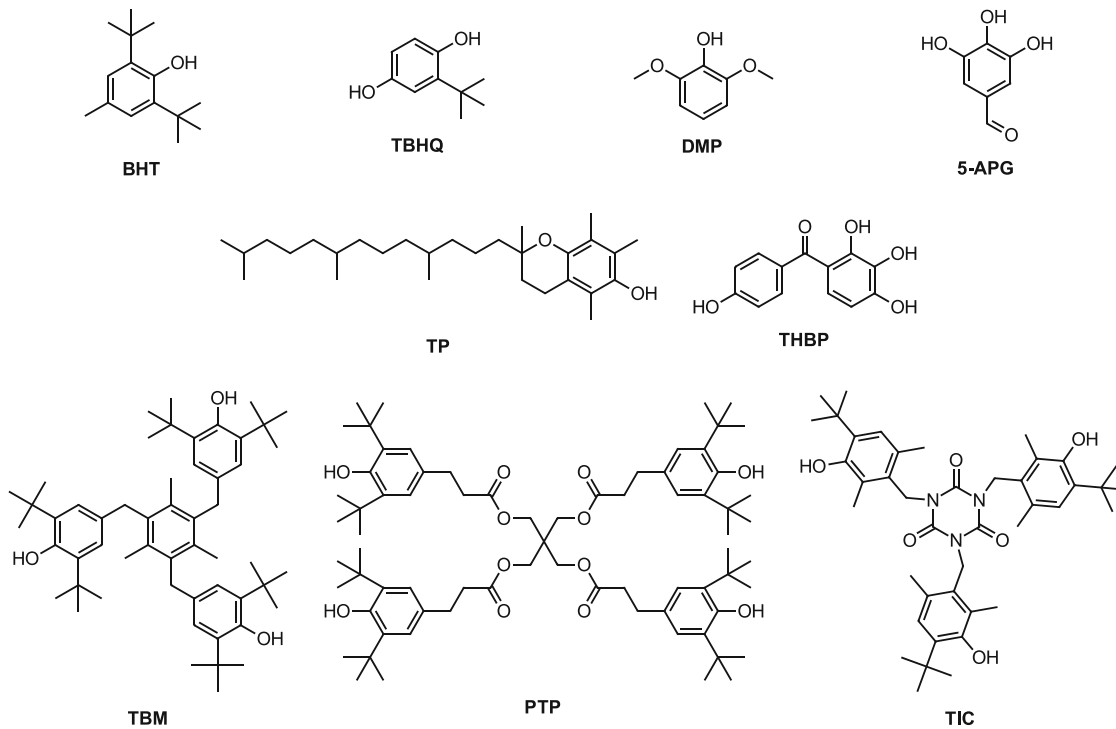
Figure 43: Tested stabilizers that exhibited additional absorbances in thin film samples.

In order to compare the different stabilizers and assess their effectiveness, the change in absorbance at 350 nm is plotted as a function of time in Figure 44. Since only measurements from one series can be compared with each other, the results are shown in three independent diagrams in comparison with a blind sample.

The stabilizer rosmarinic acid (**RA**), which does not cause any additional absorbances, was excluded from this assessment. On the one hand, due to the poor solubility of the substance, resulting in incomplete dissolution of the 1000 ppm. On the other hand, the strong absorbance of **RA** at 350 nm, precludes the possibility of evaluation at this wavelength. Consequently, the changes in absorbance were examined at 390 nm and 400 nm in comparison to the blind sample, revealing no significant differences between them. However, regarding the difference absorption spectra (see exp. part: Table 20) the long-wavelength absorbances around 450 nm could be slightly lower. Nevertheless, **RA** was not considered a suitable candidate, also due to its low solubility.
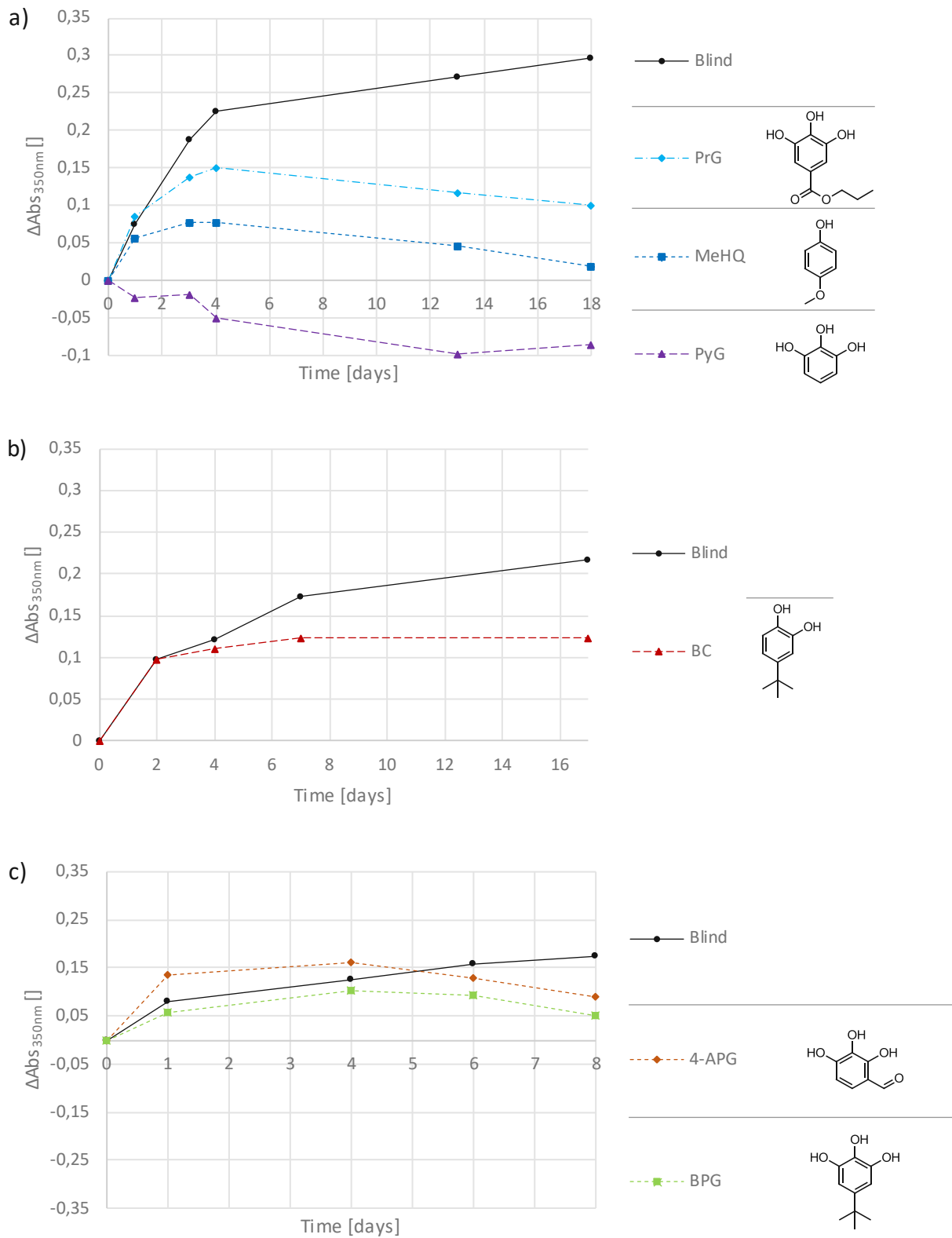
*Figure 44: Temporal change in absorbance at 350 nm of thin film samples consisting of **UDMA** (stabilized with 100 ppm **MeHQ**), **TPO** (1.07 mol%) and 1000 ppm of the investigated stabilizer.*

The first set of stabilizers (Figure 44a) examines propyl gallate (**PrG**), 4-methoxyphenol (**MeHQ**) and pyrogallol (**PyG**). All three substances notably improve the discoloration behavior, exhibiting a trend reversal by day 4 at the latest, while this was not observed in the blind sample during the evaluation period. By day 18, the absorbance at 350 nm has notably diminished with **PrG**, whereas with the application of **MeHQ**, it has nearly vanished, showcasing a remarkable enhancement compared to the blind sample. The results of **PyG** are even superior, as the application of this stabilizer can effectively suppress all occurring absorbances, thus preventing any discoloration.

In Figure 44b the results of the stabilizer 4-*tert*-butylcatechol (**BC**) can be assessed. It is evident that the addition of **BC** improves the discoloration behavior compared to the blind sample. However, the performance does not seem to match the previously evaluated stabilizers, as after 7 days no trend reversal but rather stagnation can be observed in this case.

Figure 44c presents besides 5-*tert*-butylpyrogallol (**BPG**) the special cases 2,3,4-trihydroxybenzaldehyde (**4-APG**). **BPG** again shows an improved discoloration behavior, whereby the performance seems to be comparable or slightly better than **PrG**. When the stabilizer **4-APG** is used, absorbance changes are observed at 350 nm, but the overall picture of the spectrum is clearly different here. As Figure 45b reveals, no rising absorbances can be observed above 360 nm, unlike the blind sample (Figure 45a) where increases can be detected up to 550 nm.
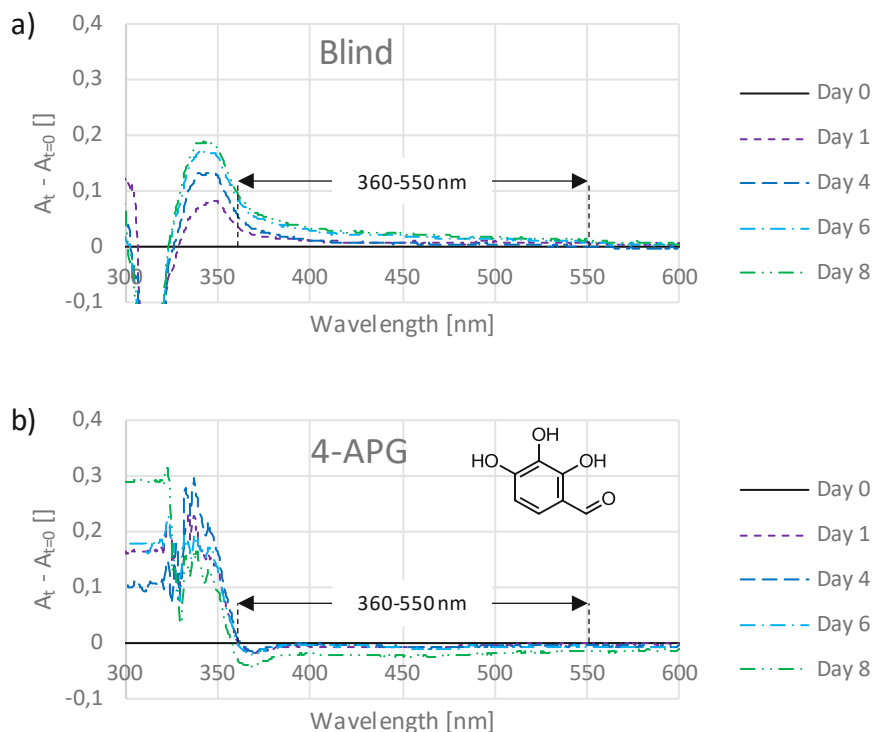
*Figure 45: Time-dependent difference absorption spectra of thin film samples consisting of **UDMA** (stabilized with 100 ppm **MeHQ**) and **TPO** (1.07 mol%) (a) and additional 1000 ppm of the stabilizer **4-APG** (b).*

The unique behavior of **4-APG** can be attributed solely to its aldehyde functionality, as otherwise there are no significant structural differences to the other stabilizers used. Only assumptions can be made about how the aldehyde prevents discoloration. It is possible that the presence of radicals induces autooxidation of the aldehyde, leading to the formation of a hydroperoxide (Figure 46). These hydroperoxides could act as oxidizing agents and may oxidize discolored species or their precursors. This assumption would also be consistent with the results in Figure 26c, where oxygen could serve as an oxidant and thus reduce discoloration. Further investigations regarding the hydroperoxide theory were performed in chapter "1.4.3 Hydroperoxides".
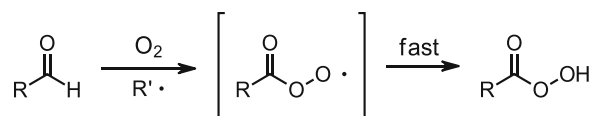

Figure 46: Mechanism of autooxidation of aldehydes.

Further analysis of the highly effective stabilizers **MeHQ** and **PyG** was conducted using measurements in the CIELAB color space. For this purpose, stabilizer-free **UDMA**

General part

monomer is formulated with 1 wt% **TPO** and either 300 ppm or 500 ppm of the respective stabilizer. The results of the color change (ΔE) are summarized in Figure 47.
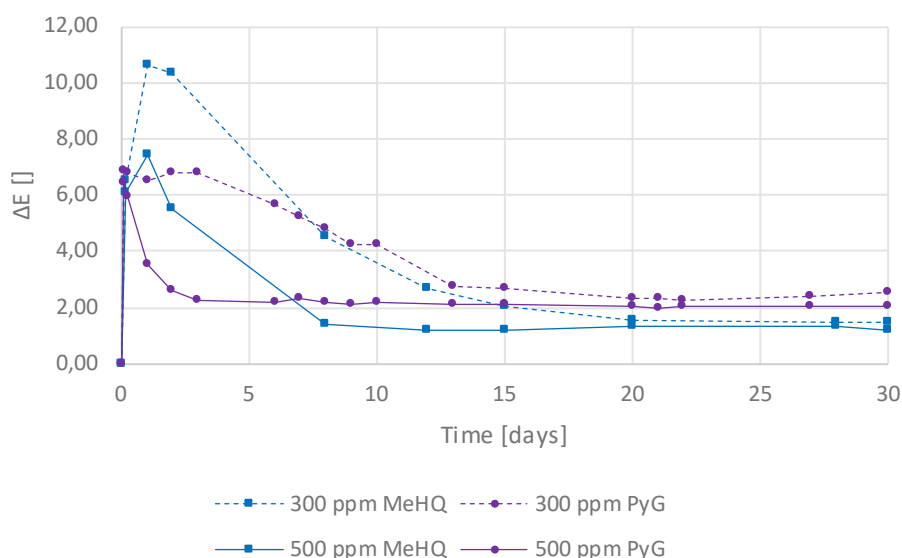

*Figure 47: Color change ΔE of samples consisting of **UDMA** (without stabilizer), **TPO** (1 wt% ≙ 1.35 mol%) and 300/500 ppm **MeHQ /PyG**, stored at 50°C immersed in water.*

The trends previously observed for **MeHQ** and **PyG** are also clearly evident in the CIELAB measurements (Figure 47). The stabilizer **PyG** again provides a better performance compared to **MeHQ** and a higher stabilizer content results in higher color stability.

1.4.3 Hydroperoxides

Experiments with different storage conditions have revealed that the presence of oxygen can significantly reduce discoloration and considerably accelerate subsequent bleaching (Figure 26c). It is hypothesized that oxidation reactions of colored species lead to their decolorization, or that the formation of colored species is prevented in advance by the oxidation of precursors. In chapter "1.4.2 Stabilizers" the stabilizer **4-APG** exhibited unexpected outcomes by the prevention of any long-wavelength absorptions in thin film samples. It is assumed that a hydroperoxide is formed by autooxidation of the aldehyde, which functions as an oxidizing agent. As explained, this could lead to the oxidation of precursors or colored substances.

To explore whether hydroperoxide formation indeed contributes to the remarkable outcomes of **4-APG** and whether hydroperoxides are viable additives for discoloration

General part

prevention, additional thin film experiments were conducted. To a standard formulation consisting of **UDMA** (stabilized with 100 ppm **MeHQ**) and **TPO** (1.07 mol%), 5 wt% of cumene hydroperoxide (**CHP**) were added. The UV-Vis measurement results of the corresponding sample are depicted in comparison to a blind sample and the **4-APG** sample in Figure 48.
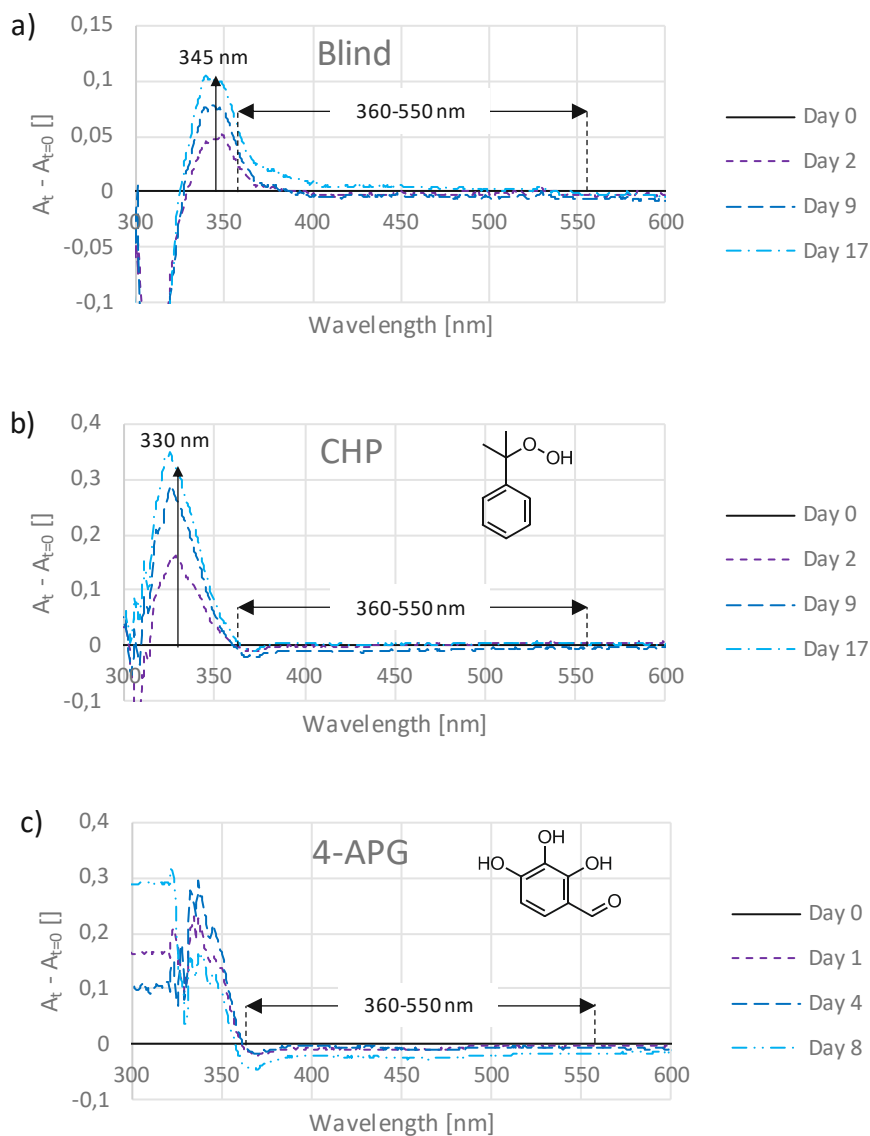
*Figure 48: Time-dependent difference absorption spectra of thin film samples consisting of **UDMA** (stabilized with 100 ppm **MeHQ**) and **TPO** (1.07 mol%) (a) and additional 5 wt% **CHP** (b) or 1000 ppm **4-APG** (c).*

Indeed, the addition of **CHP** completely suppresses any absorptions occurring at wavelengths higher than 360 nm (Figure 48b), while the blind sample exhibits

absorbances up to 550 nm (Figure 48a). In addition, the maximum change in absorbance has shifted from 345 nm to 330 nm, indicating the oxidation of the substance usually absorbing at 345 nm. The comparison between the **CHP** sample (Figure 48b) and the **4-APG** sample (Figure 48c) reveals striking similarities between the two samples, leaving little doubt that the same processes are leading to the extraordinary color-stability.

This hypsochromic shift and suppression of long-wavelength absorbances lead to the complete absence of discoloration in the sample containing **CHP**. To illustrate this conspicuously, the samples evaluated in Figure 48a and Figure 48b (Day 17) were heated to 110°C for 15 minutes and subsequently photographed. The pictures of these samples are displayed in Figure 49 and depict the deep yellow coloration of the blind sample (Figure 49a) compared to the completely colorless sample to which **CHP** was added (Figure 49b).
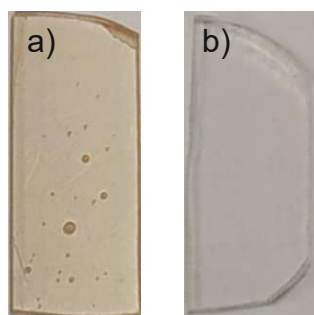

*Figure 49: Photograph of a standard thin film sample consisting of **UDMA** and **TPO** (1.07 mol%) (a) and a standard thin film sample to which 5 wt% of a **CHP** solution has been added (b). Both samples were stored under dry conditions for 17 days at 37°C and subsequently for 15 min at 110°C.*

It can be assumed that lower concentrations of **CHP** would lead to the same results and that other hydroperoxides are also suitable as additives to prevent discoloration. Both can be deduced from the example of the addition of only 1000 ppm **4-APG**, resulting in a structurally different hydroperoxide in considerably lower concentration. Furthermore, it is conceivable that other oxidizing agents might yield similar outcomes, although this aspect was not further explored in this work.

1.4.4 Further investigations

In addition to the preceding experiments, several other substances were assessed for their impact on discoloration behavior. However, no significant effects were observed with these substances. Therefore, these are only briefly outlined and summarized here:

- Ascorbic acid
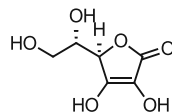
Ascorbic acid

Ascorbic acid is known as radical scavenger and reducing agent.[84] As has been shown in the chapter "1.4.3 Hydroperoxides", redox reactions appear to influence the discoloration behavior. In contrast to the oxidizing agent **CHP**, the reductive properties of ascorbic acid could possibly lead to stronger discoloration. The ability to capture radicals could lead to less discoloration in a similar way to section "1.4.2 Stabilizers". In fact, the addition of 1000 ppm ascorbic acid did not result in any significant differences compared to the standard blind sample.

- Secondary antioxidants

Synergistic effects of phenolic antioxidants with secondary antioxidants such as phosphites are described in the literature.[85] These phosphites are known to reduce hydroperoxides on the one hand, and to suppress discoloration by reacting with chromophores of, for example, colored products of phenolic antioxidants on the other. Thin film experiments were carried out in which the phenolic antioxidants **TIC**, or **TP** were combined with Doverphos 11. The samples consisted of **UDMA**, **TPO** (1.07 mol%), 1000 ppm of the respective phenolic antioxidant and 5000 ppm of the secondary antioxidant Doverphos 11. However, no significant differences to the respective samples without Doverphos 11 could be recognized in the tests.
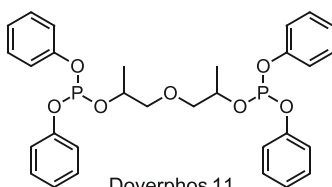
Doverphos 11

- Hydrogen atom transfer

The preliminary tests with different photoinitiators ("1.3.3 Photoinitiator") gave rise to the assumption that benzoyl radicals cause the observed discoloration. An attempt was made to reduce discoloration by the addition of substances from which hydrogen abstraction occur readily. For these experiments thin film samples were produced consisting of **UDMA**, **TPO** (1.07 mol%) and 1000 ppm of the respective hydrogen donating substance. The used hydrogen donors are depicted in Figure 50. No significant improvement in the discoloration behavior could be observed with the addition of these substances.
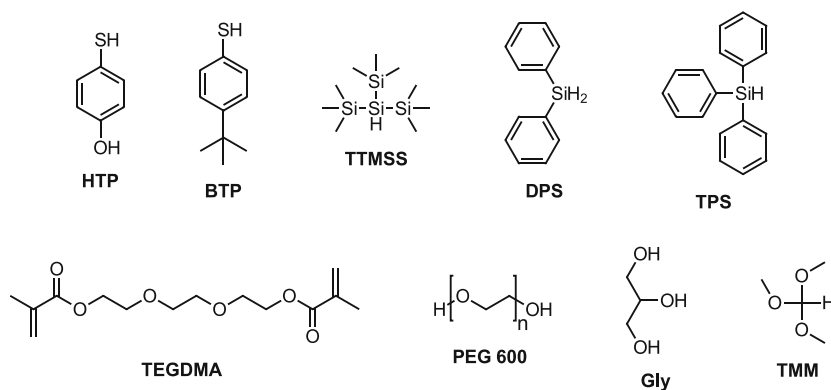
Figure 50: Hydrogen donating substances which have been evaluated for their ability to reduce discoloration.

- Siccatives

Siccatives are used as oil drying agents, which promote the free-radical autoxidation of oils with air. It is to be investigated whether these compounds also cause changes in the discoloration behavior in thin film samples. Thin film samples consisting of **UDMA**, **TPO** (1.07 mol%) and 1 wt% of the colorless siccative zirconium octoate[86] should be examined for this purpose. However, the resulting thin film sample revealed no significant changes in the discoloration behavior compared to a blind sample.

Zirconium octoate

Figure 51: Structure of the siccative zirconium octoate.

1.5 Hypotheses for causes of discoloration

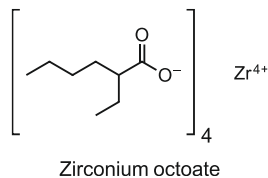Since the substances accountable for the discoloration remained unidentified, efforts continued to formulate hypotheses regarding their origins. In the preliminary tests, it has been established that photoinitiators play a crucial role in the discoloration behavior. It was demonstrated that the benzoyl chromophore determines the wavelength range where absorbances occur. Furthermore, it was shown that the use of stabilizers can significantly reduce discoloration, indicating that radicals may be involved in the discoloration process. The presence of persistent radicals was confirmed by EPR measurements, although these were not benzoyl radicals. Moreover, it has been shown that the decolorization process can be accelerated by the presence of an oxygen and that no discoloration could be observed in the presence of the oxidizing agent **CHP**. This indicates that an oxidation reaction either decolorizes the colored substances, or prevent them from forming in the first place.

Two hypotheses have been proposed regarding the potential causes of discoloration, each with some validity but also with certain contradictions.

1.5.1 Hypothesis 1

In hypothesis 1, it is proposed that at the end of the polymerization process, residual benzoyl radicals react with unreacted methacrylate double bonds, form the persistent radicals, shown in Figure 52. Subsequently, the discoloration product could be generated by a disproportionation reaction.
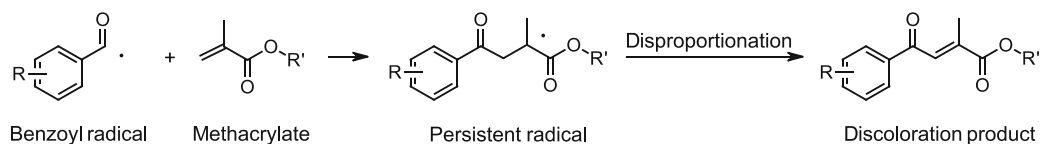
Figure 52: Postulated mechanism of the development of discoloration in hypothesis 1.

This theory was further investigated using model compounds (**MC**) 1-3, where **MC1** was commercially available and **MC2** and **MC3** were synthesized. The respective structures and the corresponding UV-Vis spectra are depicted in Figure 53.
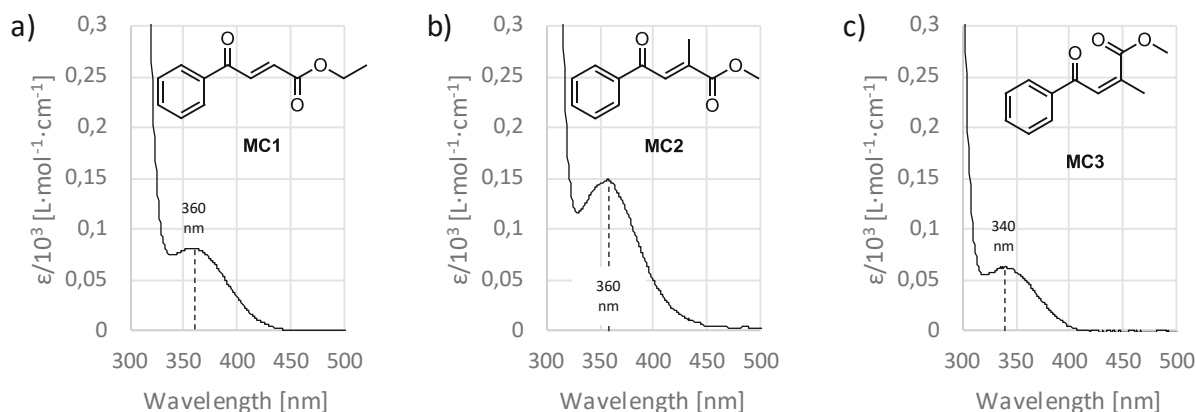
Figure 53: Structures and UV-Vis absorption spectra of the model compounds 1-3 measured in acetonitrile.

MC2 and **MC3** differ structurally from **MC1** by one methyl group attached to the double bond. Therefore, **MC2** and **MC3** are closer to reality since methacrylate monomers are used in the formulations. **MC1** and **MC2** represent the thermodynamically more stable *trans* isomers, **MC3** the *cis* isomer. Regarding the absorption spectra of these substances, it is noticeable that the methyl group does not make a decisive difference for the absorption behavior. In this context it may be mentioned that **MC1** is technical grade with a purity of about 92%, which may contribute to the slightly lower extinction. The observed absorbances (Figure 53) are quite similar to the absorbances of the thin film samples (Figure 28) in terms of shape and shift. It should be noted that the model substances exhibit a benzoyl chromophore, but depending on the photoinitiator used in the thin film samples, this chromophore can be modified. Therefore, the comparison with the **D1173**-based sample (Figure 28c) is most meaningful, as it also contains an unmodified benzoyl chromophore. The absorption maximum in the **D1173** sample is around 375 nm and is therefore at slightly higher wavelengths than MC2, which exhibits a maximum around 360 nm. However, the polymer matrix and steric effects can lead to certain shifts compared to the model substance.

Two further experiments were performed to validate this hypothesis. In the first one, a standard thin film sample was spiked with 1 mol% of **MC1** and examined with regard to the discoloration behavior. Figure 54 shows the results in comparison with the corresponding blind sample and a sample based on **D1173**, which was evaluated in a separate series of measurements.
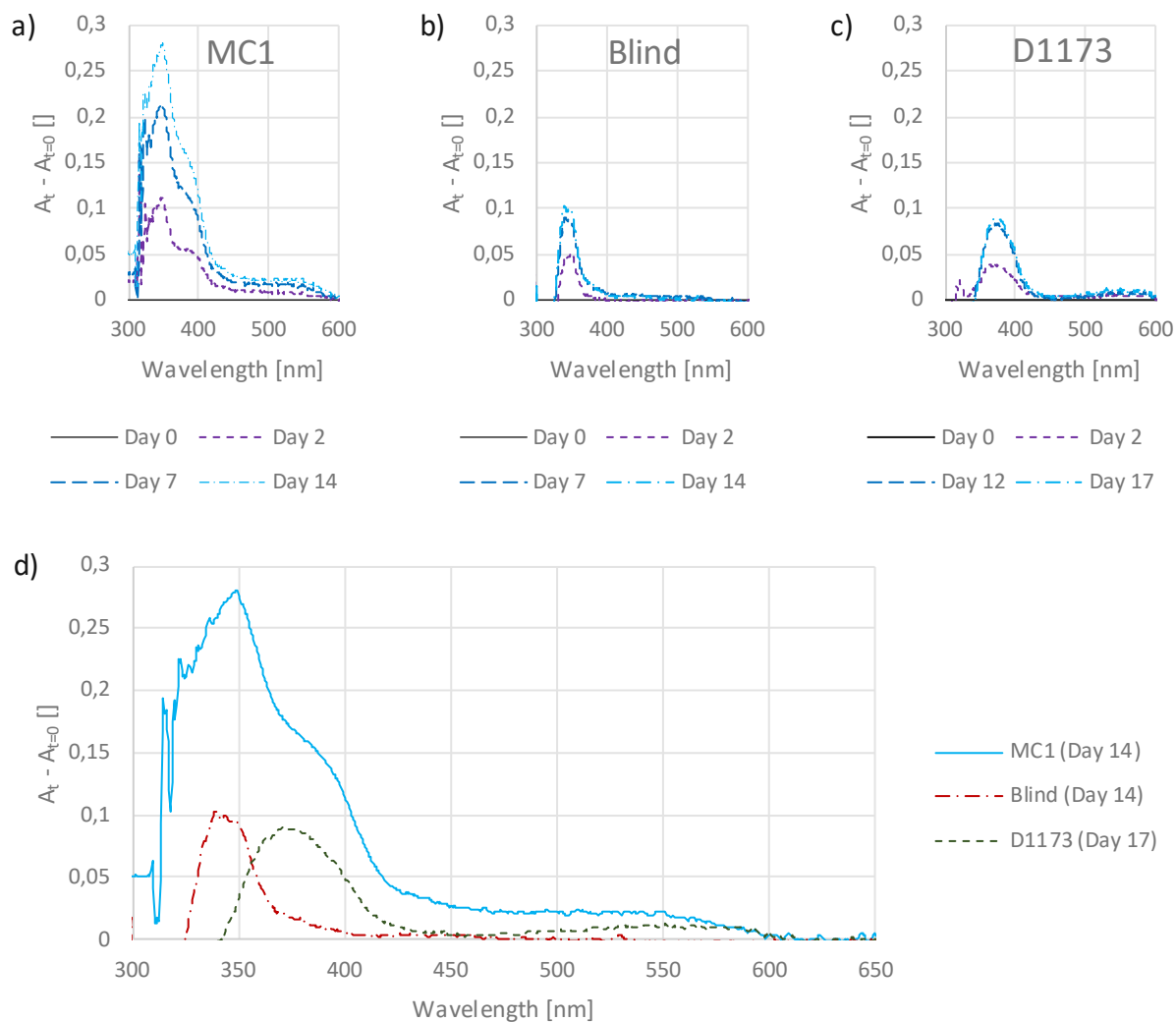
General part

*Figure 54: Time-dependent difference absorption spectra of thin film samples consisting of a): **UDMA**, **TPO** (1.07 mol%), **MC1** (1 mol%); b): **UDMA**, **TPO** (1.07 mol%); c) **UDMA**, **D1173** (1.07 mol%). In d) the final measurements are presented together in one diagram.*

The addition of **MC1** (Figure 54a) results in a significant increase in absorbance compared to the blind sample (Figure 54b). Furthermore, additional absorbance bands are evident in the **MC1** spiked sample, which are most likely attributed to the presence of the benzoyl chromophore in **MC1**. This could induce slightly different absorbances compared to the mesitoyl chromophore of the photoinitiator **TPO**. Hence, for comparison, measurements of a **D1173** sample (Figure 54c), which also features the benzoyl chromophore, are included. The final measurements of all three samples are plotted together in Figure 54d, revealing that the **MC1** sample seems to be a combination of the other two. At first sight it appears to be an indication that the theory depicted in Figure 52,

is supported by this experiment. Upon reflection, it is also conceivable that **MC1** itself may function as a photoinitiator, undergoing cleavage upon irradiation to produce benzoyl radicals, which could be accountable for the discoloration. However, detailed investigations into this behavior were not carried out.

Overall, there are some arguments in favor of this hypothesis. For example, the persistent radicals that are shown in Figure 52, would match the signals observed in the EPR measurements (Figure 34). The absorption spectra of the model substances closely resemble the observed discolorations in thin film samples, and introducing these substances results in more pronounced discolorations. Also, the temporal behavior of the occurring discolorations would be consistent with this theory, since the persistent radicals could gradually transform into the discoloration product. The observation that the addition of stabilizers reduces discoloration aligns well with the hypothesis, as they might trap the persistent radicals before they induce discoloration.

But there are also decisive arguments against this theory. Since difunctional monomers are used in the experiments, it is it is improbable that the discoloration substances can be leached out, as demonstrated in section "1.3.6 Leaching tests". Also, the weaker absorbances at higher wavelengths are not explained by the model substances, even if strong absorbances were observed in the **MC1** spiked sample. Furthermore, an experiment has shown that **MC1** cannot be oxidized by the hydroperoxide **CHP** (Figure 102). If the hypothesis holds true, the persistent radicals would need to be oxidized by **CHP** before the discoloration compounds are generated. Nevertheless, there is still no explanation why the samples would bleach again after prolonged storage, as the model substances appear to be very stable.

1.5.2 Hypothesis 2

In hypothesis 2, it is assumed that photolysis products cause the discoloration of the thin film samples. In the work of Kirchmayr et al. particularly benzil, benzoin and benzaldehyde are mentioned as possible colored photolysis products, which are related to the benzoyl chromophore.[66] Figure 55 illustrates the possible mechanism for the formation of these discolorations and potential oxidation reactions thereof.
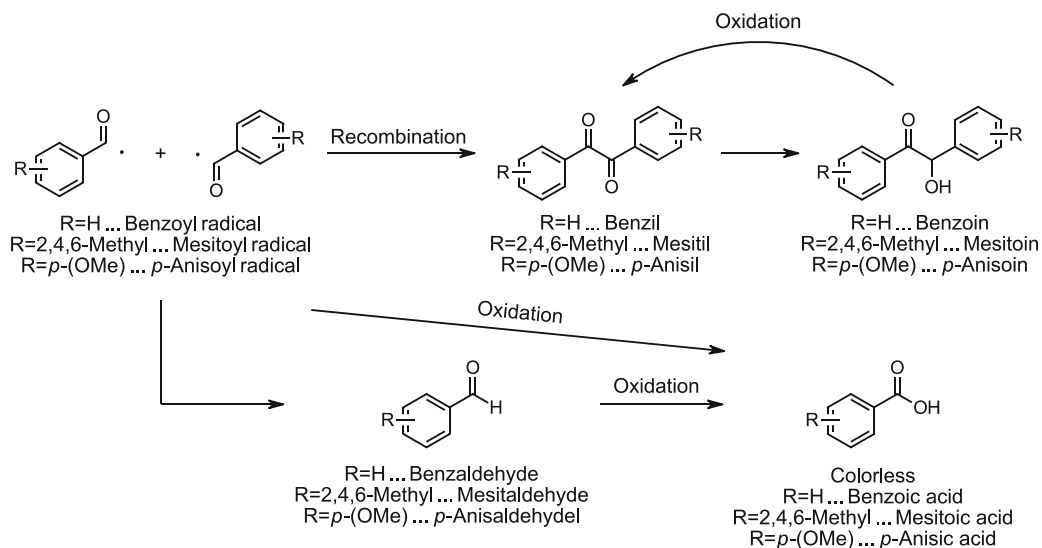
Figure 55: Postulated mechanism for the formation of photolysis products leading to discoloration and potential oxidation reactions thereof in hypothesis 2.

To further investigate this hypothesis, absorption spectra of these possible discoloration products were recorded and compared with the corresponding thin film samples. In Figure 56 the benzoyl chromophore is analyzed with the possible photolysis products benzaldehyde (a), benzoin (b) and benzil (c). A **D1173**-based thin film sample (d) is used for comparison.
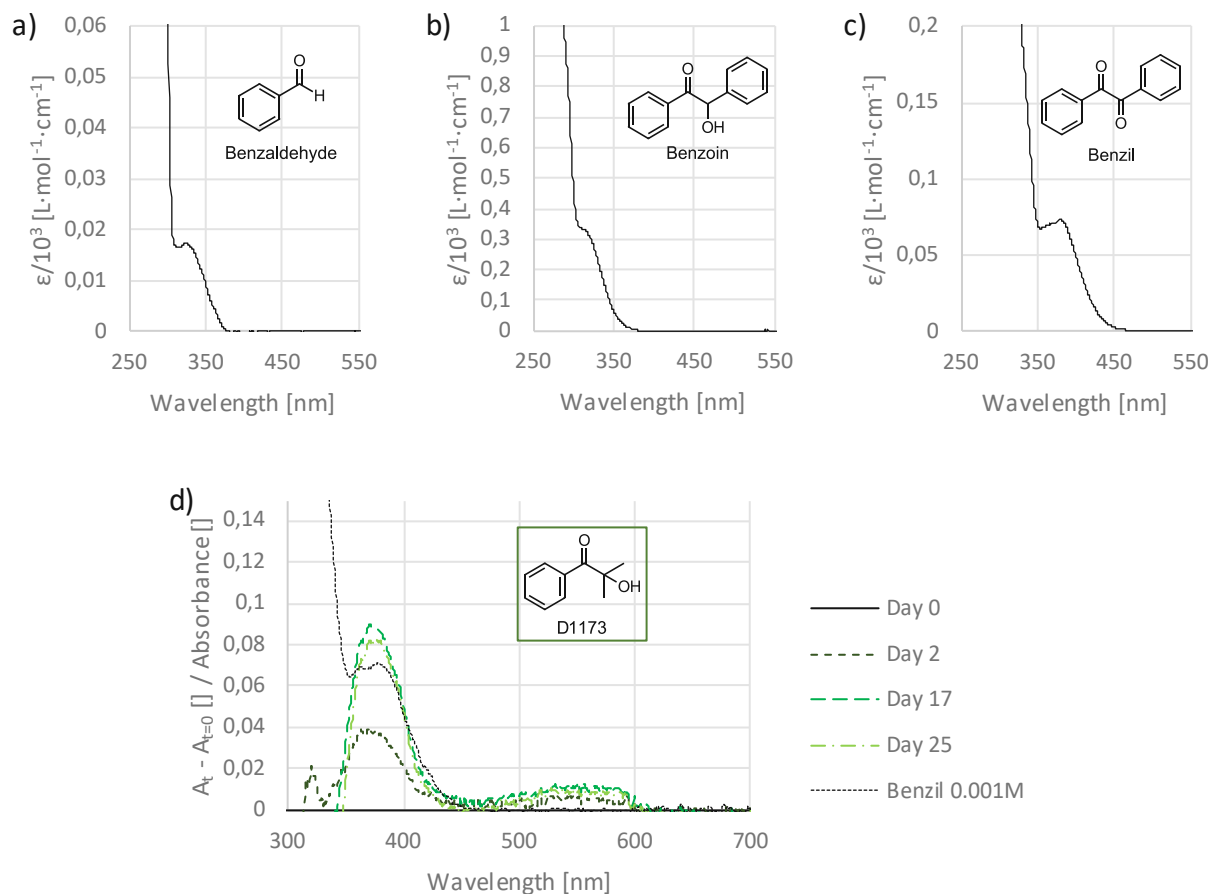
*Figure 56: UV-Vis absorption spectra of benzaldehyde (a), benzoin (b) and benzil (c) in acetonitrile. A comparison of the difference absorption spectra of the **D1173**-based thin film sample and the absorption spectrum of benzil (0.001 M) in acetonitrile is shown in diagram d).*

When comparing the absorption measurements (Figure 56a-c) with the thin film sample (Figure 56d), only benzil shows an absorption band in the appropriate wavelength range. The benzil measurement was inserted in the diagram of the thin film sample to show how exactly the absorbances overlap. Only the typical benzil band shape cannot be recognized in the thin film sample. Potentially another absorbance in this area overlaps with that of benzil, distorting the shape. It should also be noted that even at increased concentrations of the examined substances, no absorptions at higher wavelengths could be observed, as is the case with the **D1173** sample.

Next, possible products involving the anisoyl chromophore were investigate in Figure 57 and compared with an Ivocerin®-based thin film sample.
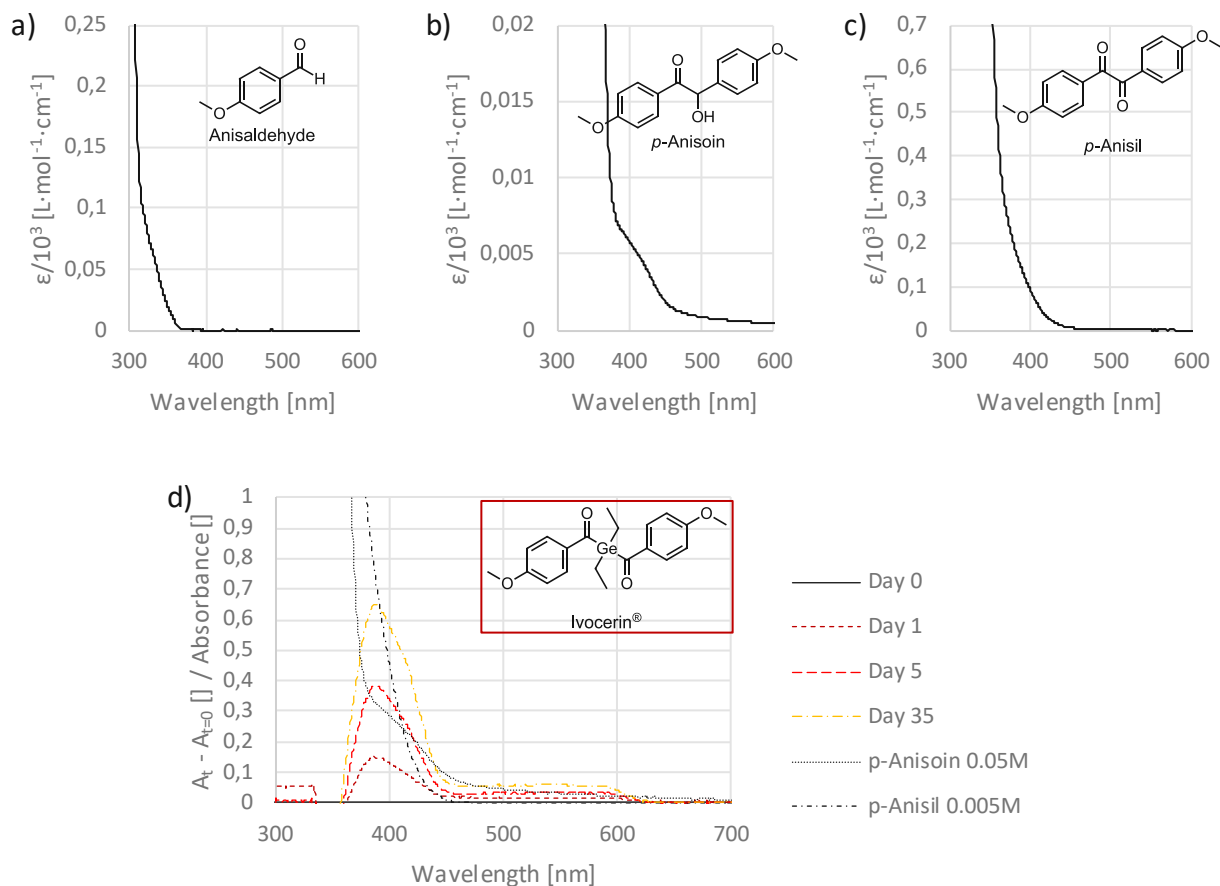
Figure 57: UV-Vis absorption spectra of anisaldehyde (a), p-anisoin (b) and p-anisil (c) in acetonitrile. A comparison of the difference absorption spectra of the Ivocerin®-based thin film sample and the absorption spectra of p-anisoin (0.05 M) and p-anisil (0.005 M) in acetonitrile is illustrated in diagram d).

The absorption spectrum of anisaldehyde (Figure 57a) does not match the observed absorbance bands of the Ivocerin®-based thin film sample (Figure 57d). *p*-Anisoin and *p*-anisil, in contrast, exhibit absorbances that are in the correct wavelength range. With regard to the shape of the absorbances, however, only *p*-anisoin matches with the absorbance observed in the thin film sample (Figure 57d).

Also in this case, the long-wavelength absorption of the thin film sample in the range of 450 nm – 625 nm cannot be explained by the substances investigated, only *p*-anisoin exhibits an absorption above 450 nm, but this decreases continuously in contrast to the observed absorbance of the thin film sample.

The investigations of the mesitoyl chromophore are less comprehensive than the previous ones, as mesitil and mesitoin were not commercially available. For mesitil, a literature-based absorption spectrum was used for the evaluation. Efforts were made to synthesize mesitoin, however, no conversion was observed (Exp. part: 1.5.2). Since no literature spectrum of mesitoin was found, either, it wasn't included in this assessment. The available data is compared with a **TPO**-based thin film sample, depicted in Figure 58.
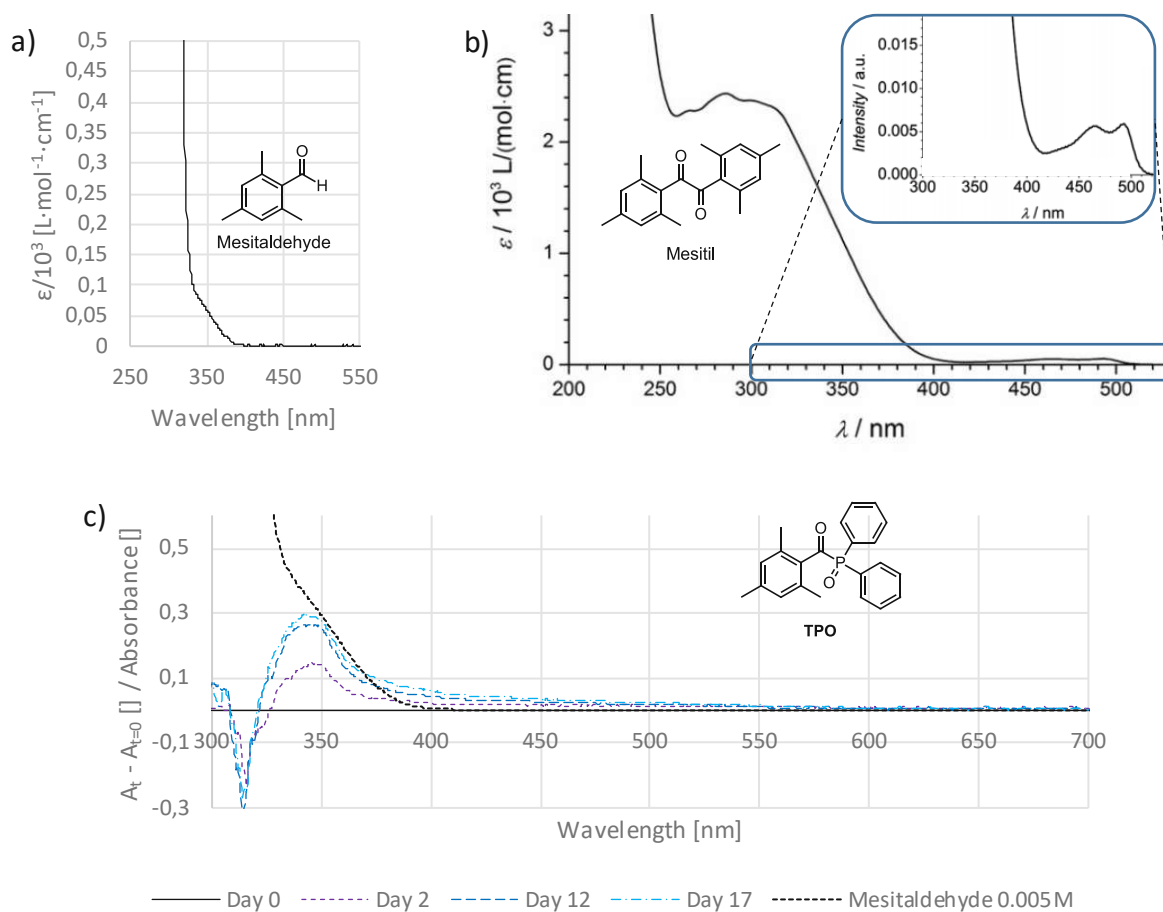

*Figure 58: a): UV-Vis absorption spectra of mesitaldehyde in acetonitrile. b): UV-Vis absorption spectrum of mesitil in methanol from the work of Wolf et al.[80] c): A comparison of the difference absorption spectra of the **TPO**-based thin film sample and the absorption spectra of mesitaldehyde (0.005 M) in acetonitrile.*

When comparing the absorption spectrum of mesitaldehyde with the difference spectrum of a **TPO**-based thin-film sample (Figure 58c), a striking correspondence of the absorbance around 345 nm can be seen. Regarding the absorption spectrum of mesitil (Figure 58b) potential matches with the thin film sample could be observed in the wavelength region above 400 nm. For the thin film sample a continuous decrease is

visible from 400 nm – 550 nm, while an absorbance with two distinct peaks characterizes the spectrum of mesitil. The long-wavelength absorbance in the **TPO**-based thin film sample thus cannot be explained by the formation of mesitil alone, but possibly by an overlap with a further absorbance. The absorption behavior of mesitoin, which could possibly also contribute to the discoloration, could not be assessed.

In the UPLC-MS measurement of a DCM extract of a strongly colored **TPO**-based polymer sample (Figure 37b, Figure 98) a substance was detected that exhibits similar absorption behavior to mesitaldehyde (Figure 58a). A certain shift could be explained by the fact that the UPLC-MS measurement was carried out under basic conditions, which can change the absorption behavior of substances to a certain degree. However, the detected masses of 305 g/mol [M+H], 141 g/mol [M-H] and 175 g/mol [M-H] do not correspond to that of mesitaldehyde [148.2], or those of mesitil [294.4] or mesitoin [296.4].

For all three chromophores investigated, matches were found between the suspected substances and the observed absorbances of the corresponding thin film samples. Other evidence also supports this hypothesis. For example, the fact that the discolorations can be leached from the thin film samples, indicating small molecules that are not covalently bound to the polymer matrix. The application of stabilizers could result in benzoyl radicals being scavenged before they form colored species to diminish discoloration. The decrease in discoloration resulting from the use of sterically hindered photoinitiators may be attributed to the reduced accessibility of benzoyl radicals for recombination or other subsequent reactions. In the presence of oxygen or by the addition of hydroperoxides remaining benzoyl radicals, aldehydes, or benzoin derivatives may be oxidized to prevent discoloration. In addition to these indications that support this theory, there is also a major contradiction of this hypothesis. If recombination products of two benzoyl radicals are responsible for the discoloration, the radicals would have to be trapped in the polymer matrix for several days before they recombine and cause discoloration. Although long-lived radicals could be detected in EPR measurements, benzoyl-like radicals would generate different signals, which were not found. Moreover, the long-wavelength absorptions in the thin film samples are scarcely explicable by the substances examined, indicating further unknown substances or another discoloration mechanism.

Nevertheless, hypothesis 2 seems to be more consistent with the observed results and also some preceding literature has described photolysis products as the cause of discoloration.

2 Photoinitiators

2.1 State of the art

To develop highly reactive Type I photoinitiators, it is essential that they effectively undergo cleavage at the irradiated wavelength and that the resulting radicals exhibit a high addition rate to the monomers utilized. Previous studies have explored the structure-reactivity relationship of phosphinoyl radicals, noting a correlation between reactivity and the s-character of localized orbitals, as well as steric effects.[87-89] Nevertheless, high radical reactivity alone does not necessarily guarantee that a photoinitiator will be efficient. Efficiency is also significantly influenced by the absorption behavior and the capability to undergo α-scission.

The long-wavelength absorption of the n→π* transition of acylphosphine oxides can be explained in two ways. Firstly, the overlap of the π*-orbital of carbonyl C with the empty d-orbital on phosphorus can be considered.[12] Secondly, the interaction of the filled nonbonding orbital of the phosphonyl oxygen with the π-orbital of the carbonyl C is postulated (Figure 59).[26]
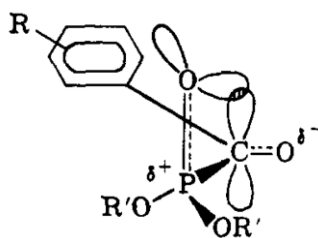

Figure 59: Overlap of a nonbonding filled phosphonyl oxygen orbital with the π-orbital of the carbonyl C.[26]

Assuming sp²-hybridization of the phosphonyl oxygen the overlap could be maximum if the P–O bond is perpendicular to the plane composed of the aryl ring, carbon and phosphorous.[26, 27] Also the work of Spichty et al. shows on the basis of calculations that the angle of the bond between C=O and P=O is of decisive importance for the α-scission of acylphosphine oxides.[90] In addition to steric effects, which can cause a favorable

spatial position of the orbitals, electronic effects influence the absorption behavior. In the work of Terauchi et al. it is assumed that the inductive effects of *p*-substituents on the benzoyl moiety of aroylphosphonic acids result in a change in the electron density at the carbonyl C atom, which alters the absorption behavior.[27] Generally, there have been numerous studies on the modification of acylphosphine oxides, however, predominantly with the focus on verifying the benzoyl part.

In the work of Sumiyoshi and Schnabel the influence of methyl substituents on the benzoyl moiety on the photolytic properties was investigated, with the result that 4-methyl-benzoyldiphenylphosphine oxide (**PBPO**) achieves a quantum yield almost twice as high as the other derivatives (Figure 60).[91]
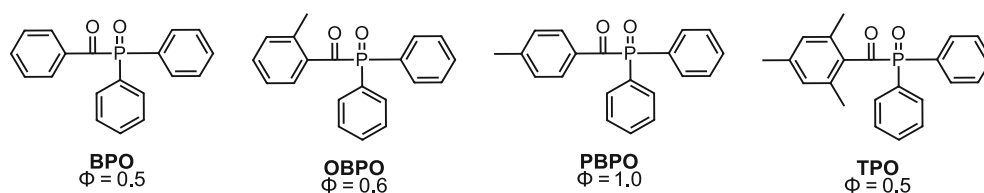

BPO
Φ = 0.5

OBPO
Φ = 0.6

PBPO
Φ = 1.0

TPO
Φ = 0.5

Figure 60: Structures and corresponding quantum yields for α-scission (Φ) investigated in the work of Sumiyoshi and Schnabel.[91]

In the work of Dietlin et al. molecular modeling was used to select potentially reactive acyldiphenylphosphine oxide (**ADPO**) compounds (Figure 61), which were synthesized and analyzed.[83] These compounds were evaluated for their reactivity in equivalent weight proportions, compared to the commercial substances **TPO-L** and **BAPO**. Especially in the case of **ADPO-2**, a very efficient photoinitiator could be produced, which showed a higher reactivity than **TPO-L** and **BAPO** in the conducted experiments. However, the study did not include a comparison with the commercial photoinitiator **TPO**, which would have been a more suitable match in terms of structure and molecular weight.
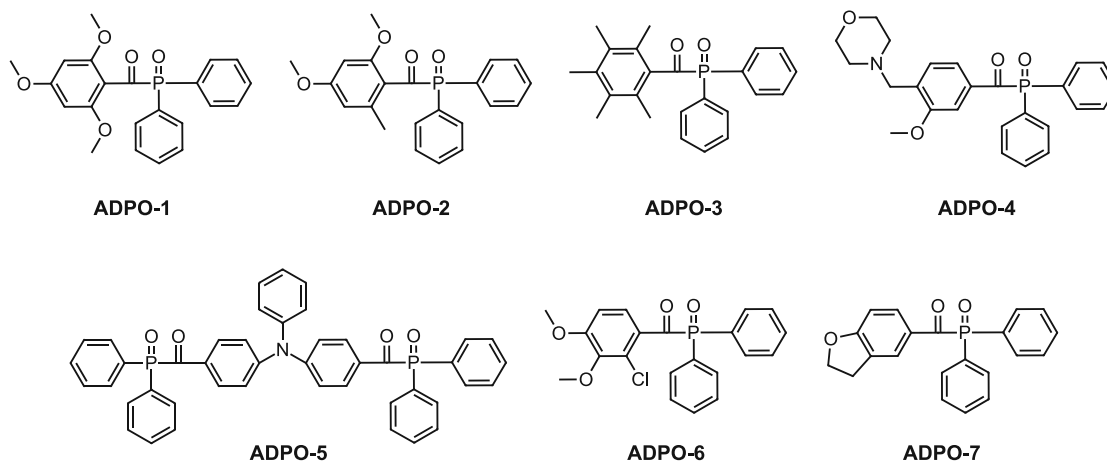
Figure 61: Acyldiphenylphosphine oxide (ADPO) structures calculated, synthesized and evaluated in the work of Dietlin et al.[83]

Xie et al. produced a MAPO derivative with a diethylamino functionality at the benzoyl moiety (Figure 62), which shows a bathochromic shift, a higher reactivity and lower migration compared to the commercial photoinitiator **TPO**. In addition, this photoinitiator has the exceptional feature to act as hydrogen donor for Type II photoinitiator systems. Despite these excellent properties, the use of this substance could lead to problems with discoloration, in the dental field. Photobleaching does not seem to be highly efficient regarding the steady-state photolysis experiment. Additionally, amines frequently contribute to discoloration through oxidation reactions.[70, 74] Another aspect that was not investigated in this work is the storage stability of this substance, due to the absence of methyl groups in ortho position of the benzoyl part, the substance could be easily decomposed by nucleophiles.
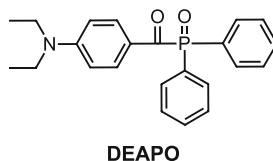

Figure 62: Highly efficient photoinitiator synthesized and evaluated in the work of Xie et al.[92]

In the work of Liu et al. several naphthyl-based MAPOs were synthesized (Figure 63), which exhibit bathochromic shifts in their absorption spectra, lower migration and especially in the case of **N3** an improved reactivity compared to **TPO**.[93]
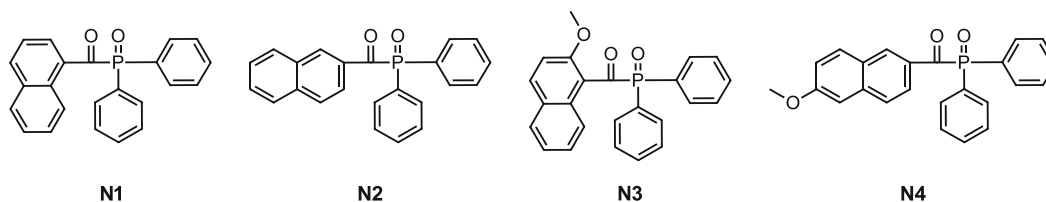
Figure 63: Structures of naphthyl-based acylphosphine oxide investigated by Liu et al.[93]

The aim of the work of Wu et al. was also the preparation of low migration acyl phosphine oxide photoinitiators.[94] Although the quantum yields (Φ) of the synthesized photoinitiators (Figure 64) **APO** (Φ=0.48) and especially **DAPO** (Φ=0.26) are significantly lower than those of **TPO** (Φ=0.56), they exhibit higher initiation efficiencies at 385 nm and 420 nm. Besides that, an improved migration ratio of two thirds in the case of **APO** and one third in the case of **DAPO** was observed.
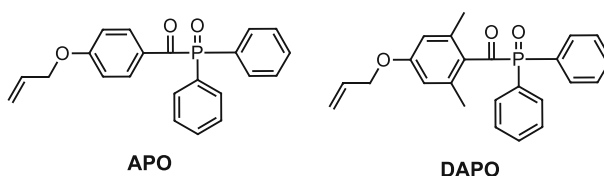

Figure 64: Synthesized and evaluated photoinitiators from the work of Wu et al.[94]

Although to a lesser extent, studies addressing the modification of monoacylphosphine oxides at the phosphorus atom have been conducted.

The work of Baxter et al. compared the reactivity of acylphosphine oxides and acylphosphonates (Figure 65).[95] While **TPO** and **DMBPO** exhibited high rates of polymerization and low induction periods, the acylphosphonates **TMBEP** and **TMBMP** exhibited significantly inferior performance in these parameters.
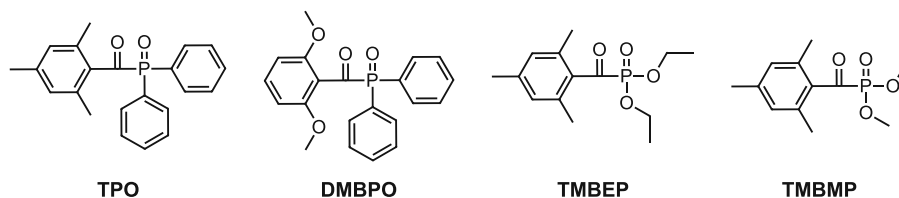

Figure 65: Structures of acylphosphine oxides and acylphosphonates evaluated in the work of Baxter et al.[95]

In the work of Oesterreicher et al. the alkyne functionalized acylphosphinic acid ester PI-9 (Figure 66) was synthesized, with the aim of achieving low migration.[96] This photoinitiator

does indeed have a lower migration rate compared to **TPO-L**, but also a somewhat lower reactivity.
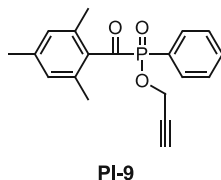

PI-9

The most relevant research on monoacylphosphine oxides with substituents within the phosphonyl moiety is undoubtedly that of Duan et al.[97] In the first part of the study the stability and the absorption behavior of **TPO**, **BPO** and **TMBPO** (Figure 67) was evaluated. It was shown that **TMBPO** exhibits a similar stability in methanol as **TPO**, due to the steric hindrance on the phosphorus, while **BPO** is apparently decomposed through the nucleophilicity of methanol. The absence of the methyl groups on the benzoyl moiety, results in **TMBPO** exhibiting an absorption behavior that is nearly identical to that of **BPO**. In contrast, **TPO** exhibits a significant blue shift, which is explained by the destruction of the π-π conjugation of the carbonyl group and the adjacent phenyl ring. In the second part of the work, the substances **4-MTPO** and **2,4-DMTPO** (Figure 67) were investigated with regard to their absorption behavior, quantum yields, reactivity and migration behavior and compared to **TPO**. The substances surpassed **TPO** in all aspects, with **2,4-DMTPO** performing even better than **4-MTPO** and also showing a slight bathochromic shift in the absorption spectrum.

TPO   BPO   TMBPO   4-MTPO   2,4-DMTPO
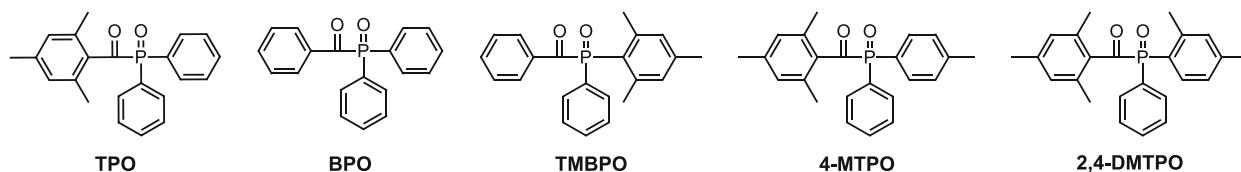
Figure 67: Investigated monoacylphosphine oxides from the work of Duan et al.[97]

In the work of Majimat and Schnabel the double-bonded oxygen atom on the phosphorus of **TPO** was replaced with a sulphur atom (Figure 68).[98] As a result, slightly lower quantum yields and radical reactivities were observed. Nevertheless, it has been shown that it is possible to replace this oxygen atom to obtain reactive photoinitiators.
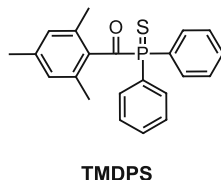
General part

TMDPS

In their research, Zhang et al. developed a highly efficient synthesis route (Figure 69) to produce different acylphosphine oxides.[99] The substances manufactured by this method include a variety of MAPOs which exhibit modifications on both the acyl and the phosphorus part. Although intriguing photoinitiators were produced within this research, no results were presented regarding the absorption behavior or reactivities of the compounds.
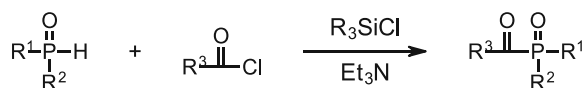
Parts of the results presented in the following will be published in our work "Size Matters: The Effect of Steric Hindrance of Substituents in the Phosphonyl Moiety on Monoacylphosphine Oxide Photoinitiators".[ii]

2.2 Benzoyl modified MAPOs

In this part of the work, the aim was to positively influence the discoloration behavior of MAPOs, by the modification of the benzoyl moiety. As described in chapter 1.4.1, it is assumed that this could be achieved by introducing sterically demanding substituents in the ortho positions of the phenyl ring of the benzoyl group. In order to investigate this, the four benzoyl modified target structures **B1** – **B4** (Figure 70) were selected to be prepared and evaluated.

[ii] By David Bassenheim, Konstantin Knaipp, Georg Gescheidt, Norbert Moszner, Yohann Catel, Robert Liska, Patrick Knaack. In preparation.
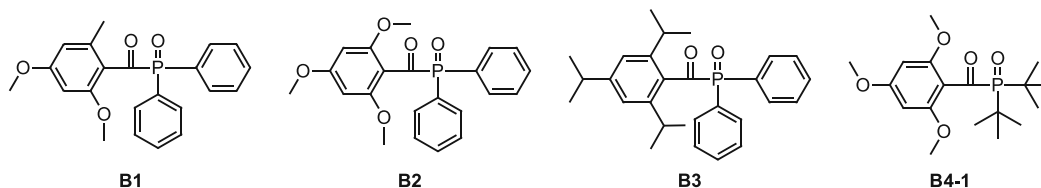
Figure 70: Selection of benzoyl modified MAPO target structured.

The substances **B1** and **B2** are known from the work of Dietlin et al., where they achieved a good performance in comparison with **TPO-L** and **BAPO**.[83] In their work, however, no comparison was made with **TPO** and no investigations regarding the discoloration behavior were conducted. **B1** and **B2** are now to be prepared and examined with regard to these aspects. In **B1** and **B2**, varying numbers of methyl groups in **TPO** are substituted with methoxy groups, altering both the steric and the electronic situation. In the case of the literature unknown substance **B3**, the electronic structure is less strongly modified, but the steric demand is significantly increased due to the presence of the *i*-propyl groups. The compound **B4-1** is an attempt to combine the steric demand of the benzoyl part of **B2** with an increased steric demand on the phosphorus through the presence of *tert*-butyl groups.

2.2.1 Synthesis

2.2.1.1 Synthesis of 2,4-dimethoxy-6-methylbenzoyldiphenylphosphine oxide (**B1**)

The photoinitiator B1 is already known from the work of Dietlin et al.[83] The molecule was synthesized and characterized by the company Ivoclar AG, analogously to the literature. The synthetic route is based on the work of Nazir et al.[100] This involves the addition of 6-methyl-2,4-dimethoxybenzaldehyde (**DMBA**) to diphenylphosphine oxide (**DPO**) in the presence of Na_2CO_3 and subsequent oxidation of the α-hydroxyphosphine oxide by MnO_2.
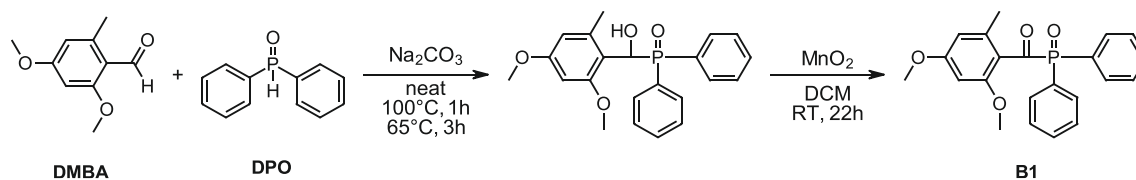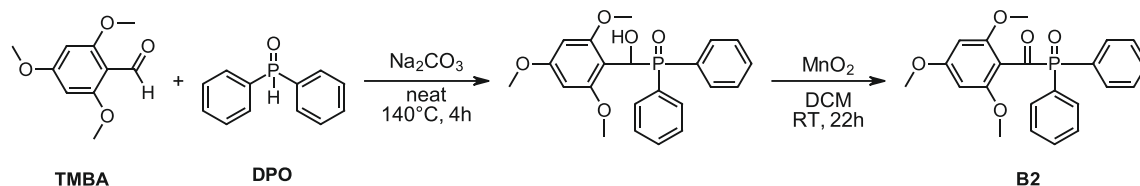
2.2.1.2 Synthesis of 2,4,6-trimethoxybenzoyldiphenylphosphine oxide (**B2**)

The photoinitiator B2 is also known from the work of Dietlin et al.[83] This substance was synthesized and characterized by the company Ivoclar AG, analogously to the literature. In comparison to the synthesis of **B1** (2.2.1.1) 2,4,6-trimethoxybenzaldehyd (**TMBA**) was used as aldehyde component and the reaction temperature was increased to 140°C.

2.2.1.3 Synthesis of 2,4,6-triisopropylbenzoyldiphenylphosphine oxide (**B3**)

The reaction for the preparation of this **TPO** derivative, exhibiting strong steric hindrance on the benzoyl moiety was performed based on the literature of Zhang et al.[99] In this synthesis, a P-O-Si intermediate is prepared first, which is then reacted with an acid chloride to form the desired target product **B3**. The route via the intermediate product is important, as the same reaction without TMS-Cl would predominantly cause a P-O-C coupling instead of P(O)-C.[99]
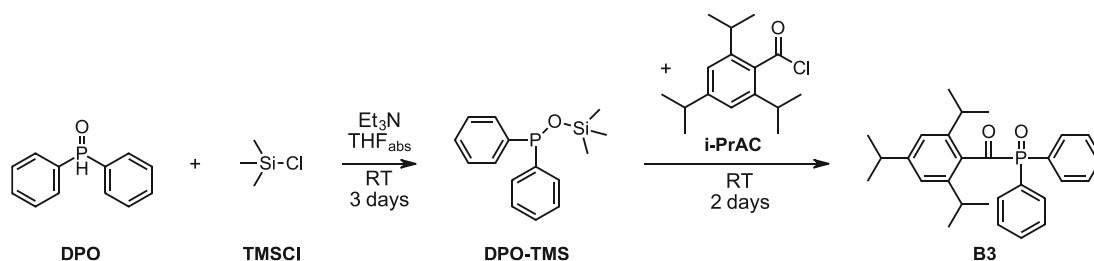
In a first step diphenylphosphine oxide (**DPO**) was reacted with 1.2 eq. of TMSCl in the presence of 1.2 eq. Et$_3$N to prepare the intermediate DPO-TMS. The acid chloride 2,4,6-triisopropylbenzoylchloride (**i-PrAC**) was freshly prepared by reacting the corresponding acid with thionyl chloride and then added to the reaction mixture. The crude product was purified by column chromatography to yield the target compound as a pale-yellow solid in 29% of the theory.

2.2.1.4 Synthesis of 2,4,6-trimethoxybenzoyl-di-*tert*-butylphosphine oxide (**B4-1**)

The photoinitiator **B4-1** is intended to combine the sterically demanding benzoyl part of **B2** with a sterically demanding phosphorus part, which exhibits two *tert*-butyl groups. For this purpose a Grignard like reaction as described in the patent literature of Suzuki et al. was attempted.[101]
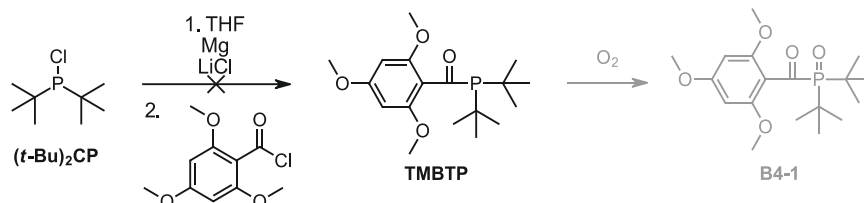
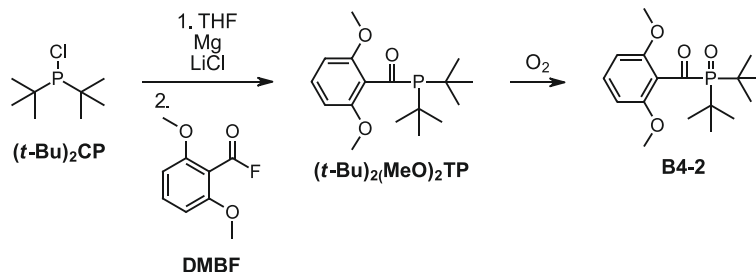For this reaction di-*tert*-butylchlorophosphine should be converted with magnesium and lithium chloride to form a reactive complex. Despite the addition of iodine to activate this reaction, heating until boiling and placing the reaction vessel in an ultrasonic bath for 15 min, no clear start of the reaction could be determined. Since magnesium and lithium chloride were suspended in the reaction mixture and the batch size was relatively small, it was also assumed that the start of the reaction had taken place but was not clearly visible, therefore the reaction procedure was continued. When the deep red colored, freshly prepared 2,4,6-trimethoxybenzoyl chloride was added, no obvious reaction or color change was observed. A reaction control using UPLC-MS also showed no conversion, indicating that the conversion with magnesium was not successfully initiated.

2.2.1.5 Synthesis of 2,6-dimethoxybenzoyl-di-*tert*-butylphosphine oxide (**B4-2**)

Pathway A)

Since the reaction of **B4-1** (2.2.1.4) failed and the educt 2,4,6-trimethoxybenzoic acid was no longer available, the target structure **B4-2** was designed, which differs from **B4-1** only in the absence of the *p*-methoxy group on the benzoyl part. For this reaction the acid fluoride 2,6-dimethoxybenzoylfluoride (**DMBF**), which was available in the working group, was used instead of an acid chloride. Apart from that, the reaction was carried out as described in the patent literature of Suzuki et al.[101]

(t-Bu)₂CP   **DMBF**   **(t-Bu)₂(MeO)₂TP**   **B4-2**

In this approach, the start of the reaction of magnesium, LiCl and di-*tert*-butylchlorophosphine again could not be clearly observed even after adding iodine and heating to boiling point. But after the mixture was stirred for two hours at room temperature a gray turbidity was visible, indicating the actual start of the reaction. The addition of DMBF resulted in a deep red solution which turned yellow within two days. After workup of the reaction, the product was exposed to air for subsequent oxidation to **B4-2**. The success of the reaction was determined using UPLC-MS measurements. Purification should be carried out using column chromatography by elution with a mixture of PE and EE. Despite washing the column with pure EE, the product could not be recovered. Only a mixture of MeOH and EE could successfully elute the product, which had a significantly higher affinity to the stationary phase than expected. In order to obtain a finally pure product, it was recrystallized from a mixture of PE and toluene. The pale-yellow solid was obtained in a total yield of 36% of the theory.

Pathway B)

Since it was not certain whether the desired product could be obtained and isolated using pathway A, another reaction was attempted for the synthesis of **B4-2**. The synthesis was performed in a similar way as in the work of Ullrich et al., but with a monofunctional phosphine and 2,6-dimethoxybenzoylfluoride (**DMBF**) instead of an acid chloride.[102]

(t-Bu)₂CP   **DMBF**   **(t-Bu)₂(MeO)₂TP**   **B4-2**
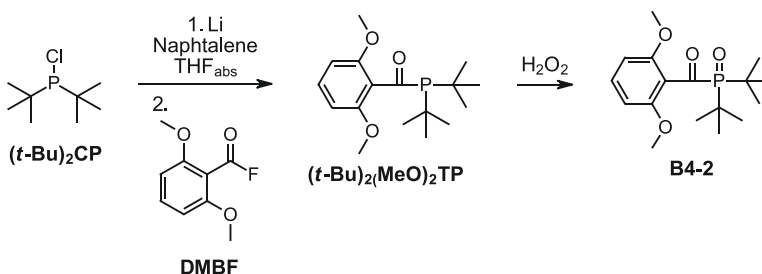
The reaction of the lithium foil and naphthalene was clearly visible by the dark color of the reaction mixture, the addition of di-*tert*-butylchlorophosphine again led to a color change of the reaction mixture, which ended in a reddish-brown suspension. After the addition of DMBF the reaction mixture was stirred for 2 h and for 16 h, before the resulting crude products were converted with hydrogen peroxide and worked up. Control by UPLC-MS measurements showed that the desired product was obtained with both reaction times, but work up after 2 h showed a relatively higher product content. No further purification of the crude products was carried out, as the desired substance was already available in sufficient quantity and purity from pathway A.

2.2.2 Characterization

The benzoyl modified photoinitiators **B1** – **B4-2** were investigated with regard to their absorption behavior, their reactivity and their discoloration behavior in polymer samples. The commercial MAPOs **TPO** and **TPO-L** were used as references for these studies.

2.2.2.1 UV-Vis spectroscopy

For the investigation of the absorption behavior of the benzoyl modified MAPOs, UV-Vis spectra of 0.001 M solutions in acetonitrile were recorded. Figure 71 illustrates the absorption bands of the n→π* transition of **B1** – **B4-2** in comparison to **TPO** and **TPO-L**. The resulting values for λ_{max} (n→π*) and the extinction coefficients (ε) at 385 nm and 400 nm are summarized in Table 2.
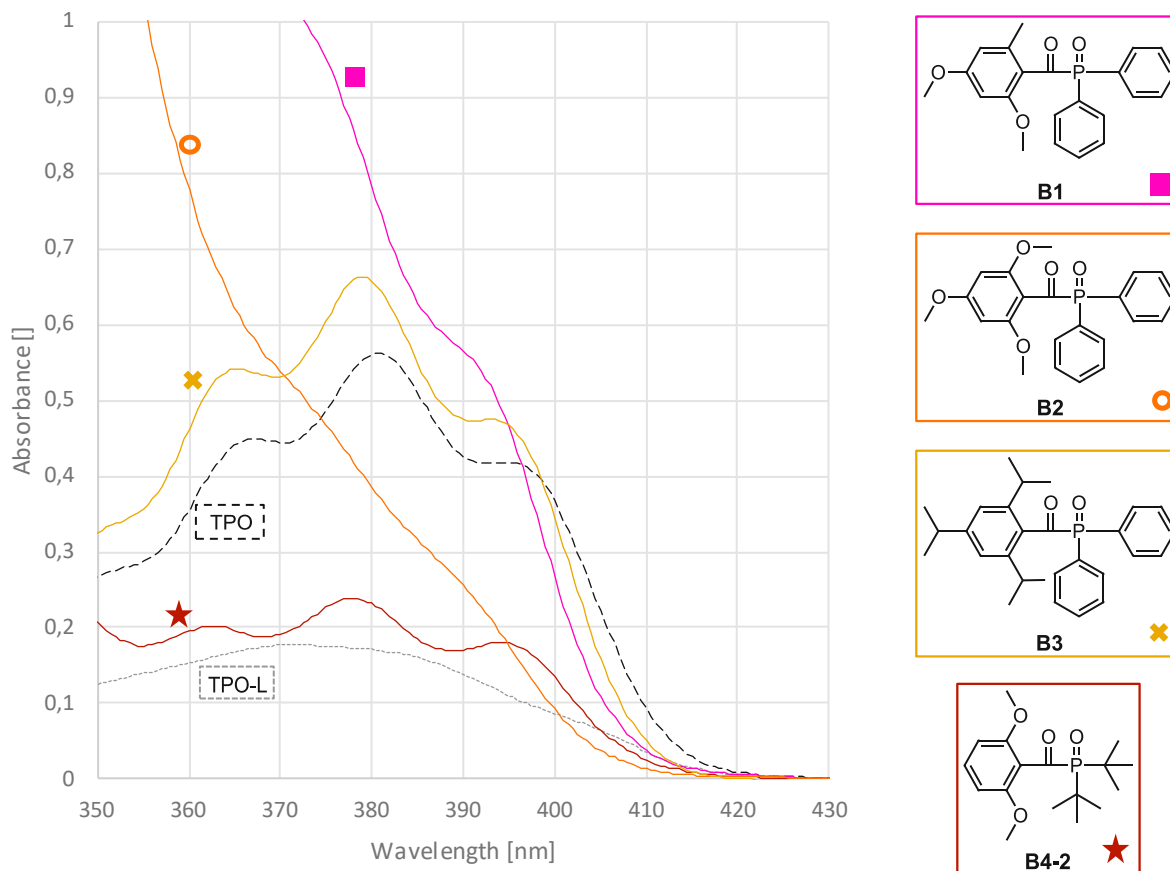
Figure 71: UV-Vis spectra of solutions of benzoyl modified MAPO derivatives B1 – B4-2 (0.001 M in acetonitrile).

*Table 2: Wavelength of the absorption maximum (λ_{max} ($n\rightarrow\pi^*$)) and molar extinction coefficient (ε) at 385 nm and 400 nm of benzoyl modified MAPO derivatives **B1** – **B4-2**.*

	λ_{max} ($n\rightarrow\pi^*$)	$\varepsilon_{\lambda max}$ (L·mol^{-1}·cm^{-1})	$\varepsilon_{385\,nm}$ (L·mol^{-1}·cm^{-1})	$\varepsilon_{400\,nm}$ (L·mol^{-1}·cm^{-1})
TPO	381	561	510	367
TPO-L	371	178	161	86
■ **B1**	374	-	629	267
○ **B2**	372	-	316	92
✖ **B3**	379	662	550	344
★ **B4-2**	378	239	185	135

Figure 71 reveals that all MAPO derivatives with a modified benzoyl moiety (**B1** – **B4-2**) exhibit a hypsochromic shift compared to **TPO**. Most probably the steric hindrance of the introduced substituents places the phenyl ring of the benzoyl group in an unfavorable

General part   75

spatial position. This effect was also described in the work of Duan et al. when comparing **BPO**, which has no substituents on the benzoyl unit, with **TPO**, which contains three methyl substituents.[97] Their explanation for this behavior was the hindered π-π conjugation of the carbonyl group and the adjacent phenyl ring. Considering the absorption spectra of **B1** and **B2**, a sudden increase in absorption at wavelengths below 375 nm is apparent. It is assumed that the electronic effects of the methoxy substituents cause a bathochromic shift of the π→π* transition, causing a partial overlap with the n→π* transition. Since this effect is not present in **B4-2**, it appears to be caused only by methoxy substituents in the *para*-position. Comparing **B2** and **B4**, it is also noticeable that **B4** is characterized by a λ_{max} (n→π*) at higher wavelengths. In this case, it is assumed that the steric hindrance on the phosphorus part by the two *tert*-butyl groups causes a favorable configuration of the molecule. This can either push the phenyl ring adjacent to the carbonyl group into a more favorable spatial position, which in turn increases the π-π conjugation described above, or bring the carbonyl and phosphonyl groups into a more favorable angle, resulting in greater orbital overlap, as described in the state of the art (2.1).

2.2.2.2 Photo-DSC

Photo-DSC measurements were carried out to determine the reactivity of the benzoyl modified MAPO photoinitiators (**B1** – **B4-2**). In the evaluation of these measurements, the parameter t_{max} is a measure for the speed of an initiator and indicates the time after which the maximum heat flow is reached. The rate of polymerization R_P is proportional to the height of the peak and indicates how efficiently a photoinitiator polymerizes the monomer used. The parameter $t_{95\%}$ indicates the time after which 95% of the total heat flow is reached, while DBC gives the final double bond conversion. The further parameters and the exact evaluation of the measurements are described in the experimental part (2.2.2.2).

For the measurements homogenous formulations consisting of 1.0 mol% of the respective photoinitiator in **UDMA** were prepared. As the individual initiators differ in terms of their absorption behavior, they were evaluated using three different light sources.
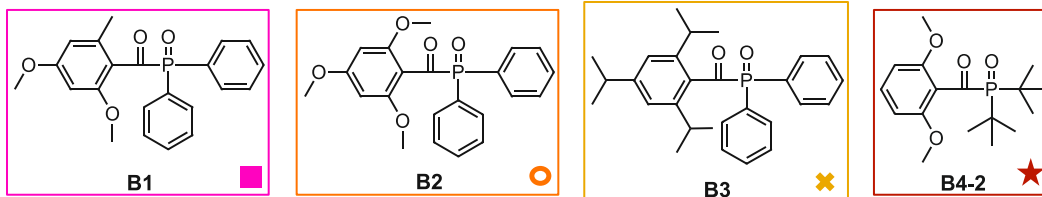
<u>320 – 500 nm broadband light source (OmniCure® S2000)</u>

For these measurements an OmniCure® S2000 high pressure mercury vapor light source equipped with a 320 – 500 nm filter was used as light source. The light intensity at the sample surface was set to 64 mW/cm^2. The main results are summarized in Table 3, the complete data of the measurements can be found in the experimental section (2.2.2.2).

*Table 3: Results of photo-DSC measurements of formulations, consisting of 1 mol% photoinitiator in the monomer **UDMA**, under irradiation with a broadband light source (320-500 nm) with an intensity of 64 mW/cm^2.*

320-500 nm	t_{max} [s]			R_p [mmol*L^{-1}*s^{-1}]			$t_{95\%}$ [s]			DBC [%]		
TPO	4.3	±	0.2	176.0	±	3.5	34.0	±	1.6	64.2	±	0.1
TPO-L	5.1	±	0.3	147.8	±	5.3	32.4	±	1.5	58.9	±	0.5
■ B1	5.1	±	0.2	142.8	±	4.4	35.4	±	1.0	59.3	±	0.4
○ B2	5.4	±	0.2	137.2	±	11.4	34.9	±	1.5	59.4	±	2.9
✖ B3	10.6	±	0.2	81.3	±	2.0	43.7	±	0.8	48.8	±	0.6
★ B4-2	5.0	±	0.1	148.3	±	6.7	29.9	±	1.3	56.8	±	2.0

When using a broadband light source (320-500 nm), it is evident that the performance of **TPO** is not achieved by any of the tested benzoyl modified photoinitiators. However, **B1** and **B4-2** achieve comparable results to **TPO-L**, whereby **B4-2** appears to be slightly faster in terms of t_{max} and R_P, but exhibits a slightly lower DBC than the others. **B2** on the other hand is somewhat slower, but yielded a higher DBC. The *iso*-propyl substituents of **B3**, appear to massively impair the reactivity, as evidenced in all measured values.

<u>385 nm LED light source</u>

For the measurements with a 385 nm light source the corresponding OmniCure® Max LED head was used. The light intensity at the sample surface was set to 10 mW/cm^2. The main results are summarized in Table 4, the complete data of the measurements can be found in the experimental section (2.2.2.2).

Table 4: Results of photo-DSC measurements of formulations, consisting of 1 mol% photoinitiator in the monomer UDMA, under irradiation with a LED light source (385 nm) with an intensity of 10 mW/cm².

385 nm	t_{max} [s]			R_p [mmol*L⁻¹*s⁻¹]			$t_{95\%}$ [s]			DBC [%]		
TPO	5.5	±	0.2	138.5	±	1.5	32.2	±	1.1	57.7	±	1.5
TPO-L	6.1	±	0.0	131.0	±	4.2	35.2	±	1.5	56.3	±	0.8
■ B1	5.8	±	0.1	132.5	±	3.3	33.3	±	1.3	56.9	±	1.7
○ B2	6.2	±	0.0	134.7	±	4.5	32.8	±	1.6	56.7	±	2.0
✖ B3	12.5	±	0.7	57.7	±	2.6	48.7	±	0.5	43.3	±	0.5
★ B4-2	6.2	±	0.2	127.2	±	6.5	32.3	±	1.3	53.9	±	0.5

When irradiated with a 385 nm LED light source, similar trends are seen as with broadband irradiation (320-500 nm). With B1 now performing slightly better than **TPO-L** and **B2** and **B4-2** performing at a similar level with **TPO-L**.

400 nm LED light source

For the measurements with a 400 nm light source the corresponding OmniCure® Max LED head was used. The light intensity at the sample surface was set to 10 mW/cm². The main results are summarized in Table 5, the complete data of the measurements can be found in the experimental section (2.2.2.2).

Table 5: Results of photo-DSC measurements of formulations, consisting of 1 mol% photoinitiator in the monomer UDMA, under irradiation with a LED light source (400 nm) with an intensity of 10 mW/cm².

400 nm	t_{max} [s]			R_p [mmol*L⁻¹*s⁻¹]			$t_{95\%}$ [s]			DBC [%]		
TPO	5.3	±	0.1	156.8	±	1.3	30.5	±	0.3	60.8	±	0.3
TPO-L	6.4	±	0.0	134.9	±	3.1	34.7	±	1.5	56.5	±	0.9
■ B1	5.7	±	0.1	144.6	±	6.2	31.6	±	0.7	56.5	±	1.6
○ B2	6.5	±	0.1	135.5	±	0.8	31.5	±	0.9	56.1	±	0.9
✖ B3	12.9	±	0.2	63.4	±	1.7	47.6	±	0.2	43.8	±	0.4
★ B4-2	5.9	±	0.2	135.8	±	2.0	32.1	±	0.7	54.2	±	0.2

The irradiation with a 400 nm LED demonstrates the differences of the initiators. In this experiment **B1** in particular, but also **B4** are faster than **TPO-L**. Comparing the measured values of t_{max} and R_p for all initiators irradiated with 385 nm to those irradiated with 400 nm reveals that the initiators **TPO**, **B1** and **B4-2** achieved better results, whereas **TPO-L** and

B2 demonstrated inferior results. Considering the UV-Vis absorption spectra (Figure 71) these results are reasonable, since **TPO-L** and **B2** exhibit their λ_{max} at the lowest wavelengths and therefore absorb light of higher wavelengths less efficiently.

2.2.2.3 Discoloration behavior

<u>UV-Vis spectroscopy method</u>

The assessment of the discoloration behavior using the UV-Vis method was carried out as described in section 1.2.1. The resulting difference absorption spectra are summarized in Figure 72. At this point it must be noted that these spectra cannot be directly compared with each other without caution. Since the photoinitiators differ in their benzoyl chromophore, they not only cause absorbances of different intensities, but also in different wavelength ranges. This phenomenon is described in more detail in the sections 1.3.3 and 1.4.1.
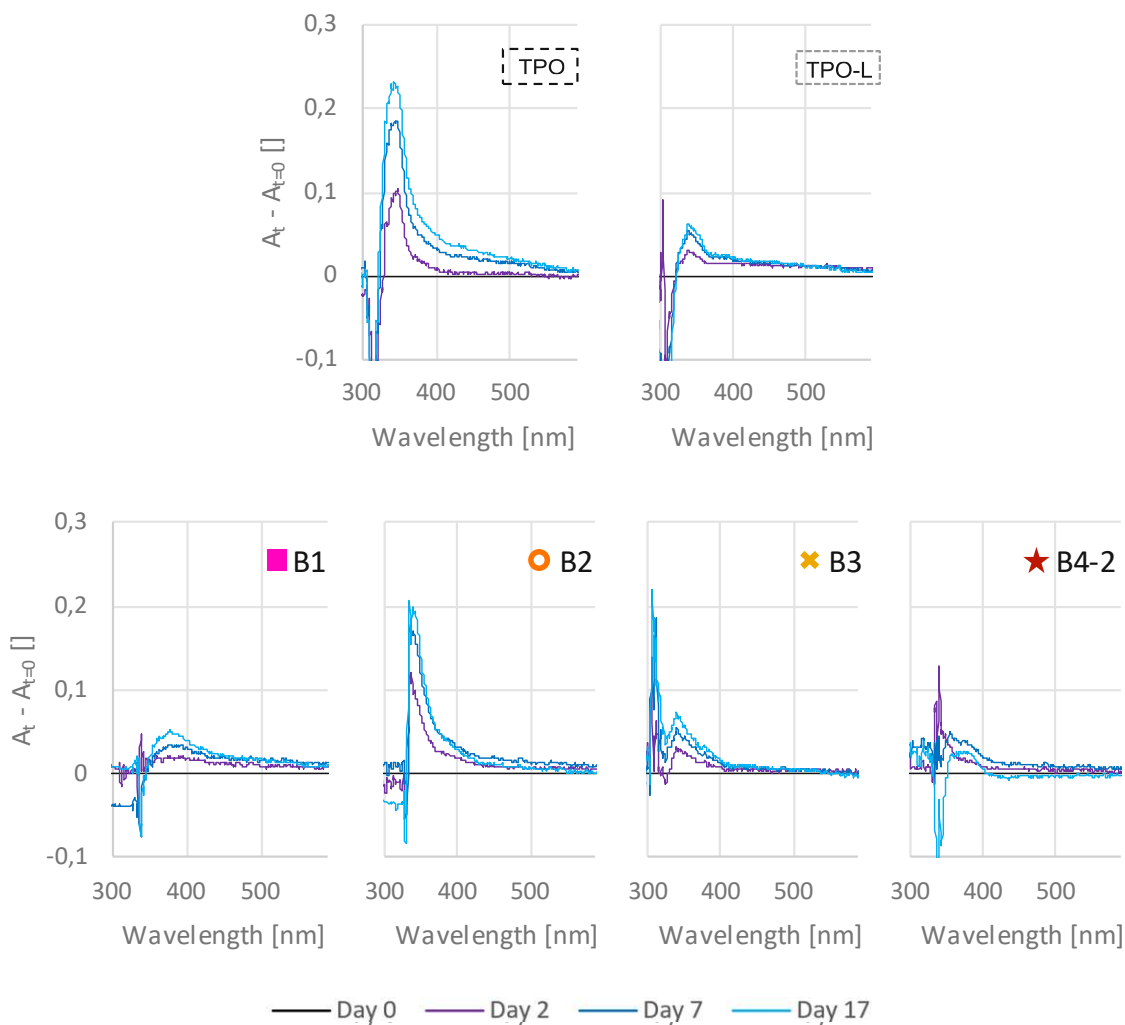
*Figure 72: Time-dependent difference absorption spectra of thin film samples consisting of **UDMA** (stabilized with 100 ppm MeHQ) and the benzoyl modified photoinitiators **B1** – **B4-2**, **TPO**, and **TPO-L** (1.07 mol%).*

Considering the measurements in Figure 72 all benzoyl modified photoinitiators (**B1** – **B4-2**) seem to exhibit lower absorption than **TPO**, in all wavelength regions. Although absorbances at higher wavelengths (<400 nm) can be observed for **B1**, **B2** and **B4-2** and these are significantly lower than in the case of **TPO**, a comparison between them would be inconclusive, as the signals are too weak to be evaluated reliably. Only **B3** seems to perform exceptionally well, as no increasing absorbances above 415 nm were observed in this sample. In order to obtain a reliable comparison of the discoloration behavior of the photoinitiators, measurements in the CIELAB color space were conducted.

CIELAB method

The CIELAB measurements were carried out by the company Ivoclar AG with samples consisting of **UDMA** and 1 mol% of the respective photoinitiator. Unfortunately, the photoinitiator **B3**, which exhibited good discoloration behavior in the experiments using the UV-Vis method, was not included in this measurements. The results for the color change ΔE are depicted in Figure 73. All additional results from the CIELAB measurements are available in the experimental section 2.2.2.3.

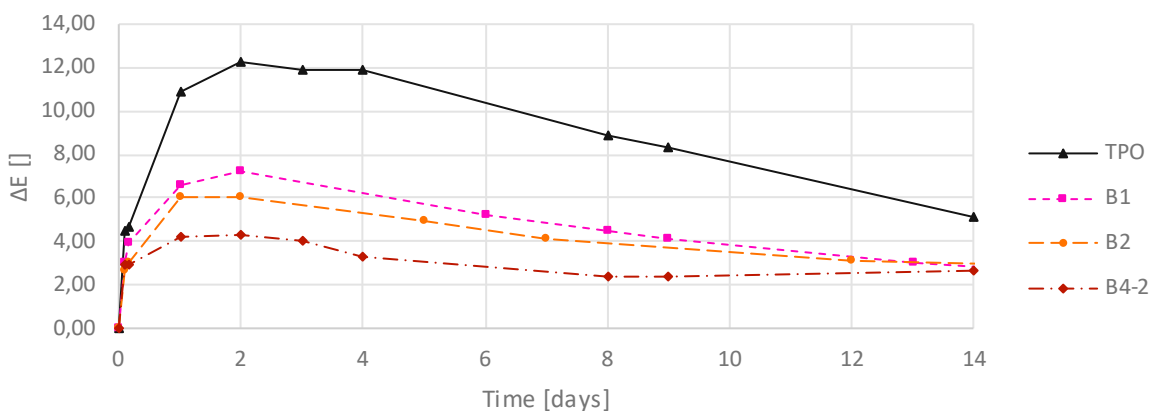*Figure 73: Color change ΔE of samples consisting of **UDMA** (stabilized with 100 ppm MeHQ) and 1 mol% of the benzoyl modified photoinitiators **B1**, **B2**, **B4-2** and **TPO**. The samples were stored at 50°C immersed in water.*

It is apparent that all investigated photoinitiators exhibit significantly improved color stability than the **TPO** reference, in the order **B1** < **B2** < **B4-2**. The fact that **B1** performs slightly worse than **B2** and **B4-2** may be explained by the fact that there is only one methoxy substituent in the *ortho*-position of the benzoyl moiety and thus the steric hindrance is lower than for the derivatives **B2** and **B4-2**. The observation that **B4-2** performs better than **B2**, on the other hand, is more difficult to explain, as radical recombination of the corresponding benzoyl radicals appears equally plausible, with regard to steric effects. However, as will be evident later, the phosphorus part is also likely to have a significant influence on the discoloration behavior, which is likely to be favorable for **B4-2**.

2.2.3 Conclusion

It has been shown that a modification of the benzoyl part can significantly influence the absorption behavior of MAPOs. The introduction of sterically demanding substituents in the *ortho*-position of the phenyl ring of the benzoyl part, seems to cause a hypsochromic shift of the n→π* transition. The substituents in *para*-position, on the other hand, seem to influence the extinction coefficients and the π→π* transition. Thus, presumably due to the absence of the *para*-substituent in the case of **B4-2**, a low absorbance can be observed. In the case of **B1** and **B2** the *p*-methoxy groups seem to cause a redshift of the π→π* transition, causing a partial overlap with the n→π* transition.

Regarding the reactivity, the photo-DSC experiments revealed that the benzoyl-modified photoinitiators achieve lower performance compared to **TPO**. **B1** performs best here, **B4-2** is generally slightly faster than **B2**, but has a lower DBC. However, in general **B2** and **B4-2** are comparable to **TPO-L**. Especially the irradiation with 400 nm is remarkable, where **B1** and **B4-2** stand out and clearly outperform **TPO-L**. **B3**, on the other hand, is in no way competitive with the other initiators and is significantly worse in all parameters. There is no apparent explanation for the low reactivity of **B3**, but maybe it is related to the +I effect of the *i*-propyl groups or the large steric hindrance of the formed benzoyl radicals. The methoxy groups of **B1**, **B2** and **B4** also appear to have a negative effect on reactivity. Here, too, steric hindrance and electronic effects are possible causes, which cannot be clearly separated from each other on the basis of the substances tested.

Nevertheless, all of the used benzoyl-modified photoinitiators, fulfilled the actual intention of this study, namely to improve the discoloration behavior of the polymer samples. **B1** and **B4-2** in particular must be highlighted. **B1** effectively reduces discoloration and still delivers a good performance with all tested light sources, which is equal or superior to **TPO-L** and **B4-2** reduces the discoloration to an absolute minimum and still provides reasonable performance, especially at higher wavelengths.

2.3 Phosphorus modified MAPOs with different alkyl/phenyl substituents

In this chapter, the phosphorus-bound phenyl substituents of **TPO** will be modified or replaced by aliphatic residues (P-modified MAPOs). As the work of Duan et al. shows, this can lead to an improvement in absorption behavior and reactivity.[97] It is suspected that particularly sterically demanding substituents on the phosphorus could have a positive effect. To investigate this in more detail the following target structures were selected.
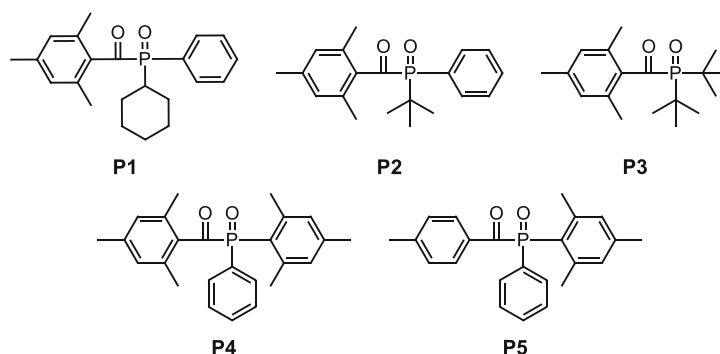
P1 was selected as a comparison to **TPO**. By replacing one phenyl substituent of **TPO** with a cyclohexyl ring, it will be investigated to which extent the two initiators, which should have a similar spatial conformation, differ from each other. In the case of **P2**, the introduction of a P-bonded *tert*-butyl group is intended to increase the steric demand around the phosphorous compared to **TPO**. In **P3**, this will be further enhanced by the introduction of a second *tert*-butyl substituent. In the MAPO **P4**, the basic structure of **TPO** is to be retained and the steric requirement around the phosphorus is to be increased by introducing 3 methyl groups on a P-bonded phenyl ring. This substance has already been tried to be prepared by Duan et al., but without success.[97] In their work, they also showed that the stability of **BPO**, which exhibits no methyl groups on the phenyl ring of the benzoyl part, can be increased by the introduction of 3 methyl groups on a P-bonded phenyl ring. In the work of Sumiyoshi and Schnabel it was shown that by introducing a methyl group in the *para*-position of the benzoyl moiety of **BPO**, excellent quantum yields can be achieved.[91] Therefore, an attempt was made to combine these two findings by developing the structure **P5**.

2.3.1 Synthesis

2.3.1.1 Synthesis of 2,4,6-trimethylbenzoyl-cyclohexylphenylphosphine oxide (**P1**)

In a first approach the precursor cyclohexylphenylphosphine oxide (**CHPO**) was prepared by a Grignard reaction. The synthesis was carried out based on the literature of Zhang et al., but using dichlorophenylphosphine (**DCPP**) instead of a various dichlorophosphites.[103]
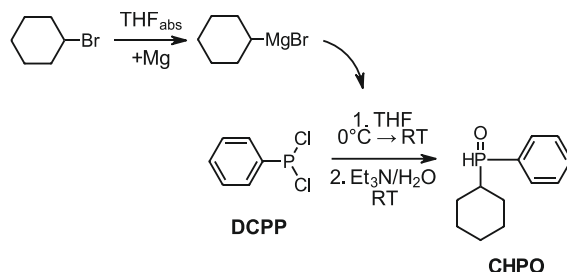
The reaction basically worked well and the desired structure was obtained as the main ingredient in the crude product. In addition, based on the molar masses detected in a UPLC-MS measurement, it is assumed that the corresponding phosphinic acid and the disubstituted derivative were obtained as side-products of the reaction. Despite the fact that good separation and no degradation were observed on a 2D TLC sample, no pure products could be isolated by repeated column chromatography. It is assumed that the product degrades slowly and continuously under the conditions of column chromatography and therefore could not be isolated as a pure substance. Therefore, a different approach to synthesize **CHPO** was sought in order to obtain a crude product with higher purity, that can be used directly for the subsequent reaction.

In the second attempt **CHPO** was produced as described in the work of Beaud et al.[104] Firstly ethyl phenylphosphinate (**EPP**) was prepared, which is converted without further purification with a freshly prepared Grignard reagent to yield the product. Using this method, should avoid a multiple attack of the Grignard reagent and could possibly prevent from undesired hydrolysis products, potentially resulting in a pure crude product
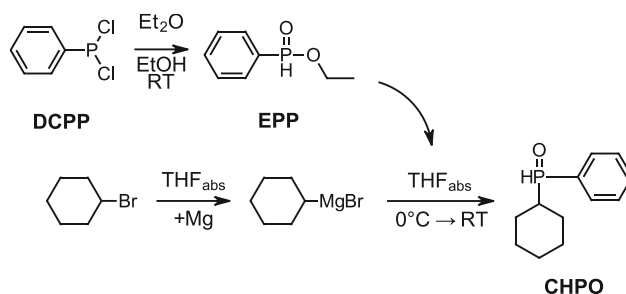
The synthesis proceeded as described and indeed yielded a crude product of high purity. Since the purification by column chromatography was not successful in the first synthesis route, it was not performed in this case. Instead, literature was found describing purification of similar phosphine oxides by distillation.[105] The product was thus successfully purified by means of Kugelrohr distillation to yield a colorless oil in 43% of the theory.
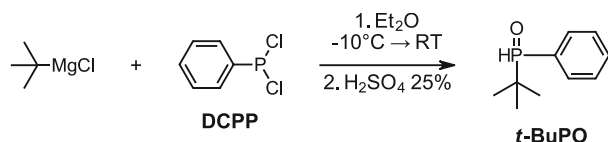
The subsequent reaction to produce the desired photoinitiator **P1** was conducted with the synthesis method of Zhang et al. which was already successful in the synthesis of **B3** (2.2.1.3).[99]
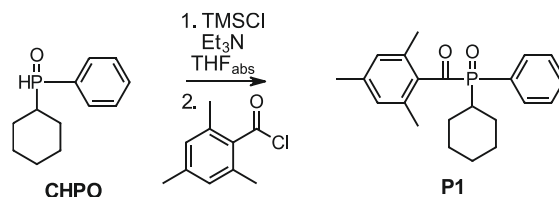
The coupling reaction took place as intended with full conversion within 67 h. The product was purified by means of solid-loaded column chromatography and a pale-yellow solid was obtained in 69% yield.

2.3.1.2 Synthesis of 2,4,6-trimethylbenzoyl-phenyl(*tert*-butyl)phosphine oxide (**P2**)

For the synthesis of the **TPO** derivative **P2**, exhibiting a steric hindrance at the phosphorus part by the introduction of a *tert*-butyl moiety, the precursor *tert*-butylphenylphosphine oxide (*t*-**BuPO**) had to be prepared first. The synthesis of this precursor was performed analogously to literature.[105]

The reaction was conducted as described and produced the desired target substance as the main component. Purification by Kugelrohr distillation yielded the product in sufficient purity as white solid in 61% yield.
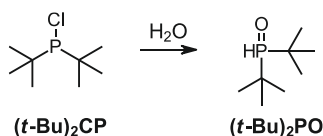
The subsequent reaction to produce the desired photoinitiator **P2** was conducted with the established synthesis method of Zhang et al.[99]
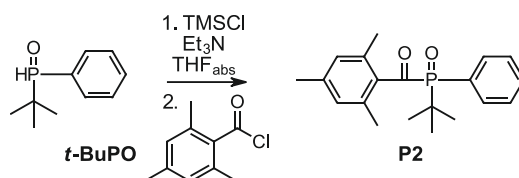
The coupling reaction of **t-BuPO** with 2,4,6-trimethylbenzoyl chloride was conducted at room temperature. Most probably due to the steric hindrance the reaction mixture had to be stirred for 8 days, to achieve an almost complete conversion. By increasing the temperature to 100°C, the conversion could be accelerated as described in the literature.[99] The crude product obtained was purified by column chromatography and resulted in a pale-yellow solid with a yield of 57 % of theory.

2.3.1.3 Synthesis of 2,4,6-trimethylbenzoyl-di-*tert*-butylphosphine oxide (**P3**)

In order to synthesize the **TPO** derivative **P3**, which exhibits a large steric hindrance on the phosphorus due to two *tert*-butyl groups, the precursor di-*tert*-butylphosphine oxide (**(t-Bu)₂PO**) was prepared in a first attempt. For this purpose, di-*tert*-butylchlorophosphine (**(t-Bu)₂CP**) was hydrolyzed according to literature.[106]


The reaction proceeded without difficulties and yielded the desired product as a white solid with sufficient purity and a yield of 91%.

The subsequent coupling reaction to produce the desired photoinitiator **P3** was attempted with the established synthesis method of Zhang et al.[99]
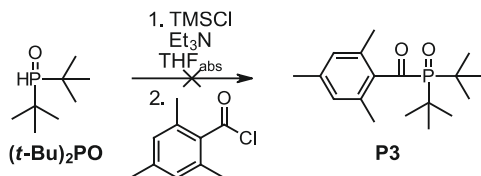
In this reaction, no conversion to the desired target product was observed after 6 days of stirring at room temperature, although the silylated intermediate was detected. It is assumed that the coupling could not take place under these reaction conditions due to the large steric hindrance of **(t-Bu)₂PO**. Consequently, the reaction mixture was heated to reflux to enhance the driving force of the reaction. However, even after another 18 h, no progress of the reaction was observed, prompting the search for an alternative synthesis route.

To reduce the steric demand of the phosphorus component for the coupling reaction, an attempt was made to link the non-oxidized **(t-Bu)₂CP** directly to 2,4,6-trimethylbenzoyl chloride. For this purpose a Grignard-like reaction, described in the patent literature of Suzuki et al. is to be used.[101] This procedure should yield the intermediate **(t-Bu)₂TP**, which is to be oxidized by atmospheric oxygen or in presence of an oxidizing agent to the desired product **P3**.
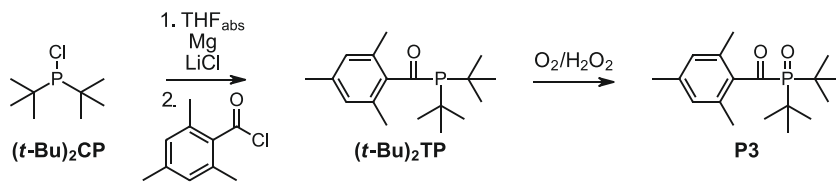

As there were difficulties when starting this reaction in previous attempts, special emphasis was placed on establishing particularly favorable conditions for this approach. All ingredients were weighed in a glove box and the glassware was flame-dried with particular care. Anhydrous LiCl was dried again by heating it under high vacuum, the magnesium shavings were finely ground in inert gas atmosphere to break a potential passivation layer and increase the surface for the reaction. A graine of iodine was added to promote the start of the reaction. After heating the reaction mixture, it was initially presumed that the first step of the reaction had started. However, this assumption was

brought into question upon the addition of the remaining (**t-Bu)₂CP**. Reaction controls with GCMS and NMR confirmed that the reaction had indeed not started. A distinct gray turbidity of the reaction mixture appeared spontaneously soon after these controls, which was considered as a definite indication of the start of the reaction. The mixture was stirred for 2 h before the second reaction step was conducted. A red coloration of the solution was observed when 2,4,6-trimethylbenzoyl chloride was added, indicating the success of the reaction. After stirring for 3 h the reaction was stopped and the crude product was processed in two different ways. One part was attempted to be purified by fractioned distillation. However, some of the distillate got stuck in the distillation bridge and no pure product could be obtained this way. The other part was oxidized with H_2O_2 and subsequently purified via column chromatography. Through this method, a pure pale-yellow solid was obtained with a yield of 39%.
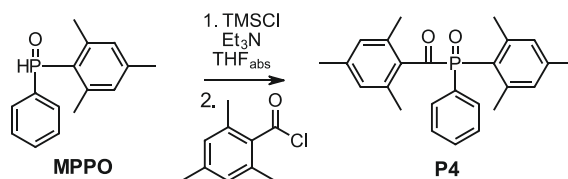
2.3.1.4 Synthesis of 2,4,6-trimethylbenzoyl-phenyl(2,4,6-trimethylphenyl)phosphine oxide (**P4**)

In a first step the precursor phenyl(2,4,6-trimethylphenyl)phosphine oxide (**MPPO**) was prepared by a Friedel-Crafts reaction according to the literature.[107]
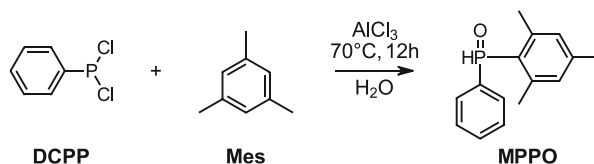
The reaction was simple and yielded the desired product as described. The purification was performed by column chromatography and the white solid product was obtained in 87% yield.

For the synthesis of the target structure **P4**, exhibiting a steric hindrance at the phosphorus part by the introduction of the mesityl group, the established reaction described by Zhang et al. was used.[99]

The first reaction step was conducted as described. In the second step of the reaction, only little conversion was observed after 2 days. Therefore, the reaction time was extended to 8 days in total. Although some remaining reactant was visible in the UPLC-MS control, the reaction was stopped at this point in time. The crude product was purified by solid loaded column chromatography with a mixture of dichloromethane and methanol. The yield of the pale-yellow solid was 17% of the theory. A higher yield could probably be achieved by a longer reaction time, or by an increase of the reaction temperature.

2.3.1.5 Synthesis of 4-methylbenzoyl-phenyl(2,4,6-trimethylphenyl)phosphine oxide (P5)

<u>Pathway A)</u>

The precursor **MPPO** was prepared as described in 2.3.1.4. In a first approach, P5 should be prepared using a mild synthesis described by Duan et al.[97] In the literature, benzaldehyde is first converted with **MPPO** to form a α-hydroxyphosphine, which is then oxidized with active MnO_2. In this synthesis, *p*-tolualdeyhde was used instead of benzaldehyde.
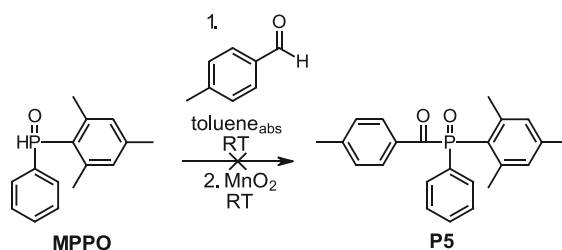
Although the reaction was performed precisely as described in the literature, no conversion of the reactants was detected with TLC control. Even longer reaction times and an increase of the reaction temperature to 100°C did not result in any conversion.

<u>Pathway B)</u>

In another experiment, an attempt was made to produce the substance with the reaction described by Zhang et al., which had already been successful in previous synthesis.[99]

1. TMSCl
Et$_3$N
THF$_{abs}$

2.

MPPO

P5
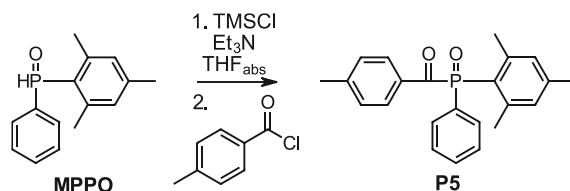
The reaction was conducted as described to yield the desired crude product. An attempt was made to purify the substance using column chromatography, which resulted in partial decomposition of the substance. As it was suspected that the product could be unstable in general, NMR experiments were carried out. A measured sample was exposed to the air atmosphere and then remeasured. The ¹H-NMR and ³¹P-NMR spectra show certain changes in ppm ranges where product signals are expected (Experimental part: Figure 105 and Figure 106). As these are NMR spectra of the crude product, the individual signals cannot be clearly assigned, therefore, it cannot be stated with certainty that it is actually the product that degrades or a by-product. Nevertheless, it seems likely that is the product, since the *ortho*-methyl groups on the benzoyl part, which usually provide stability, are missing. This, and the fact that the crude product could not be purified by conventional column chromatography, led to the decision not to analyze the substance in detail.

2.3.2 Characterization

The phosphorous modified photoinitiators **P1** – **P4** were investigated with regard to their absorption behavior, their reactivity and their discoloration behavior in polymer samples. The commercial MAPOs **TPO** and **TPO-L** were used as references for these studies. Furthermore, DFT calculations were performed to predict the reactivity of the respective phosphanoyl radicals. Laser flash photolysis experiments should then be used to determine whether these predictions are correct on the basis of **P1** and **P2**. In addition, steady-state photolysis experiments were conducted for **TPO**, **P1** and **P2** to investigate the bleaching behavior and to determine the quantum yield (Φ).

2.3.2.1 UV-Vis spectroscopy

For the investigation of the absorption behavior of the phosphorous modified MAPOs, UV-Vis spectra of 0.001 M solutions in acetonitrile were recorded. In the case of the

potentially unstable substance **P5**, a very rough estimate of the purity of the crude product was made using the ^{1}H-NMR spectrum. This resulted in a purity of about 33%, which is why the triple amount of crude substance was weighed in for the UV-Vis sample. As this is only a rough estimate, the intensity of the corresponding absorption of **P5** cannot be considered accurate. The resulting absorption spectra of **P1** – **P5** are depicted in Figure 74, the derived values for λ_{max}, ε_{385nm} and ε_{400nm} in Table 6.

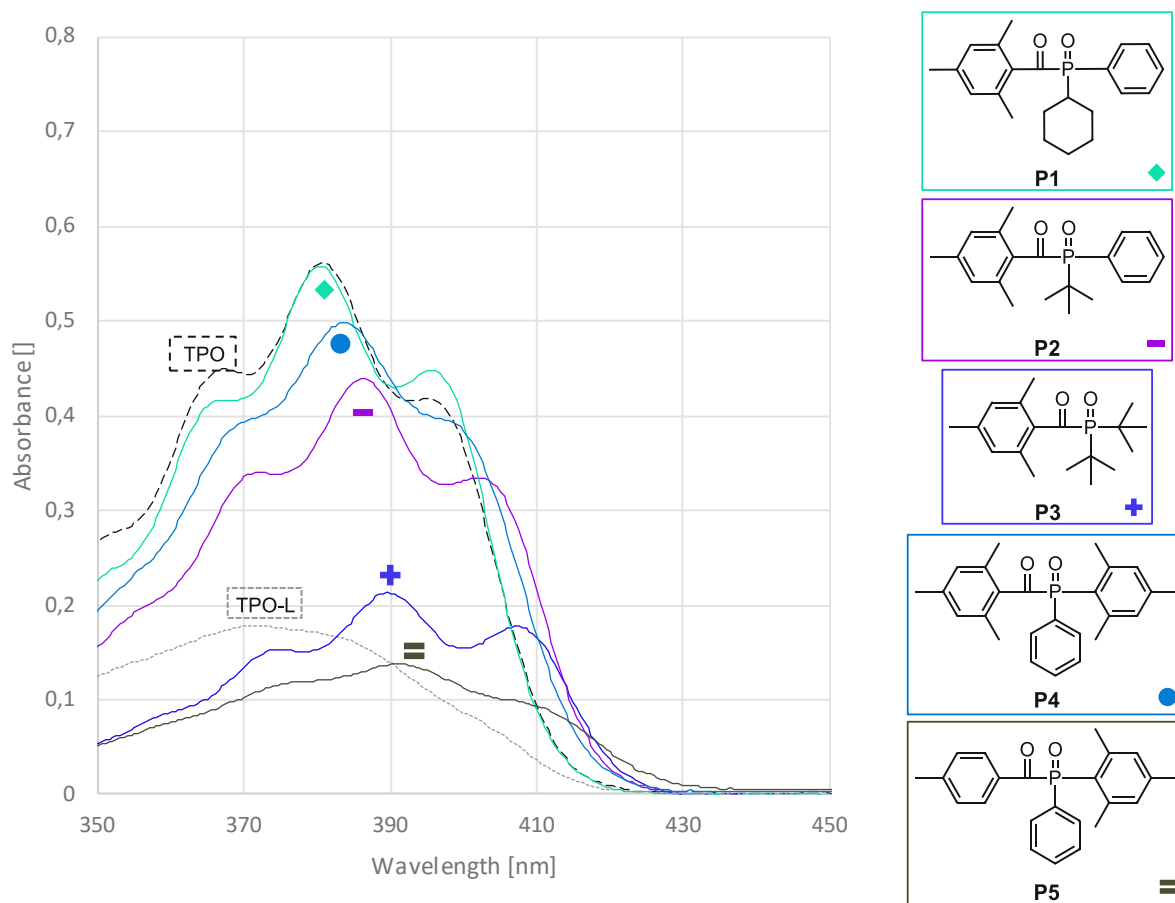*Figure 74: UV-Vis spectra of solutions of the phosphorous-modified MAPOs **P1** – **P5** (c = 0.001 M in acetonitrile). For P5 a purity of 33% was assumed.*

*Table 6: Wavelength of the absorption maximum (λ_{max} ($n\rightarrow\pi^*$)) and molar extinction coefficient (ε) at 385 nm and 400 nm of the phosphorous-modified MAPOs **P1** – **P5**. The ε-values for P5 are not reliable, as the assumed purity of 33% was only a rough estimation.*

	λ_{max} ($n\rightarrow\pi^*$)	$\varepsilon_{\lambda max}$ (L·mol^{-1}·cm^{-1})	$\varepsilon_{385\,nm}$ (L·mol^{-1}·cm^{-1})	$\varepsilon_{400\,nm}$ (L·mol^{-1}·cm^{-1})
TPO	381	561	510	367
TPO-L	371	178	161	86
◆ **P1**	380	558	497	392
▬ **P2**	386	439	435	331
✚ **P3**	390	213	186	154
● **P4**	384	498	494	384
═ **P5**	391	(137)	(127)	(113)

Considering Figure 74 and Table 6, a trend of increasing bathochromic shift can be observed in the following order: **TPO-L < P1 < TPO < P4 < P2 < P3 < P5**. **P1**, which is structurally very similar to **TPO**, also exhibits an almost identical absorption spectrum, only the shoulders next to the main peak are shaped slightly differently. In contrast to **TPO** and **P1**, **P2** exhibits a redshift of approximately 5 nm. It is assumed that this bathochromic shift is caused by a favorable conformation, induced by the steric demand of the sterically demanding *tert*-butyl substituent. In **P3**, this steric requirement at the phosphorous is further increased by the introduction of a second *tert*-butyl group and consequently the redshift is also increased to about 9 nm. In the case of **P4**, the effect of the three methyl substituents on the P-bonded phenyl ring appears to be smaller than that of the *tert*-butyl group in **P2**, as the bathochromic shift is only 3 nm. The absorption spectrum of **P5**, on the other hand, shows the great influence of the *ortho*-methyl groups on the benzoyl part. In contrast to **P4**, **P5** not only has a strong redshift of 10 nm compared to **TPO** in terms of λ_{max}, but also a far tail out to about 435 nm. Furthermore, a trend can be seen across the P-modified photoinitiators, that the extinction seems to decrease with increasing redshift.

2.3.2.2 Steady-state photolysis

The steady-state photolysis experiments were conducted in order to evaluate the photobleaching behavior and subsequently determine the quantum yields of the individual photoinitiators. For this purpose, solutions of **TPO** (0.001 M), **P1** (0.001 M) and

P2 (0.002 M) in acetonitrile were prepared and degassed. The photoinitiators **P3**, **P4** and **P5** were not evaluated. For the experiments the samples were irradiated with a high-power LED at 385 nm and UV-Vis spectra were recorded every 10 s. The resulting spectra are depicted in Figure 75.
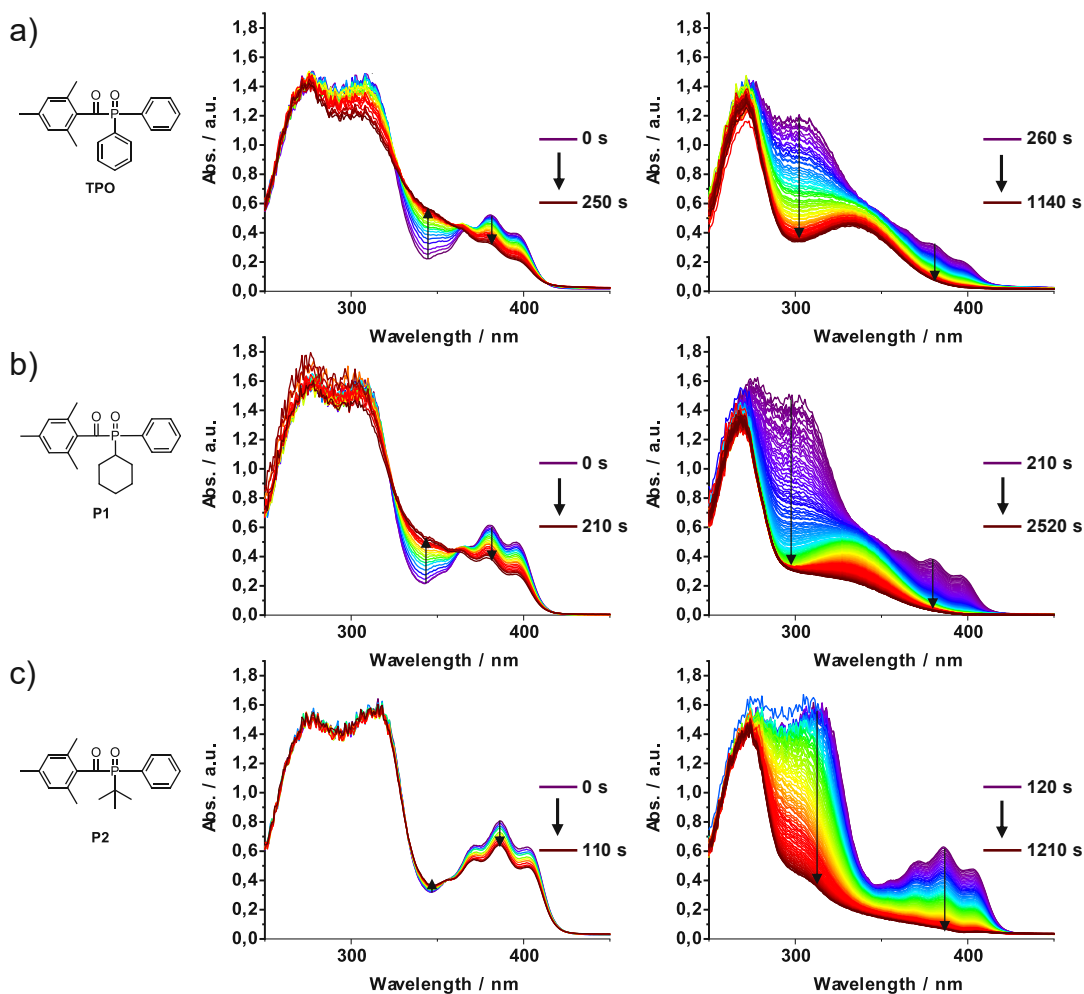

*Figure 75: Steady-state photolysis experiments of solutions of **TPO** (0.001 M), **P1** (0.001 M) and **P2** (0.002 M) in acetonitrile.*

In addition to **TPO**, the photoinitiators **P1** and **P2** also provide excellent photobleaching. The typical absorbance caused by the n→π* transition in the range of about 350 – 420 nm disappears completely in all cases. The time-dependent decrease of this absorbance can be used to determine the quantum yields (Φ), this method is explained in more detail in the experimental section (2.3.2.2) and in the literature.[108] The quantum

yields (Φ) are a measure of the efficiency with which a photoinitiator cleaves when exposed to the applied light source. The results for a 385 nm LED light source are summarized in Table 7.

*Table 7: Results for quantum yield determination of **TPO**, **P1** and **P2** irradiated with a 385 nm LED.*

MAPO	Quantum Yield Φ		
TPO	0.43	±	0.02
P1	0.43	±	0.02
P2	0.45	±	0.02

Based on these results, it can be concluded that **TPO** and the structurally very similar **P1** cleave equally efficiently when irradiated with a 385 nm LED light source. **P2** in comparison exhibits slightly higher quantum yields than **TPO** and **P1**. The higher quantum yields of **P2** can only be attributed to the *tert*-butyl substituent. It is assumed that this sterically demanding group brings the molecule in a favorable conformation, resulting in advantageous orbital overlap and therefore higher quantum yields.

2.3.2.3 Density functional theory (**DFT**) calculations of phosphanoyl radicals

DFT calculations were carried out at TU Graz in the working group of Prof. Georg Gescheidt and were used to determine the phosphorous hyperfine coupling constant a(P), of phosphanoyl radicals with different phosphorous-bound substituents. A high a(P) is associated with a high quenching constant and thus a high radical reactivity. Table 8 shows the calculated values for a(P) with varying alkyl and phenyl substituents for R^1 and R^2.

General part

Table 8: DFT calculated ^{31}P hyperfine coupling constants a(P) for different phosphanoyl radicals.

		R^1	
		Ph	*t*-Bu
R^2	Ph	320 **TPO**	
	Me	323	
	Et	311	
	Cyclohexyl	297 **P1**	
	t-Bu	292 **P2**	268 **P3**
	OEt	434 **TPO-L**	

$$\cdot \underset{R^2}{\overset{\displaystyle O}{\underset{|}{\overset{\|}{P}}}} - R^1$$

Table 8 shows that a substitution of the phenyl rings with aliphatic residues has rather negative effects on the reactivity of the P-centered radicals. If the aliphatic chains are longer, or increasingly branched, the value for a(P) decreases, which could be explained by the increasing +I effect of these substituents. The strong +M and weak -I effects of the OEt substituent of **TPO-L** on the other hand, seems to increase a(P) drastically.

2.3.2.4 Laser flash photolysis (LFP)

Laser flash photolysis experiments were conducted at TU Graz in the working group of Prof. Georg Gescheidt and are used to determine the addition rate of butyl methacrylate to primary phosphanoyl radicals. For this purpose, solutions of **TPO** (0.001 M), **P1** (0.001 M) and **P2** (0.002 M) in acetonitrile were prepared and evaluated. The exact procedure and the evaluation of this experiments are described in the experimental part (2.3.2.4).

The results for the rate constants of the addition of butyl methacrylate to the P-centered radicals of **TPO**, **P1** and **P2** are summarized in Table 9.

*Table 9: Rate constants for the addition of butyl methacrylate to the P-centered radicals of **TPO**, **P1** and **P2**.*

	Rate constant / 10^7 [$M^{-1} \cdot s^{-1}$]		
TPO	9.3	±	0.2
P1	6.4	±	0.2
P2	5.7	±	0.4

It can be seen that the measured rate constants of the P-centered radicals decrease from **TPO** to **P1** to **P2**. This is the same trend that was predicted from the DFT calculations in section 2.3.2.3. In Figure 76 the measured rate constants are plotted against the calculated phosphorous hyperfine coupling constant a(P) (Table 8).
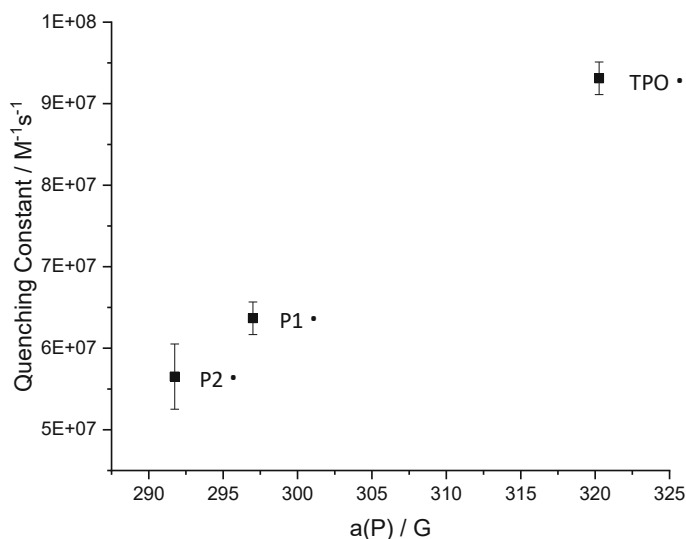

*Figure 76. Correlation between DFT calculated ^{31}P isotropic hyperfine coupling constants (a(P)) and the rate constants for the addition of butyl acrylate to P-centered radicals of **TPO**, **P1** and **P2** (k).*

This diagram demonstrates the direct correlation between the calculated values for a(P) with the measured quenching constants and indicates that the DFT-calculations achieve quite reliable results.

2.3.2.5 Photo-DSC

Photo-DSC measurements were carried out to determine the reactivity of the phosphorous-modified MAPO photoinitiators (**P1** – **P4**). Homogenous formulations consisting of 1.0 mol% of the respective photoinitiator in **UDMA** were prepared. As the individual initiators differ in terms of their absorption behavior, they were evaluated using three different light sources.
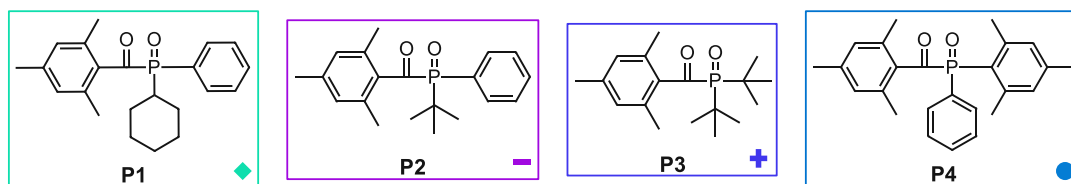
<u>320 – 500 nm broadband light source (OmniCure® S2000)</u>

For the first set of measurements an OmniCure® S2000 high pressure mercury vapor light source equipped with a 320 – 500 nm filter was used as light source. The light intensity at the sample surface was set to 64 mW/cm². The main results are summarized in Table 10, the complete data of the measurements can be found in the experimental section (2.3.2.5).

*Table 10: Results of photo-DSC measurements of formulations, consisting of 1 mol% photoinitiator in the monomer **UDMA**, under irradiation with a broadband light source (320-500 nm) with an intensity of 64 mW/cm².*

320-500 nm	t_{max} [s]			R_p [mmol*L^{-1}*s^{-1}]			$t_{95\%}$ [s]			DBC [%]		
TPO	4.3	±	0.2	176.0	±	3.5	34.0	±	1.6	64.2	±	0.1
TPO-L	5.1	±	0.3	147.8	±	5.3	32.4	±	1.5	58.9	±	0.5
◆ **P1**	4.4	±	0.1	175.2	±	4.3	30.8	±	1.0	61.4	±	0.6
▬ **P2**	4.3	±	0.2	184.7	±	5.0	29.3	±	2.2	65.1	±	1.2
✚ **P3**	4.3	±	0.2	168.4	±	1.5	32.2	±	1.4	61.4	±	1.2
● **P4**	4.7	±	0.0	159.4	±	3.7	36.1	±	0.4	59.5	±	0.4

Comparing the structurally very similar photoinitiators **P1** and **TPO** with each other, it can be recognized, that **P1** performs slightly worse than **TPO** in the speed-determining parameters t_{max} and R_p, as well as in the DBC. **P2** outperforms **TPO**, with higher R_P and DBC and equal t_{max}. **P3** is equal with regard to t_{max}, but is inferior to **TPO** in terms of R_P and DBC. The performance of **P4** is between **TPO** and **TPO-L**.

<u>385 nm LED light source</u>

Next the samples were examined using a 385 nm LED light source with a light intensity of 10 mW/cm² at the surface of the samples. The main results are summarized in Table 11, the complete data of the measurements is available in the experimental section (2.3.2.5).

Table 11: Results of photo-DSC measurements of formulations, consisting of 1 mol% photoinitiator in the monomer UDMA, under irradiation with a LED light source (385 nm) with an intensity of 10 mW/cm².

385 nm	t_{max} [s]			R_p [mmol*L^{-1}*s^{-1}]			$t_{95\%}$ [s]			DBC [%]		
TPO	5.5	±	0.2	138.5	±	1.5	32.2	±	1.1	57.7	±	1.5
TPO-L	6.1	±	0.0	131.0	±	4.2	35.2	±	1.5	56.3	±	0.8
◆ P1	5.6	±	0.1	139.9	±	2.4	31.5	±	1.0	56.0	±	1.3
▬ P2	5.4	±	0.1	151.4	±	2.1	30.4	±	1.2	58.5	±	0.5
✚ P3	6.1	±	0.2	135.1	±	4.4	31.7	±	1.6	56.5	±	1.0
● P4	6.6	±	0.1	118.0	±	1.5	35.2	±	1.8	54.5	±	0.4

As with broadband irradiation, **P1** is also slightly inferior to **TPO** at 385 nm. **P2** on the other hand proves its superiority over **TPO** even more at this wavelength. The performance of P3, which performed significantly better than **TPO-L** with broadband irradiation, can only match it at 385 nm. Surprisingly, **P4** performs worse at 385 nm than **TPO-L**, despite similar extinction coefficients at this wavelength as **TPO** and **P1** (see Table 6).

400 nm LED light source

The examination of the samples using a 400 nm LED light source was also conducted with a light intensity of 10 mW/cm² at the surface of the samples, to obtain comparability with the values at 385 nm. The main results are summarized in Table 12, the complete data of the measurements is available in the experimental section (2.3.2.5).

Table 12: Results of photo-DSC measurements of formulations, consisting of 1 mol% photoinitiator in the monomer UDMA, under irradiation with a LED light source (400 nm) with an intensity of 10 mW/cm².

400 nm	t_{max} [s]			R_p [mmol*L^{-1}*s^{-1}]			$t_{95\%}$ [s]			DBC [%]		
TPO	5.3	±	0.1	156.8	±	1.3	30.5	±	0.3	60.8	±	0.3
TPO-L	6.4	±	0.0	134.9	±	3.1	34.7	±	1.5	56.5	±	0.9
◆ P1	5.6	±	0.1	150.6	±	4.7	29.7	±	1.3	58.5	±	0.8
▬ P2	5.1	±	0.3	159.1	±	7.7	30.2	±	2.0	63.3	±	2.0
✚ P3	5.7	±	0.2	145.1	±	7.6	30.8	±	1.3	58.3	±	0.4
● P4	5.8	±	0.2	136.5	±	4.8	33.9	±	1.6	56.7	±	0.4

Irradiation of the photoinitiators at 400 nm instead of 385 nm leads to improved performance of all initiators except **TPO-L**. In this case, too, a slightly worse performance

of **P1** and a slightly better performance of **P2** compared to **TPO** can be observed. The performance of **P3** is between that of **TPO** and **TPO-L** and **P4** achieves slightly better results than **TPO-L** at this wavelength.

2.3.2.6 Discoloration behavior

<u>UV-Vis spectroscopy method</u>

The assessment of the discoloration behavior using the UV-Vis method was carried out as described in section 1.2.1. Since all phosphorous-modified photoinitiators exhibit the same 2,4,6-trimethylbenzoyl chromophore, the assessment of the discoloration behavior using the UV-Vis method is reasonable. The resulting difference absorption spectra are depicted in Figure 77.
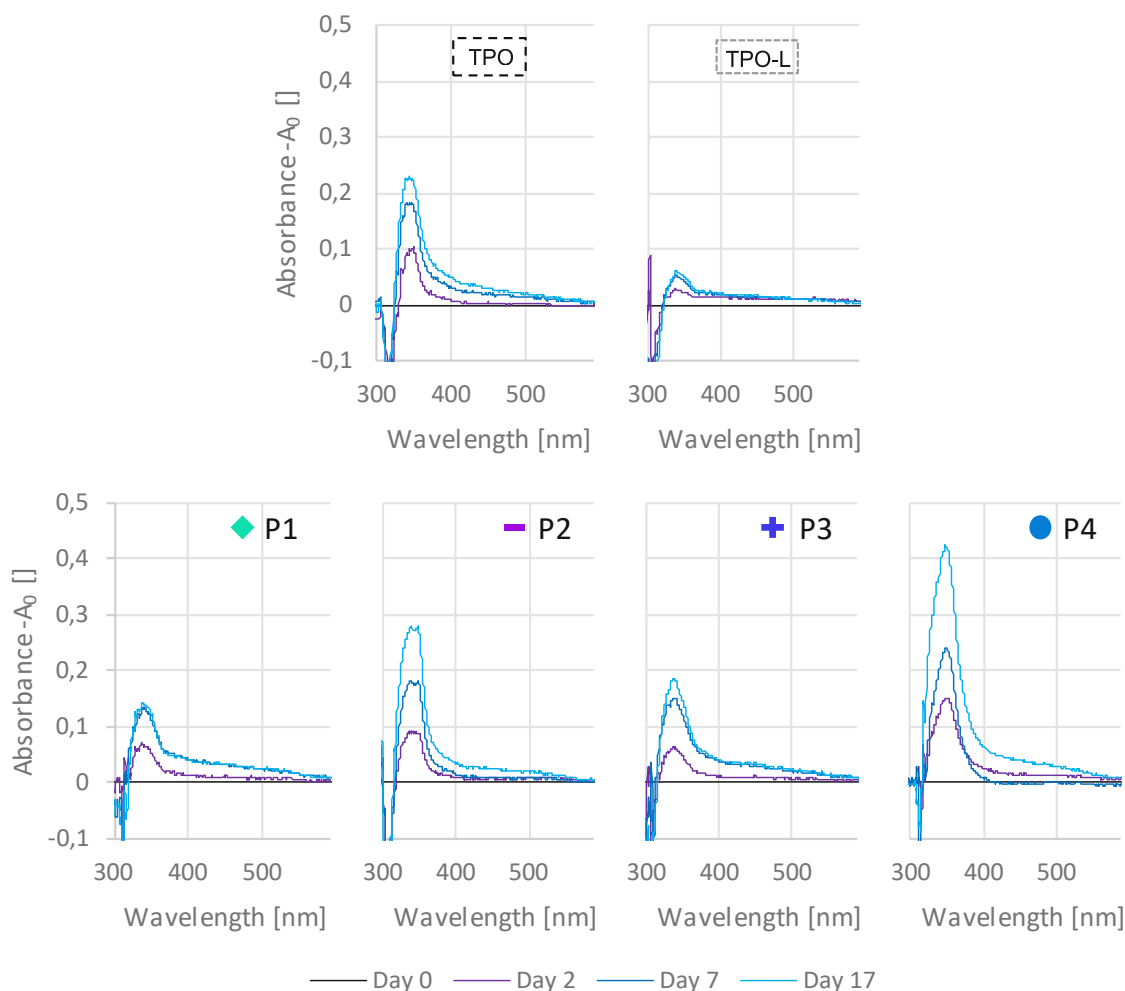
*Figure 77: Time-dependent difference absorption spectra of thin film samples consisting of **UDMA** (stabilized with 100 ppm **MeHQ**) and the phosphorous-modified photoinitiators **P1** – **P4**, **TPO**, and **TPO-L** (1.07 mol%).*

Comparing the difference absorption spectra of the P-modified photoinitiators **P1** – **P4** with those of **TPO**, **P1** in particular, but also **P2**, exhibit an improved discoloration behavior. **P3** causes similar absorbances, which are only slightly higher than those of **TPO**. **P4**, on the other hand, produces significantly stronger discoloration. However, none of these initiators can compete with the discoloration behavior of **TPO-L**. It is unclear why the discoloration behavior of the P-modified photoinitiators differ from **TPO** despite the fact that they have the same benzoyl chromophore. Initially, it was assumed that a lower P-radical reactivity would allow more free benzoyl radicals to react and thus cause less discoloration, but this hypothesis is disproved by these experiments. The fact is that the P-radical generated from **TPO-L** has the highest and **P2** and especially **P3** have a lower

P-radical reactivity than **P1** (see 2.3.2.3). The intensity of the discoloration should therefore decrease in the following order: **TPO-L** > **TPO** > **P1** > **P2** > **P3**, but this is completely wrong with regard to Figure 77. P4 has been excluded here as no calculated P-radical reactivities are available.

2.3.3 Conclusion

P1 is structurally very similar to **TPO** and most likely has a similar spatial conformation. This similarity is also reflected in the UV-Vis absorption spectrum, which is almost congruent with that of **TPO**. Nevertheless, **P1** is slightly inferior to **TPO** in all photo-DSC experiments. In the steady-state photolysis experiments (2.3.2.2), **P1** and **TPO** achieved equal quantum yields (Φ) at 385 nm, so they should cleave equally efficiently. The DFT calculations (2.3.2.3) and the LFP experiments (2.3.2.4), on the other hand, revealed that the P-radical generated by **P1** is less reactive than that of **TPO**. This lower radical reactivity is likely to be the decisive factor for the lower performance of **P1** in the photo-DSC measurements. Furthermore, **P1** has shown the best discoloration behavior of the P-modified initiators, outperforming **TPO**.

P2 exhibits a distinct bathochromic shift of about 5 nm in terms of λ_{max} in comparison to **TPO**. It is assumed that the sterically demanding *tert*-butyl group brings the molecule into a favorable spatial conformation, requiring less energy for the n→π* transition and thus shifting it to higher wavelengths. P2 showed a lower P-radical reactivity than **TPO** in the DFT calculations (2.3.2.3) and the LFP experiments (2.3.2.4), but achieved higher quantum yields (Φ) at 385 nm (2.3.2.2). The photo-DSC measurements revealed that **P2** performs better than **TPO** with all used light sources. Therefore, it appears that the higher quantum yield overcompensates the lower P-radical reactivity.

In **P3**, the steric demand was further increased, resulting in an even stronger bathochromic shift of about 9 nm with respect to λ_{max}. The calculated P-radical reactivity is even lower than that of **P2** and also in the photo-DSC experiments, **P3** could not match the performance of **TPO**, **P1** and **P2**. Nevertheless, an enhancement in performance was noted with irradiation at higher wavelengths, thus exposure to light of even higher

wavelengths than 400 nm could potentially lead to higher reactivity and consequently to a superiority of **P3**.

A redshift of about 3 nm in the absorption spectrum was observed for **P4**. Apart from that, the results of **P4** were surprisingly disappointing. In the photo-DSC measurements, **P4** performed significantly worse than **TPO** with all light sources used, and even worse than **TPO-L** at 385 nm. Also, with regard to the discoloration behavior, **P4** performed worst. The reason for the poor results is unclear, but perhaps the resonance stabilization of the P-radical through the mesitylene ring plays a role.

In the case of **P5**, no detailed investigations were carried out, as it is assumed that the molecule is not sufficiently stable and purification of the substance appears difficult. Nevertheless, a highly promising UV-Vis absorption spectrum of the raw product was recorded. This revealed a strong bathochromic shift of about 10 nm regarding λ_{max} compared to **TPO** and a far tail out to 435 nm. The possible instability is most likely due to the absence of the *ortho*-methyl groups on the benzoyl moiety, allowing nucleophiles to cleave the molecule. If the steric demand on the phosphorus would be increased further, nucleophilic attacks could possibly be prevented.

Furthermore, it could be shown that the trends of the DFT calculations of the phosphorous hyperfine coupling constant a(P) correlate well with the measured addition rate constants of butyl methacrylate to the corresponding phosphanoyl radicals. This shows that the radical reactivity can be predicted well by these calculations. Nevertheless, they do not give any information about how efficiently a photoinitiator cleaves upon irradiation. This is particularly evident in the example of **TPO-L**, which exhibits exceptionally high values for a(P) but shows low performance in the photo-DSC.

2.4   Phosphorus-modified MAPOs with heteroatom substituents (PH-modified)

In this chapter the aim is to produce and evaluate MAPOs that carry substituents linked to phosphorus via a heteroatom. The photoinitiators with such phosphorus-heteroatom linkages are labeled with PH. The literature shows on the basis of **TPO-L**, such derivatives

could be superior to **TPO** in terms of toxicological properties.[31, 33] However, **TPO-L** exhibits lower reactivity compared to **TPO**, prompting efforts to enhance its reactivity through modifications. In section 2.3 it was demonstrated that sterically demanding substituents on the phosphorous can improve the absorptions behavior and the reactivity of MAPOs. Therefore, the following target structures were selected to be prepared and characterized.
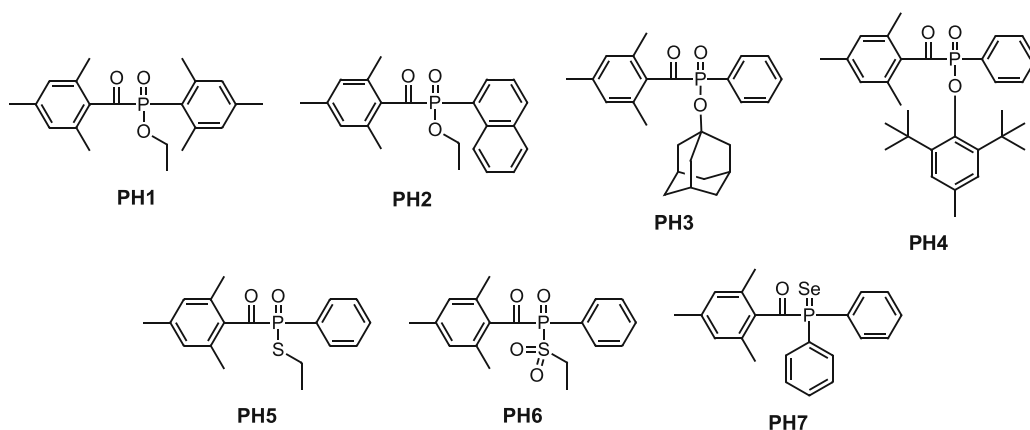

For **PH1** and **PH2**, **TPO-L** should be modified by introducing three methyl groups (**PH1**), or an additional phenyl ring (**PH2**) to the P-bonded phenyl ring. In the case of **PH3** and **PH4** the steric demand should be enhanced by replacing the oxygen-bonded ethyl group with an adamantanyl (**PH3**) or a 2,6-bis(1,1-dimethylethyl)-4-methylphenyl (**PH4**) group. In **PH5** the oxygen atom is replaced by a larger sulfur atom. This sulfur should then be oxidized, resulting in the very bulky sulphone group of **PH6**. In the case of **PH5** and particularly **PH6**, not only the spatial configuration, but also the electronic situation of the phosphorus changes significantly, which can also affect the absorption behavior and reactivity. With **PH7**, a completely different approach is to be tried to change the situation around the phosphorus by replacing the double-bonded oxygen with a considerably larger selenium atom.

2.4.1 Synthesis

2.4.1.1 Synthesis of 2,4,6-trimethylbenzoyl-ethoxy(2,4,6-timethylphenyl)phosphine oxide (**PH1**)

In order to prepare the PH-modified derivative, the precursor ethyl *P*-(2,4,6-trimethylphenyl)phosphinate (**EMP**) had to be synthesized. The first reaction was carried out analogously to the description of Zhang et al.[103]
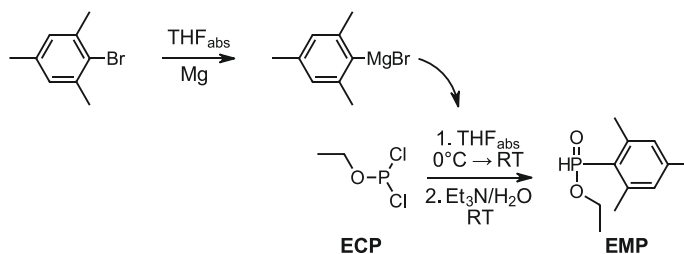
Ethyldichlorophoshite (**ECP**) was converted by the addition of a freshly prepared mesitylmagnesiumbromide solution. Care was taken to ensure that the Grignard reagent was added slowly to avoid multiple substitution. Nonetheless, at the end of the reaction a mixture of substances was obtained. While the literature reports successful purification of similar molecules from the same substance class using column chromatography, attempts of purification were not successful in this case.[103] Column chromatography produced mixed fractions containing the desired product, but also impurities. When these presumably pre-purified fractions were tried to be purified again by column chromatography, however, only mixed fractions were obtained. As no product of adequate purity was obtained in this approach, another method was attempted to obtain the desired precursor.

In the work of Schuman et al. the synthesis of the desired substance **EMP** is described.[109] Here the purification of the intermediate product is performed by Kugelrohr distillation, eliminating the need for further purification of the final product. In addition, the use of diethyl *P*-(2,4,6-trimethylphenyl)phosphonite (**DECP**) as the starting material could reduce the possibility of undesired side reactions.
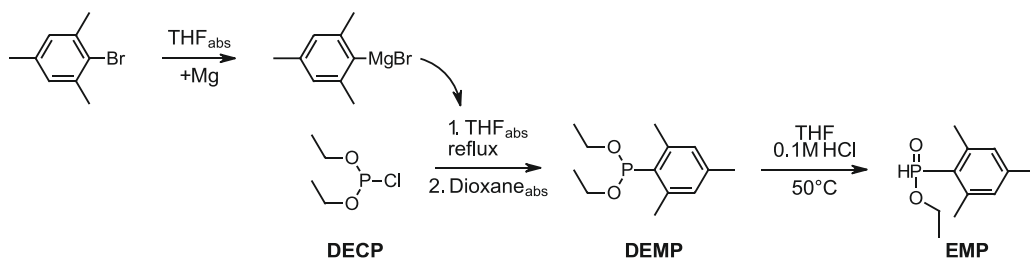
The reaction proceeds as described, during the purification of the intermediate stage **DEMP** using Kugelrohr distillation, the inert gas atmosphere was maintained as best as possible to avoid premature oxidation of this phosphine. The last reaction step was quantitative and resulted in a colorless oil with a total yield of 67 %.

The precursor **EMP** obtained by this method was then coupled with 2,4,6-trimethylbenzoyl chloride according to the proven method of Zhang et al. to synthesize the desired product **PH1**.[99]
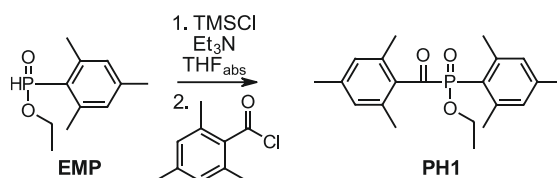
The crude product obtained in the reaction, was purified by column chromatography to give a pale-yellow solid in 53% yield and moderate purity. In order to obtain a pure product, this pre-cleaned product was recrystallized from heptane, resulting in a reduction of the overall yield to 41 %.

2.4.1.2 Synthesis of 2,4,6-trimethylbenzoyl-ethoxy(1-naphthyl)phosphine oxide (**PH2**)

For the preparation the naphthyl containing PH-modified derivative **PH2**, the precursor *P*-1-naphthalenylphosphinate (**ENP**) had to be synthesized. This reaction was carried out analogously to literature.[103]
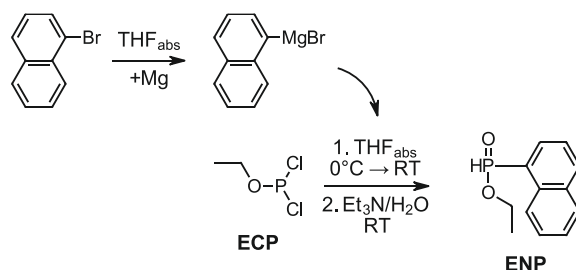
The reaction proceeded without any notable problems, but yielded a mixture of several substances. The purification by column chromatography was performed twice, as the initial choice of the eluent mixture was found to be unfavorable. The desired product was obtained as a yellow oil, with a poor yield of 10%. Despite two purification steps, the product was obtained with a certain degree of impurity. This and the conspicuously low yield could indicate that this product degrades slowly due to the conditions during column chromatography, as already described in 2.3.1.1 and 2.4.1.1.

Nevertheless, the mostly pure **ENP** was used for the follow-up reaction, which was conducted with the repeatedly successful method from the work of Zhang et al.[99]
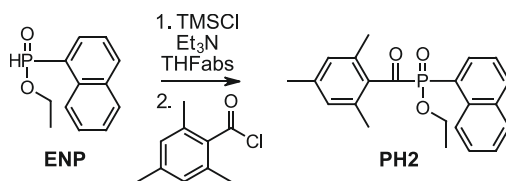
The reaction proceeded as intended and yielded the desired product. Similar to the preparation of the precursor, also in this case the solvent mixture for the column chromatography (DCM:MeOH, 99:1) was chosen to polar, resulting in mixed fractions. These pre-purified fractions were then subjected to further column chromatography (PE:EE, 9:1) to yield the pure product as yellow liquid in a yield of 29%.

2.4.1.3 Synthesis of *P*-2,4,6-trimethylbenzoyl-*P*-phenylphosphinic acid 1-adamantyl ester (**PH3**)

For the preparation the PH-modified derivative **PH3**, exhibiting a sterically demanding adamantanyl ester, the precursor 1-adamantanyl *P*-phenylphosphinate (**AdPO**) had to be prepared first. This substance was already synthesized in the work of Gatineau et al. and should be produced using the same method.[110] In this procedure, 1-adamantaol is deprotonated using pyridine, to enable nucleophilic attack on dichlorophenylphosphine (**DCPP**). The subsequent hydrolysis should then yield the precursor **AdPO**.
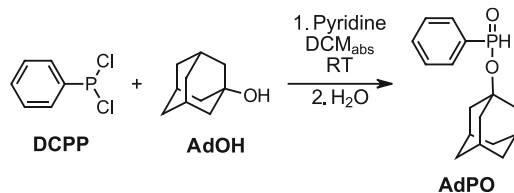
The reaction proceeded as intended and yielded a white crystalline crude product of quite high purity in 87% yield. Small scale experiments to recrystallize the crude product from EtOH, EE, or hexane failed. Purification by column chromatography led to problems in previous attempts with similar precursor substances, which is why the substance was used for the subsequent reaction without further purification.

For the coupling reaction of the **AdPO** precursor with 2,4,6-trimethylbenzoyl chloride the well-established method from the work of Zhang et al. was used.[99]
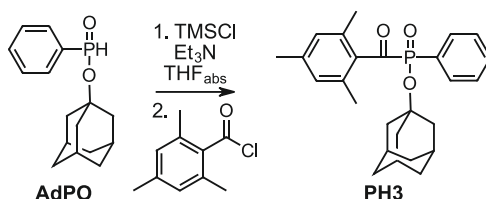
The reaction proceeded as anticipated and yielded the desired product. As with previously synthesized products, purification of the viscous product should be carried out using column chromatography. Unexpectedly, the product was not recovered after column chromatography with a solvent mixture of PE and EE, although a 2D TLC did not show degradation. With regard to UPLC-MS measurements, 2,4,6-trimethylbenzoic acid seems to be the main impurity of the crude product. This substance might be separated by distillation due to its higher volatility compared to the product. Consequently, a Kugelrohr distillation was conducted under high vacuum conditions with a maximum temperature of 140°C. This process actually removed the majority of the 2,4,6-trimethylbenzoic acid. Unfortunately, the product appears to start degrading at these temperatures, evidenced by the emergence of new impurities following the distillation.

Since no suitable method was found to purify the substance, an alternative synthesis route was explored with the aim of obtaining a purer end product or improving purification options. This method was basically described by Oesterreicher et al. and Roszkowski et

al.[96, 111] It involves the reaction of a phosphinic acid chloride with an alcohol, thiol or amine in the presence of a base. Where the phosphinic acid chloride is produced from the photoinitiator **TPO-L** via the intermediate stages sodium 2,4,6-trimethylbenzoylphenylphosphinate (**Na-TPO**) and 2,4,6-trimethylbenzoylphenylphosphinic acid (**TPO-OH**).
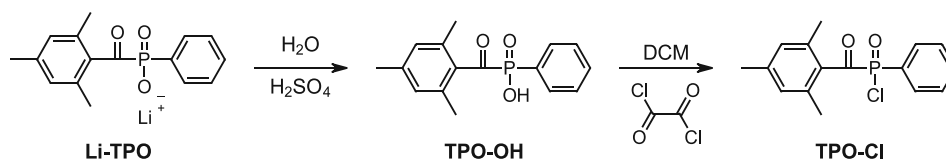
Lithium 2,4,6-trimethylbenzoylphenylphosphinate (**Li-TPO**), which was available in the working group was used instead of **Na-TPO** for the preparation of **TPO-OH**. The subsequent conversion with oxalyl chloride to 2,4,6-trimethylbenzoylphenylphosphinic acid chloride (**TPO-CI**) was carried out without any issues, following the procedure described in the literature.[111] The resulting brown oil was used for subsequent reactions without further purification.

For the preparation of the photoinitiator **PH3**, 1 eq. of **TPO-CI** was reacted with 1.1 eq. of 1-adamantanol (**AdOH**) in the presence of the base Et$_3$N (2.2 eq).
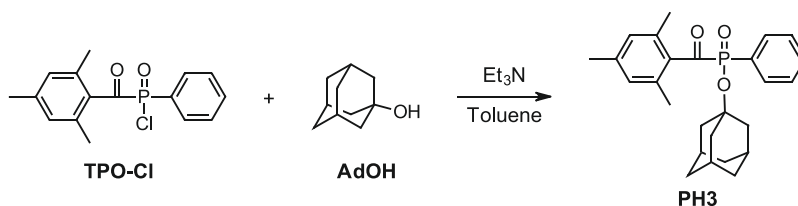
After a reaction time of 2 h, complete conversion could be determined. After washing and evaporation of volatile components, a solid crude product was obtained. The only significant impurity in this product appeared to be excess **AdOH**. To isolate the product an attempt was made to wash out the product using refrigerated toluene, as the product is well and **AdOH** barely soluble in it. Although the purity of the product could be increased with this method, it was not possible to completely separate **AdOH**, even when repeated. In another experiment, an attempt was made to separate the remaining **AdOH** by distillation. As in the first synthesis of **PH3** a degradation of this substance at higher temperatures was observed, an attempt was made to carry out the separation as quickly

as possible at the lowest possible temperature. By Kugelrohr distillation at high vacuum at 85°C for about 10 min. the desired product was obtained in good purity as highly viscous orange substance in 21% yield.

2.4.1.4 Synthesis of *P*-2,4,6-trimethylbenzoyl-*P*-phenylphosphinic acid 2,6-bis(1,1-dimethylethyl)-4-methylphenyl ester (**PH4**)

During the synthesis of **PH3** (2.4.1.3), a highly efficient method for preparing monoacylphosphine oxides with phosphorus-bound heteroatoms was discovered, leading to the development of the target structure **PH4**. In this structure, the bulky substance BHT is to be bound to the phosphinic acid chloride **TPO-Cl**.
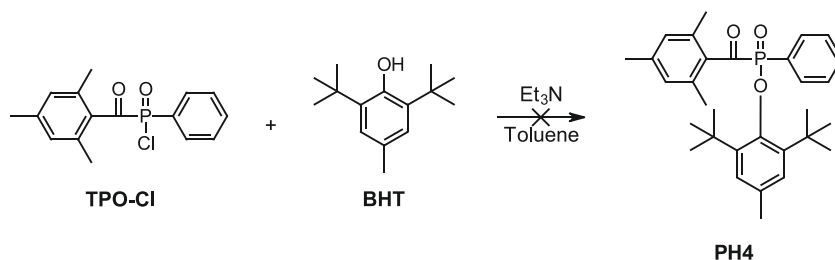
The preparation of **TPO-Cl** was conducted as described in the section 2.4.1.3. The subsequent reaction with 3,5-di-*tert*-butyl-4-hydroxytoluol (**BHT**) was carried out analogously to the literature.[111] No product formation could be observed at any time, and after work up, only the hydrolysis product of **TPO-Cl**, namely **TPO-OH** (Figure 78), was detected in the aqueous phase. It is assumed that the product formation is not possible due to the exceptional steric hindrance of **BHT**.
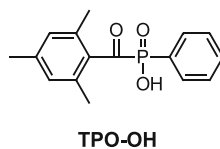
*Figure 78: Undesired hydrolysis product 2,4,6-trimethylbenzoylphenylphosphinic acid (**TPO-OH**).*

2.4.1.5 Synthesis of 2,4,6-trimethylbenzoyl-(ethylthio)phenyl-phosphine oxide (**PH5**)

The sulfur-substituted **TPO-L** pendant has been attempted to be synthesized using three different methods.

In the first approach, an attempt was made to conduct a Grignard-like reaction, as described in the patent literature of Suzuki et al.[101] This method would not have been the initial choice, but, the patent literature of Ye et al., detailing the synthesis of the precursor *S*-ethyl *P*-phenylphosphinothioate (**EtSPO**) resulted in the formation of another product, namely phenylphosphonochloridothious acid ethyl ester (**PCS**).[112]
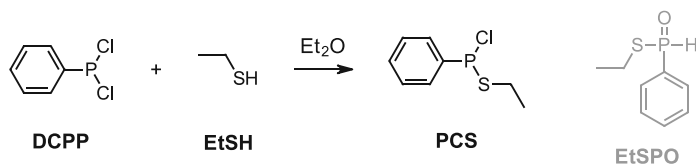
The crude product was attempted to be purified by fractional distillation, but minor impurities, most likely the disubstituted compound, could not be fully separated using this method. With a contamination of about 7% this liquid product which was obtained in 51% yield was used for the subsequent reaction.
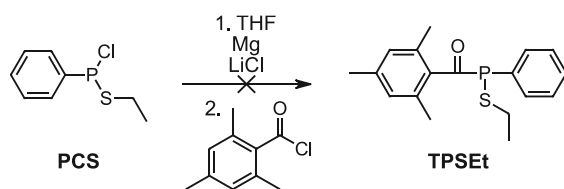
The reaction was performed based on the literature of Suzuki et al.[101] As previously described in section 2.3.1.3, the reaction encounters the challenge of having an unclear initiation phase. In this case it was assumed that the start of the reaction had been observed, which is why the further procedure was continued. However, contrary to previous experiments, no obvious reaction could be seen with the addition of 2,4,6-trimethylbenzoyl chloride, which could indicate that the conversion with magnesium was not successful. Since no conversion could be determined by reaction controls either, the reaction was discarded.

In the second approach, the reaction described by Ye et al. was repeated and extended with a hydrolysis step at the end to produce the desired precursor **EtSPO**.[112]
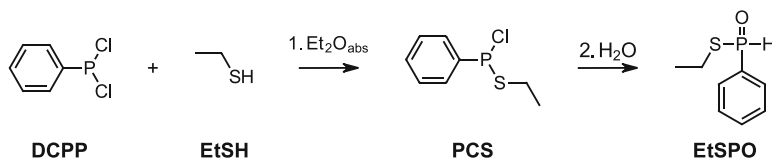
The reaction control of the first reaction step, detected the intermediate **PCS**, and residual educt **DCPP**. To avoid the formation of the disubstituted side-product, the reaction was stopped before full conversion was obtained. The reaction mixture was hydrolyzed by the addition of water and stirring for 10 min. After processing a mixed product containing **EtSPO** and most probably the corresponding disubstituted derivative were obtained, as suggested by UPLC-MS and NMR analysis. Since purification of similar substances has posed challenges, and it was assumed that this side-product would not impede the subsequent reaction, the substance mixture was used without further purification.

For the coupling reaction of **EtSPO** with 2,4,6-trimethylbenzoyl chloride the established method from the work of Zhang et al. was used.[99]
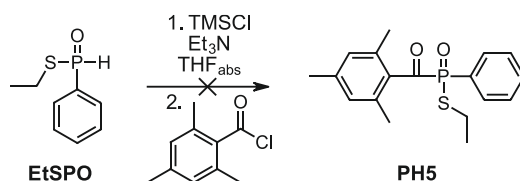
The reaction control by UPLC-MS confirmed that, as assumed, the side product from the precursor synthesis was evidently not involved in the reaction, as indicated by the consistent peak in the chromatogram. The precursor **EtSPO** itself, on the other hand, is reacted, but without forming the desired target molecule. At this point, it is unclear whether the reaction itself is unable to proceed, or if major or minor impurities from the precursor synthesis are inhibiting the reaction.

In the third attempt the highly efficient method for the preparation of monoacylphosphine oxides with phosphorus-bound heteroatoms, described in the work of Roszkowski et al. was used to prepare **PH5**.[111]
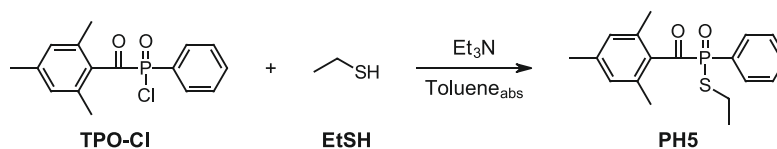
TPO-Cl was freshly prepared as described in section 2.4.1.3. The reaction mixture was stirred for 1 h, when complete conversion without any undesirable side reactions was

determined. After work up, the desired product was obtained nearly quantitatively as an orange viscous substance of high purity with a yield of 95%.

2.4.1.6 Synthesis of 2,4,6-trimethylbenzoyl-(ethylsulfonyl)phenyl-phosphine oxide (**PH6**)

To enhance the steric hindrance adjacent to the phosphorus and simultaneously modify the electronic situation, an attempt is made to oxidize the sulfur atom of **PH5**.

The first approach was carried out similarly to the procedure of Wu et al., using *meta*-chloroperoxybenzoic acid (***m*-CPBA**) as oxidizing agent.[113]
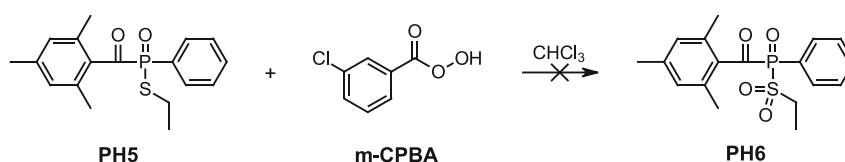
For this purpose, 1.5 eq. of ***m*-CPBA** were used and the reaction mixture was analyzed after 4 min., 30 min and 2 days reaction time with UPLC-MS. Reaction times longer than 4 min. did not result in any further reaction progress. The desired target product could not be detected, the majority part of **PH5** was still present at the end of the reaction and only a small part of the educt appears to have been converted to the undesired side-product **TPO-OH** (Figure 78).

In a second attempt using ***m*-CPBA**, **PH5** was directly mixed with 4 eq. of the oxidizing agent. This resulted in an exothermic reaction, which yielded complete conversion of PH5 to the undesired product **TPO-OH** (Figure 78).

The third approach was conducted using the monopersulfate compound Oxone® as oxidizing agent in analogy to the literature, where thioanisol was oxidized to the corresponding sulfone.[114]
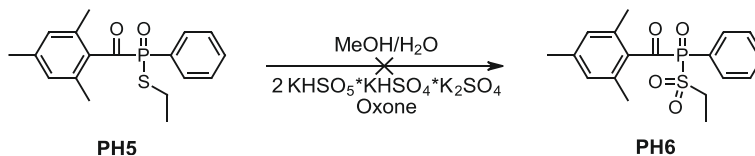
After 1 h 45 min and after 24 h reaction controls were carried out using UPLC-MS measurements. The desired target product could not be detected at any point in time.

Nevertheless, the educt **PH5** seems to be converted to two other monoacylphosphine oxides over time. One was identified as **TPO-OH** (Figure 78), which was formed to an extent of about 4% after 24h regarding the peak area at 254 nm in the UPLC-MS measurement. The second could be **TPO-OMe** (Figure 79), which would be appropriate with regard to the detected molecular weight of 302 g/mol. This product was formed to an extend of about 17% within 24 h, regarding the peak area at 254 nm in the UPLC-MS measurement. The conversion could be achieved by the reaction of **PH5** or the intermediate **TPO-OH** with methanol. Since this substance does not appear promising in terms of its absorption properties (λ_{max} (n→π*): 371 nm) and similarity to **TPO-L** as a photoinitiator, it was not further investigated.

TPO-OMe
[302.30]
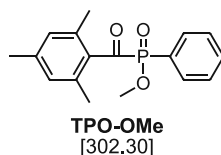
*Figure 79: Possible structure of the 2nd formed substance during the reaction of **PH5** with Oxone®.*

2.4.1.7 Synthesis of (2,4,6-trimethylbenzoyl)diphenylphosphine selenid (**PH7**)

<u>Pathway A)</u>

In the first attempt the target structure **PH7** was tried to be synthesized with the established synthesis method of Zhang et al.[99] For this synthesis the precursor diphenylphosphine selenide was commercially available.
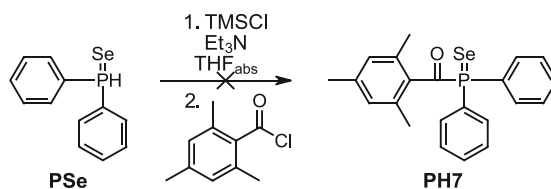
Reaction controls using UPLC-MS, ^{1}H-NMR and ^{31}P-NMR showed no evidence of a successful reaction at any point in time, therefore this reaction was discarded.

Pathway B)

In the second attempt, the non-oxidized precursor **TP** should be prepared in the first step, according to literature.[115] In a subsequent reaction this precursor is to be oxidized by elemental selenium, as described by Kumar et al., to yield **PH7**.[116]
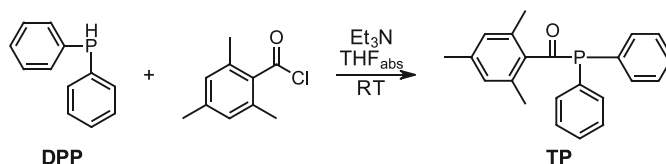
The reactants diphenylphosphine (**DPP**) and 2,4,6-trimethylbenzoyl chloride were used in equimolar amounts. After stirring for 24 h full conversion of 2,4,6-trimethylbenzoyl chloride was determined by GCMS and ^{31}P-NMR, but residual DPP was observed. After filtration through a bed of silica and evaporation of the solvent, residual **DPP** was removed at high vacuum at 70°C. An attempt was made to purify the crude product by recrystallization from methanol, but no precipitation could be achieved. Therefore, the solvent was removed and the crude product was used without further purification for the subsequent reaction.

In the subsequent reaction TP was stirred vigorously with 1.2 eq. elemental selenium for 16 h.
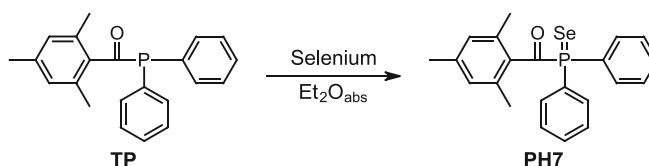
The reaction control by ^{31}P-NMR, revealed the formation of a P-Se bond by a strong signal with a typical triplet coupling pattern. An UPLC-MS measurement, in which aqueous non-inert conditions prevailed, showed a large number of peaks, one of which produced an absorption spectrum similar to that of **TPO** (Figure 81). In the corresponding mass spectrum, a pattern typical for selenium was detected, but no clear molecular peak. In the positive mode m/z values of 547 and 559 are most prominent with the selenium pattern, in the negative those at 281 and 343. No observed signal matches the molecular mass of 411.33 of the target molecule.

After workup and removing the solvent, the crude product was analyzed by ^{31}P-NMR, whereby the typical P-Se coupling and the supposed product were no longer observed. A repeated measurement of the inert filled ^{31}P-NMR reaction control also did not show this signal anymore. It is therefore assumed that the product is highly unstable, which is why its preparation is not pursued further.

2.4.2 Characterization

The PH-modified photoinitiators **PH1** – **PH3** and **PH5** were investigated with regard to their absorption behavior, their reactivity and their discoloration behavior in polymer samples. Furthermore, DFT calculations were performed to predict the reactivity of some relevant phosphanoyl radicals.

2.4.2.1 UV-Vis spectroscopy

For the investigation of the absorption behavior of the MAPOs modified with substituents linked to phosphorus via a heteroatom (PH-modified), UV-Vis spectra of 0.001 M solutions in acetonitrile were recorded. Figure 80 illustrates the absorption bands of the n→π* transition of **PH1** – **PH3** and **PH5** in comparison to **TPO** and **TPO-L**. In Table 13 the corresponding values for λ_{max} (n→π*) and the extinction coefficients (ε) at 385 nm and 400 nm are summarized.
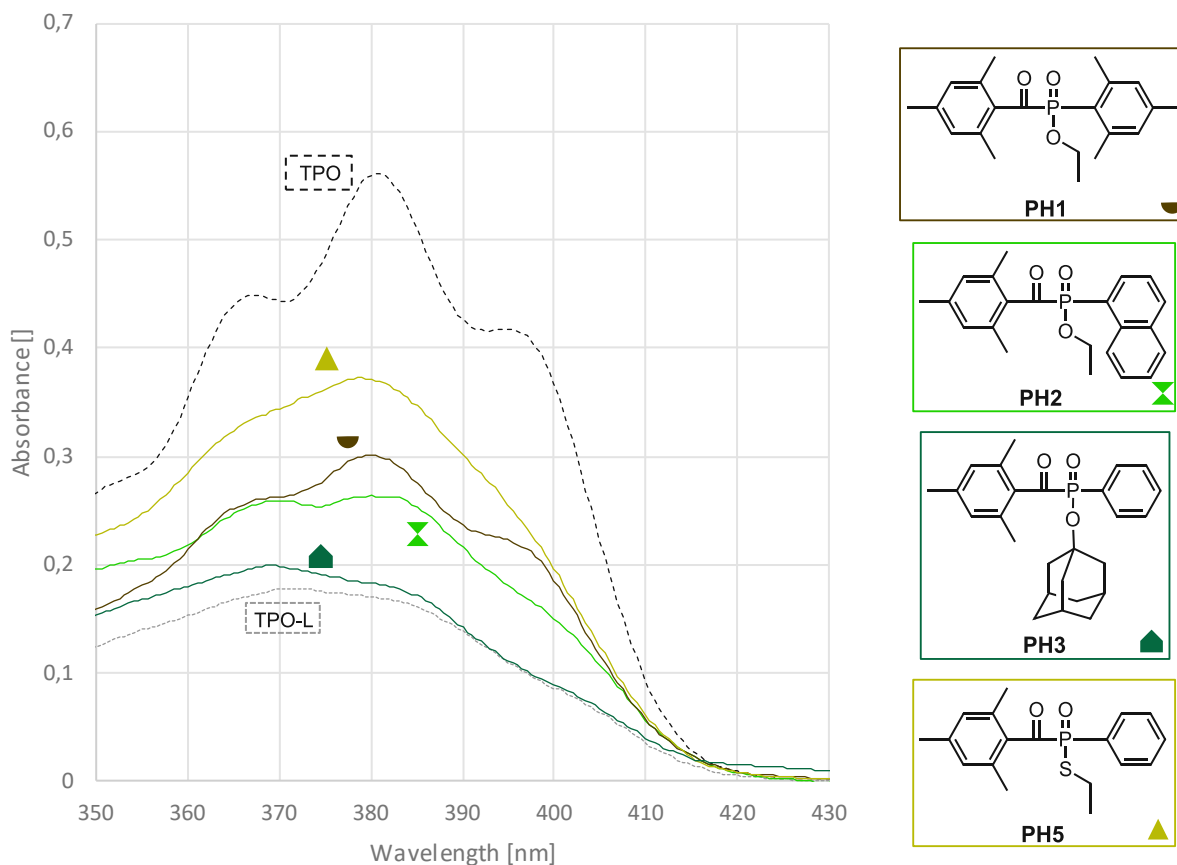
*Figure 80: UV-Vis spectra of solutions of the PH-modified MAPOs **PH1** – **PH3** and **PH5** in comparison with **TPO** and **TPO-L** (c = 0.001 M in acetonitrile).*

Table 13: Wavelength of the absorption maximum (λ_{max} (n→π)) and molar extinction coefficient (ε) at 385 nm and 400 nm of the PH-modified MAPOs **PH1** – **PH3** and **PH5** in comparison to **TPO** and **TPO-L**.*

	λ_{max} (n→π*)	$\varepsilon_{\lambda max}$ (L·mol^{-1}·cm^{-1})	$\varepsilon_{385\ nm}$ (L·mol^{-1}·cm^{-1})	$\varepsilon_{400\ nm}$ (L·mol^{-1}·cm^{-1})
TPO	381	561	510	367
TPO-L	371	178	161	86
PH1	380	301	276	186
PH2	380	264	254	150
PH3	369	199	172	89
PH5	379	373	347	196

Considering Figure 80, it can be seen that all PH-modified derivatives show improved absorption behavior compared to **TPO-L**. The absorption spectrum of **PH1** has a main peak with two shoulders that resemble the shape of the absorbance of **TPO**, although the

General part

extinction is comparatively lower. The three methyl groups of **PH1** therefore appear to bring the chromophore into a favorable spatial position. In the case of **PH2** the naphthyl substituent seems to have a similar effect, but particularly the left shoulder of the absorbance is pronounced. The adamantanyl ring of **PH3**, on the other hand, did not achieve the desired result. Although a certain improvement in terms of extinction can be observed compared to **TPO-L**, this is only marginal. In this case, the left shoulder appears to be even more prominent than in **PH2**, so that this represents the absorption maximum (λ_{max}) and thus causes a hypsochromic shift of λ_{max} compared to **TPO-L**. **PH5** shows an absorption spectrum with the comparatively highest extinction coefficients of this series. The shoulders that can be seen in the absorption spectrum of **TPO** are less pronounced but can already be recognized. Whether this improved absorption behavior is due to the steric requirement of the sulfur atom or its electronic effects is not certain at this point.

In addition to the actually produced and isolated PH-modified MAPOs, the attempt to synthesize the selenium-containing **PH7** (2.4.1.7) revealed a substance with an absorption behavior similar to **TPO**. Whether this is actually attributable to the target structure **PH6** remains unclear. The absorption spectrum recorded in the UPLC-MS measurement of the reaction mixture is shown in Figure 81.
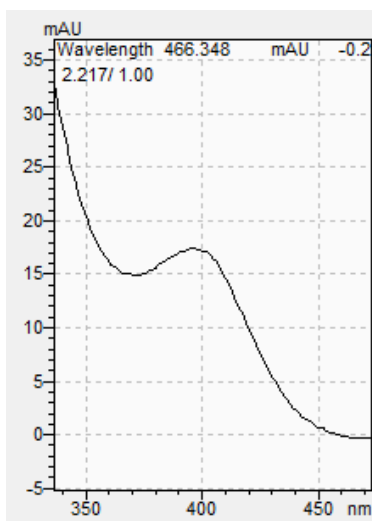
*Figure 81: Absorption spectrum of a substance separated from the reaction mixture of the synthesis of **PH7** by UPLC. The spectrum was recorded with a PDA-detector.*

If this spectrum is indeed attributed to the substance **PH7**, replacing the double-bonded oxygen at the phosphorus of **TPO** with selenium would result in a distinct bathochromic shift of λ_{max} of about 9 nm. In addition, the tail out is extended to about 450 nm in this spectrum, whereas with **TPO** it is only up to 420 nm.

2.4.2.2 DFT calculations of phosphanoyl radicals

DFT calculations were carried out at TU Graz in the working group of Prof. Georg Gescheidt and were used to determine the phosphorous hyperfine coupling constant a(P), of phosphanoyl radicals with different phosphorous-bound substituents. A high a(P) is associated with a high quenching constant and thus a high radical reactivity. Table 14 shows the calculated values for a(P) with varying heteroatom containing substituents for R^1 and R^2.

Table 14: DFT calculated ^{31}P hyperfine coupling constants a(P) for different phosphanoyl radicals.

		R^1	
		Ph	
R^2	Ph	320	**TPO**
	OMe	434	
	OEt	434	**TPO-L**
	SEt	400	**PH5**
	S(O)$_2$Et	302	**PH6**

The comparison of the OMe and the OEt substituent shows that the length of the alkyl residue on the oxygen atom does not appear to have a major effect on the a(P) value. Replacing the oxygen with sulphur appears to reduce the reactivity of the resulting P-radical. For this, the lower +M and -I effects of the sulfur could be a contributing factor. In the case of S(O)$_2$Et rather a -M effect can be assumed, which seems to have a negative influence on a(P).

2.4.2.3 Photo-DSC

Photo-DSC measurements were carried out to determine the reactivity the photoinitiators of the PH-modified MAPO photoinitiators (**PH1** – **PH3**, **PH5**). Homogenous formulations

General part

consisting of 1.0 mol% of the respective photoinitiator in **UDMA** were prepared. As the individual initiators differ in terms of their absorption behavior, they were evaluated using three different light sources.
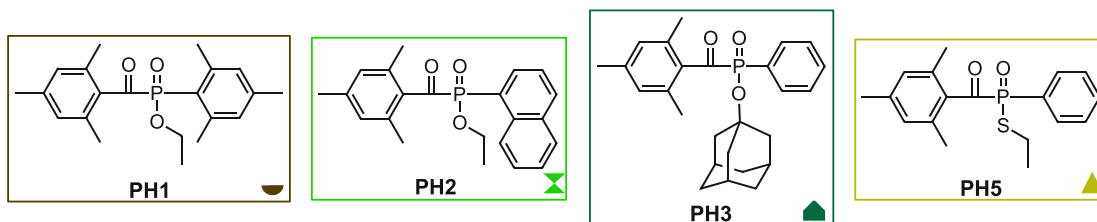
320 – 500 nm broadband light source (OmniCure® S2000)

For the first set of measurements an OmniCure® S2000 high pressure mercury vapor light source equipped with a 320 – 500 nm filter was used as light source. The light intensity at the sample surface was set to 64 mW/cm². The main results are summarized in Table 15, the complete data and the corresponding diagrams of the measurements can be found in the experimental section (2.4.2.3).

Table 15: Results of photo-DSC measurements of formulations, consisting of 1 mol% photoinitiator in the monomer UDMA, under irradiation with a broadband light source (320-500 nm) with an intensity of 64 mW/cm².

320-500 nm	t_{max} [s]	R_p [mmol*L⁻¹*s⁻¹]	$t_{95\%}$ [s]	DBC [%]
TPO	4.3 ± 0.2	176.0 ± 3.5	34.0 ± 1.6	64.2 ± 0.1
TPO-L	5.1 ± 0.3	147.8 ± 5.3	32.4 ± 1.5	58.9 ± 0.5
PH1	5.1 ± 0.1	147.6 ± 2.3	33.6 ± 0.9	57.6 ± 0.9
PH2	6.3 ± 0.3	137.5 ± 1.6	35.9 ± 1.7	58.0 ± 0.5
PH3	5.6 ± 0.1	141.9 ± 0.7	32.7 ± 0.6	57.0 ± 0.5
PH5	6.3 ± 0.2	121.8 ± 2.0	36.7 ± 0.9	54.9 ± 1.0

When irradiating the samples using a broadband light source (320-500 nm) the prepared PH-modified photoinitiators cannot compete with **TPO**. In comparison with **TPO-L**, only **PH1** exhibits a performance that is on an equal level with **TPO-L**. **PH3** is slightly inferior to **TPO-L**. **PH2** performs worse especially in terms of t_{max}, R_P and $t_{95\%}$ but achieves similar values at the DBC. **PH5**, on the other hand, performs worse than **TPO-L** in all measured parameters, which is obviously attributed to the phosphorous bound sulfur.

385 nm LED light source

Next the samples were examined using a 385 nm LED light source with a light intensity of 10 mW/cm^2 at the surface of the samples. The main results are summarized in Table 16, the complete data of the measurements is available in the experimental section (2.4.2.3).

*Table 16: Results of photo-DSC measurements of formulations, consisting of 1 mol% photoinitiator in the monomer **UDMA**, under irradiation with a LED light source (385 nm) with an intensity of 10 mW/cm^2.*

385 nm	t_{max} [s]	R_p [mmol*L^{-1}*s^{-1}]	$t_{95\%}$ [s]	DBC [%]
TPO	5.5 ± 0.2	138.5 ± 1.5	32.2 ± 1.1	57.7 ± 1.5
TPO-L	6.1 ± 0.0	131.0 ± 4.2	35.2 ± 1.5	56.3 ± 0.8
PH1	6.2 ± 0.0	126.4 ± 1.8	35.5 ± 0.7	54.8 ± 0.5
PH2	7.5 ± 0.1	108.8 ± 3.6	38.2 ± 1.7	51.6 ± 0.7
PH3	6.3 ± 0.3	124.8 ± 1.6	36.6 ± 0.7	53.6 ± 0.6
PH5	7.8 ± 0.2	101.3 ± 1.5	38.7 ± 0.9	50.8 ± 0.9

When irradiated with a 385 nm LED light source, similar trends are observed as with broadband irradiation (320-500 nm). Whereby the performance of **PH1** in this case is also slightly inferior to that of **TPO-L**. **PH3** exhibits a similar performance in relation to **TPO-L** as before, but **PH2** and **PH5** seem to lag even further behind.

400 nm LED light source

The examination of the samples using a 400 nm LED light source was also conducted with a light intensity of 10 mW/cm^2 at the surface of the samples, to obtain comparability with the values at 385 nm. The main results are summarized in Table 17, the complete data of the measurements is available in the experimental section (2.4.2.3).

Table 17: Results of photo-DSC measurements of formulations, consisting of 1 mol% photoinitiator in the monomer UDMA, under irradiation with a LED light source (400 nm) with an intensity of 10 mW/cm².

400 nm	t_{max} [s]			R_p [mmol*L^{-1}*s^{-1}]			$t_{95\%}$ [s]			DBC [%]		
TPO	5.3	±	0.1	156.8	±	1.3	30.5	±	0.3	60.8	±	0.3
TPO-L	6.4	±	0.0	134.9	±	3.1	34.7	±	1.5	56.5	±	0.9
⏏ PH1	5.8	±	0.0	129.6	±	5.2	35.6	±	0.2	55.2	±	0.9
⏳ PH2	7.5	±	0.4	113.8	±	1.5	38.9	±	1.6	53.5	±	0.7
⬟ PH3	7.2	±	0.2	114.5	±	1.8	35.5	±	1.3	51.4	±	1.0
▲ PH5	8.0	±	0.1	104.8	±	1.7	37.3	±	0.0	51.7	±	0.7

When irradiated with 400 nm the overall performance of **PH1** has improved compared to 385 nm and is prior to **TPO-L** with regard to t_{max}. This indicates effective cleavage of **PH1** at this wavelength. In terms of R_p and DBC, however, **PH1** is slightly behind, which in turn could suggest a lower radical reactivity. The reactivity of **PH2** has also improved minimally compared to irradiation with 385 nm. **PH3**, on the other hand, worsened in all values in this comparison. **PH5** gives similar results at both wavelengths.

2.4.2.4 Discoloration behavior

<u>UV-Vis spectroscopy method</u>

The assessment of the discoloration behavior using the UV-Vis method was carried out as described in section 1.2.1. The resulting difference absorption spectra are summarized in Figure 82. Since all PH-modified photoinitiators exhibit the same 2,4,6-trimethylbenzoyl chromophore, the assessment of the discoloration behavior using the UV-Vis method is reasonable.
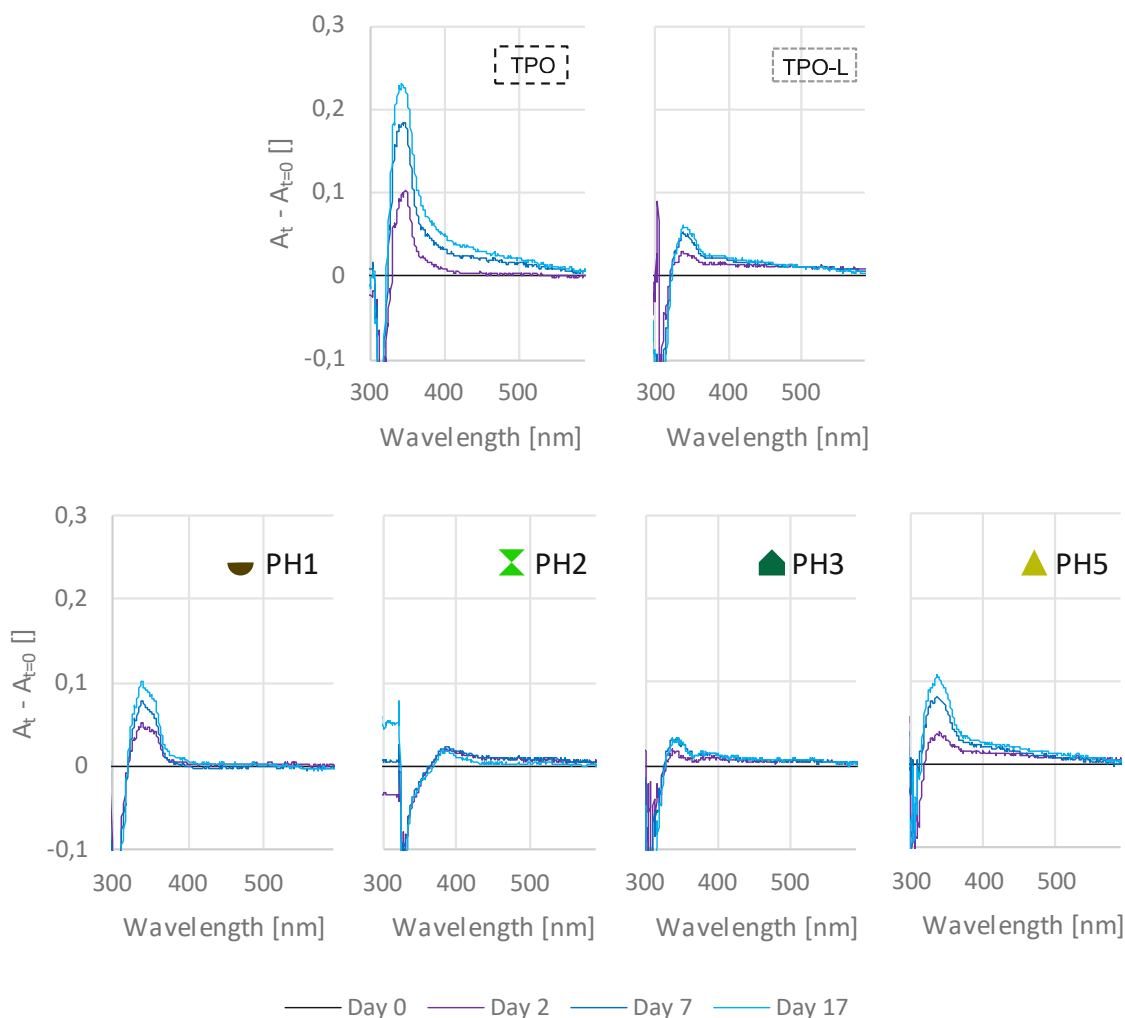
*Figure 82: Time-dependent difference absorption spectra of thin film samples consisting of **UDMA** (stabilized with 100 ppm **MeHQ**) and the PH-modified photoinitiators **PH1**– **PH3**, **PH5**, **TPO**, and **TPO-L** (1.07 mol%).*

Figure 82 demonstrates that all PH-modified photoinitiators exhibit improved discoloration behavior compared to **TPO**. The absorbances caused by **PH1** and **PH5** are between those of **TPO** and **TPO-L**, while those of **PH2** and **PH3** are the same or even slightly lower than those of **TPO-L**.

2.4.3 Conclusion

It has been shown that the absorption behavior of PH-modified MAPOs can be adjusted depending on the substituents. Although no bathochromic shift of the n→π* transition could be achieved with these modifications, the absorbance of **TPO-L** could be adjusted towards that of **TPO**. Thus, by introducing a large sulfur atom in **PH5**, a mesitylene ring

in **PH1** or a naphthyl group in **PH2**, higher extinction coefficients and a more **TPO**-like shape could be achieved. The introduction of the sterically demanding adamantanyl substituent, which is bound to oxygen in **PH3**, had only a minor effect on the absorption behavior.

Despite some promising absorption spectra, the substances could achieve satisfactory results in the photo-DSC experiments. Only **PH1** could partially match the performance of **TPO-L**, while **PH3** could only approach it at 385 nm. **PH2** and especially **PH5** have performed significantly worse. It is possible that the resulting P-radicals of **PH1** and **PH2** are significantly less reactive than those of **TPO-L** due to resonance stabilization via the mesitylene or naphthyl residue. In the case of **PH3** the size of the resulting P-radical could limit mobility and thus make it less reactive. The P-radical of **PH5** is known to be less reactive from the DFT calculations.

Regarding the discoloration behavior, **PH2** and **PH3** seem to achieve similarly good results as the **TPO-L** reference. Analogous to the P-modified equivalent **P4**, the PH-modified **PH1** also exhibits a stronger discoloration than the reference. Therefore, the mesitylene residue obviously has a negative effect on the discoloration behavior. The sulfur containing **PH5** exhibits not only low reactivity, but also worsened discoloration behavior compared to **TPO-L**.

Summary

The color stability of dental restorative materials holds paramount importance in modern dentistry, in order to meet the esthetic expectations of modern standards. Particularly, photopolymers, which are now indispensable for a large number of dental applications, are unable to consistently meet these high requirements. Due to intrinsic factors, they tend to discolor to a certain degree over time, necessitating improvements in this aspect. Literature suggests various causes for this discoloration, but particularly the monomers and photoinitiators used seem to have a significant influence on the discoloration behavior.[10, 29, 30, 57-65] Concerning monomers, unreacted double bonds are considered to be responsible for discoloration, but correlations have also been found between water absorption and water solubility of the monomer and the discoloration behavior.[10, 58] As for photoinitiators, higher concentrations may lead to incomplete bleaching, resulting in discoloration due to residual photoinitiator.[62-64] Additionally, distinct photoinitiators are associated with varying discolorations, with suspected contributions from the photolysis products formed.[65, 66] Within this thesis, the underlying causes of these discolorations and factors influencing them were investigated, in order to develop solutions for mitigating or entirely eliminating them.

Indeed, an influence of the applied monomer on both the intensity and duration of the discoloration was observed, although not on the type of discoloration. Additionally, storage conditions such as temperature, humidity and atmosphere were identified as factors influencing the quantitative aspect of discoloration. However, the photoinitiators appear to be the underlying cause of the discoloration. The structure of their benzoyl chromophore emerged as the decisive factor influencing the wavelengths at which specific absorbances occur. While the exact nature of the species responsible for the observed absorbances remains unclear, it appears that certain radicals become trapped in the polymer matrix, leading to discoloration over time.

Three different strategies were developed to counteract discoloration. The first method directly addresses the photoinitiator. By incorporating sterically demanding substituents at the *ortho*-positions of the benzoyl moiety, discoloration can be effectively reduced. It is assumed that due to the steric requirement, the resulting radicals are less accessible and

therefore preventing the formation of colored secondary products. However, regrettably, the exceptionally high reactivity of **TPO** could not be entirely retained with this method.

The second approach achieves improved discoloration behavior by the targeted incorporation of stabilizers. Interestingly, significant variations were observed depending on the type of stabilizer added. While certain stabilizers induce the formation of colored species during the stabilization process, and thus counteract the actual purpose, others prove highly effective in reducing discoloration. Pyrogallol (**PyG**) and 4-methoxyphenol (**MeHQ**), in particular, exhibited exceptional efficacy in this regard. The stabilizer 2,3,4-trihydroxybenzaldehyde (**4-APG**) seems to suppress the discoloration completely, although a different mechanism is suspected here.
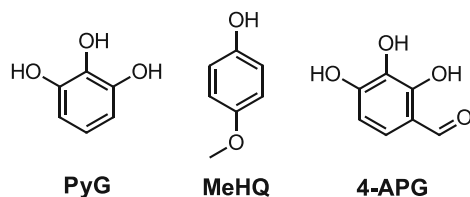
The observation that the samples stored in an oxygen atmosphere experienced less discoloration and the distinct discoloration behavior exhibited by the stabilizer **4-APG**, led to the third and most effective method of suppressing discoloration. Through the addition of the oxidizing agent cumene hydroperoxide (**CHP**) the emergence of absorbances in the visible wavelength range is completely prevented. It is assumed that **CHP** promptly oxidizes precursors of the substances responsible for discoloration and thereby suppress their formation entirely.
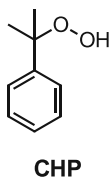
In the second part of the study, alternative options to **TPO** as a photoinitiator were explored due to concerns regarding potential health hazards. As **TPO** finds application in 3D printing of dental materials, any appropriate substitute must fulfill a multitude of criteria. These include high reactivity, effective absorption at the wavelength of the printing device (385 nm), excellent photobleaching properties and high color-stability of the resulting polymers.

In order to meet these requirements, diverse monoacylphosphine oxide derivatives were designed, synthesized, and characterized. As previously mentioned, the modification of the benzoyl part with sterically demanding substituents, resulted in photoinitiators capable of producing particularly color stable polymers. Although these initiators did not reach the performance of **TPO**, some were prepared that outperformed **TPO-L**. Particularly, photoinitiators **B1** and **B4-2** achieved a favorable balance between superior color stability and reactivity. Furthermore, these experiments elucidated how certain *ortho-* and *para*-substituents on the benzoyl part affect the absorption behavior.

B1　　　　　　　　　　　B4-2
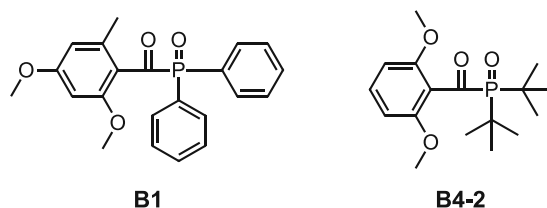
The exploration extended to derivatives modified at the phosphorus atom of **TPO**. By introducing altered alkyl and phenyl substituents an improvement of both the absorption properties and the reactivity of the photoinitiators could be achieved. Especially the modification with the sterically demanding *tert*-butyl groups of **P2** and **P3** resulted in particularly favorable properties. For **P2** a bathochromic shift of λ_{max} by 5 nm could be achieved, for **P3** it was even 9 nm, compared to **TPO**. Moreover, **P2** demonstrated the highest reactivity, outperforming **TPO** across all tested wavelengths in photo-DSC experiments. These remarkable results were attributed, through steady state photolysis experiments, laser flash photolysis experiments and DFT calculations, mainly to the higher quantum yields of **P2**. Although **P3** did not achieve the same performance as **TPO** in these experiments, it demonstrated a significant improvement in performance when irradiated with a 400 nm LED in comparison to the 385 nm LED. This suggests that this derivative, with a pronounced bathochromic shift in the absorption spectrum, may achieve its maximum performance at even higher wavelengths. Another outcome of this series of experiments was that the DFT calculations could indeed accurately predict radical reactivities of P-centered radicals.

P2 **P3**
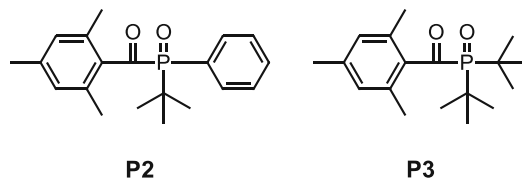
Lastly, the investigation extended to the modification of phosphorus with heteroatom substituents, similar to **TPO-L**, with the anticipation of potentially enhancing the toxicological properties compared to **TPO**. Based on the success of prior approaches, attempts were made to introduce sterically demanding residues in this context as well. Indeed, contrary to **TPO-L**, an improved absorption behavior could be achieved. However, in the photo-DSC experiments, only one derivative, namely **PH1**, could at least compete with the performance of **TPO-L**.

PH1
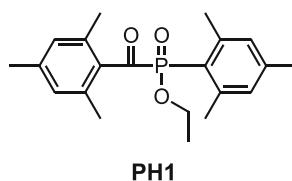
Experimental part

1 Color-stability of light cured dental materials

1.2 Determination of the color change

1.2.1 UV-Vis method

<u>Sample preparation</u>

For the preparation of the formulations all ingredients are weighed into amber glass vials and alternately heated to 50°C, homogenized using a vortex mixer and placed into an ultrasonic bath until all components are completely dissolved. A standard formulation consists of the monomer **UDMA** (stabilized with 100 ppm **MeHQ**) and 1.07 mol% of the photoinitiator **TPO**. From these formulations thin film samples are produced using a photorheometer coupled with suitable light source. The exact construction and possible applications of this device are described in the work of Gorsche et al.[78] For the preparation of the polymer samples, a polyethylene tape (TESA 4668 MDPE) is applied to the glass plate of the photorheometer and the light intensity on the surface is calibrated to 10 mW/cm². An adequate sample quantity is applied, the gap width is fixed at 1200 µm and the temperature is set to 25°C. Afterwards the samples are irradiated for 300 seconds to be cured. Subsequently the stamp is removed and the samples carefully detached from the PE tape. The samples are then post-cured on both sides using the PrograPrint® Cure device (405 nm/460 nm; Program: "Model"; 3 min; 270 mW/cm²). Using a scalpel and if necessary, sandpaper, strips no wider than 10 mm were cut from the round samples, fitting upright in a 10x10 mm quartz glass cuvette of a spectrophotometer.

<u>Light sources</u>

The applied light source was selected depending on the photoinitiator used. For curing **TPO** and **BAPO** based samples, an OmniCure® LX500 LED Spot UV Curing System with a 385 nm LED head was used. A medium pressure mercury lamp in an OmniCure® S2000 Spot UV curing system together with a 400-500 nm filter was used for curing Ivocerin®-based samples and a 320-500 nm filter was applied for curing **I2959**-, **D1173**- and **I184**-based samples. Furthermore, the samples including **I2959**, **D1173** and **I184**

were not post-cured with the PrograPrint® Cure device, but with an Uvitron IntelliRay 600 UV flood curing system (broadband, 15 min., UV-A: 125 mW/cm², Vis: 125 mW/cm²).

Storage

The samples were stored in light-protected polypropylene containers and occasionally removed to be measured. For dry stored samples, the lid is placed on the container without any further precautions. Wet stored samples are completely immersed in deionized water, before the container is closed. To provide specific atmospheres (argon, oxygen), the samples are placed in round bottom flasks with stopcocks, which are evacuated and ventilated with the desired gas for three times. For the UV-Vis absorption measurements the samples were removed and the desired atmosphere recreated afterwards. For storage at certain temperatures, the containers were placed a in drying oven at the desired temperature. The thin film samples are stored at 37°C under dry conditions as standard.

Measurements

The absorption spectra are recorded using a Thermo Scientific™ NanoDrop™ One spectrophotometer. The cut thin film samples are measured standing upright in a 10x10 mm quartz cuvette. Liquid samples are measured as solutions in acetonitrile, in a 10x10 mm quartz cuvette, unless otherwise noted. The spectra are recorded from 250 nm – 850 nm and a baseline correction is executed at 750 nm.

Evaluation

To create the diagrams of the absorption measurements, the measured absorbance values are plotted against the wavelength. For the creation of the difference spectra the absorbance values at a respective wavelength of day 0 are subtracted from those of the other days. For the graphs depicting the change in absorbance over time at a particular wavelength, the absorbance values for each time measurement at the certain wavelength are plotted against the time.

1.2.2 CIELAB

The measurements in the CIELAB color space are carried out by the company Ivoclar AG. Formulations are prepared for the measurements, which are homogenized with a magnetic stirrer. The respective compositions are stated with the individual measurements. The test specimens are produced in a steel ring mold (Ø=20 mm, H=2 mm) and cured on both sides using the PrograPrint® Cure device (405 nm/460 nm; Program: "Splint"). The cured polymer samples are stored at 50°C immersed in water. The measurements are performed using a CM3700d (Konica Minolta) spectrophotometer, in transmitted light against black and white reference surfaces. The color change (ΔE) is determined using the following formula:

$$\Delta E = \sqrt{\Delta L^2 + \Delta a^2 + \Delta b^2}$$

1.3 Studies on the discoloration of polymers

1.3.1 Preliminary tests

<u>UDMA purification</u>

Conventional **UDMA** (stabilized with 100 ppm **MeHQ**) was purified by column chromatography. For this purpose, 10 g of **UDMA** were applied in liquid form to a column loaded with 435 g silica gel and conditioned with PE:EE (70:30). A pure **UDMA** fraction was obtained by gradient elution. The solvent was removed and the product dried at high vacuum. The monomer obtained was used to prepare a thin film sample with **TPO** (1.07 mol%). The sample was stored together with a reference sample consisting of untreated **UDMA** and **TPO** (1.07 mol%) under standard storage conditions. The difference spectra of the corresponding absorption measurements are shown in Figure 83.
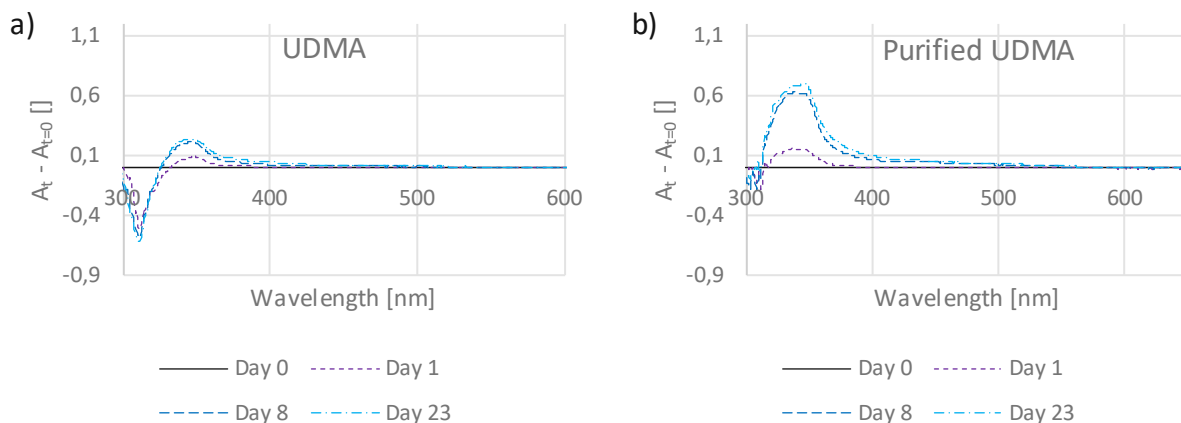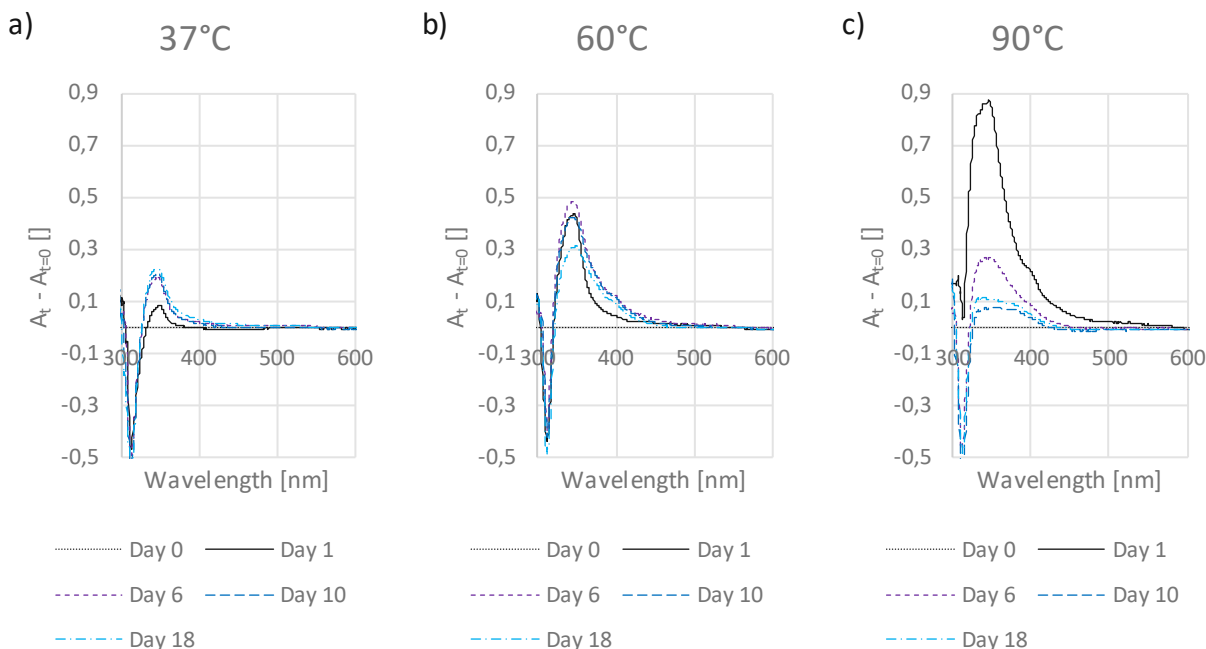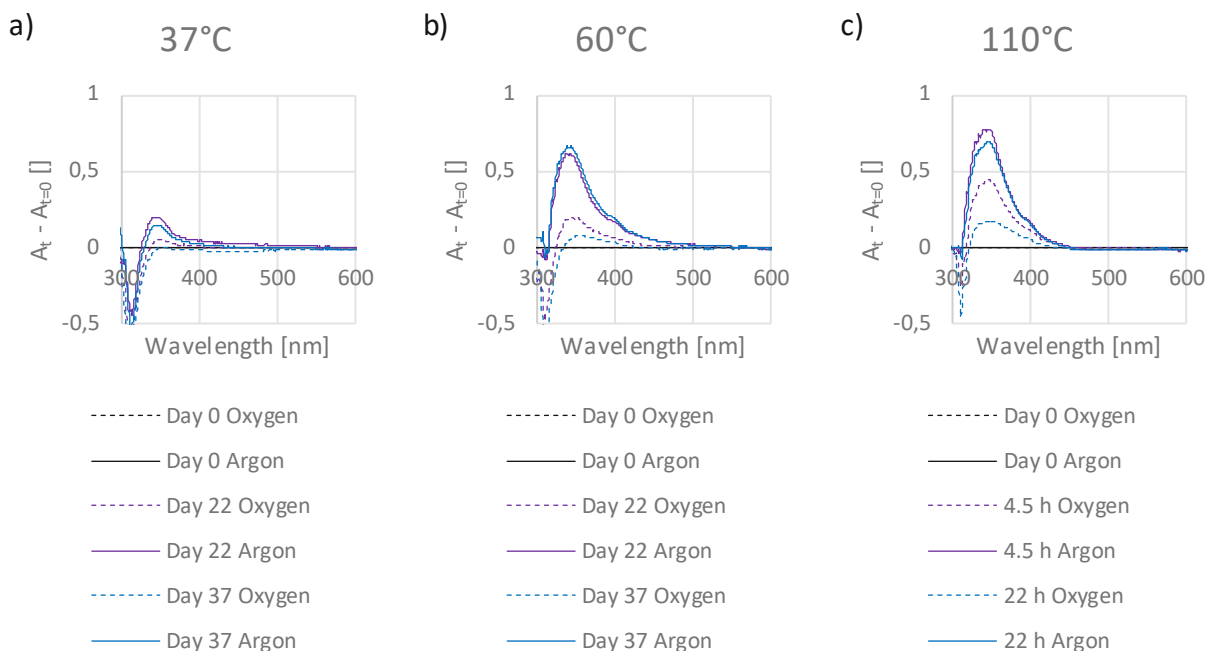
*Figure 83: Time-dependent difference absorption spectra of thin film samples consisting of **TPO** (1.07 mol%) and untreated **UDMA** (a), or purified **UDMA** (b).*

MeHQ addition test

For the formulation with additional **MeHQ**, a small quantity of **MeHQ** was initially added to determine the appropriate quantities of the other ingredients thereafter. In this way, a sample consisting of **UDMA** (stabilized with 100 ppm **MeHQ**), **TPO** (1.07 mol%) and additional 300 ppm **MeHQ** was produced. This sample is designated as "400 ppm **MeHQ**" and compared with a standard blind sample (100 ppm **MeHQ**). The resulting difference spectra of these samples are shown in Figure 84.
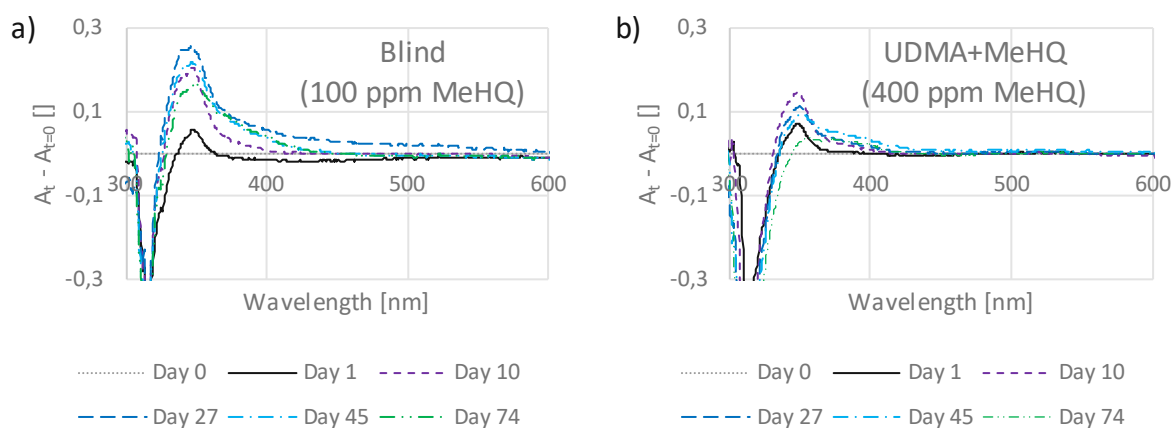
*Figure 84: Time-dependent difference absorption spectra of thin film samples consisting of **UDMA** (stabilized with 100 ppm **MeHQ**) and **TPO** (1.07 mol%) (a) and additional 300 ppm **MeHQ** (b), stored dry at 37°C.*

Experimental part

1.3.2 Storage conditions

Standard thin film samples consisting of **UDMA** and **TPO** (1.07 mol%) were exposed to different storage conditions and evaluated by means of UV-Vis absorption measurements. Figure 85 depicts the difference spectra of two samples stored at 37°C, one under dry conditions (a) and one under wet conditions, immersed in deionized water (b).

a)

b)
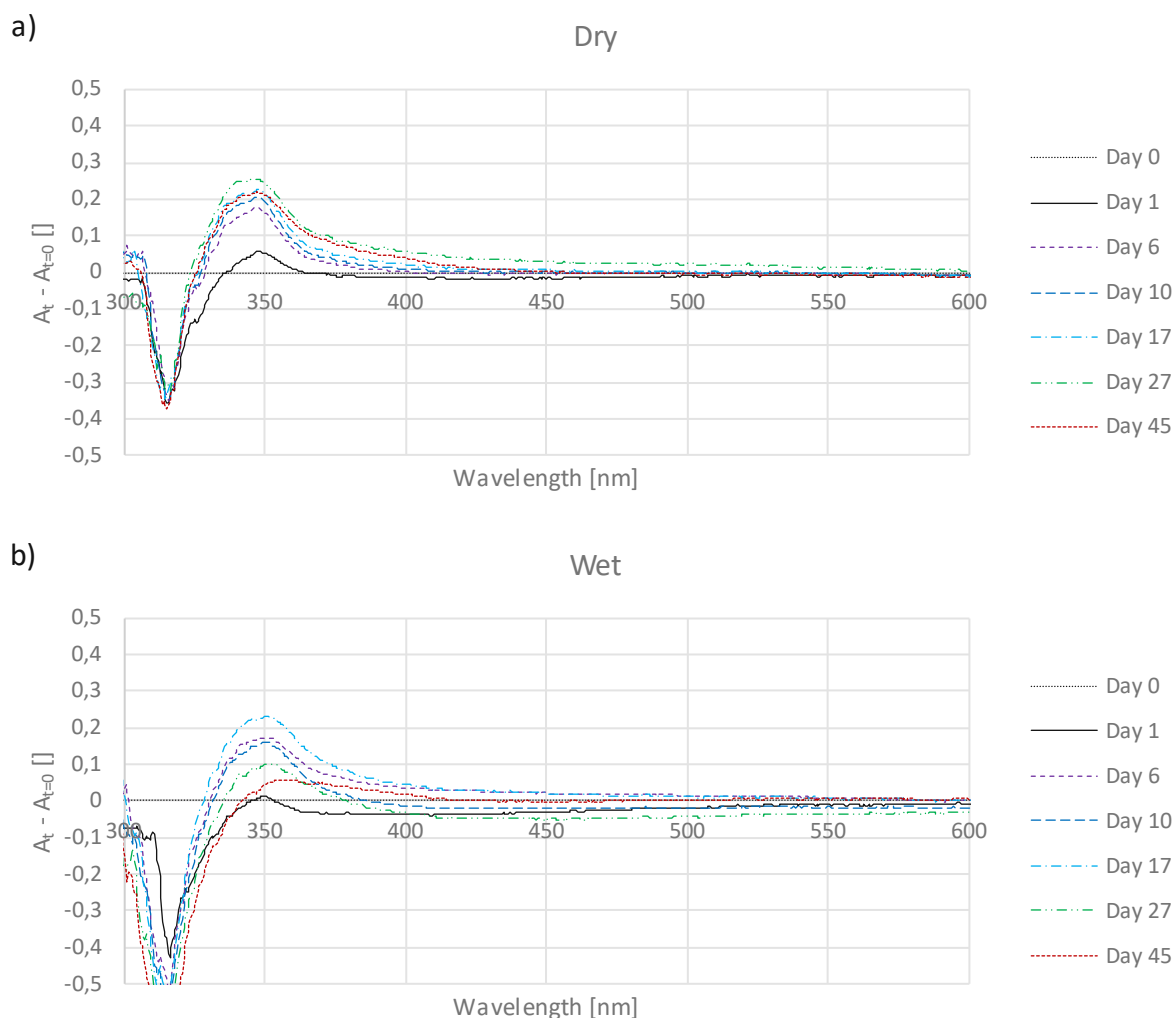
*Figure 85: Time-dependent difference absorption spectra of standard thin film samples consisting of **UDMA** and **TPO** (1.07 mol%), stored at 37°C under dry (a) or wet (b) conditions.*

In Figure 86 standard difference absorption spectra of thin film samples, stored dry at different temperatures are shown.

a) **37°C**

b) **60°C**

c) **90°C**

Day 0 .... Day 1 ——— Day 6 ------ Day 10 ----- Day 18 –·–·–

*Figure 86: Time-dependent difference absorption spectra of standard thin film samples consisting of **UDMA** and **TPO** (1.07 mol%), stored under dry conditions at 37°C (a), 60°C (b), or 90°C (c).*

The difference spectra shown in Figure 87 compare standard thin film samples, stored under oxygen or argon atmosphere, at different temperatures. The samples were stored in tightly sealed round-bottom flasks equipped with a stopcock. The particular atmosphere was achieved by alternately evacuating and ventilating the flasks three times with the respective gas using a balloon. For the absorption measurements, the samples were removed and the respective atmosphere was recreated afterwards.

*Figure 87: Time-dependent difference absorption spectra of standard thin film samples consisting of **UDMA** and **TPO** (1.07 mol%), stored under oxygen (dashed lines), or argon (solid lines) atmosphere, at 37°C (a), 60°C (b), or 110°C (c).*

1.3.3 Photoinitiators

Figure 88 depicts difference absorption spectra of thin film samples, consisting of **UDMA** and varying concentrations of the photoinitiator **TPO**. The specimens were stored at 37°C under dry conditions.

Experimental part

a) **0.4 wt%**

b) **0.8 wt%**

c) **1.2 wt%**
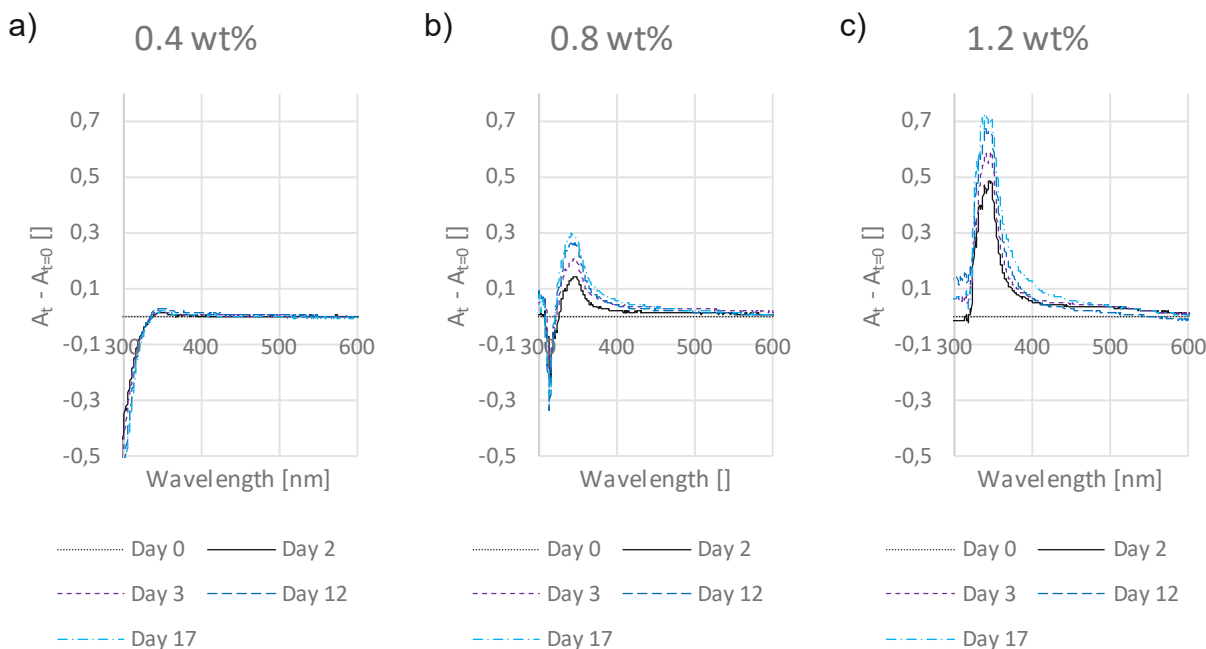
*Figure 88: Time-dependent difference absorption spectra of standard thin film samples, consisting of **UDMA** and 0.4 wt%% ≙ 0.54 mol% (a); 0.8 wt% ≙ 1.1 mol% (b); 1.2 wt% ≙ 1.62 mol% (c) of the photoinitiator **TPO**, stored dry at 37°C.*

The preparation of the samples containing different photoinitiators was basically carried out as described in "1.2.1 UV-Vis method", but the light sources for curing and post-curing had to be adapted to the respective initiator. This adaptation is necessary to properly stimulate, cleave and bleach the photoinitiator and thus obtain solid specimens. The light sources and curing parameters used for the respective photoinitiators are summarized in Table 18.

Table 18: Curing and post-curing parameters for thin film samples containing different photoinitiators.

	TPO / BAPO	Ivocerin®	I2959 / D1173 / I184
Curing (Photorheometer)	OmniCure® LX500 LED	OmniCure® S2000 (medium pressure mercury lamp)	OmniCure® S2000 (medium pressure mercury lamp)
	385 nm	400 – 500 nm	320 – 500 nm
	300 s	300 s	300 s
	10 mW/cm²	10 mW/cm²	10 mW/cm²
Post-curing	PrograPrint® Cure	PrograPrint® Cure	Uvitron IntelliRay 600 UV flood curing system
	405 nm / 460 nm (LED)	405 nm / 460 nm (LED)	broadband
	Program: "Model" 2 x 180 s	Program: "Model" 2 x 180 s	15 min.
	270 mW/cm²	270 mW/cm²	UV-A: 125 mW/cm² Vis: 125 mW/cm²

The formulations for these samples consist of **UDMA** and 1.07 mol% of the respective photoinitiator, only the sample containing **I2959** was prepared with twice the initiator concentration (2.14 mol%), as the long-wavelength absorbance was rather weak in the 1.07 mol% sample and therefore difficult to evaluate.

The **AIBN**-based thin film sample consists of **UDMA** and 1.07 mol% of the thermal initiator **AIBN**. In analogy to the other samples, the curing process was carried out on the photorheometer with a gap width of 1200 µm, but without using a light source. Instead, the thermostat temperature was increased from 25°C to 90°C and the sample was cured for 30 min at this temperature. Thus, a solid colorless test specimen was obtained which was examined in the same way as the other specimens.

1.3.4 Photoreactor

The photoreactor experiments were carried out entirely in the absence of light. Solutions of defined concentrations of **TPO** in acetonitrile were prepared in glass vials and sealed with a septum. These solutions were degassed with an argon balloon and a needle as

pressure equalization for 5 min. A quartz glass cuvette with a magnetic stirring bar is flooded with argon while 3 ml of the test solution were transferred into it. Subsequently the cuvette is tightly sealed with a lid and parafilm. A schematic illustration of the setup for the photoreactor study is shown in Figure 89.
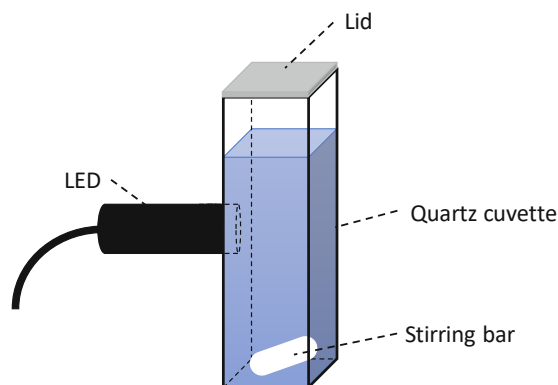
Figure 89: Schematic illustration of the setup used for the photoreactor experiments.

In this setup, a LED light source is positioned plane at the side of the quartz cuvette and fixed in position using a universal clamp. A magnetic stirrer in combination with the stirring bar are used to ensure the permanent homogeneity of the solution. Prior the experiments, the light intensity is adjusted. For this purpose, a spectrophotometer is positioned on the opposite side of the light source and the intensity of the light that has passed through the cuvette filled with acetonitrile is determined. As light source an OmniCure® LX500 equipped with a 385 nm LED head was used and the light intensity was set to 100 mW/cm². After defined times, the light source was switched off, the cuvette was transferred to a spectrophotometer, an absorption spectrum was recorded, the cuvette was transferred back and the irradiation process continued.

1.3.5 Persistent radicals – EPR

All EPR experiments were conducted at the TU Graz by Max Schmallegger within the research group of Prof. Georg Gescheidt. Two thin film samples consisting of **UDMA** and **TPO** (1.07 mol%) stored for 22 days and 271 days at 37°C under dry conditions were prepared at TU Wien and sent to TU Graz for the measurements. Figure 90 shows a photogrpah of the two samples, on the left the sample stored for 22 days, which has a yellow stain, and on the right the sample stored for 271 days, which appears colorless.
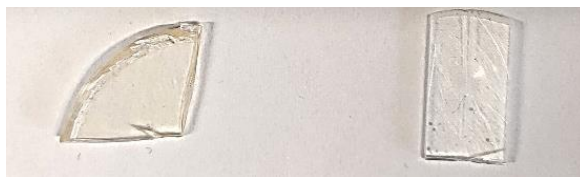
Figure 90: Photograph of the two thin film samples stored for 22 day (left) and 271 days right.

Small pieces of the polymer thin films were broken off, placed in an NMR tube (diameter = 5 mm) and measured directly by EPR. For each measurement, 25 spectra were recorded. The measurements were performed using the following parameters: Sweep Width = 20 mT, Modulation = 0.2 mT, Receiver Gain = 1 x 102.

Further polymer samples were prepared directly at the TU Graz. Different monomers and photoinitiators were mixed, light-cured in NMR tubes for 15 minutes and then measured by EPR spectroscopy. In Figure 91 the results of samples consisting of **UDMA** and either the photoinitiator **TPO** (a) or **D1173** (b) are shown.
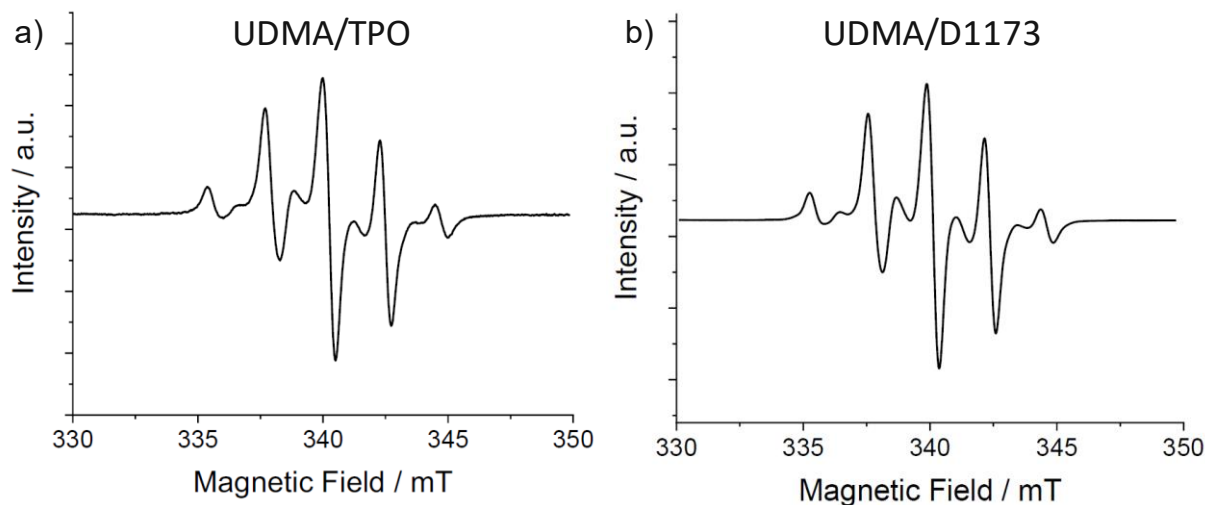
*Figure 91: EPR spectra of polymer samples consisting of **UDMA** and **TPO** (a) or **D1173** (b), 15 minutes after preparation.*

In addition, samples consisting of **TPO** and the monomers shown in Figure 92 were prepared and measured. The corresponding results are depicted in Figure 93.
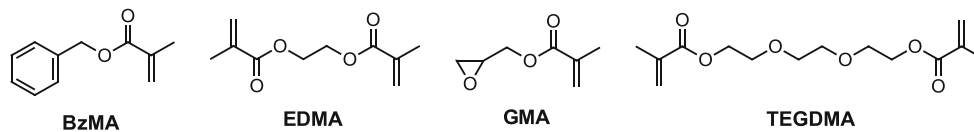
Figure 92: Structures of monomers used for EPR measurements.
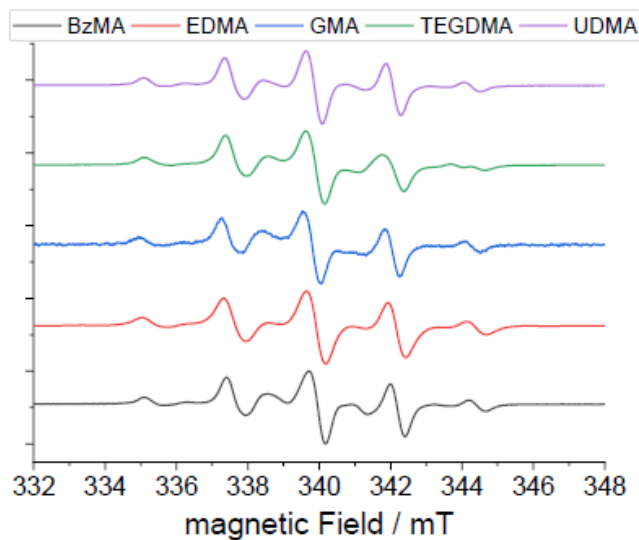
*Figure 93: EPR spectra of polymers consisting of **TPO** and different monomers.*

1.3.6 Leaching tests

For leaching tests, a thin film sample consisting of **UDMA** and **TPO** (1.07 mol%) was stored for 23 days dry at 37°C. To increase the discoloration of the specimen, the sample was stored at 110°C for 15 minutes. Afterwards the polymer was ground to a powder using sanding paper. This powder was extracted in DCM for 14 days while stirring. The solids were separated by filtration. The extract obtained was analyzed using UV-Vis absorption (Figure 94), UPLC-MS (Figure 95) and TLC measurements (Figure 96).
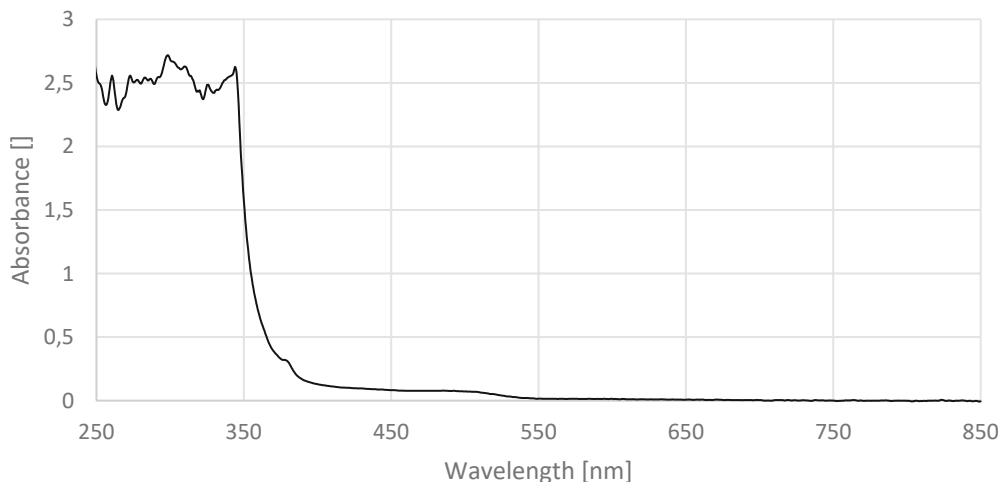
Figure 94: UV-Vis absorption measurement of the extract of a standard thin film sample stored for 23 days at 37°C and for 15 min at 110°C.Tthe sample was extracted for 14 days in DCM.
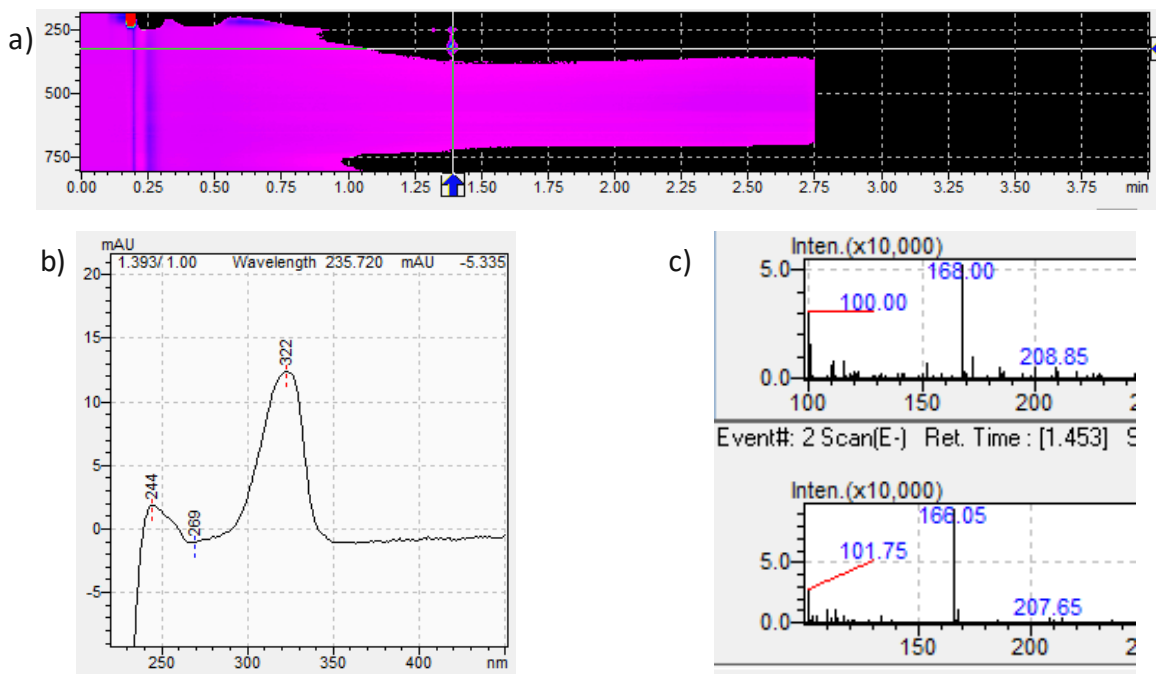
Figure 95: Results of UPLC-MS measurements of the DCM extract of a standard thin film sample stored for 23 days at 37°C and for 15 min at 110°C. a): Detector signal of the PDA (photo diode array) detector. b): Absorption signal of the substance at a retention time of 1.4 min. c): Mass signal (top: positive mode; bottom: negative mode) of the substance at a retention time of 1.4 min.
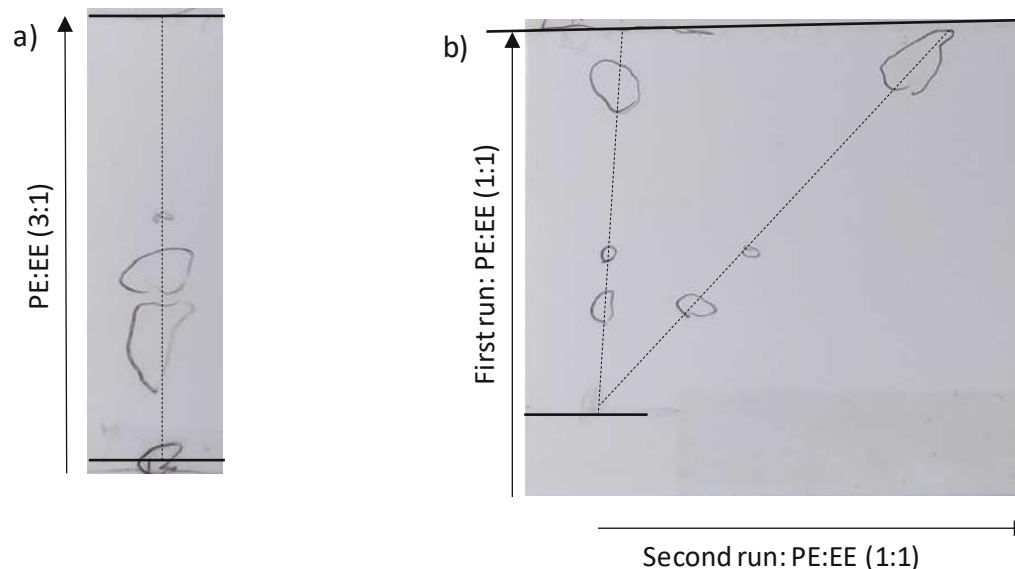
Figure 96: 1D (a) and 2D (b) TLC (silica gel) experiments of the DCM extract of a standard thin film sample stored for 23 days at 37°C and for 15 min at 110°C, using different solvent compositions.

Upscaling experiments were carried out to obtain larger quantities of the colored substances, to perform column chromatography:

<u>1st attempt</u>

10 g formulation consisting of **UDMA** and **TPO** (1.07 mol%) were cured in a silicone mold with the PrograPrint® Cure device (405 nm; 100%, 2*10 min.) from both sides. Subsequently the polymer sample was stored for 30 min. in a 110°C drying oven, resulting in a deep orange discoloration. The polymer was ground to a fine powder using a cryogenic mill, before being extracted with DCM for 3 days. The resulting extract and the polymer appeared colorless and was discarded.

<u>2nd attempt</u>

10 g formulation consisting of **UDMA** and **TPO** (1.07 mol%) were cured in a silicone mold with the PrograPrint® Cure device (405 nm/460 nm; Program: "Model"; 2*3 min; 270 mW/cm²) from both sides. Subsequently the polymer sample was stored for 15 min. in a 110°C drying oven, resulting in a deep orange discoloration. The sample was then stored for 1 day at 37°C before being ground to a fine powder using a cryogenic mill. Around 5 g of the powder has been tried to be extracted with ACN for 1 day, whereby no

colored solution was obtained. The other 5 g were extracted with DCM for 1 day. After filtration and evaporation of the solvent 32 mg of a yellowish viscous mass were obtained, which may contain some small polymer particles which could not be removed by filtration. The insufficient amount of extract was not further processed.

3rd attempt

15 g formulation consisting of **UDMA** and **TPO** (1.07 mol%) were cured in a silicone mold with the PrograPrint® Cure device (405 nm/460 nm; Program: "Model"; 2*3 min; 270 mW/cm²) from both sides. Subsequently the polymer sample was stored for 15 min. in a 110°C drying oven, resulting in a deep orange discoloration. The polymer was ground to a fine powder using a cryogenic mill, before being extracted with DCM in a Soxhlet apparatus. After 1 day both, the polymer and the solvent appeared completely colorless.

4th attempt

10 g formulation consisting of **UDMA** and **TPO** (1.07 mol%) were cured in a silicone mold with the PrograPrint® Cure device (405 nm/460 nm; Program: "Model"; 2*3 min; 270 mW/cm²) from both sides. Subsequently the polymer sample was stored for 15 min. in a 110°C drying oven, resulting in a deep orange discoloration. The polymer stored for 2 days at room temperature before it was ground to a fine powder using a cryogenic mill. This powder was extracted with DCM in a Soxhlet apparatus. After 1 day both, the polymer and the solvent appeared completely colorless.

5th attempt

10 g formulation consisting of **UDMA** and **TPO** (1.07 mol%) were cured in a silicone mold with the PrograPrint® Cure device (405 nm/460 nm; Program: "Model"; 2*3 min; 270 mW/cm²) from both sides. Subsequently the polymer sample was stored for 1 day at 37°C before it was stored for 15 min. in a 110°C drying oven to yield a deep orange discoloration. Afterwards, the sample was ground to a fine powder using a cryogenic mill and extracted for 14 days with DCM while stirring. After filtration and evaporation of the solvent, 381 mg of a yellowish viscous mass were obtained, which contained some small polymer particles. These particles could not be separated using multi-layer paper filters

Experimental part

or fine-pored glass frit, syringe filters clogged immediately and centrifuging did not produce the desired result either. Therefore, the particles were not be removed before proceeding. The extract was applied to a column loaded with 20 g silica and an attempt was made to separate it using gradient elution from PE:EE. Several yellow fractions were obtained, all of which appear to be mixed fractions in TLC experiments. A 2D TLC experiment revealed the yellow substance is not stable under the conditions of the column chromatography (Figure 97). The fact that this behavior was not noticed in the previous 2D TLC experiment (Figure 96) is probably due to the now more concentrated sample.
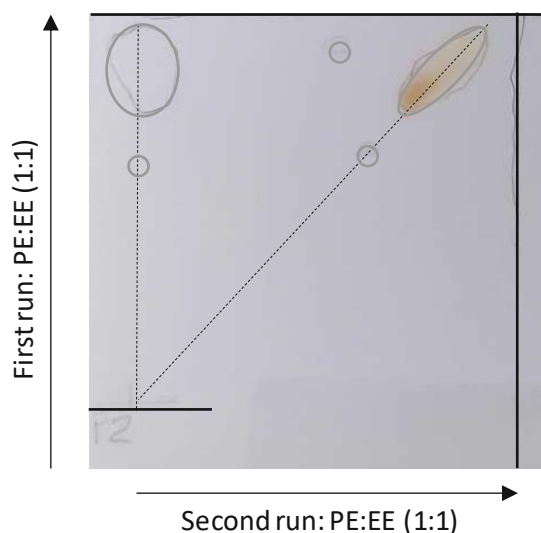
Figure 97: 2D TLC (silica gel) experiment of a yellow fraction, obtained during a column chromatography of the DCM extract from attempt 5.

Based on the assumption that the acidic conditions of the silica gel led to decomposition, an UPLC-MS measurement of the crude extract was carried out under basic instead of normally acidic conditions. Figure 98 depicts the results for the substance that produced the longest wavelength absorbance on the PDA detector at a retention time of 1.8 min.
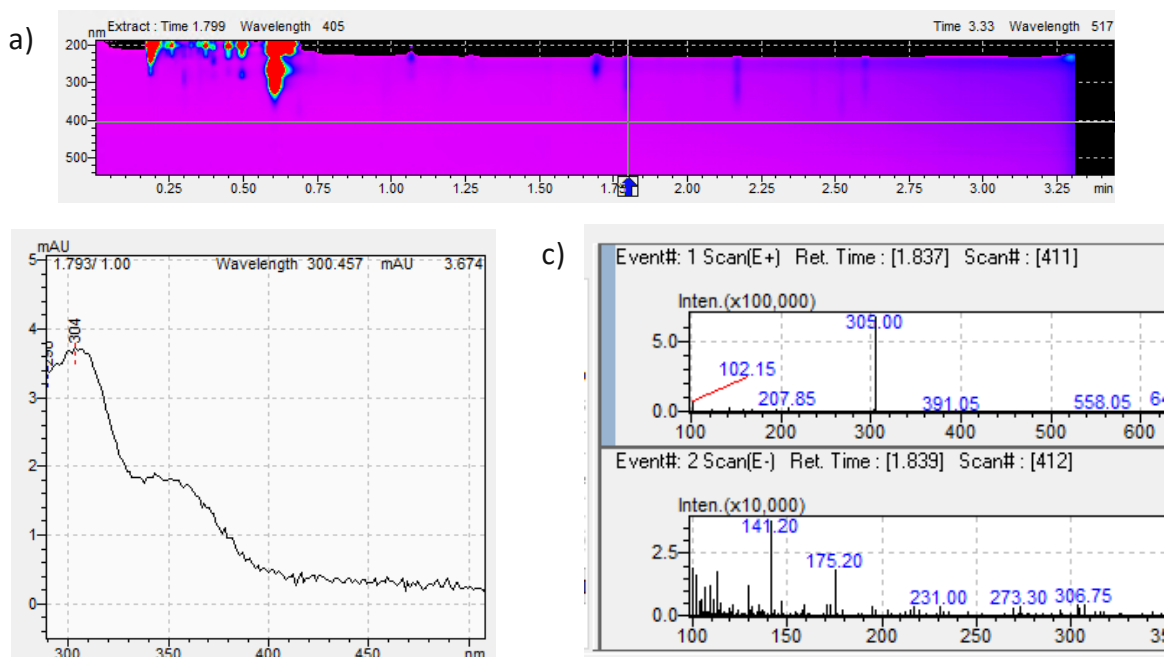
Figure 98: Results of UPLC-MS measurements performed under basic conditions, of the DCM extract from attempt 5. a): Detector signal of the PDA (photo diode array) detector. b): Absorption signal of the substance at a retention time of 1.8 min. c): Mass signal (top: positive mode; bottom: negative mode) of the substance at a retention time of 1.8 min.

6th attempt

12 g formulation consisting of **UDMA** and **TPO** (1.07 mol%) were cured in a silicone mold with the PrograPrint® Cure device (405 nm/460 nm; Program: "Model"; 2*3 min; 270 mW/cm²) from both sides. Subsequently the polymer sample was stored for 1 day at 37°C before it was stored for 15 min. in a 110°C drying oven to yield a deep orange discoloration. Afterwards the sample was ground to a fine powder using a cryogenic mill. Extraction tests with the solvents DCM, Et$_2$O, PE and Toluene were carried out. For each test 1 g of sample were used. Only the use of the solvents DCM and Et$_2$O yielded yellow extracts.

The residual 8 g were extracted for 5 days with Et$_2$O while stirring. Around 220 mg yellow extract including small polymer particles were obtained after filtration and evaporation of the solvent. The sample was attempted to be separated by column chromatography over 20 g of neutral aluminum oxide. Gradient elution starting with pure PE and increasing EE content yielded one yellow fraction. It consisted of 6 mg of two substances, which exhibit a very similar retention time on aluminum oxide. The corresponding TLC is depicted in Figure 99.

PE:EE (9:1)
neutral aluminum oxide
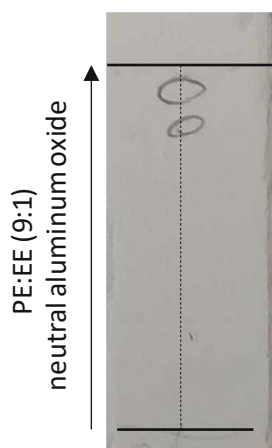
Figure 99: TLC of the yellow fraction of the column chromatography performed with neutral aluminum oxide in attempt 6.

An ^{1}H-NMR experiment of this impure fraction showed a variety of mainly aliphatic signals and did not provide any information about the identity of the substances. The corresponding spectrum of this experiment can be found in the appendix (Figure 110).

1.4 Approaches to enhance color-stability

1.4.1 Photoinitiators

The literature known photoinitiators **B1** and **B2** were synthesized by the company Ivoclar AG, analogously to the work of Dietlin et al.[83] The general synthesis route and the structures of the synthesized compounds are illustrated below.

Na$_2$CO$_3$
neat
100-140°C
4-6h

MnO$_2$
DCM
20°C, 22h

B1

B2
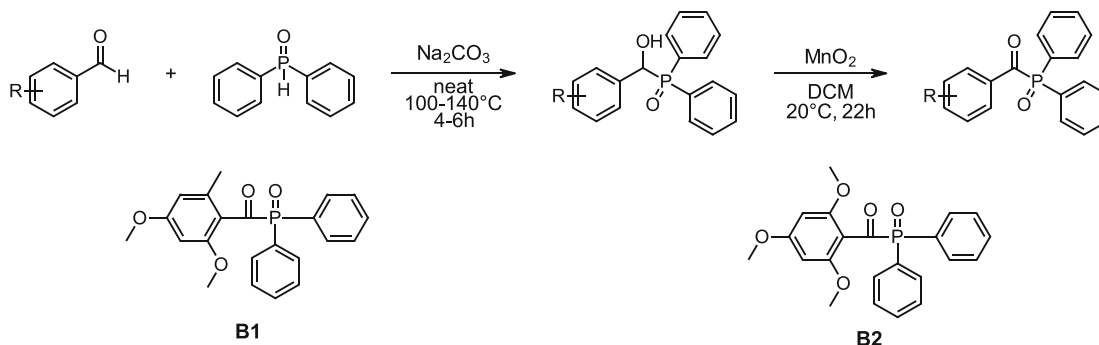
For the synthesis of **B1**, the starting material 2,4-dimethoxy-6-methylbenzaldehyde was used. In the case of **B2**, this was 2,4,6-trimethoxybenzaldehyde. For the evaluation of the discoloration behavior thin film samples consisting of **UDMA** (stabilized with 100 ppm **MeHQ**) and 1.07 mol% of B1 or B2 photoinitiator were prepared, as described in 1.2.1,

using a 385 nm LED for curing. The samples were stored under dry conditions at 37°C and analyzed by means of UV-Vis absorption measurements.

Additionally, polymer samples were prepared, which were evaluated in the CIELAB color space, as described in 1.2.2. Those samples consist of **UDMA** (stabilized with 100 ppm **MeHQ**) and 1.0 mol% of the photoinitiator **B1**, **B2**, or **TPO**. The prepared specimens were stored immersed in water at 50°C. The changes of the values L, a and b are illustrated in Figure 100 the absolute values are depicted in Figure 101.

Experimental part
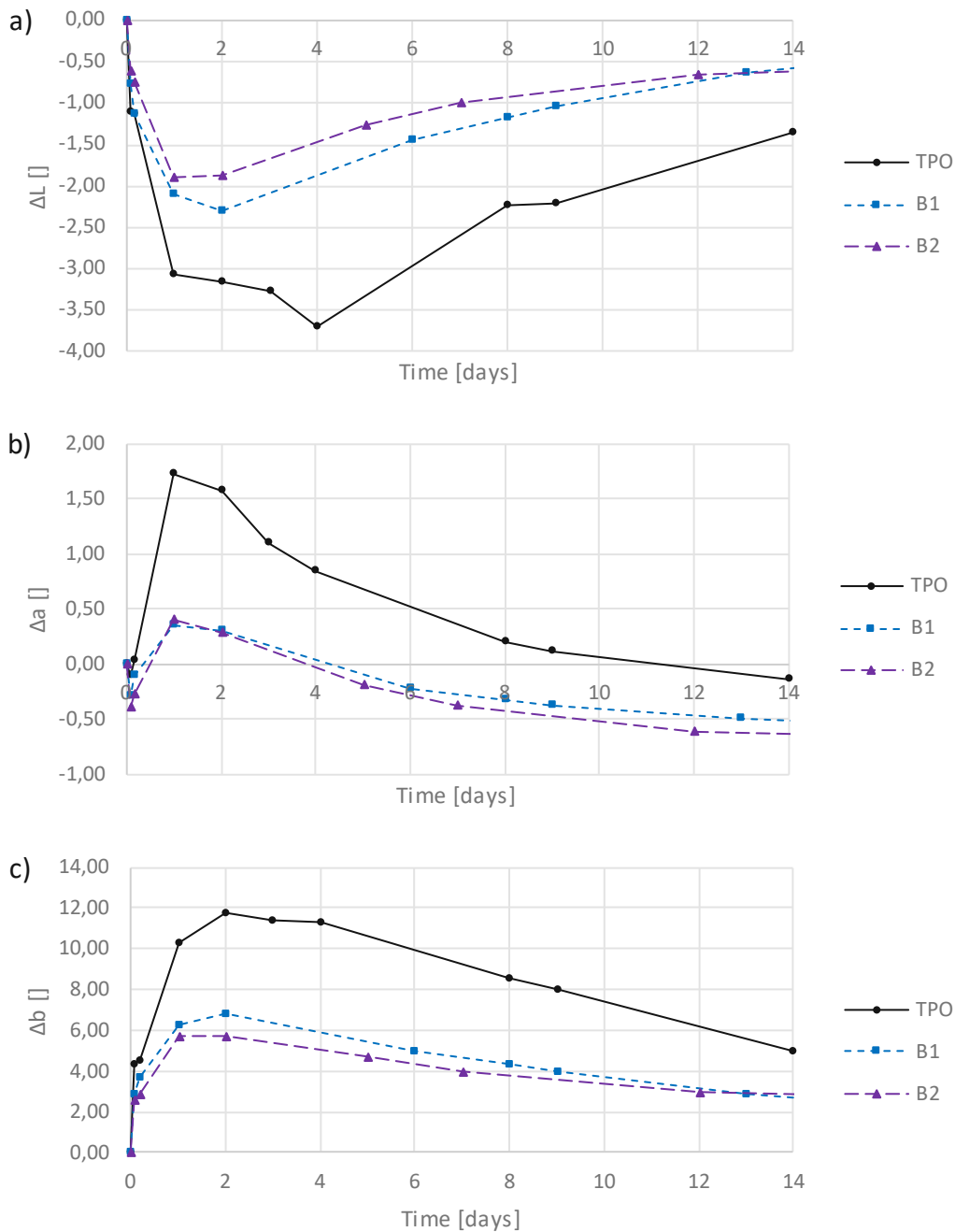
*Figure 100: Change of the lightness ΔL (a), on the green-red axid Δa (b) and on the blue-yellow axis Δb (c) of samples consisting of **UDMA** (stabilized with 100 ppm **MeHQ**) and 1 mol% of the respective photoinitiator. The thin film samples were stored at 50°C immersed in water.*
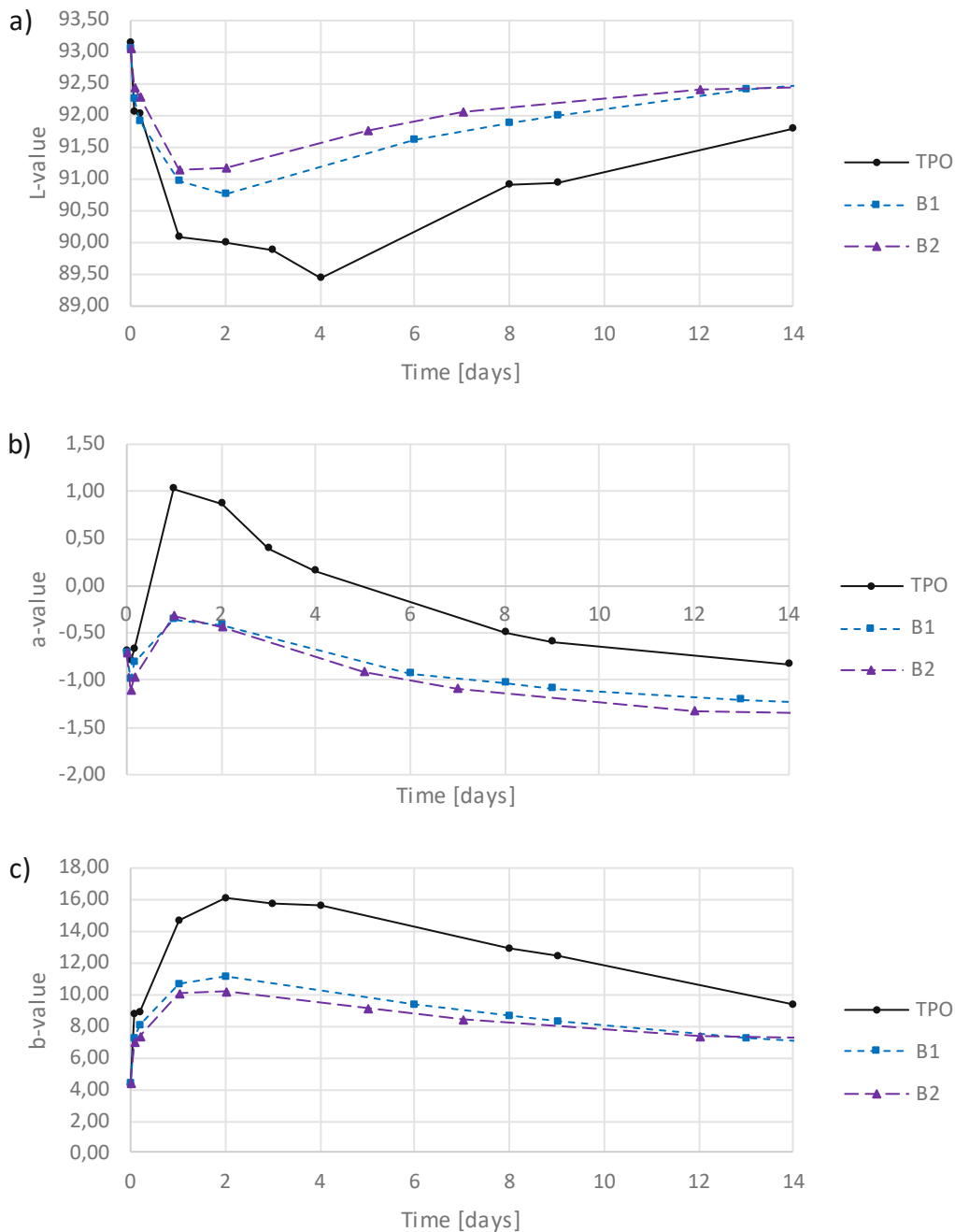
*Figure 101: L-values (a), a-values (b) and b-values (c) of samples consisting of **UDMA** (stabilized with 100 ppm **MeHQ**) and 1 mol% of the respective photoinitiator. The thin film samples were stored at 50°C immersed in water.*

1.4.2 Stabilizers

For the evaluation of the effect of stabilizers on the discoloration behavior, thin film samples consisting of **UDMA** (stabilized with 100 ppm **MeHQ**), 1.07 mol% **TPO** and

1000 ppm of the investigated stabilizer were produced, according to the description in 1.2.1. As the formulations necessitate low quantities of stabilizer, which are difficult to weigh precisely, a small portion of stabilizer was weighed in a glass vial, and the other components of the formulation were adjusted accordingly. The prepared samples were stored under dry conditions at 37°C and analyzed by means of UV-Vis absorption measurements. 3 series of measurements using different stabilizers were carried out. The structures and designations of the stabilizers used and the resulting difference absorption spectra are compiled in Table 19 – Table 21.

*Table 19: Stabilizer measurement series 1 – Time-dependent difference absorption spectra of thin film samples consisting of **UDMA**, **TPO** (1.07 mol%) and 1000 ppm stabilizer, stored dry at 37°C.*
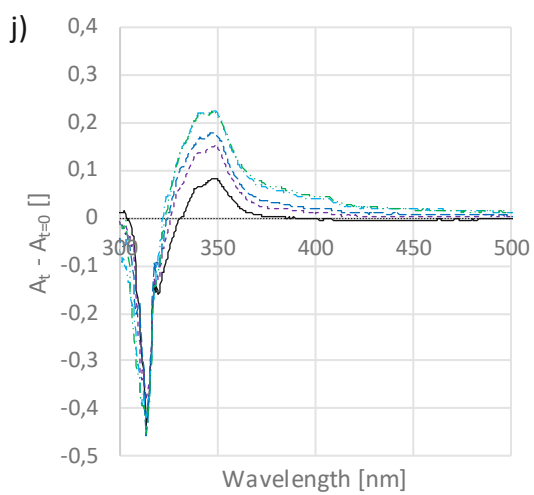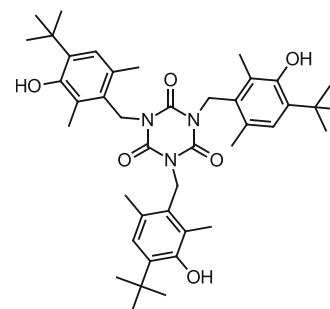
c)

d)

e)

Experimental part

f)

g)

h)

i)

j)

Experimental part
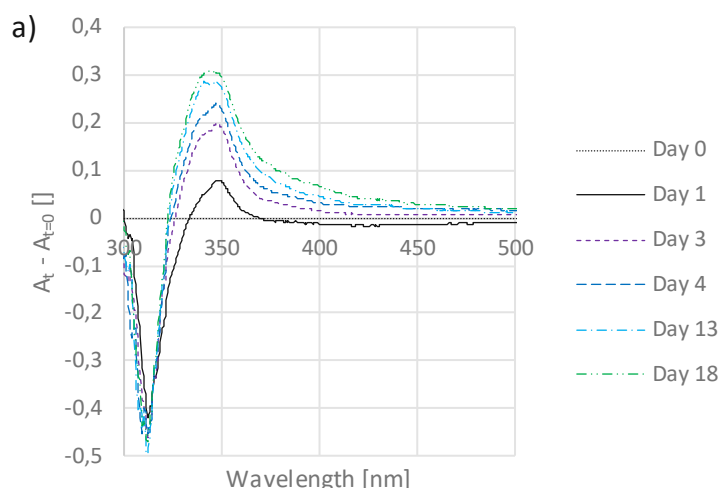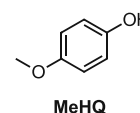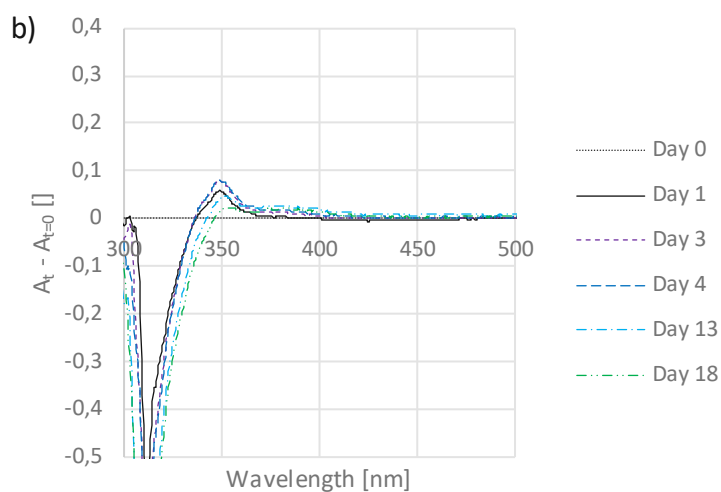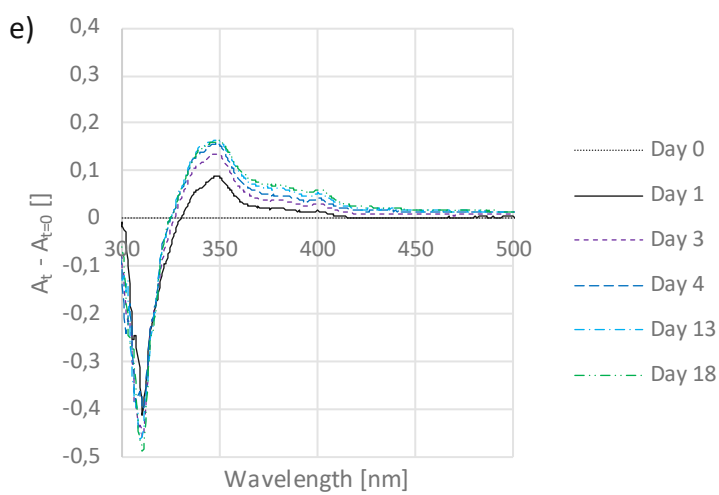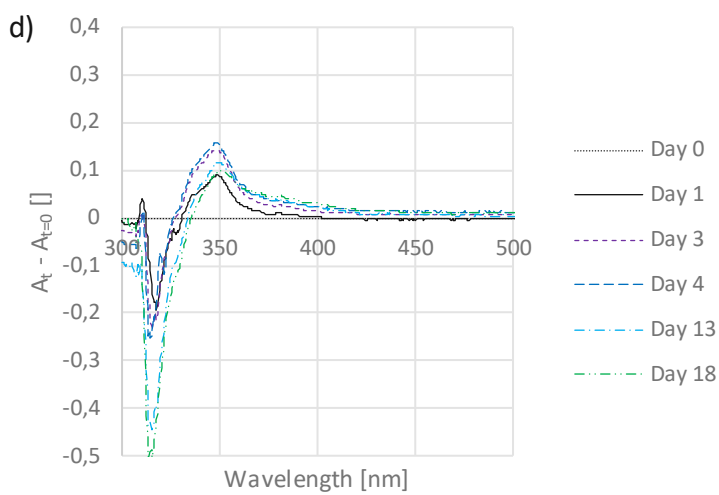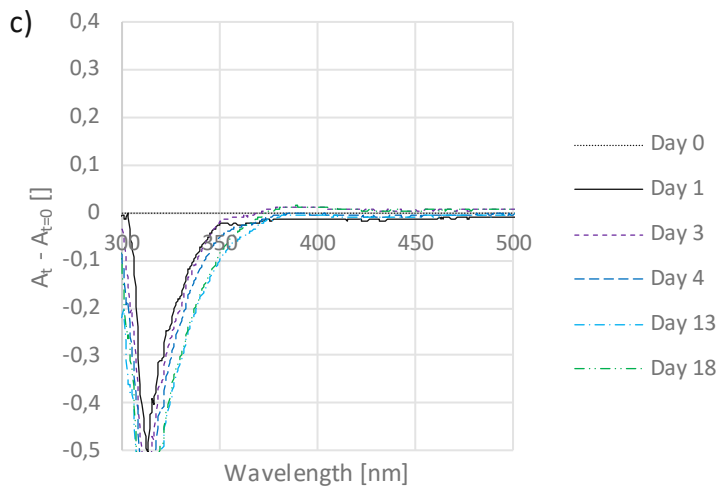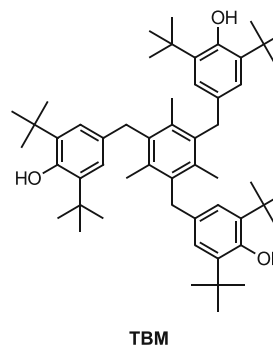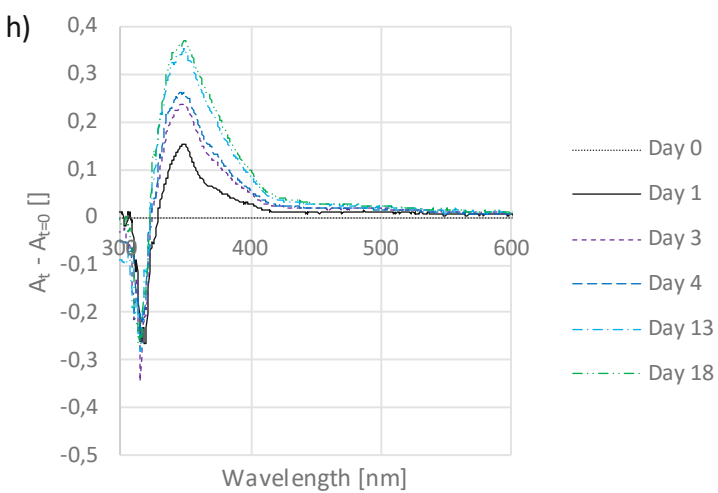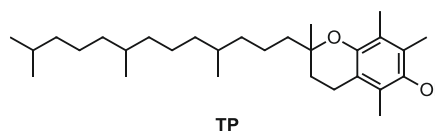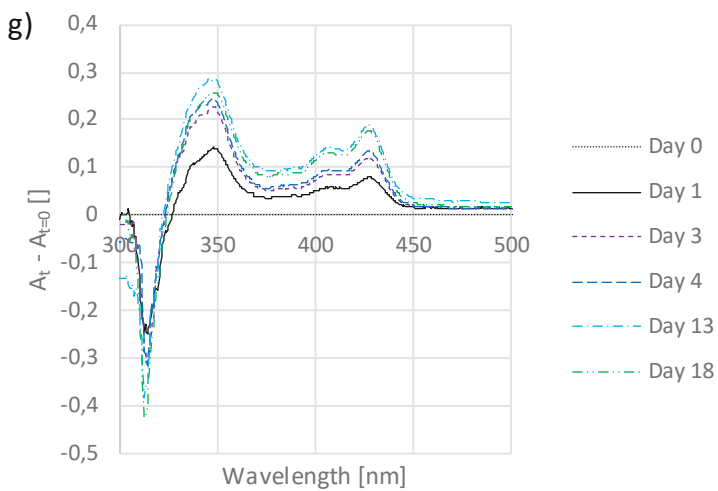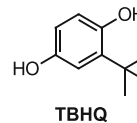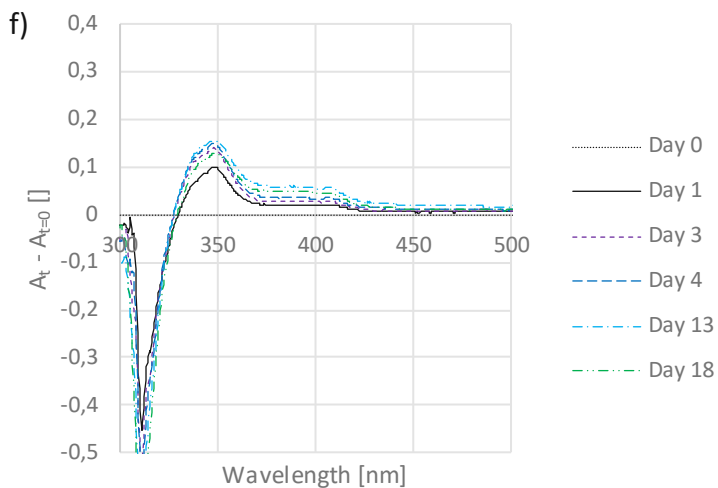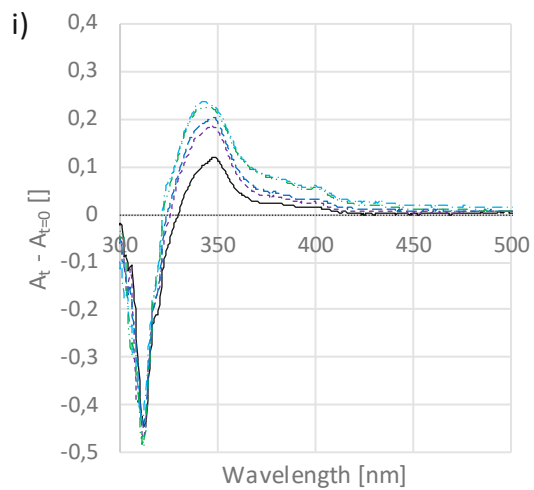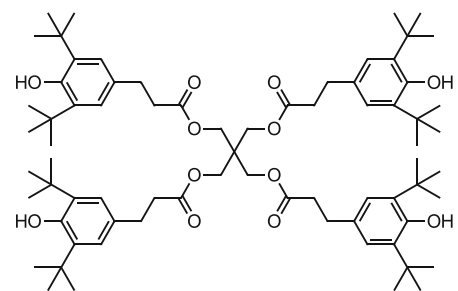
*Table 20: Stabilizer measurement series 2 – Time-dependent difference absorption spectra of thin film samples consisting of **UDMA**, **TPO** (1.07 mol%) and 1000 ppm stabilizer, stored dry at 37°C.*

a)

Blind

b)

BPG

c)

d)

e)

Experimental part

f)

5-APG

g)

THBP
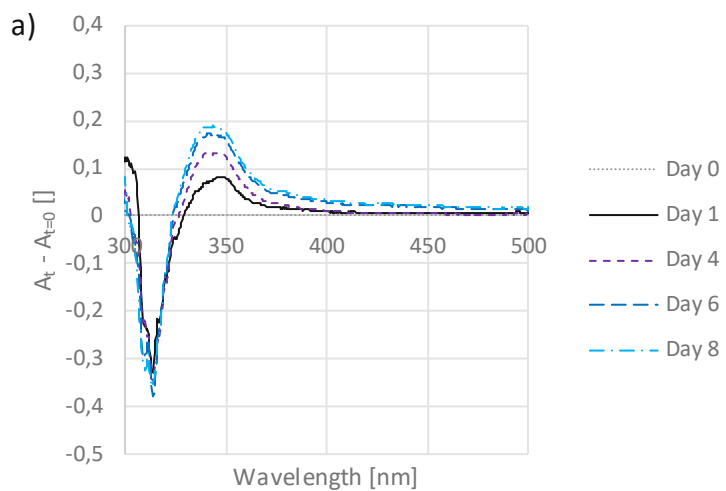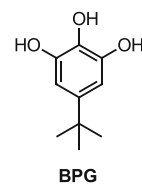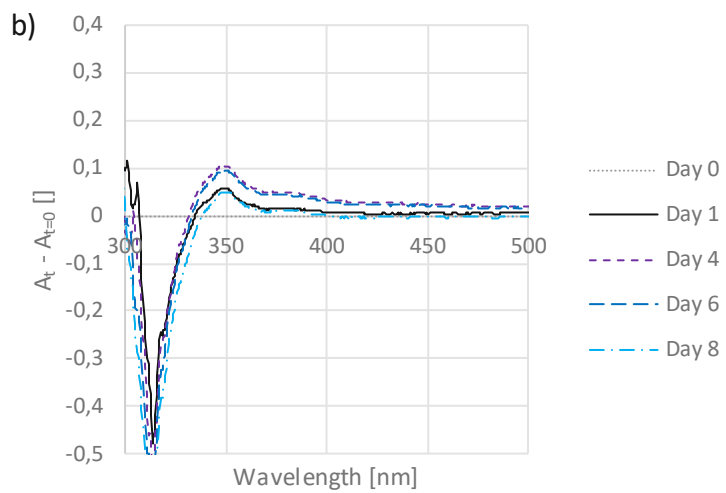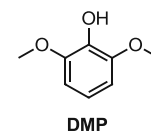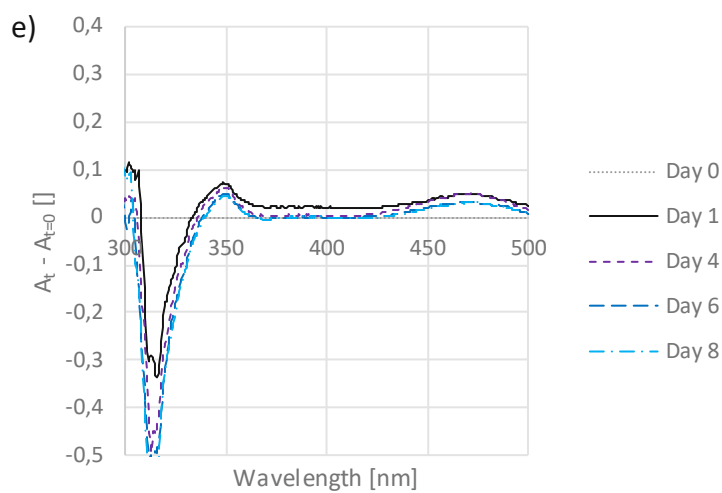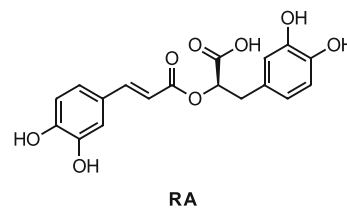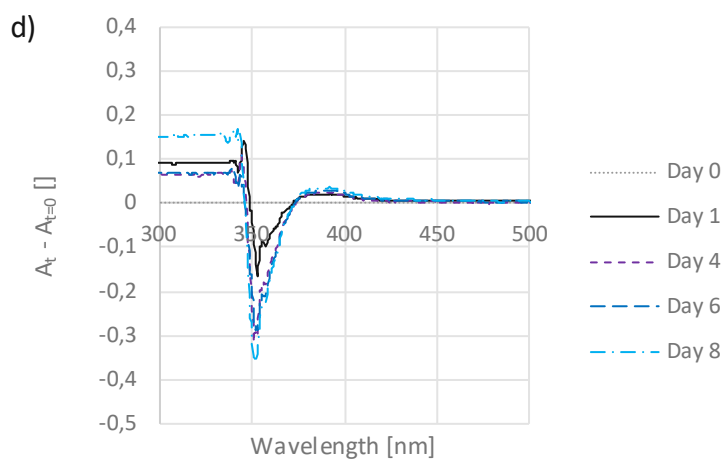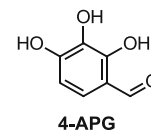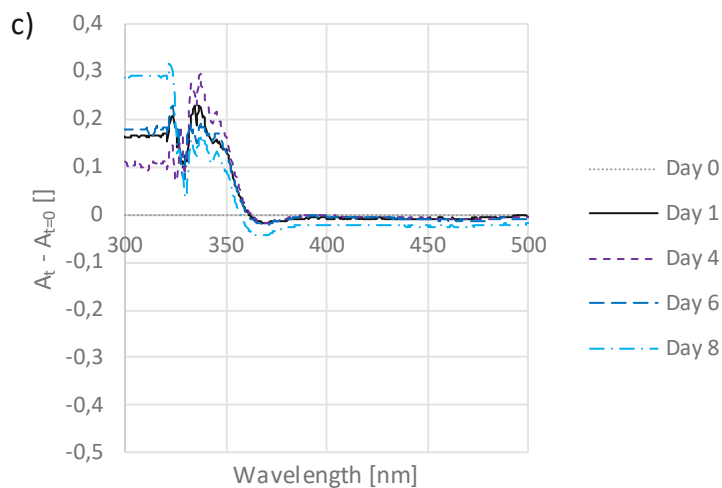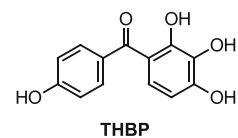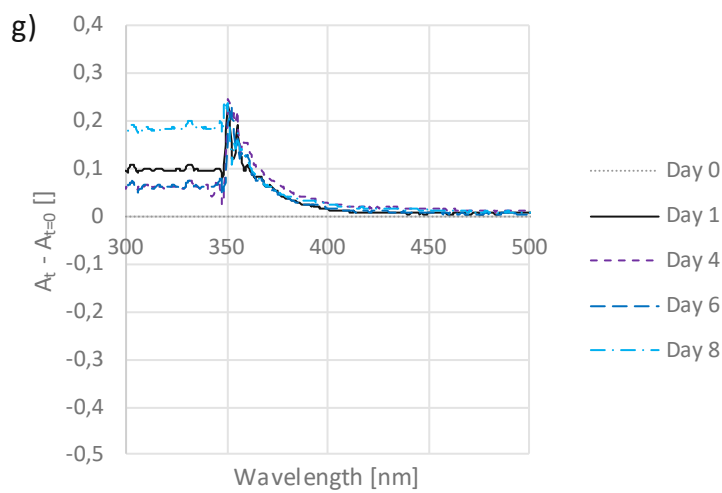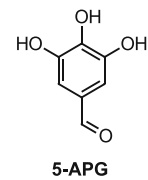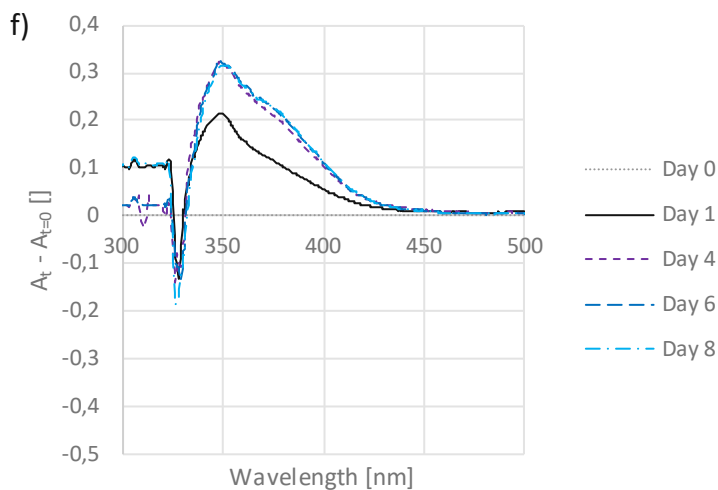
*Table 21: Stabilizer measurement series 3 – Time-dependent difference absorption spectra of thin film samples consisting of **UDMA**, **TPO** (1.07 mol%) and 1000 ppm stabilizer, stored dry at 37°C.*

a)

blind

b)

BC
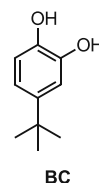
1.4.3 Hydroperoxides

For the evaluation of the effect of hydroperoxides on the discoloration behavior, a formulation consisting of **UDMA** (stabilized with 100 ppm **MeHQ**), 1.07 mol% **TPO** and 5 wt% of cumene hydroperoxide (**CHP**, 80% solution in cumene) were added and homogenized. This and a second thin film sample without CHP were prepared, as described in 1.2.1 and analyzed using UV-Vis absorption measurements. The difference absorption spectra of these samples are depicted in Table 22.

*Table 22: Time-dependent difference absorption spectra of thin film samples consisting of **UDMA** and **TPO** (1.07 mol%) (a) and additional 5 wt% of **CHP** (80% solution in cumene) (b), stored dry at 37°C.*

a)

Blind

b)

CHP
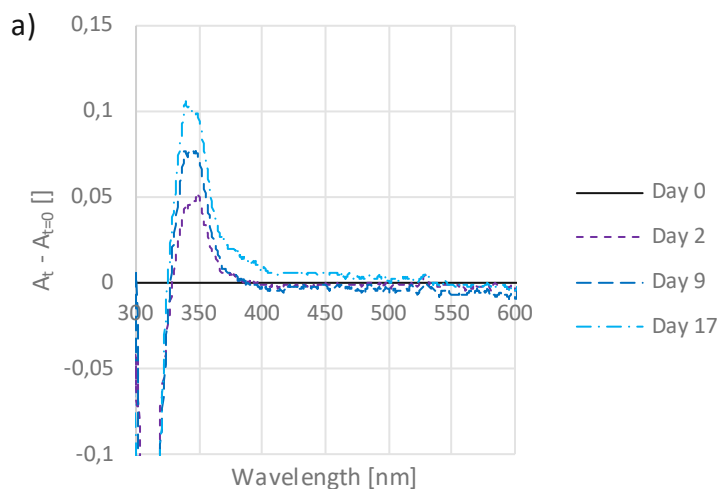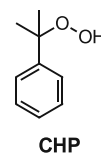
1.4.4 Further investigations

- Ascorbic acid

A thin film sample consisting of **UDMA** (stabilized with 100 ppm **MeHQ**), 1.07 mol% **TPO** and 1000 ppm of ascorbic acid was prepared, as described in 1.2.1. This sample together with a prepared standard reference sample without ascorbic acid were stored dry at 37°C and analyzed using UV-Vis absorption measurements. The resulting difference absorption spectra are depicted in Table 23.

*Table 23: Time-dependent difference absorption spectra of thin film samples consisting of **UDMA** and **TPO** (1.07 mol%) (a) and additional 1000 ppm of ascorbic acid (b), stored dry at 37°C.*
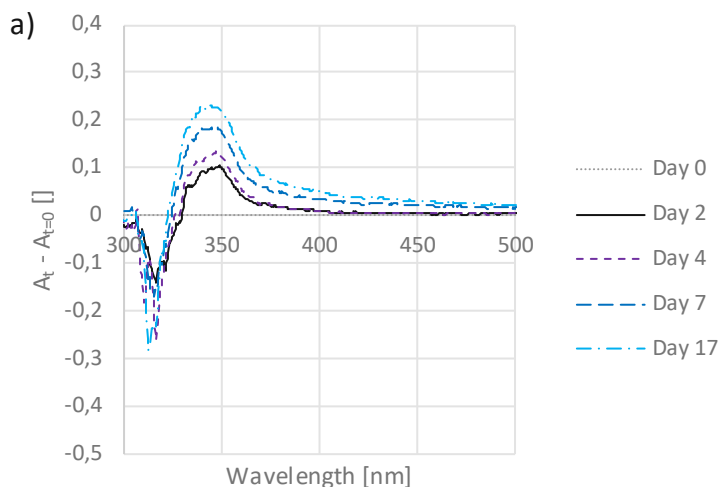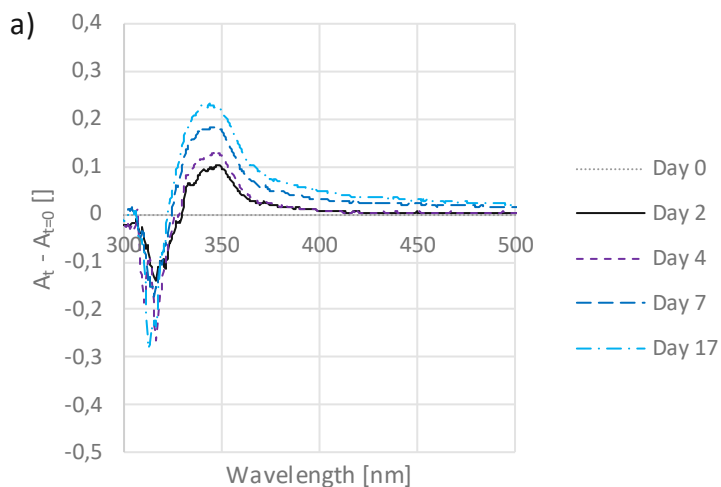

a) Blind

b) Ascorbic acid
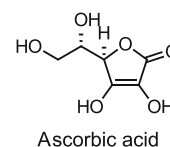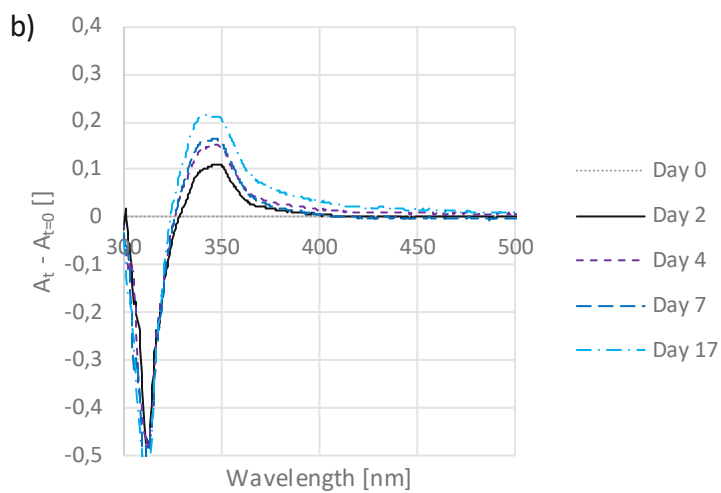
- Secondary antioxidants

For the evaluation of synergistic effects of stabilizers with secondary antioxidants, thin film samples consisting of **UDMA**, **TPO** (1.07 mol%) and 1000 ppm of **TIC** or **TP** were compared with the respective samples consisting of **UDMA**, **TPO** (1.07 mol%), 1000 ppm of **TIC** or **TP** and additional 5000 ppm Doverphos 11. The comparison is made on the basis of difference absorption spectra illustrated in Table 24 for **TIC** containing samples and in Table 25 for **TP** containing ones.

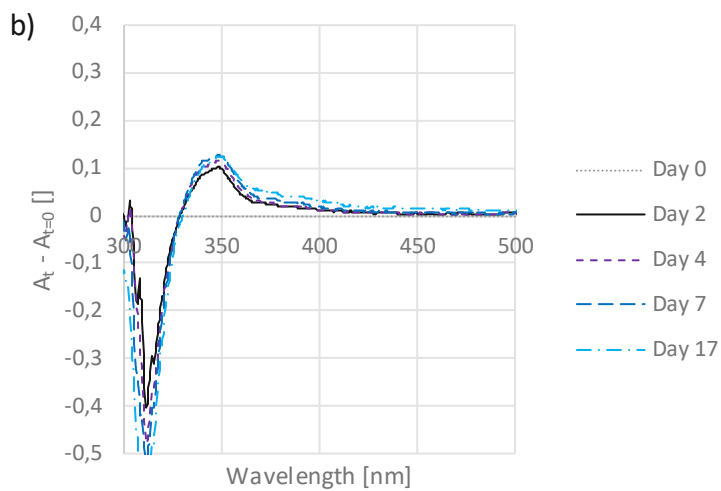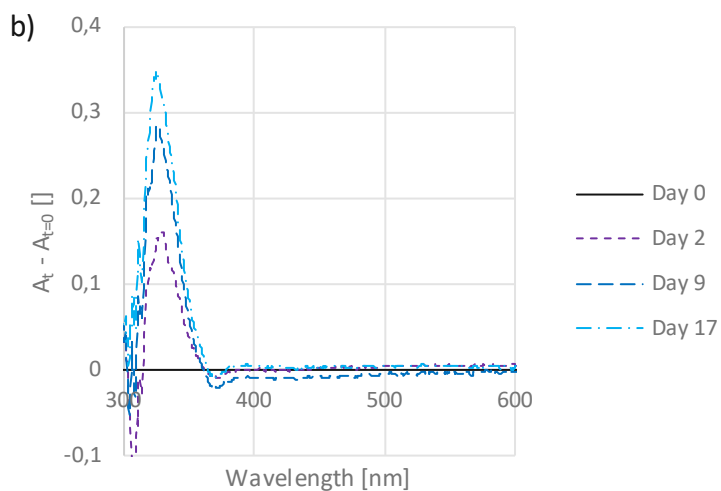*Table 24: Time-dependent difference absorption spectra of thin film samples consisting of **UDMA**, **TPO** (1.07 mol%) and 1000 ppm **TIC** (a) and additional 5000 ppm Doverphos 11 (b), stored dry at 37°C.*
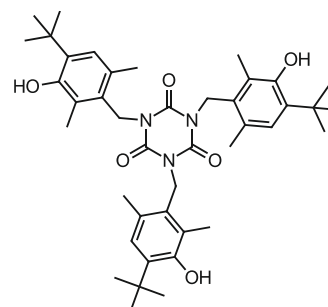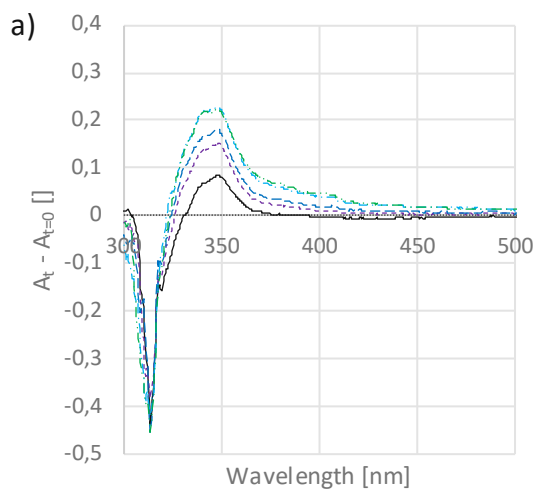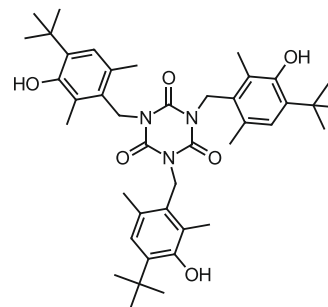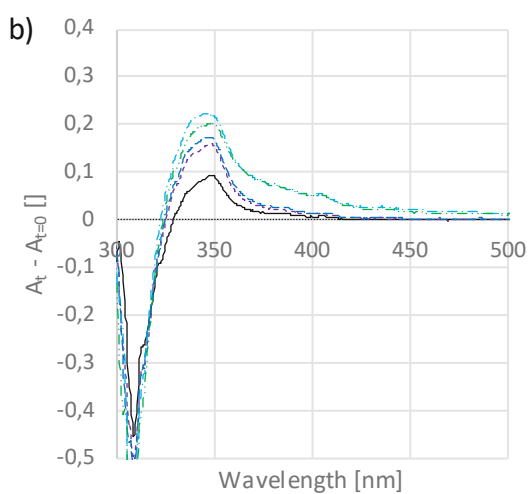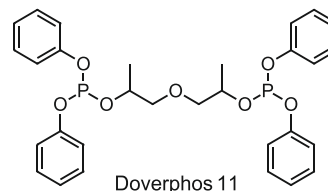
*Table 25: Time-dependent difference absorption spectra of thin film samples consisting of **UDMA**, **TPO** (1.07 mol%) and 1000 ppm **TP** (a) and additional 5000 ppm Doverphos 11 (b), stored dry at 37°C.*
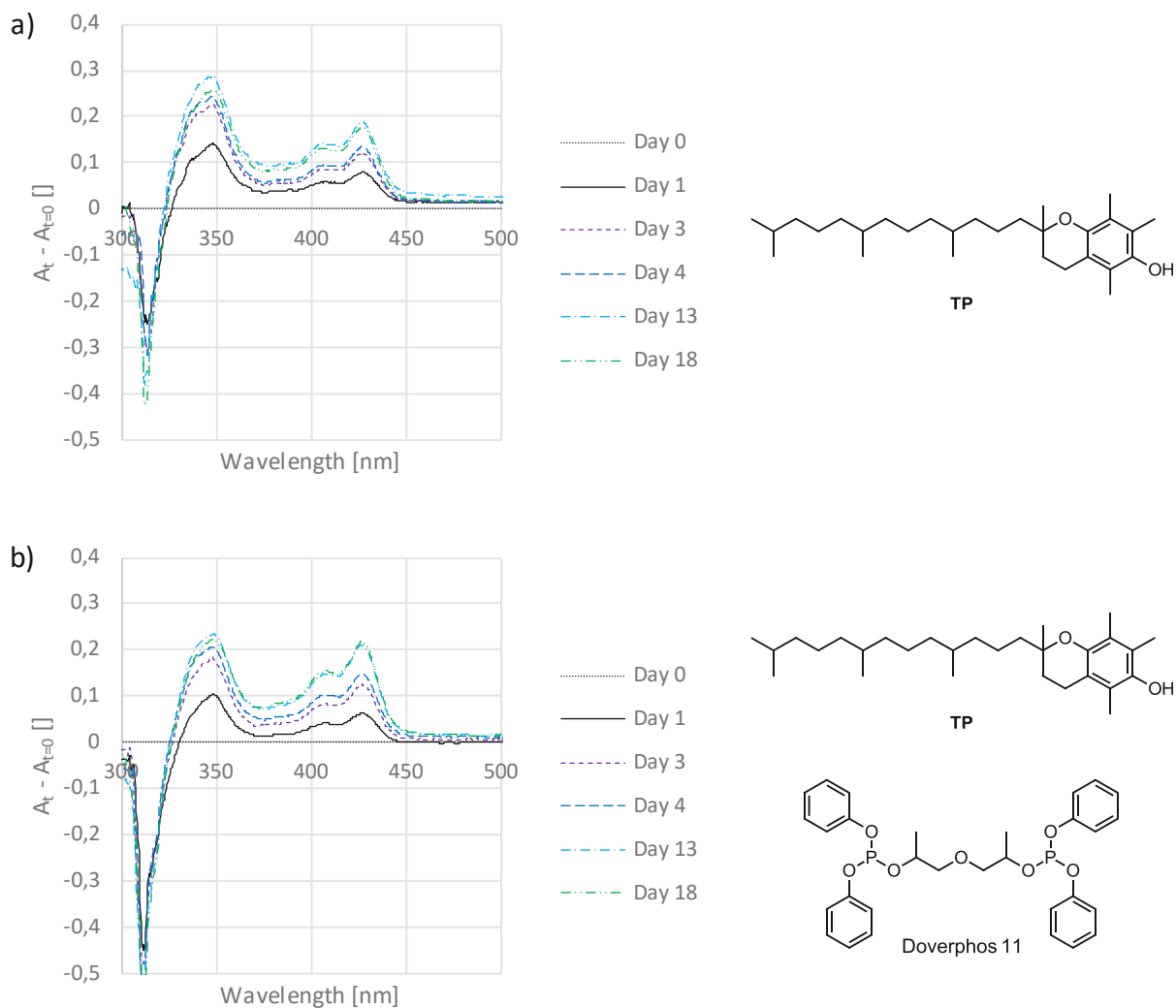

- Hydrogen atom transfer

For the evaluation of the effect of hydrogen donor substances on the discoloration behavior, thin film samples consisting of **UDMA** (stabilized with 100 ppm **MeHQ**), 1.07 mol% **TPO** and 1000 ppm of the respective hydrogen donating substance were prepared, as described in 1.2.1. The samples were analyzed using UV-Vis absorption measurements and stored under dry conditions at 37°C. The used substances, their designations and the resulting difference absorption spectra of these samples are depicted in Table 26.

Experimental part

*Table 26: Time-dependent difference absorption spectra of thin film samples consisting of **UDMA**, **TPO** (1.07 mol%) and 1000 ppm of different hydrogen donating substances, stored dry at 37°C.*

a)

Day 0
Day 1
Day 4
Day 6
Day 20

Blind

b)

Day 0
Day 1
Day 4
Day 6
Day 20

SH

OH

HTP

c)

d)

e)

Experimental part

f)

TPS

g)

TEGDMA

h)

PEG 600

i)

j)
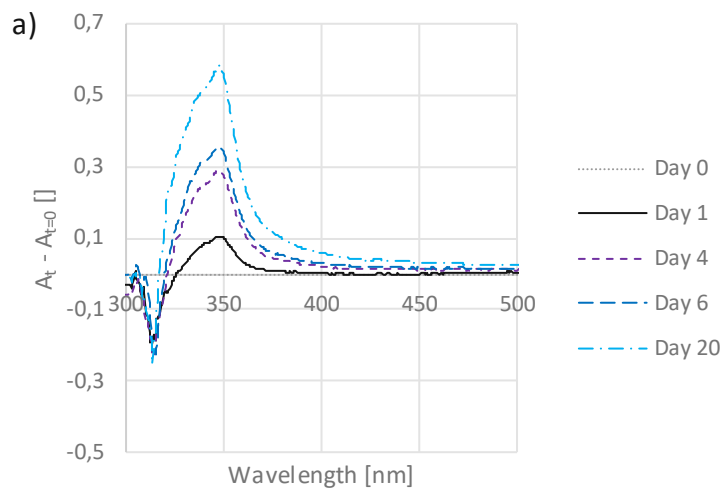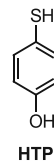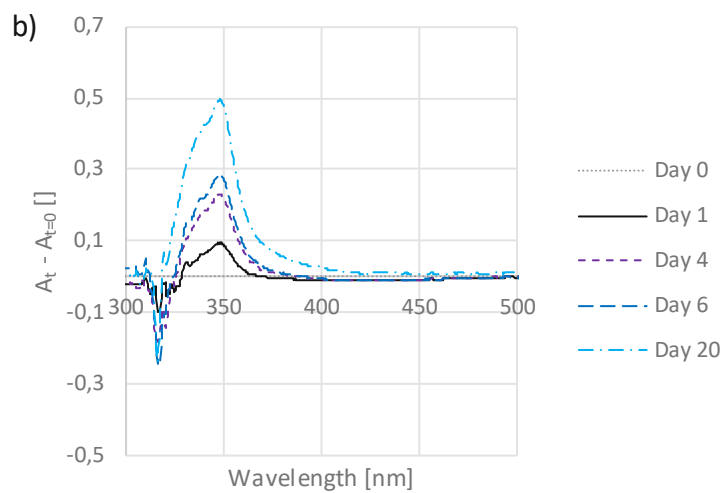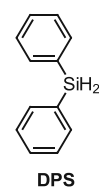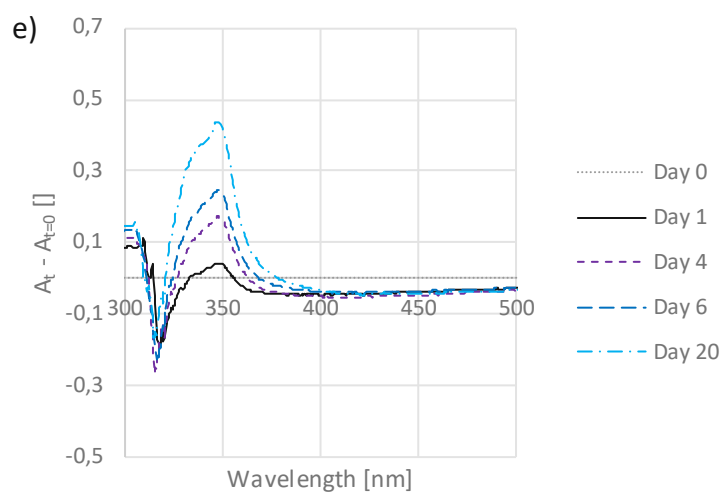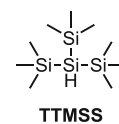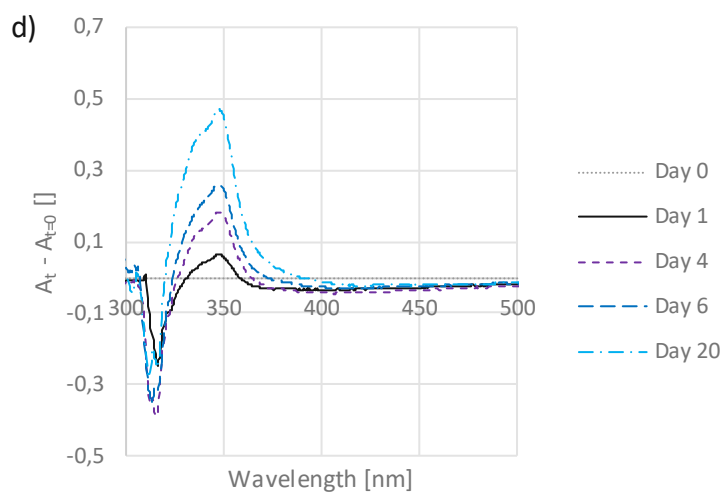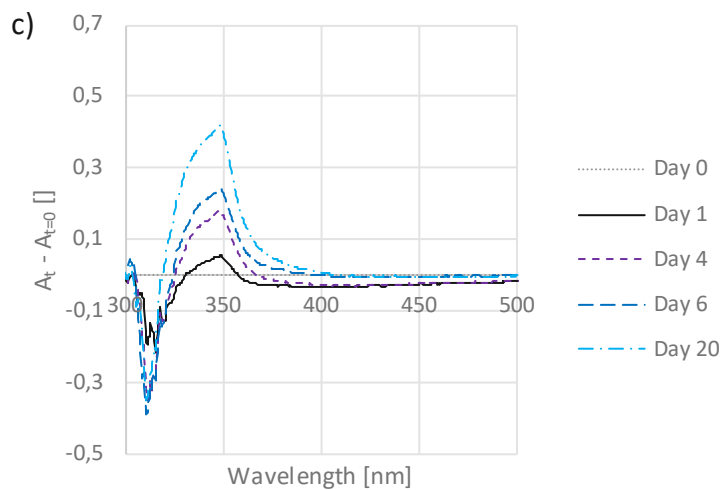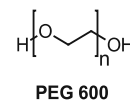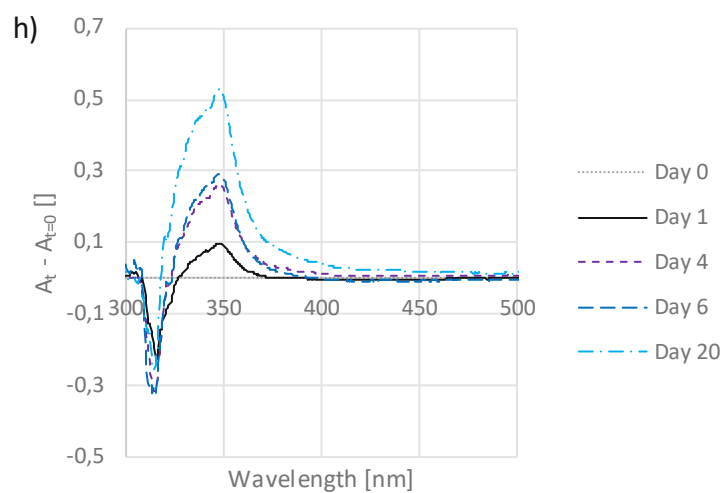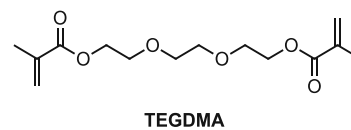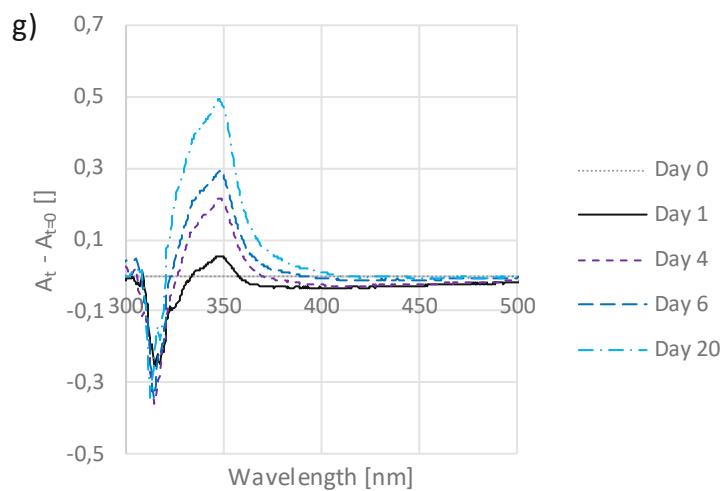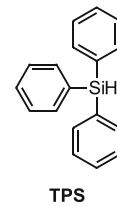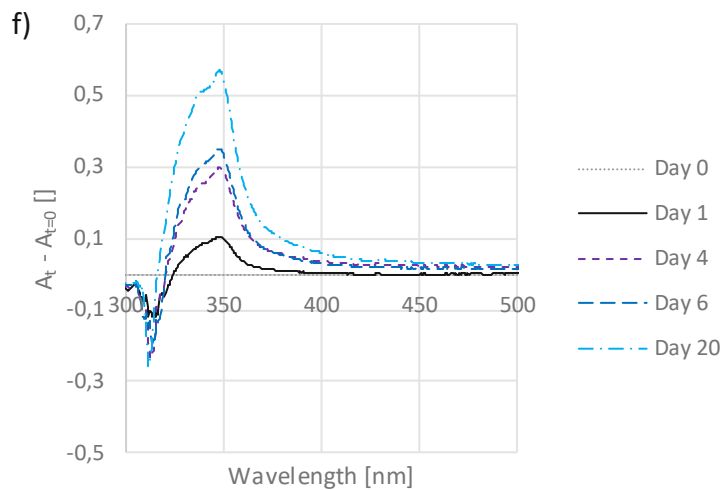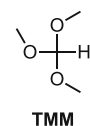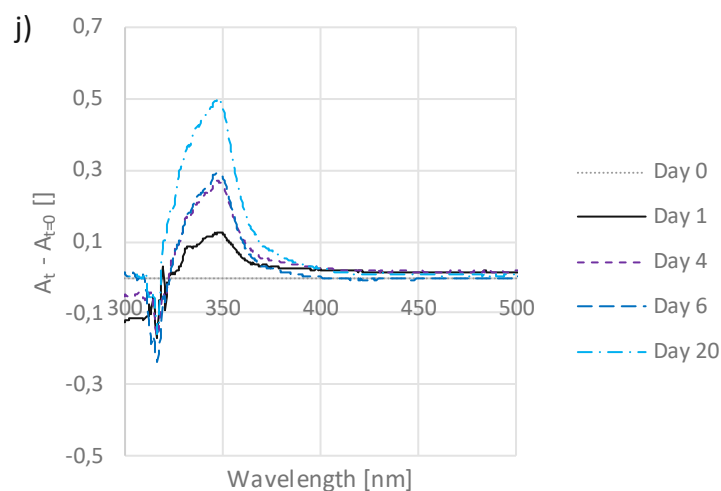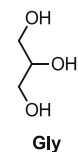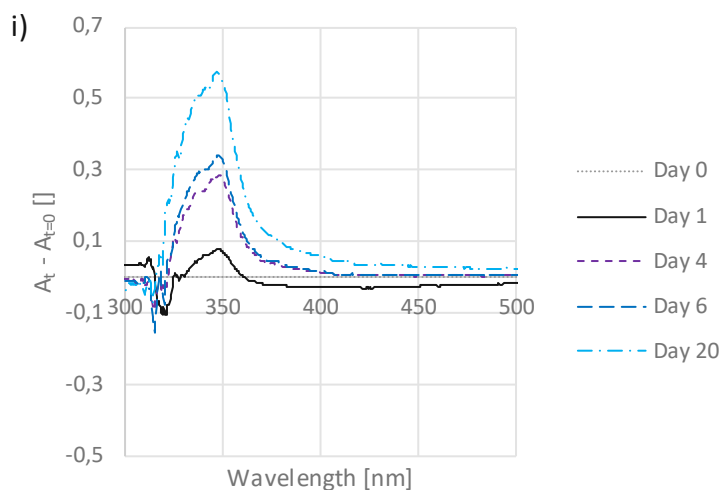
- Siccatives

For the evaluation of the effect of siccatives on the discoloration behavior, formulations consisting of **UDMA**, **TPO** (1.07 mol%) and 1 wt% of the siccative zirconium octoate should be prepared. Zirconium octoate was obtained as a 6% solution in mineral spirits. For the preparation of the formulation, an unspecified amount of this siccative was filled in a tared sample vial, the solvent was evaporated, the amount of zirconium octoate was determined and **UDMA** and **TPO** were added in adequate quantities. The resulting thin film sample was then stored dry at 37°C and analyzed using UV-Vis absorption measurements. The corresponding difference absorption spectra are depicted in comparison with a blind sample in Table 27.

*Table 27: Time-dependent difference absorption spectra of thin film samples consisting of **UDMA** and **TPO** (1.07 mol%) (a) and additional 1 wt% of zirconium octoate (b), stored dry at 37°C.*

a)

Blind

b)

Zirconium octoate
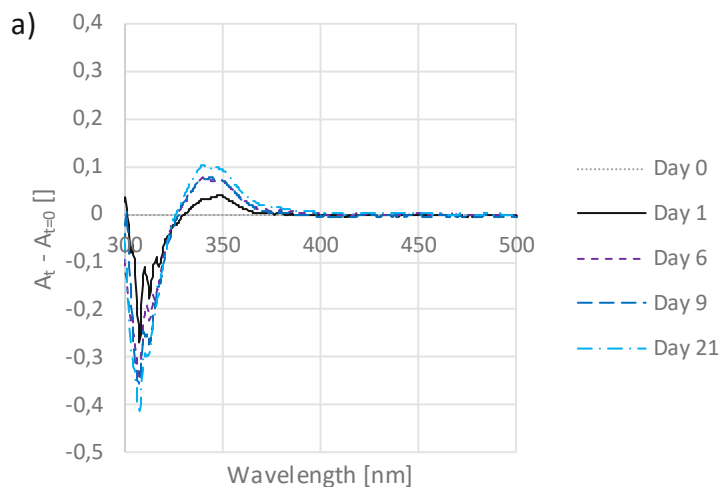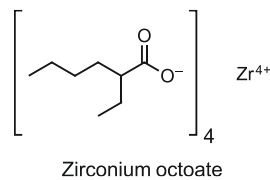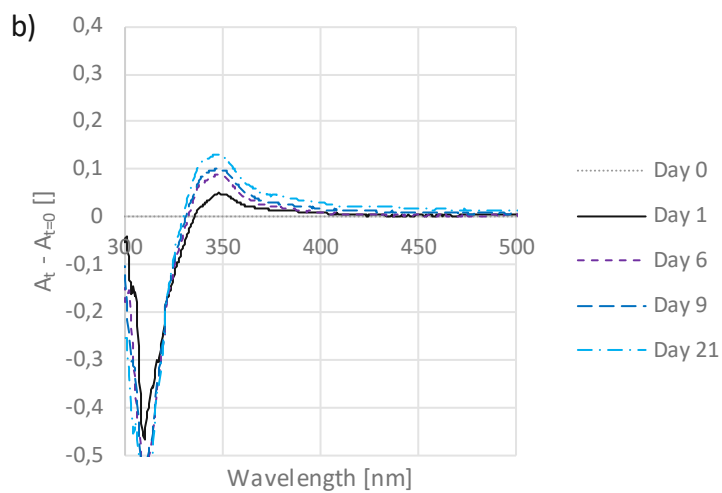
## 1.5 Hypotheses for causes of discoloration

1.5.1 Hypothesis 1

1.5.1.1.1 Synthesis of MC2 and MC3

The model compounds **MC2** and **MC3** were synthesized analogously to literature.[117]
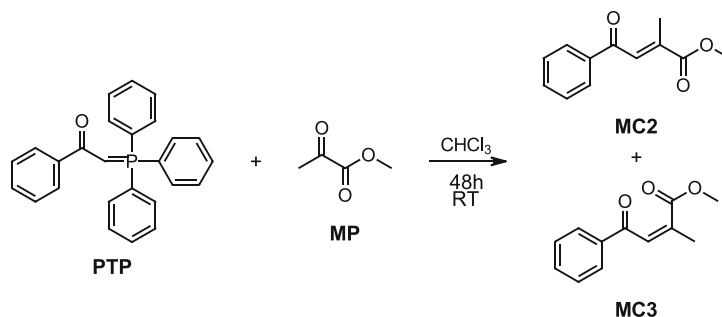
PTP (3.00 g, 7.88 mmol, 1.1 eq.) was dissolved in 12 mL chloroform$_{abs}$ under inert gas atmosphere. While stirring **MP** (0.73 g, 7.17 mmol, 1 eq.) was added dropwise to the yellow PTP solution. After stirring the mixture for 48 hours at room temperature, the TLC control showed full conversion. The crude mixture was concentrated and about one half of it was separated by means of column chromatography. A column loaded with 42 g silica gel, conditioned with PE:EE (98:2) was used. The products were eluted by gradient elution. The separation was only partially successful and several mixed fractions were obtained. The pure fractions were combined and evaporated to obtain the yellow liquid products **MC2** and **MC3**. The remaining crude product and mixed fractions were not further processed, explaining the low yields.

MC2:

Yield	176.5 mg (12% of the theory)
¹H-NMR (400 MHz, CDCl₃)	δ 7.96 (dd, J = 8.4, 1.4 Hz, 2H, C-**H**$_{Ar}$), 7.72 (q, J = 1.5 Hz, 1H, -C**H**=C-), 7.59 (tt, J = 7.4, 2.0 Hz, 1H, C-**H**$_{Ar}$), 7.49 (t, J = 7.5 Hz, 2H, C-**H**$_{Ar}$), 3.85 (s, 3H, -O-C**H₃**), 2.19 (d, J = 1.6 Hz, 3H, CH=C-C**H₃**). – Corresponds to literature.[118]
λ$_{max}$ (n-π*):	356 nm (in acetonitrile)

MC3:

Yield	42.9 mg (3% of the theory)
¹H-NMR (400 MHz, CDCl₃)	δ 7.92 (dd, J = 8.4, 1.4 Hz, 2H, C-**H**$_{Ar}$), 7.57 (tt, J = 7.5, 1.4 Hz, 1H, C-**H**$_{Ar}$), 7.46 (t, J = 7.5 Hz, 2H, C-**H**$_{Ar}$), 6.76 (q, J = 1.6 Hz, 1H, -C**H**=C-), 3.64 (s, 3H, -O-C**H₃**), 2.15 (d, J = 1.6 Hz, 3H, CH=C-C**H₃**). Corresponds to literature.[119]
λ$_{max}$ (n-π*)	339 nm (in acetonitrile)

A thin film sample consisting of **UDMA**, **TPO** (1.07 mol%) and **MC1** (1 mol%) (Figure 53a) was prepared, as described in 1.2.1. The sample was analyzed using UV-Vis absorption measurements and compared with a blind sample without MC1. The specimens were stored under dry conditions at 37°C.

An experiment to oxidize **MC1** with the hydroperoxide **CHP** was conducted. For this purpose, a sample solution of **MC1** (0.005 M) in acetonitrile was compared with a solution consisting of **MC1** (0.005 M) and **CHP** (0.005 M) in acetonitrile using UV-Vis absorption measurements. Additionally, the solution containing **MC1** and **CHP** was briefly heated several times with a heat gun and then measured again. The results are illustrated in Figure 102. The respective spectra are virtually congruent, which means that **CHP** has no effect on **MC1**.
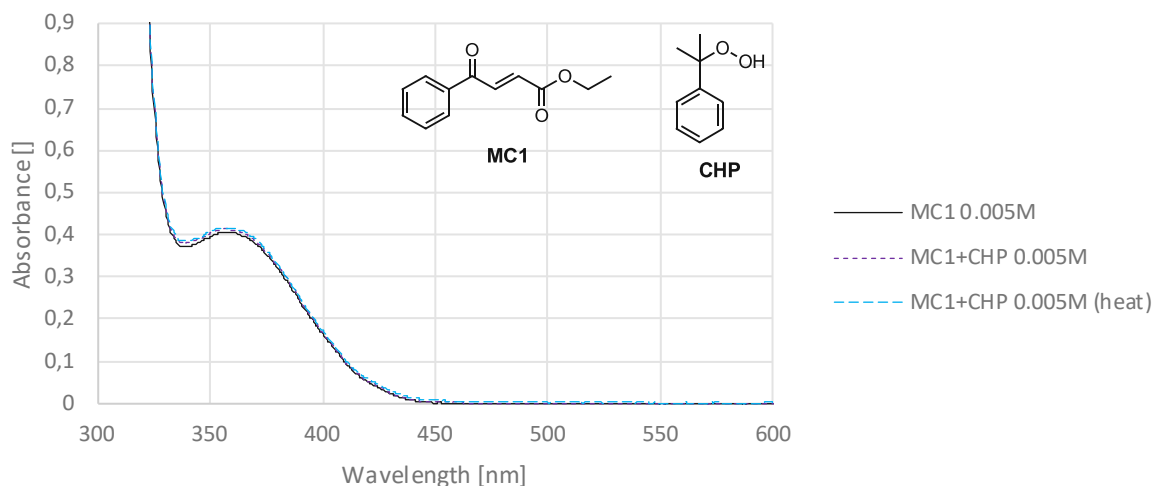
*Figure 102: UV-Vis absorption measurements of solutions of **MC1** and **CHP** in acetonitrile.*

1.5.2 Hypothesis 2

UV-Vis absorption spectra of the purchased substances benzaldehyde, benzoin, benzil, anisaldehyde, anisoin, anisil and mesitaldehyde dissolved in acetonitrile were recorded. The absorption spectrum of mesitil was obtained from the work of Wolf et al.[80] One attempt was made to synthesize mesitoin.

Synthesis of Mesitoin

The reaction was performed analogously to literature.[120]

TMB + NaCN → Mesitoin
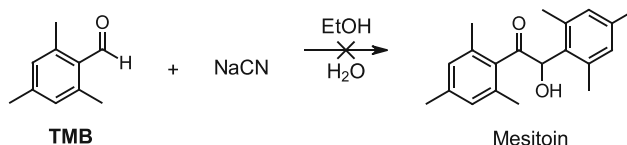
NaCN (2.14 g, 43 mmol, 4.3 eq.) was dissolved in a mixture of ethanol (3 mL) and deionized water (2 mL). Trimethylbenzaldehyde (TMB, 3.00 g, 20 mmol, 2 eq.) was added to the stirring solution. The reaction mixture was heated to reflux for 3 h. The reaction control by TLC showed no conversion of TMB, even after a further 2 hours of refluxing. The reaction mixture was discarded and no further attempts were made for this reaction.

2 Photoinitiators

2.2 Benzoyl modified MAPOs

2.2.1 Synthesis

2.2.1.1 Synthesis of 2,4-dimethoxy-6-methylbenzoyldiphenylphosphine oxide (**B1**)

DMBA + **DPO**
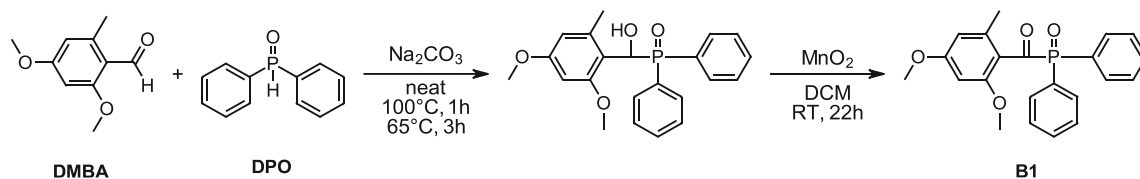
The literature known photoinitiator **B1** was synthesized and characterized by the company Ivoclar AG, analogously to the work of Dietlin et al.[83]

2.2.1.2 Synthesis of 2,4,6-trimethoxybenzoyldiphenylphosphine oxide (**B2**)

TMBA + **DPO**
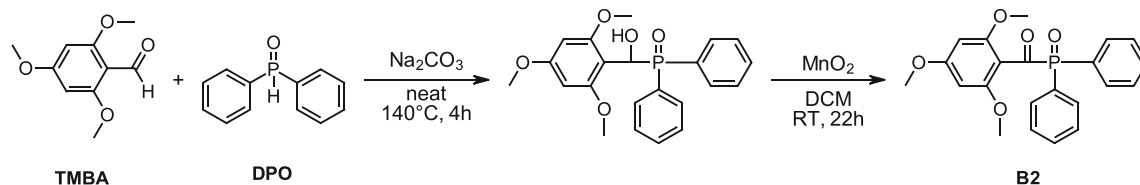
The literature known photoinitiator **B2** was synthesized and characterized by the company Ivoclar AG, analogously to the work of Dietlin et al.[83]

2.2.1.3 Synthesis of 2,4,6-triisopropylbenzoyldiphenylphosphine oxide (B3)

2.2.1.3.1 Synthesis of 2,4,6-triisopropylbenzoylchloride
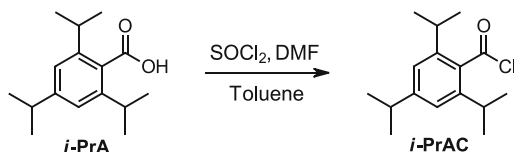
In a first step, 2,4,6-triisopropylbenzoyl chloride (*i*-PrAC) was prepared according to literature, but using 2,4,6-triisopropylbenzoic acid (*i*-PrA) as reactant and toluene as solvent.[121] The reaction was conducted in argon atmosphere. 2,4,6-Triisopropylbenzoic acid (*i*-PrA, 2.28 g, 9.2 mmol, 1 eq.) was dissolved in 10 mL toluene$_{abs}$ and one drop of DMF was added. Afterwards thionylchloride (SOCl$_2$, 4.59 g, 38.6 mmol, 4.2 eq.) was dropped into the mixture, before refluxing for 3.5 hours. The volatile components were separated by distillation to yield the slightly yellow solid product *i*-PrAC. This crude product was used without further purification for the subsequent reaction.

m.p.	81.5 – 83.5°C
^{1}H-NMR (400 MHz, CDCl$_3$)	δ 7.03 (s, 2H, C-**H**$_{Ar}$), 3.05 (hept, *J* = 6.8 Hz, 2H, C**H**-(CH$_3$)$_2$), 2.90 (hept, *J* = 6.7 Hz, 1H, C**H**-(CH$_3$)$_2$), 1.28 (d, *J* = 6.8 Hz, 12H, CH-(C**H$_3$**)$_2$), 1.26 (d, *J* = 6.9 Hz, 6H, CH-(C**H$_3$**)$_2$).

2.2.1.3.2 Synthesis of 2,4,6-triisopropylbenzoyldiphenylphosphine oxide (B3)
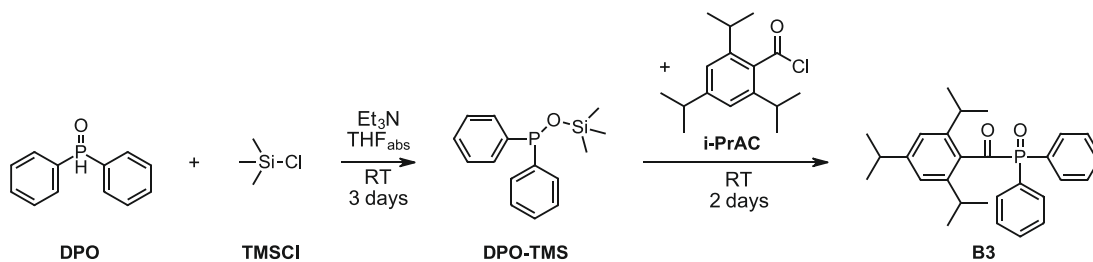
The reaction for the preparation of **B3** was performed based on the literature of Zhang et al., under light exclusion and argon atmosphere.[99] Dry Et$_3$N (0.40 g, 3.9 mmol, 1.2 eq.) was added to a solution of diphenylphosphine oxide (**DPO**, 0.65 g, 3.2 mmol, 1.0 eq.), dissolved in 7 mL THF$_{abs}$. Freshly distilled **TMSCl** (0.42 g, 3.9 mmol, 1.2 eq.) was added while stirring and white solid precipitated immediately. The reaction was stirred at room

temperature for 3 days before a solution of *i*-**PrAC** (0.96 g, 3.6 mmol 1.1 eq.) in 3 mL THF$_{abs}$ was added dropwise. The mixture was then stirred for another 2 days at room temperature. The solids were filtrated, and the solvent evaporated. The crude product was purified by column chromatography to yield 0.40 g (29% of theory) of the light-yellow solid product **B3**.

¹H-NMR (600 MHz, CDCl₃)	δ 7.99 (dd, *J* = 11.0, 7.1 Hz, 4H, C-**H**$_{Ar}$), 7.57 (td, *J* = 7.5, 1.3 Hz, 2H, C-**H**$_{Ar}$), 7.50 (td, *J* = 7.5, 3.1 Hz, 4H, C-**H**$_{Ar}$), 6.97 (s, 2H, C-**H**$_{Ar}$), 2.86 (hept, *J* = 6.9 Hz, 1H, C$_{Ar}$-**CH**-(CH₃)₂), 2.43 (hept, *J* = 6.7 Hz, 2H, C$_{Ar}$-**CH**-(CH₃)₂), 1.22 (d, *J* = 6.9 Hz, 6H, CH-(**CH₃**)₂), 1.00 (d, *J* = 6.7 Hz, 12H, CH-(**CH₃**)₂).
³¹P-NMR (243 MHz, CDCl₃)	δ 12.88.
¹³C-NMR (151 MHz, CDCl₃)	δ 221.17 (d, *J* = 72.1 Hz), 151.48, 145.91, 134.46 (d, *J* = 38.6 Hz), 132.45 (d, *J* = 2.8 Hz), 132.03 (d, *J* = 8.5 Hz), 130.00 (d, *J* = 92.6 Hz), 128.79 (d, *J* = 11.6 Hz), 121.45, 34.58, 31.92, 24.01.
UPLC-MS	2.22 min; [M+H]⁺ 433.15
HRMS	Calculated: [M + Na]⁺ 455.2108; Found: 455.2112

2.2.1.4 Synthesis of 2,4,6-trimethoxybenzoyl-di-*tert*-butylphosphine oxide (**B4-1**)

2.2.1.4.1 <u>Synthesis of 2,4,6-trimethoxybenzoylchloride</u>
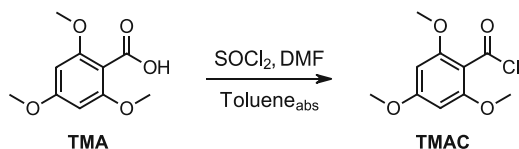
In a first step, 2,4,6-trimethoxybenzoic acid chloride (**TMAC**) was prepared according to literature, but using toluene as a solvent instead of DCM.[121] The reaction was conducted in argon atmosphere. 2,4,6-Trimethoxybenzoic acid (**TMA**, 2.50 g, 11.8 mmol, 1eq.) was dissolved in 10 mL toluene$_{abs}$ and one drop of DMF. Afterwards, thionylchloride (**SOCl₂**, 7.02 g, 59.0 mmol, 5 eq.) was dropped into the mixture, which was then refluxed for 4 hours. The volatile components were separated by distillation to yield the deep red

viscous product **TMAC**. This crude product was used without further purification for the subsequent reaction.

UPLC-MS 1.70 min.

2.2.1.4.2 Synthesis of 2,4,6-trimethoxybenzoyl-di-tert-butylphosphine oxide (**B4-1**)
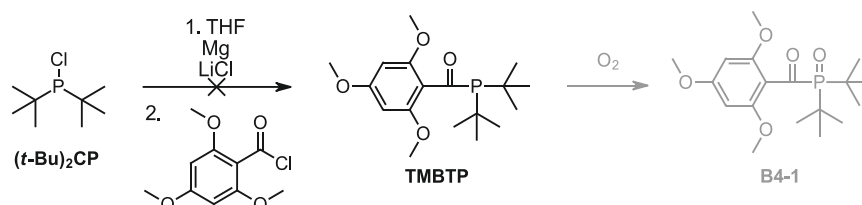
The reaction was performed analogously to the patent literature of Suzuki et al., under inert gas atmosphere and light exclusion.[101] Metal Mg (0.50 g, 20.6 mmol, 1.75 eq.) and LiCl anhydrous (0.50 g, 11.8 mmol, 1 eq.) were suspended in 2 mL THF$_{abs}$. Two drops of (***t*-Bu)₂CP** and one grain of iodine were added and briefly heated to boiling point. No distinct start of the Grignard-like reaction could be observed, therefore another 5 drops of (***t*-Bu)₂CP** and one more grain of iodine were added and heated, before the mixture was placed in an ultrasonic bath for 15 minutes. Despite the fact that no clear start of the reaction was detected, the remaining (***t*-Bu)₂CP** (in total: 2.14 g, 11.8 mmol, 1 eq.) was added and stirred for 3 hours at room temperature. The excess Mg was removed by transferring the reaction solution using a transfer cannula. The mixture was then cooled using an ice bath and the previously prepared acid chloride **TMAC** (2.72 g, 11.8 mmol, 1 eq.) dissolved in 30 mL toluene$_{abs}$ was added dropwise. No obvious reaction could be observed. A reaction control using UPLC-MS showed no conversion and further stirring at RT overnight could not achieve a reaction either. Therefore, the reaction was stopped and discarded.

2.2.1.5 Synthesis of 2,6-dimethoxybenzoyl-di-*tert*-butylphosphine oxide (**B4-2**)

2.2.1.5.1 Synthesis of 2,6-dimethoxybenzoylfluoride (**DMBF**)
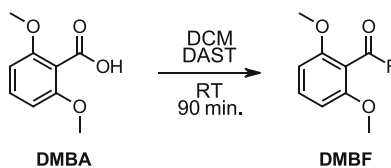
The synthesis was performed analogously to the work of Kaduk et al.[122] The reaction was carried out in argon atmosphere. 2,6-Dimethoxybenzoic acid (**DMBA**, 3.64 g, 19.98 mmol, 1 eq.) was suspended in 90 mL DCM$_{abs}$. The suspension was cooled with an ice bath and diethylaminosulfur trifluoride (**DAST**, 2.8 mL, 20.98 mmol, 1.05 eq.) was added dropwise. The yellow solution was stirred over an ice bath for 90 min. Then 20 mL saturated NH$_4$Cl solution were added dropwise. The organic phase was separated and the aqueous phase was extracted with 30 mL DCM. The combined organic phases were dried with Na$_2$SO$_4$. The solvent was removed to obtain the yellow solid product. This crude product was used without further purification for the subsequent reaction.

2.2.1.5.2 Pathway A) Synthesis of 2,6-dimethoxybenzoyl-di-*tert*-butylphosphine oxide (B4-2)
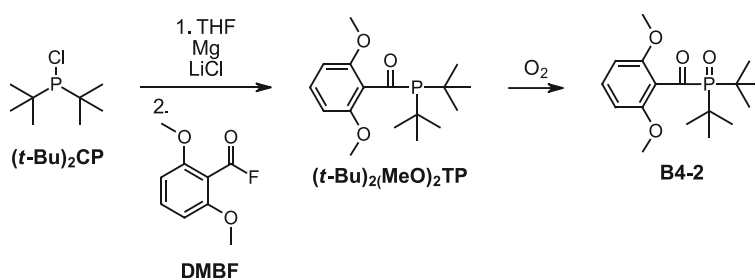

The reaction was carried out under inert gas atmosphere and in the absence of light, similarly to the patent literature by Suzuki et al., but with a slightly lower amount of **DMBF**.[101] Metal Mg (0.57 g, 23.49 mmol, 1.8 eq.) and LiCl anhydrous (0.64 g, 15.1 mmol, 1.1 eq.) were suspended in 2 mL THF$_{abs}$. One grain of iodine and 3 drops of (**t-Bu)$_2$CP** were added and the mixture was heated to start the reaction. The reaction was cooled with an ice bath and the remaining (**t-Bu)$_2$CP** (2.70 g, 15.0 mmol, 1.1 eq.) diluted in 15 mL THF$_{abs}$ was added dropwise. After stirring for 2 h at room temperature, the actual start of the reaction could be observed by means of a gray turbidity. The excess Mg was removed by transferring the reaction solution using a transfer cannula. **DMBF** (2.46 g, 13.35 mmol, 1 eq.) was dissolved in 5 mL THF$_{abs}$ and slowly added to reaction mixture which was cooled with an ice bath. The ice bath was removed and the initially deep red solution is stirred for 2 days at room temperature, whereby it turned yellow. The reaction was quenched by the addition of 10 mL 3% aqueous H$_2$SO$_4$. The organic phase was

separated, washed with water and saturated NaCl solution, before being dried with Na$_2$SO$_4$. The solvent was removed to yield an oily crude product. The product was exposed to air for 2 days, before it was attempted to be purified by column chromatography over silica. The product could not be recovered by gradient elution with a mixture of PE and EE. After 12 days, the column was washed with an EE:MeOH mixture to obtain an orange solid containing the product. Further purification by column chromatography with a mixture of EE:MeOH was necessary to yield a mostly pure product (2.17 g, 50% of theory, m.p.: 114 – 126°C). In a further purification step, 1.09 g of the solid were recrystallized from a mixture of PE and toluene. The pure yellow solid product (0.786 g) was obtained in a total yield of 36% of the theory.

m.p.	136.6 – 138.4°C
^{1}H-NMR (600 MHz, CDCl$_3$)	δ 7.32 (t, *J* = 8.4 Hz, 1H, C-**H**$_{Ar}$), 6.57 (d, *J* = 8.4 Hz, 2H, C-**H**$_{Ar}$), 3.81 (s, 6H, O-C**H$_3$**), 1.33 (s, 9H, C-(C**H$_3$**)$_3$), 1.30 (s, 9H, C-(C**H$_3$**)$_3$)
^{31}P-NMR (243 MHz, CDCl$_3$)	δ 50.57
^{13}C-NMR (151 MHz, CDCl$_3$)	δ 217.17 (d, *J* = 59.0 Hz), 158.18, 132.98, 119.53 (d, *J* = 34.8 Hz), 104.85, 56.03, 37.00 (d, *J* = 51.0 Hz), 27.12.
UPLC-MS	1.63 min.; [M+H]$^+$ 327.05
HRMS	Calculated: [M + H]$^+$ 327.1719;
	Found: 327.1733

2.2.1.5.3 <u>Pathway B) Synthesis of 2,6-dimethoxybenzoyl-di-*tert*-butylphosphine oxide (**B4-2**)</u>
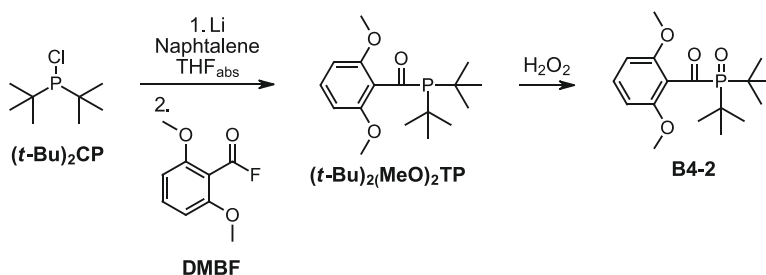
The synthesis was performed under argon atmosphere and in absence of light, analogously to the work of Ullrich et al.[102] Lithium foil (0.19 g, 26.97 mmol, 2.15 eq.) was

suspended in 10 mL THF$_{abs}$. Naphthalene (10.6 mg, 0.08 mmol, 0.007 eq.) was dissolved in 2 mL THF$_{abs}$ and added to the stirring suspension. The mixture was stirred for 15 minutes, whereby it first turned green and then dark brown. (**t-Bu)$_2$CP** (2.30 g, 12.75 mmol, 1 eq.) in 5 mL THF$_{abs}$ was dropped in slowly and the solution became clear and yellow in color. The reaction was stirred for 1 h at room temperature, whereby turbidity appeared again and the color changed to reddish brown. The mixture was filtered under inert conditions to separate the remaining solids and to obtain an orange solution. **DMBF** (2.47 g, 13.40 mmol, 1.05 eq.) was dissolved in a total of 20 mL THF$_{abs}$ and added dropwise to the solution, which turned red as a result. Half of the solution was worked up after 2 h stirring, the other half after 16 h. For this, the solvent was removed and the crude product was suspended in 13 mL toluene, then 30% H$_2$O$_2$ (1.3 mL, 12.75 mmol, 1 eq.) was added and stirred for 20 min at room temperature. 100 mL EE were added and washed with 50 mL saturated NaHCO$_3$. The aqueous phase was extracted 3 times with 50 mL EE each and the combined organic layers were washed with saturated NaCl, dried with Na$_2$SO$_4$ and evaporated to yield a yellow oil. Both fractions contained the desired product, whereby the one stirred for only 2 h contained relatively higher amounts of the desired product according to the UPLC-MS measurements. No further purification of the crude products was carried out, as the desired substance was already available in sufficient quantity and purity from pathway A).

UPLC-MS   1.67 min.; [M+H]$^+$ 327.05

2.2.2 Characterization

2.2.2.2 Photo-DSC

For the quantification of the photo-DSC measurements, several parameters were used. The time until heat flow maximum is reached (t_{max}), the heat of polymerization (Area), the time to reach 95 % of the total heat flow ($t_{95\%}$) and the onset of the polymerization are obtained directly from the evaluation of the photo-DSC curves. The rate of polymerization (R_P) is calculated from the peak height using the following Equation 1:

$$R_P \left[\frac{mmol}{s * L} \right] = \frac{h * \rho}{\Delta H_0} * 1000$$

<div align="right">*Equation 1*</div>

h	*Maximal height of the photo-DSC peak [mW/mg]*
ρ	*Density of the monomer [g/L]: ρ(UDMA) = 1100 g/L*
ΔH_0	*Theoretical polymerization heat of the monomer [J/mol]: ΔH_0(UDMA)≈112000 J/mol. The theoretical polymerization heat of monofunctional methacrylates is around 56000 J/mol.[123, 124]*

The calculation of the double bond conversion (DBC) is determined by Equation 2.

$$DBC \ [\%] = \frac{\Delta H_P * M_M * W_M}{\Delta H_0}$$

<div align="right">*Equation 2*</div>

ΔH_P	*Heat of polymerization [J/g]*
M_M	*molecular weight of the monomer [g/mol]: M_M(UDMA) = 470.56 g/mol*
W_M	*weight percentage of the monomer in the formulation [%]*
ΔH_0	*Theoretical polymerization heat of the monomer [J/mol]: ΔH_0(UDMA)=112000 J/mol. The theoretical polymerization heat of monofunctional methacrylates is around 56000 J/mol.[123, 124]*

320 – 500 nm broadband light source (OmniCure® S2000)

For these measurements an OmniCure® S2000 high pressure mercury vapor light source equipped with a 320 – 500 nm filter was used as light source. The light intensity at the sample surface was set to 64 mW/cm². The results are summarized in Table 28.

Table 28: Results of photo-DSC measurements of formulations, consisting of 1 mol% photoinitiator in the monomer UDMA, under irradiation with a broadband light source (320-500 nm) with an intensity of 64 mW/cm².

320-500 nm	t_{max} [s]	R_p [mmol*L⁻¹*s⁻¹]	$t_{95\%}$ [s]	Onset [s]	Area [J/g]	DBC [%]
TPO	4.3 ± 0.2	176.0 ± 3.5	34.0 ± 1.6	1.7 ± 0.1	154.0 ± 0.2	64.2 ± 0.1
TPO-L	5.1 ± 0.3	147.8 ± 5.3	32.4 ± 1.5	2.1 ± 0.2	141.1 ± 1.3	58.9 ± 0.5
■ B1	5.1 ± 0.2	142.8 ± 4.4	35.4 ± 1.0	1.6 ± 0.0	142.4 ± 0.9	59.3 ± 0.4
○ B2	5.4 ± 0.2	137.2 ± 11.4	34.9 ± 1.5	1.8 ± 0.1	142.7 ± 7.0	59.4 ± 2.9
✖ B3	10.6 ± 0.2	81.3 ± 2.0	43.7 ± 0.8	3.5 ± 0.2	117.2 ± 1.5	48.8 ± 0.6
★ B4-2	5.0 ± 0.1	148.3 ± 6.7	29.9 ± 1.3	2.1 ± 0.0	136.0 ± 4.7	56.8 ± 2.0

385 nm LED light source

For the measurements a 385 nm OmniCure® Max LED light source was used. The light intensity at the sample surface was set to 10 mW/cm². The results are summarized in Table 29.

Table 29: Results of photo-DSC measurements of formulations, consisting of 1 mol% photoinitiator in the monomer UDMA, under irradiation with a LED light source (385 nm) with an intensity of 10 mW/cm².

385 nm	t_{max} [s]	R_p [mmol*L^{-1}*s^{-1}]	$t_{95\%}$ [s]	Onset [s]	Area [J/g]	DBC [%]
TPO	5.5 ± 0.2	138.5 ± 1.5	32.2 ± 1.1	1.9 ± 0.0	138.3 ± 3.6	57.7 ± 1.5
TPO-L	6.1 ± 0.0	131.0 ± 4.2	35.2 ± 1.5	2.5 ± 0.1	134.9 ± 2.0	56.3 ± 0.8
■ B1	5.8 ± 0.1	132.5 ± 3.3	33.3 ± 1.3	1.9 ± 0.0	136.6 ± 4.0	56.9 ± 1.7
○ B2	6.2 ± 0.0	134.7 ± 4.5	32.8 ± 1.6	2.1 ± 0.0	136.1 ± 4.7	56.7 ± 2.0
✖ B3	12.5 ± 0.7	57.7 ± 2.6	48.7 ± 0.5	3.0 ± 0.2	104.0 ± 1.2	43.3 ± 0.5
★ B4-2	6.2 ± 0.2	127.2 ± 6.5	32.3 ± 1.3	2.5 ± 0.1	129.2 ± 1.2	53.9 ± 0.5

400 nm LED light source

For the measurements with a 400 nm light source the corresponding OmniCure® Max LED head was used. The light intensity at the sample surface was set to 10 mW/cm². The results are summarized in Table 30.

Table 30: Results of photo-DSC measurements of formulations, consisting of 1 mol% photoinitiator in the monomer UDMA, under irradiation with a LED light source (400 nm) with an intensity of 10 mW/cm².

400 nm	t_{max} [s]	R_p [mmol*L^{-1}*s^{-1}]	$t_{95\%}$ [s]	Onset [s]	Area [J/g]	DBC [%]
TPO	5.3 ± 0.1	156.8 ± 1.3	30.5 ± 0.3	2.1 ± 0.0	145.8 ± 0.8	60.8 ± 0.3
TPO-L	6.4 ± 0.0	134.9 ± 3.1	34.7 ± 1.5	2.7 ± 0.0	135.4 ± 2.2	56.5 ± 0.9
■ B1	5.7 ± 0.1	144.6 ± 6.2	31.6 ± 0.7	2.3 ± 0.0	135.6 ± 3.9	56.5 ± 1.6
○ B2	6.5 ± 0.1	135.5 ± 0.8	31.5 ± 0.9	2.7 ± 0.1	134.7 ± 2.2	56.1 ± 0.9
✖ B3	12.9 ± 0.2	63.4 ± 1.7	47.6 ± 0.2	4.5 ± 0.2	105.2 ± 1.1	43.8 ± 0.4
★ B4-2	5.9 ± 0.2	135.8 ± 2.0	32.1 ± 0.7	2.5 ± 0.1	129.9 ± 0.5	54.2 ± 0.2

2.2.2.3 Discoloration behavior

CIELAB method

The CIELAB measurements were carried out by the company Ivoclar AG with samples consisting of **UDMA** and 1 mol% of the respective photoinitiator. The exact procedure is described in section 1.2.2. The results for ΔL, Δa and Δb are depicted in Figure 103, those of the values L, a and b are shown in Figure 104.
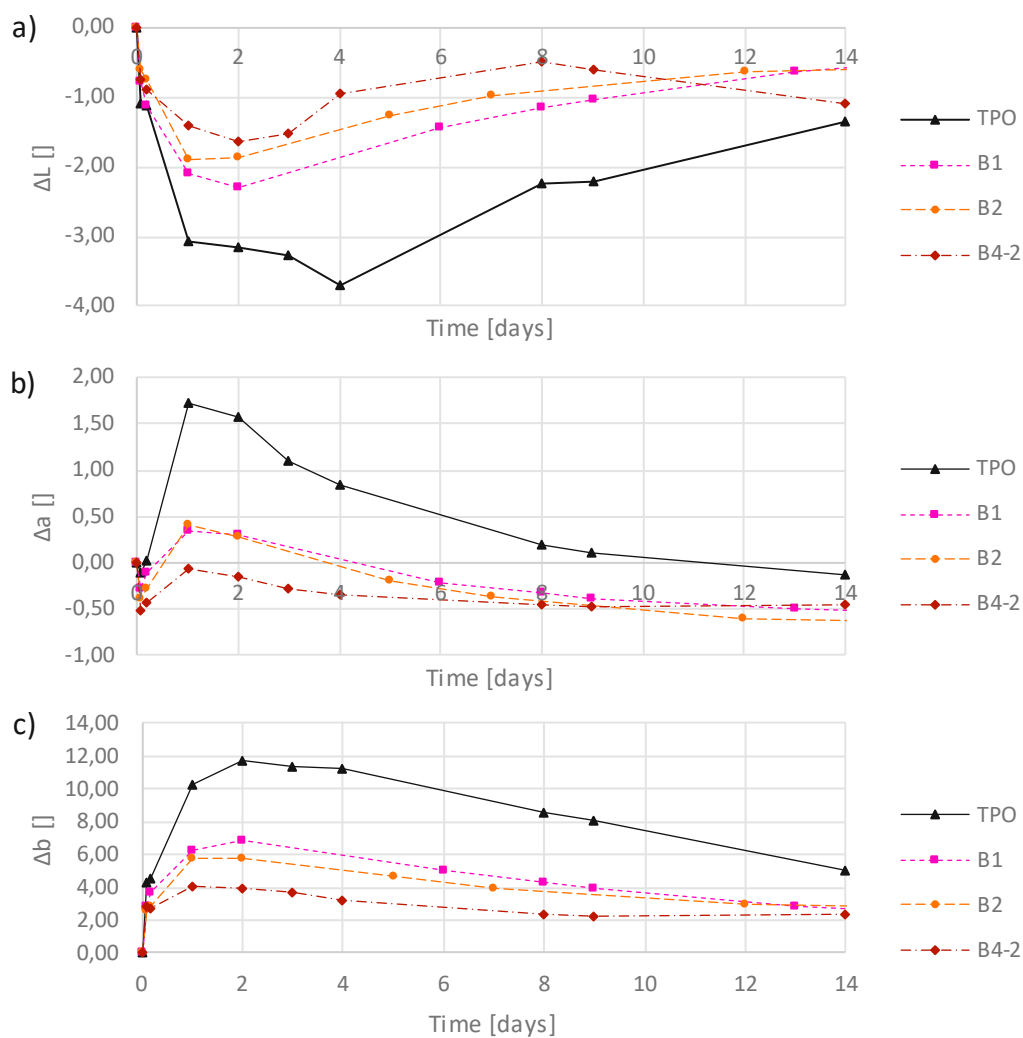
*Figure 103: Change of lightness ΔL (a), green-red error Δa (b) and blue-yellow error Δb (c) of samples consisting of **UDMA** (stabilized with 100 ppm **MeHQ**) and 1 mol% of the benzoyl modified photoinitiators **B1**, **B2**, **B4-2** and **TPO**. The thin film samples were immersed in water and stored at 50°C.*
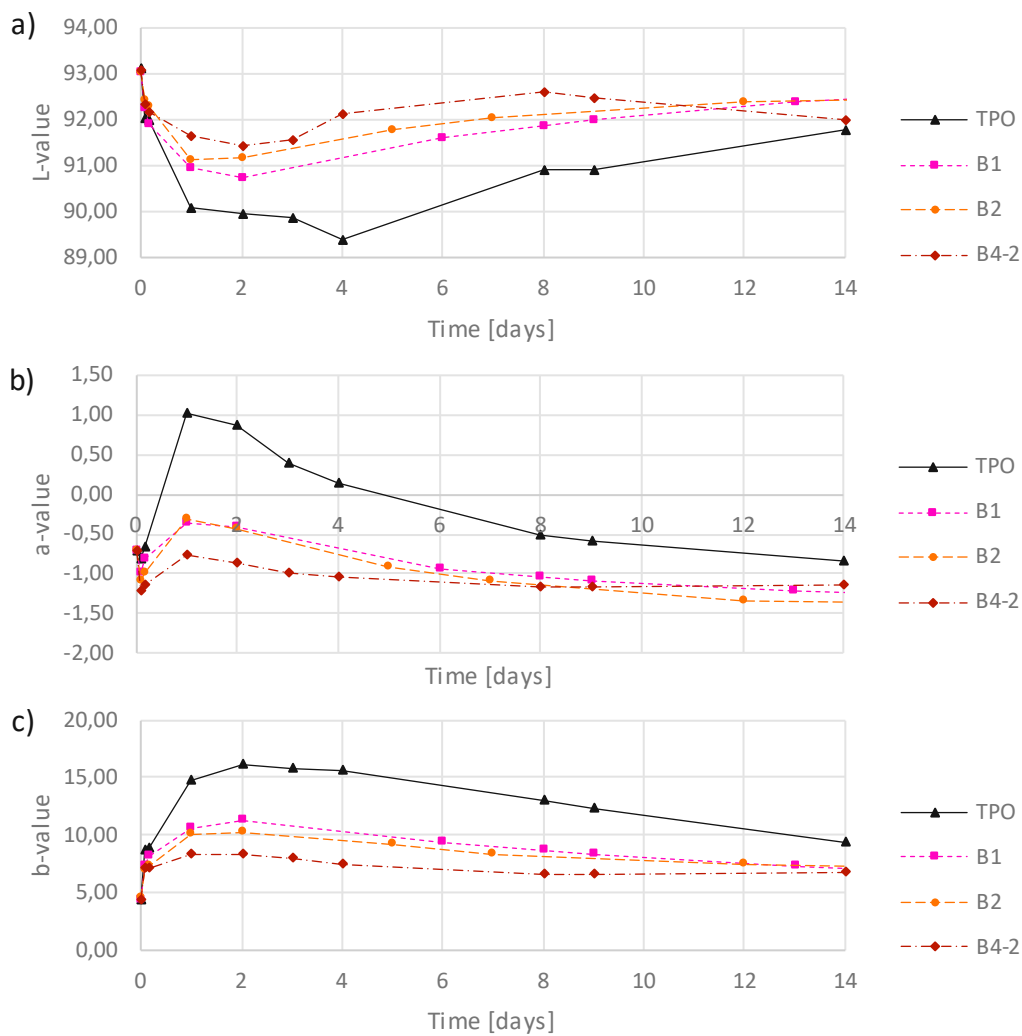
*Figure 104: L-values (a), a-values (b) and b-values (c) of samples consisting of **UDMA** (stabilized with 100 ppm **MeHQ**) and 1 mol% of the benzoyl modified photoinitiators **B1**, **B2**, **B4-2** and **TPO**. The thin film samples were immersed in water and stored at 50°C.*

2.3 Phosphorus modified MAPOs with different alkyl/phenyl substituents

2.3.1 Synthesis

2.3.1.1 Synthesis of 2,4,6-trimethylbenzoyl-cyclohexylphenylphosphine oxide (**P1**)

2.3.1.1.1 <u>Pathway A) Synthesis of cyclohexylphenylphosphine oxide (**CHPO**)</u>
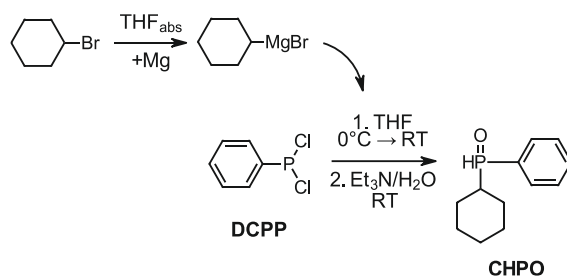
The reaction was performed in analogy to literature in inert gas atmosphere.[103] In the first step, Mg-shavings (0.73 g, 30 mmol, 1.0 eq.) are suspended in 4 ml THF$_{abs}$ and bromocyclohexane (4.92 g, 30 mmol, 1.0 eq.) is filled in a dropping funnel. 3 drops of bromocyclohexane were added to the stirring suspension and the Grignard reaction was started by heating until boiling. The remaining bromocyclohexane was diluted with 25 ml THF$_{abs}$ and slowly added to the reaction mixture. The reaction was stirred at ambient temperature for 2 h.

In a separate flask, under inert gas atmosphere, dichlorophenylphosphine (**DCPP**, 5.38 g, 30 mmol, 1.0 eq.) was dissolved in 25 mL THF$_{abs}$ and cooled with an ice bath. The cyclohexylmagnesium bromide solution was added dropwise while stirring. The ice bath was removed and after 2 h stirring the reaction was quenched by the addition of a mixture of Et$_3$N (4.55 g, 45 mmol, 1.5 eq.), water (0.81 g, 45 mmol, 1.5 eq.) and THF (6 ml). The mixture was stirred for 1 h before being filtrated, dried with Na$_2$SO$_4$ and filtrated again. After evaporation of the solvent, a white solid was obtained as crude product. UPLC-MS measurements showed that the reaction was successful, but yielded several by-products. 2D-TLC control did not show any degradation, so an attempt was made to purify the crude product by solid loaded column chromatography. Although separated peaks could be observed at the UV detector, the respective fractions appear to be mixtures of substances. Even after repeated column chromatography of the "pre-purified" products,

no pure product could be obtained. Although 2D-TLC had not shown any degradation, it is assumed that the substance is not stable against the silica under prolonged contact.

2.3.1.1.2 Pathway B) Synthesis of cyclohexylphenylphosphine oxide (**CHPO**)
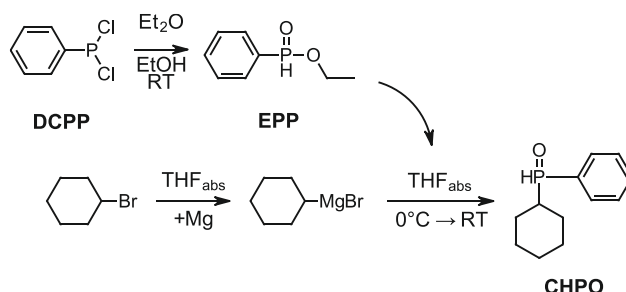
This synthesis was performed analogously to literature.[104] In the first step dichlorophenylphosphine (**DCPP**, 8.75 g, 49 mmol, 1.0 eq.) was dissolved in 80 mL Et$_2$O in an open flask and EtOH (5.65 g, 123 mmol, 2.5 eq.) was added dropwise while stirring. After 2 h the solvents were evaporated to obtain ethyl phenylphosphinate (**EPP**) quantitatively as yellow liquid.

¹H-NMR (400 MHz, CDCl$_3$)	δ 7.70 – 7.63 (m, 2H, C-**H**$_{Ar}$), 7.59 – 7.54 (m, 1H, C-**H**$_{Ar}$), 7.53 – 7.47 (m, 2H, C-**H**$_{Ar}$), 7.19 (dd, J = 456.4, 2.5 Hz, 1H, P-**H**), 1.96 – 1.78 (m, 5H, C-C**H₂**-C), 1.72 – 1.66 (m, 1H, C-C**H**-C), 1.41 – 1.16 (m, 5H, C-C**H₂**-C). Corresponds to literature.[104]

For the second step Mg-shavings (2.57 g, 106 mmol, 2.2 eq.), one grain of iodine and 10 mL THF$_{abs}$ were introduced in a flask under argon atmosphere. To the stirring suspension 5 drops of bromocyclohexane were added and the Grignard reaction was started by heating until boiling. Residual bromocyclohexane (17.22 g, 106 mmol, 2.2 eq.) was diluted with 70 ml THF$_{abs}$ and slowly added to the reaction mixture. The reaction was refluxed for 75 min. Afterwards the solution was cooled with an ice bath. Previously prepared **EPP** (49 mmol, 1.0 eq.) was dissolved in 10 mL THF$_{abs}$, before it was added dropwise to the cold cyclohexylmagnesium bromide solution. The solution was stirred for 90 min. at room temperature and then quenched with 20 mL water and 40 mL 1N HCl.

The aqueous phase was extracted 5 times with 50 mL Et$_2$O each. The organic phase was washed with 80 mL saturated NaHCO$_3$, dried with Na$_2$SO$_4$ and filtrated. The solvent was removed and a yellow crude product was obtained with 63% (6.46 g) of the theoretical yield. 4.36 g of the crude product were purified by Kugelrohr distillation at 205 – 230°C to give 3.01 g of a colorless oil, which corresponds to 43% of the theoretical yield.

^{1}H-NMR (400 MHz, CDCl$_3$)	δ 7.70 – 7.63 (m, 2H, C-**H**$_{Ar}$), 7.59 – 7.54 (m, 1H, C-**H**$_{Ar}$), 7.53 – 7.47 (m, 2H, C-**H**$_{Ar}$), 7.19 (dd, J = 456.4, 2.5 Hz, 1H, P-**H**), 1.96 – 1.78 (m, 5H, C-C**H$_2$**-C), 1.72 – 1.66 (m, 1H, C-C**H**-C), 1.41 – 1.16 (m, 5H, C-C**H$_2$**-C). Corresponds to literature.[104]
^{31}P-NMR (162 MHz, CDCl$_3$)	δ 36.54. Corresponds to literature.[104]
^{13}C-NMR (101 MHz, CDCl$_3$)	δ 132.48 (d, J = 2.8 Hz), 130.43 (d, J = 10.4 Hz), 129.59, 128.86 (d, J = 12.0 Hz), 38.75 (d, J = 69.8 Hz), 26.10 (dd, J = 14.3, 4.0 Hz), 25.88 (d, J = 1.5 Hz), 25.06 (dd, J = 69.3, 2.1 Hz). Corresponds to literature.[104]
UPLC-MS	1.45 min.; [M+H]$^+$ 209.00

2.3.1.1.3 Synthesis of 2,4,6-trimethylbenzoyl-cyclohexylphenylphosphine oxide (**P1**)
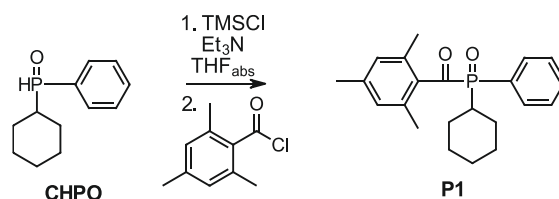
The reaction to produce the desired acylphosphine oxide **P1** was carried out analogously to the literature.[99] Under argon atmosphere and light exclusion, pure **CHPO** (2.36 g, 11 mmol, 1.0 eq.) was dissolved in THF$_{abs}$ (25 mL). Subsequently dry Et$_3$N (1.37 g, 14 mmol, 1.2 eq.) and distilled trimethylsilyl chloride (1.47 g, 14 mmol, 1.2 eq.) were added to the stirring solution. White solid precipitated and the mixture was stirred for 26 h at room temperature. Afterwards distilled 2,4,6-trimethylbenzoyl chloride (3.22 g, 17 mmol, 1.5 eq.) was added. After 67 h solids were removed by filtration and the solvent

was evaporated. The desired product was isolated by solid loaded column chromatography with gradient elution with a mixture of PE and EE. A yield of 2.76 g was obtained, corresponding to 69% of the theoretical yield of the pale-yellow solid.

m.p.	157.6 – 159.6°C
^{1}H-NMR (400 MHz, CDCl$_3$)	δ 7.82 – 7.76 (m, 2H, C-**H**$_{Ar}$), 7.57 – 7.51 (m, 1H, C-**H**$_{Ar}$), 7.50 – 7.44 (m, 2H, C-**H**$_{Ar}$), 6.75 (s, 2H, C-**H**$_{Ar}$), 2.68 – 2.57 (m, 1H, P-C**H**), 2.23 (s, 3H, C$_{Ar}$-C**H$_3$**), 1.99 (s, 6H, C$_{Ar}$-C**H$_3$**), 1.95 – 1.86 (m, 1H, C-C**H$_2$**-C), 1.84 – 1.67 (m, 3H, C-C**H$_2$**-C), 1.53 – 1.37 (m, 3H, C-C**H$_2$**-C), 1.33 – 1.21 (m, 2H, C-C**H$_2$**-C).
^{31}P-NMR (162 MHz, CDCl$_3$)	δ 31.86.
^{13}C-NMR (101 MHz, CDCl$_3$)	δ 221.80 (d, J = 64.3 Hz), 140.58, 135.37, 132.32 (d, J = 2.8 Hz), 131.86, 131.78, 129.10, 128.90 (d, J = 10.8 Hz), 128.63, 127.83, 36.00 (d, J = 67.8 Hz), 26.38 (dd, J = 13.4, 10.6 Hz), 25.81 (d, J = 1.3 Hz), 24.68 (dd, J = 116.2, 2.9 Hz), 21.30, 19.65.
UPLC-MS	2.00 min.; [M+H]$^+$ 355.05
HRMS	Calculated: [M+H]$^+$ 355.1821;
	Found: 355.182

2.3.1.2 Synthesis of 2,4,6-trimethylbenzoyl-phenyl(*tert*-butyl)phosphine oxide (**P2**)

2.3.1.2.1 Synthesis of *tert*-butylphenylphosphine oxide (*t*-BuPO)
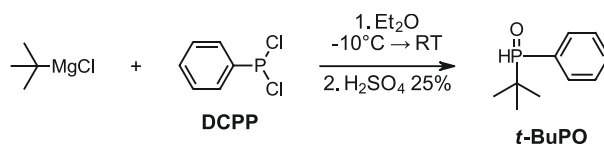
The synthesis of **t-BuPO** was performed analogously to literature.[105] In argon atmosphere a 2 M *tert*-butylmagnesium chloride solution (100 mL, 200 mmol, 4 eq.) in Et$_2$O was presented and cooled to -10°C. A solution of **DCPP** (8.95 g, 50 mmol, 1 eq.) in 10 mL Et$_2$O$_{abs}$ was added carefully to the cooled *tert*-butylmagnesium chloride solution. The cooling bath was removed and the solution stirred for 1 h at ambient temperature. Afterwards 25% aqueous H$_2$SO$_4$ (75 mL) was added slowly. The phases were separated and the aqueous phase was extracted 2 times with 20 mL DCM. The combined organic

phases were dried with Na_2SO_4, filtrated and dried to obtain a yellow crude product. The purification was achieved by Kugelrohr distillation under high vacuum at 166°C. The product **t-BuPO** was obtained as white solid with a yield of 61% of the theory.

m.p.	44.1 – 50.4°C (Literature: 46°C)[105]
¹H-NMR (400 MHz, CDCl₃)	δ 7.70 – 7.64 (m, 2H, C-**H**$_{Ar}$), 7.57 – 7.54 (m, 1H, C-**H**$_{Ar}$), 7.52 – 7.46 (m, 2H, C-**H**$_{Ar}$), 7.02 (d, J = 453.2 Hz, 1H, P-**H**), 1.14 (d, J = 16.6 Hz, 9H, C-(C**H₃**)₃).
	Corresponds to literature.[125]
³¹P-NMR (162 MHz, CDCl₃)	δ 47.51.
¹³C-NMR (101 MHz, CDCl₃)	δ 132.60 (d, J = 2.8 Hz), 131.06 (d, J = 10.0 Hz), 129.50, 128.64 (d, J = 11.8 Hz), 32.13 (d, J = 69.2 Hz), 23.59 (d, J = 2.1 Hz).
UPLC-MS	1.28 min.; [M+H]⁺ 183.00

2.3.1.2.2 Synthesis of 2,4,6-trimethylbenzoyl-phenyl(*tert*-butyl)phosphine oxide (**P2**)
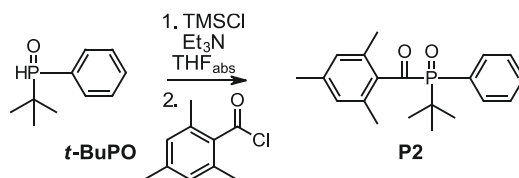
The reaction to produce the desired acylphosphine oxide **P2** was carried out analogously to the literature.[99] Under argon atmosphere and light exclusion, pure **t-BuPO** (2.50 g, 14 mmol, 1.0 eq.) was dissolved in THF$_{abs}$ (30 mL). Subsequently dry Et₃N (1.69 g, 16 mmol, 1.2 eq.) and distilled trimethylsilyl chloride (1.81 g, 16 mmol, 1.2 eq.) were added to the stirring solution. White solid precipitated and the mixture was stirred for 26 h at room temperature. Afterwards distilled 2,4,6-trimethylbenzoyl chloride (3.83 g, 21 mmol, 1.5 eq.) was added. The repeated reaction control shows that the reaction proceeds very slowly. After 200 h almost complete conversion was observed, the reaction was stopped, solids were removed by filtration and the solvent was evaporated. The oily crude product was purified by liquid loaded column chromatography with a mixture of PE and EE. 57% of the theoretical yield of the pale-yellow solid **P2** were obtained.

m.p.	163.0 – 165.2°C

¹H-NMR (600 MHz, CDCl₃)   δ 7.96 – 7.90 (m, 2H, C-**H**$_{Ar}$), 7.58 – 7.53 (m, 1H, C-**H**$_{Ar}$), 7.50 – 7.45 (m, 2H, C-**H**$_{Ar}$), 6.77 (s, 2H, C-**H**$_{Ar}$), 2.23 (s, 3H, C$_{Ar}$-**CH₃**), 2.13 (s, 6H, C$_{Ar}$-**CH₃**), 1.30 (d, J = 15.1 Hz, 9H, C-(**CH₃**)₃).

Corresponds to literature.[99]

³¹P-NMR (243 MHz, CDCl₃)   δ 31.45.

Corresponds to literature.[99]

¹³C-NMR (151 MHz, CDCl₃)   δ 140.67, 137.03 (d, J = 37.0 Hz), 135.55, 132.54 (d, J = 7.6 Hz), 132.15 (d, J = 2.8 Hz), 129.31, 128.39 (d, J = 10.6 Hz), 127.63 (d, J = 76.8 Hz), 35.60 (d, J = 61.6 Hz), 25.35, 21.28, 20.31.

UPLC-MS   1.93 min.; [M+H]⁺ 329.05

HRMS   Calculated: [M + H]⁺ 329.1664;

Found: 329.1662

2.3.1.3 Synthesis of 2,4,6-trimethylbenzoyl-di-*tert*-butylphosphine oxide (**P3**)

2.3.1.3.1 Synthesis of di-*tert*-butylphosphine oxide ((*t*-Bu)₂PO)

(*t*-Bu)₂CP   (*t*-Bu)₂PO
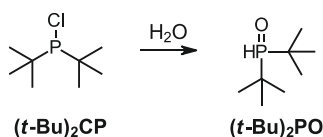
The reaction was performed analogously to literature under inert gas atmosphere.[106] To a solution of di-*tert*-butylchlorophosphine (**(*t*-Bu)₂CP**, 1.00 g, 5.5 mmol, 1.0 eq.) in 16 mL degassed THF, degassed H₂O (0.20 g, 11.1 mmol, 2.0 eq.) was added and stirred for 18 h. After full conversion was determined by UPLC-MS, Et₃N (0.62 g, 6.1 mmol, 1.1 eq.) was added carefully, which resulted in precipitation of a white solid. The solution was diluted with 7 mL Et₂O, filtrated, dried with Na₂SO₄ and filtrated again. The evaporation of the solvents gave a white solid with a yield of 0.82 g (91% of the theory).

m.p.   85.3 – 89.5°C

¹H-NMR (400 MHz, CDCl₃)   δ 6.05 (d, J = 426.5 Hz, 1H, P-**H**), 1.26 (d, J = 14.9 Hz, 18H, C-(**CH₃**)₃).

Corresponds to literature.[126]

³¹P-NMR (162 MHz, CDCl₃)   δ 65.93.

Corresponds to literature.[126]

2.3.1.3.2 Pathway A) Synthesis of 2,4,6-trimethylbenzoyl-di-*tert*-butylphosphine oxide (**P3**)
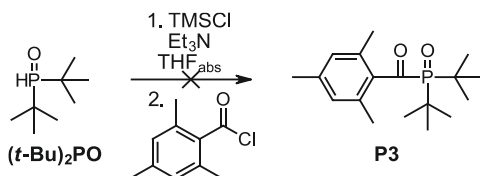
The reaction to was carried out analogously to the literature.[99] Under argon atmosphere and light exclusion, (**t-Bu)₂PO** (0.53 g, 3.2 mmol, 1.0 eq.) was dissolved in THF$_{abs}$ (10 mL). Subsequently dry Et₃N (0.39 g, 3.9 mmol, 1.2 eq.) and distilled trimethylsilyl chloride (0.42 g, 3.9 mmol, 1.2 eq.) were added to the stirring solution. White solid precipitated and the mixture was stirred for 48 h at room temperature. Afterwards, distilled 2,4,6-trimethylbenzoyl chloride (0.89 g, 4.9 mmol, 1.5 eq.) was added. After stirring for 6 days at room temperature, no conversion could be determined in any reaction control. A GC-MS measurement of the reaction mixture, showed a mass, corresponding to that of the reactive silylated intermediate. In order to promote the subsequent reaction, the mixture was refluxed for 18 h. However, no progress of the reaction was observed and therefore the reaction was not continued.

2.3.1.3.3 Pathway B) Synthesis of 2,4,6-trimethylbenzoyl-di-*tert*-butylphosphine oxide (**P3**)
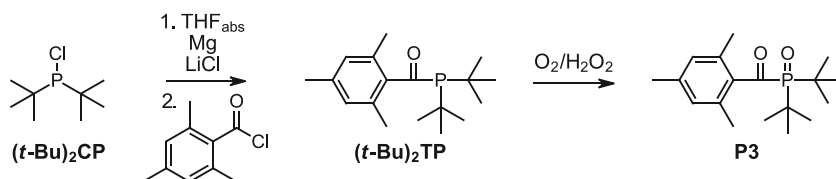
The reaction was carried out under an inert gas atmosphere and in the absence of light, as described in the patent literature of Suzuki et al.[101] The ingredients for the first reaction step were weighed in a glove box and the glassware was flame-dried with particular care. LiCl anhydrous was re-dried by heating under high vacuum, the magnesium shavings were finely ground in inert gas atmosphere, before use. Metal Mg (1.47 g, 60 mmol, 1.75 eq.), anhydrous LiCl (1.46 g, 35 mmol, 1.0 eq.) and one grain of iodine were

suspended in 5 mL THF$_{abs}$. One drop of (**t-Bu**)$_2$**CP** was added and the mixture was stirred and briefly heated to boiling, whereby a presumed turbidity was recognized, which was assumed to indicate the start of the reaction. The reaction mixture was cooled in an ice bath, the remaining (**t-Bu**)$_2$**CP** (6.34 g, 35 mmol, 1.0 eq.) was diluted with 20 mL THF$_{abs}$ and slowly added to the mixture, whereby the supposed turbidity disappeared. The reaction mixture was analyzed by GC-MS and ^{31}P-NMR and no evidence of a successful start of the reaction was found. Shortly afterwards, a distinct gray turbidity of the reaction mixture was observed, indicating the actual start of the Grignard-like reaction. The stirring was continued for 2 h on the ice bath, then the solution was filtrated in inert gas atmosphere and the solid residues were washed with 15 mL THF$_{abs}$. The solution was cooled with an ice bath, before distilled 2,4,6-trimethylbenzoyl chloride (6.39 g, 35 mmol, 1.0 eq.) in 5 mL toluene$_{abs}$ was added dropwise and the reaction mixture turned red. After 3 h of stirring at room temperature, the now colorless reaction was stopped by the addition of 22 mL of 3% aqueous H_2SO_4. The organic phase was washed with 30 mL distilled water, dried with Na_2SO_4 and evaporated to yield 9.72 g crude product.

3.47 g of the crude product were attempted to be purified by distillation. At 160°C oil bath temperature and high vacuum the (**t-Bu**)$_2$**TP** could be evaporated as described in literature.[101] However, a precipitate condensed in the distillation bridge and fractional distillation was not possible. Therefore, no pure product could be obtained with this method.

5.50 g of the crude product were dissolved in 50 mL DCM and oxidized by the dropwise addition of 30% H_2O_2 (10 mL, 94 mmol, 5 eq.). The mixture turned yellow and was stirred for 3 h at room temperature. The phases were separated, the aqueous phase extracted three times with 10 mL DCM each and the combined organic layers dried with Na_2SO_4, filtrated and evaporated to yield a yellow oil. This crude product was purified by column chromatography, using a mixture of PE and EE as eluent. A pure pale-yellow solid was obtained in a quantity of 2.36 g (39% of the theory).

m.p.	101.6 – 103.7°C
^{1}H-NMR (600 MHz, CDCl$_3$)	δ 6.83 (s, 2H, C-**H**$_{Ar}$), 2.48 (s, 6H, C$_{Ar}$-**CH$_3$**), 2.26 (s, 3H, C$_{Ar}$-**CH$_3$**), 1.34 (d, J = 13.6 Hz, 18H, C-(**CH$_3$**)$_3$).

31P NMR (243 MHz, CDCl$_3$)	δ 54.33.
13C-NMR (151 MHz, CDCl$_3$)	δ 222.63 (d, *J* = 49.7 Hz), 140.97, 138.54 (d, *J* = 35.3 Hz), 136.79, 130.02, 37.26 (d, *J* = 50.0 Hz), 27.45, 21.25, 21.19.
UPLC-MS	1.98 min.; [M+H]$^+$ 309.05
HRMS	Calculated for [M+H]$^+$: 309.1978;
	Found: 309.2004

2.3.1.4 Synthesis of 2,4,6-trimethylbenzoyl-phenyl(2,4,6-trimethylphenyl)-phosphine oxide (**P4**)

2.3.1.4.1 Synthesis of the precursor phenyl(2,4,6-trimethylphenyl)phosphine oxide (**MPPO**)
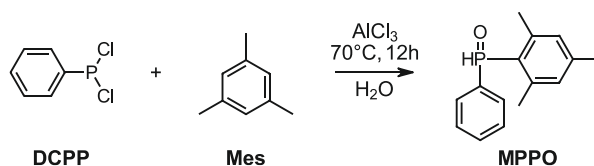
The synthesis of **MPPO** was performed analogously to literature.[107] In argon atmosphere, dichlorophenylphosphine (**DCPP**, 7.88 g, 44.0 mmol, 1 eq.) was dissolved in mesitylene (Mes, 6.95 g, 57.8 mmol, 1.3 eq.), afterwards AlCl$_3$ (7.13 g, 53.5 mmol, 1.2 eq) was added, resulting in an orange suspension. The mixture was heated in an oil bath at 70°C for 18 h. The dark green reaction mixture was allowed to cool to room temperature, before being poured into a 100 mL ice bath, precipitating a white solid. This mixture was stirred for 1 h, then the water phase was extracted 4 times with 75 mL dichloromethane each and washed with 75 mL of a saturated Na$_2$CO$_3$ solution. The combined organic layers were dried with Na$_2$SO$_4$ and evaporated to yield a yellow liquid. Purification was carried out by column chromatography using a mixture of PE and EE. A white solid product of 9.32 g (87% of the theoretical yield) was obtained.

1H-NMR (400 MHz, CDCl$_3$)	δ 8.55 (d, J = 482.6 Hz, 1H, P-**H**), 7.67 – 7.59 (m, 2H, C-**H**$_{Ar}$), 7.55 – 7.49 (m, 1H, C-**H**$_{Ar}$), 7.48 – 7.41 (m, 2H, C-**H**$_{Ar}$), 6.91 (d, J = 4.0 Hz, 2H, C-**H**$_{Ar}$), 2.46 (s, 6H, C-C**H**$_{3,Ar}$), 2.31 (s, 3H, C-C**H**$_{3,Ar}$).
	Corresponds to literature.[107]

^{31}P-NMR (162 MHz, CDCl$_3$)   δ 9.71.

Corresponds to literature.[107]

UPLC-MS   1.61 min.; [M+H]$^+$ 245.10

2.3.1.4.2 Synthesis of 2,4,6-trimethylbenzoyl-phenyl(2,4,6-trimethylphenyl)phosphine oxide (**P4**)
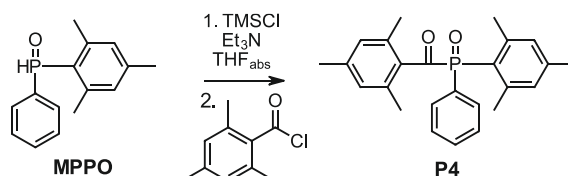
The reaction was carried out analogously to literature.[99] Under argon atmosphere and light exclusion, **MPPO** (2.73 g, 11.2 mmol, 1.0 eq.) was dissolved in THF$_{abs}$ (20 mL). Subsequently dry Et$_3$N (1.77 g, 17.6 mmol, 1.6 eq.) and distilled TMSCl (1.92 g, 17.6 mmol, 1.6 eq.) were added to the stirring solution. White solid precipitated and the mixture was stirred for 22 h at room temperature. Afterwards, distilled 2,4,6-trimethylbenzoyl chloride (2.83 g, 15.5 mmol, 1.3 eq.) was added. After 48 h only little conversion was observed, therefore the reaction time was increased to 8 days. Solids were removed by filtration and the solvent was evaporated. The crude product was purified by solid loaded column chromatography with a mixture of dichloromethane and methanol. The yield of the slightly yellow solid was 0.76 g (17% of the theoretical yield).

m.p.   146.7 – 149.9°C

^{1}H-NMR (600 MHz, CDCl$_3$)   δ 7.73 – 7.68 (m, 2H, C-**H**$_{Ar}$), 7.53 (td, 1H, C-**H**$_{Ar}$), 7.45 (td, J = 7.7, 3.0 Hz, 2H, C-**H**$_{Ar}$), 6.89 (d, J = 3.5 Hz, 2H, C-**H**$_{Ar}$), 6.81 (s, 2H, C-**H**$_{Ar}$), 2.31 (s, 3H, C$_{Ar}$-**CH$_3$**), 2.29 (s, 6H, C$_{Ar}$-**CH$_3$**), 2.27 (s, 3H, C$_{Ar}$-**CH$_3$**), 2.05 (s, 6H, C$_{Ar}$-**CH$_3$**).

^{31}P-NMR (243 MHz, CDCl$_3$)   δ 26.15.

^{13}C-NMR (151 MHz, CDCl$_3$)   δ 217.64 (d, J = 70.8 Hz), 144.80 (d, J = 10.3 Hz), 142.76 (d, J = 2.7 Hz), 140.30, 136.89 (d, J = 41.5 Hz), 135.67, 133.67 (d, J = 94.2 Hz), 132.01 (d, J = 2.7 Hz), 131.37 (d, J = 2.8 Hz), 131.36 (d, J = 18.0 Hz), 129.07, 128.91 (d, J = 11.9 Hz),

122.49 (d, J = 88.4 Hz), 23.84 (d, J = 3.6 Hz), 21.34, 21.29, 19.86.

UPLC-MS	2.10 min.; [M+H]$^+$ 391.10
HRMS	Calculated: [M+H]$^+$ 391.1821;
	Found: 391.1818

2.3.1.5 Synthesis of 4-methylbenzoyl-phenyl(2,4,6-trimethylphenyl)-phosphine oxide (**P5**)

2.3.1.5.1 Pathway A) Synthesis of 4-methylbenzoyl-phenyl(2,4,6-trimethylphenyl)phosphine oxide (**P5**)
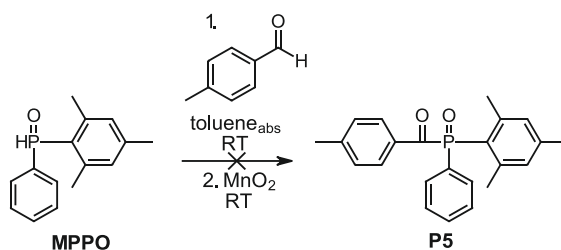
In the first approach, an attempt was made to prepare the photoinitiator **P5** using a mild synthesis route in analogy to literature.[97] The precursor **MPPO** was prepared as described in section 2.3.1.4. Under argon atmosphere and light exclusion MPPO (2.50 g, 10.2 mmol, 1.05 eq.) was stirred in toluene$_{abs}$ (100 mL), before p-tolualdeyhd (1.17 g, 9.7 mmol, 1.0 eq.) was added. After stirring for 6 hours, no conversion was observed by TLC. Another 22 hours of reaction time did not result in any change, so the reaction temperature was increased to 100°C. Even through no product formation could be observed within 3 h.

2.3.1.5.2 Pathway B) Synthesis of 4-methylbenzoyl-phenyl(2,4,6-trimethylphenyl)phosphine oxide (**P5**)
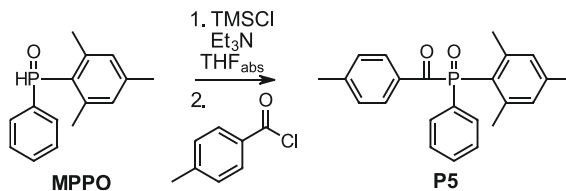
The reaction was carried out analogously to literature.[99] The precursor **MPPO** was prepared as described in section 2.3.1.4. Under argon atmosphere and light exclusion, **MPPO** (1.93 g, 7.9 mmol, 1 eq.) was dissolved in THF$_{abs}$ (30 mL). Subsequently, dry Et$_3$N (0.96 g, 9.5 mmol, 1.2 eq.) and distilled trimethylsilyl chloride (1.03 g, 9.5 mmol, 1.2 eq.) were added to the stirring solution. White solid precipitated and the mixture was stirred for 20 h at room temperature. Afterwards, distilled *p*-toluoylchlorid (1.80 g, 11.7 mmol, 1.5 eq.) was added and the mixture was stirred for another 45 h at room temperature. Solids were removed by filtration and the solvent was evaporated to yield a viscous yellow crude product. When attempting to purify the substance by column chromatography, mixed fractions were obtained. A 2D TLC experiment indicated that the substance degrades during column chromatography.

Furthermore, an NMR study was carried out, in which the same sample was measured before and after exposure to air. For air exposure, the NMR sample was bubbled with compressed air for several minutes. The ^{1}H-NMR measurements are depicted in Figure 105. The red line corresponds to the spectrum recorded before air exposure, the green line to the spectrum afterwards. The intensities of the spectra were aligned using the doublet peak at 8.28 ppm. Figure 105 a) shows the entire spectrum, with the areas, in which the signals of the target structure **P5** are expected, highlighted in yellow. The peaks highlighted in gray and are attributed to the remaining toluyl chloride. Figure 105 b) shows the first important area between 8.5 ppm and 6.6 ppm in detail, whereby the areas in which significant changes were observed are highlighted in red. The second important area between 2.6 ppm and 2.1 ppm is depicted in Figure 105 c).
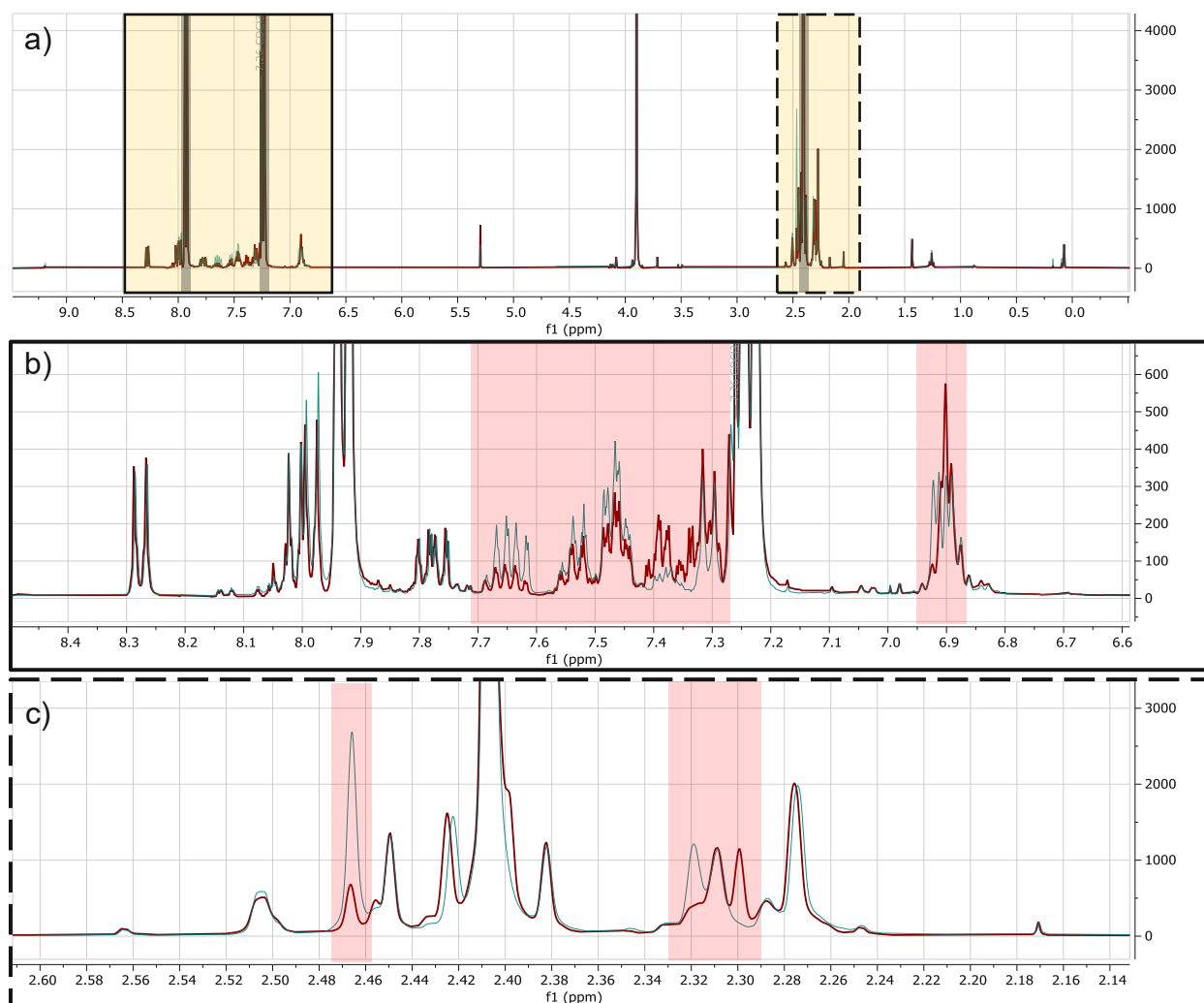
*Figure 105: ¹H-NMR spectra of the crude product **P5** dissolved in CDCl₃ before (red line) and after (green line) exposure to air. a) Whole spectrum; b) Area between 8.5 – 6.6 ppm in detail; c) Area between 2.6 – 2.1 ppm in detail.*

Figure 105 b) and Figure 105 c show that in the areas in which the product signals are expected, significant changes are caused by exposing the crude product to the air. Due to the considerable number of signals close together, it is challenging to clearly assign them to the product. Consequently, it is also uncertain whether the observed changes can be definitively attributed to the product.

Figure 106 depicts the corresponding ³¹P-NMR spectra, where a) is before and b) is after air exposure.
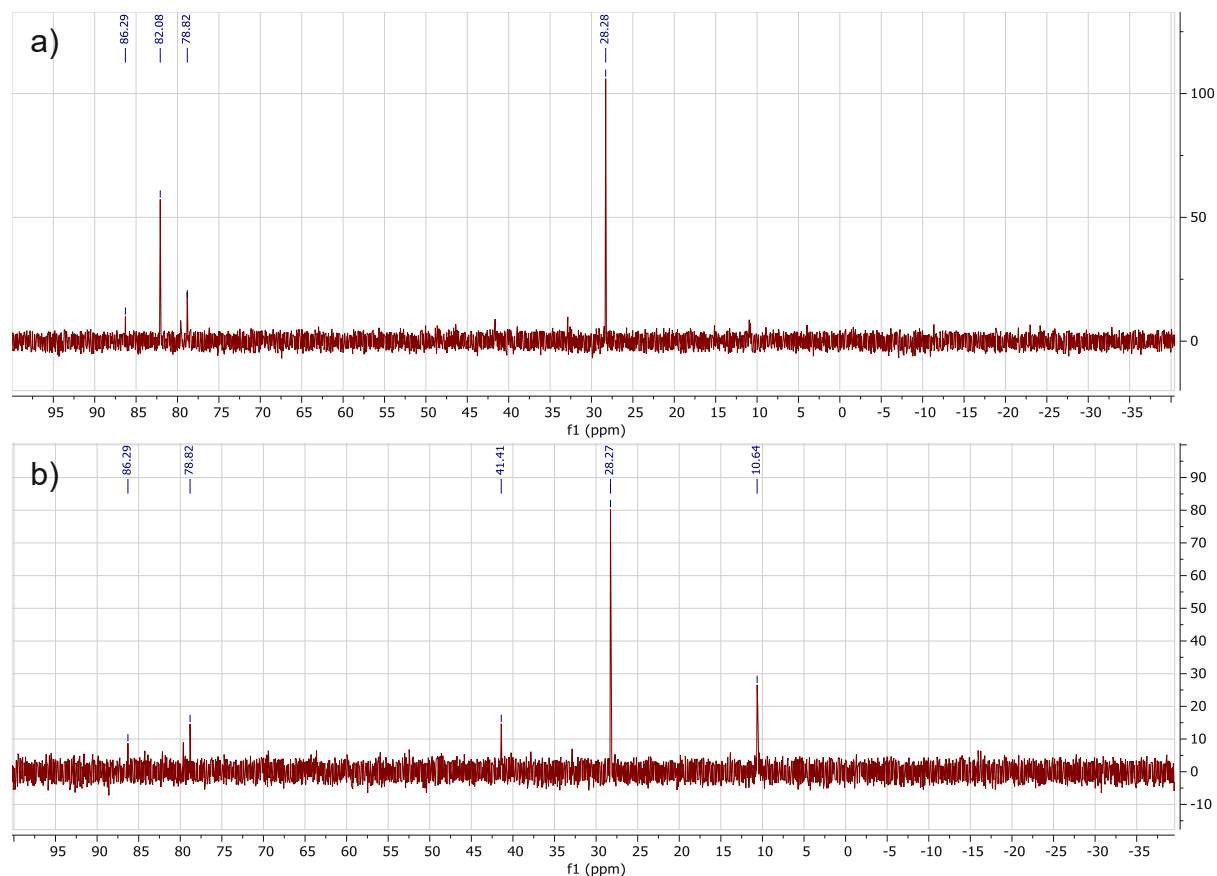
*Figure 106: ^{31}P-NMR spectra of the crude product **P5** dissolved in CDCl$_3$ before (a) and after (b) exposure to air.*

Figure 106 also shows significant changes in the spectra due to exposure to air. With regard to the shift, the signal at 28.27 ppm most likely belongs to the target product P5. Although this signal is the most prominent before and after air exposure, without an internal standard it is unclear whether the intensity has changed or not.

UPLC-MS   1.96 min.; [M+H]$^+$ 363.10

2.3.2 Characterization

2.3.2.2 Steady-state photolysis

The steady-state photolysis and the determination of the quantum yields were performed at the TU Graz within the research group of Prof. Georg Gescheidt, by Konstantin Knaipp. The UV-Vis spectra were recorded on a TIDAS fiber optics spectrometer. Solutions of the photoinitiators **TPO** (0.001 M), **P1** (0.001 M) and **P2** (0.002 M) in acetonitrile were

prepared and degassed with argon for 3 min. Afterwards the samples were irradiated with a high-power LED at 385 nm and UV-Vis spectra were recorded every 10 s. Figure 107 illustrates the absorbance traces for the photobleaching experiments of **TPO**, **P1** and **P2** at 385 nm.
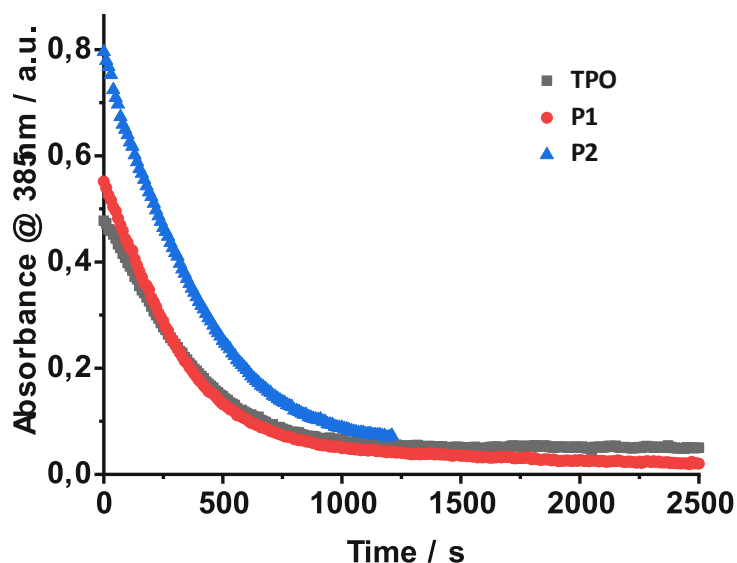
*Figure 107: Kinetic traces recorded at 385 nm for the photobleaching experiments of **TPO** (0.001 M), **P1** (0.001 M) and **P2** (0.002 M).*

For the calculation of the quantum yield Equation 3 was used.

$$\Phi = \frac{k_{fit}c_0}{I_0\left(1 - 10^{-A'_i}\right)}$$

Equation 3

Φ: *Quantum yield []*

k_{fit}: *Decay constant obtained by exponential fitting of the absorbance trace [s-1]*

c_0: *Starting concentration of the solutions [M]*

I_0: *Initial light intensity [mol·L-1·s-1]*

A'_i: *Initial absorbance at the irradiation wavelength []*

2.3.2.3 Density functional theory (DFT) calculations of phosphanoyl radicals

The DFT calculations were performed at the TU Graz in the working group of Prof. Georg Gescheidt, using GAUSSIAN16. The geometries of the phosphanoyl radicals were

optimized with the B3LYP functional and the 6-311++G** basis set. To further improve the result, Grimme's D3BJ dispersion correction was used.

2.3.2.4 Laser flash photolysis

Laser flash photolysis (LFP) experiments were performed at the TU Graz within the research group of Prof. Georg Gescheidt, by Konstantin Knaipp. The measurements were used to determine the rate constants for the addition of butyl acrylate to primary phosphanoyl radicals. Solutions of **TPO** (0.001 M), **P1** (0.001 M) and **P2** (0.002 M) in acetonitrile were prepared and degassed with argon for 3 min. before the measurements. Upon irradiation with a Innolas Spitlight Compact 100 solid state Nd:YAG laser at 355 nm (pulse width: 8 ns, energy: 10 mJ/pulse), transient spectra were taken on a LKS80 Laser Flash Photolysis Spectrometer (Applied Photophysics, UK).

Figure 108 depicts the transient absorption spectra obtained from the LFP experiments. ΔAbs was recorded from -8.11×10^{-7} s to 7.19×10^{-6} s and all traces were averaged. The absorbances around 340 nm are assigned to the P-centered radicals, which result from the irradiation of **TPO** and **P1** and **P2**.
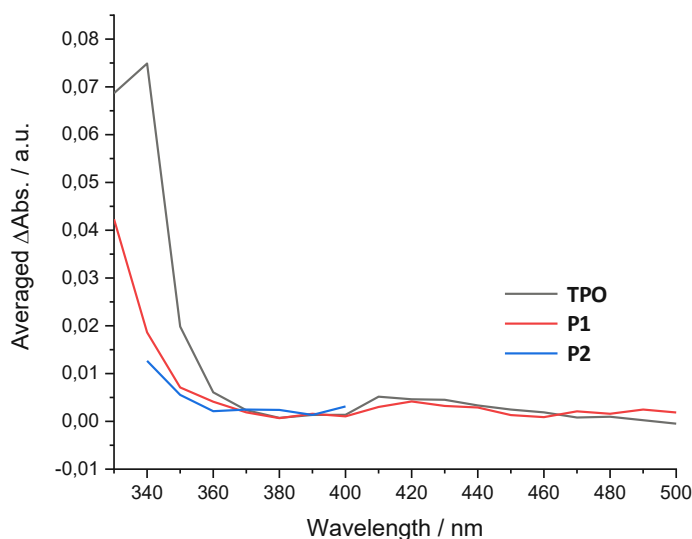
*Figure 108: Transient absorption spectra of LFP measurements of **TPO**, **P1** and **P2**.*

Tracing the formation and subsequent decay of the P-centered radicals is performed best at 340 nm for **TPO** and **P2** and at 330 nm for **P1**, as the greatest changes in absorption can be seen at these wavelengths. For **P2** only small changes in the transient absorption spectrum can be observed, necessitating a higher initiator concentration, which limits the

wavelength window in which the detector still receives enough light intensity to produce a signal. The P-centered radicals can be quenched by the addition of an excess of butyl methacrylate to the solutions. At higher methacrylate concentrations, the decrease in the absorption of radicals accelerates. The corresponding time traces of the signal intensities for **TPO**, **P1** and **P2** depending on the concentration of butyl methacrylate are depicted in Figure 115 – Figure 117 in the appendix. Fitting a monoexponential decay function to the time trace allows the determination of a pseudo-first order decay constant. Plotting these decay constants against the acrylate concentration yields a linear relationship (Figure 109), where the slope corresponds to the bimolecular quenching constant k of the phosphanoyl radicals.
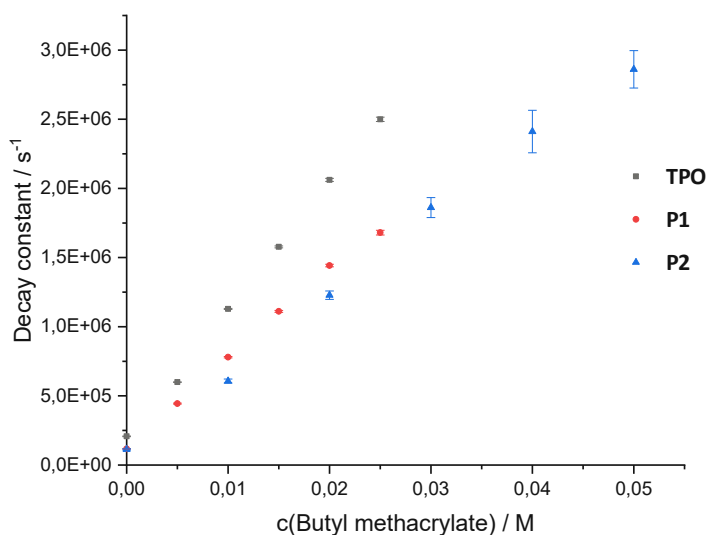
Figure 109. Stern-Vollmer plots for the determination of the second-order rate constants for the addition of butyl methacrylate to P-centered radicals of TPO, P1 and P2.

The fitted pseudo-first order decay constants and their absolute fitting errors are given in Table 37 in the appendix.

2.3.2.5 Photo-DSC

The evaluation of the photo-DSC measurements is described in section 2.2.2.2.

320 – 500 nm broadband light source (OmniCure® S2000)

For these measurements an OmniCure® S2000 high pressure mercury vapor light source equipped with a 320 – 500 nm filter was used as light source. The light intensity at the sample surface was set to 64 mW/cm^2. The complete results are summarized in Table 31.

Table 31: Results of photo-DSC measurements of formulations, consisting of 1 mol% photoinitiator in the monomer UDMA, under irradiation with a broadband light source (320-500 nm) with an intensity of 64 mW/cm^2.

320-500 nm	t_{max} [s]	R_p [mmol*L^{-1}*s^{-1}]	$t_{95\%}$ [s]	Onset [s]	Area [J/g]	DBC [%]
TPO	4.3 ± 0.2	176.0 ± 3.5	34.0 ± 1.6	1.7 ± 0.1	154.0 ± 0.2	64.2 ± 0.1
TPO-L	5.1 ± 0.3	147.8 ± 5.3	32.4 ± 1.5	2.1 ± 0.2	141.1 ± 1.3	58.9 ± 0.5
◆ P1	4.4 ± 0.1	175.2 ± 4.3	30.8 ± 1.0	1.8 ± 0.1	147.3 ± 1.4	61.4 ± 0.6
▬ P2	4.3 ± 0.2	184.7 ± 5.0	29.3 ± 2.2	1.7 ± 0.1	156.0 ± 2.9	65.1 ± 1.2
✚ P3	4.3 ± 0.2	168.4 ± 1.5	32.2 ± 1.4	1.8 ± 0.0	147.2 ± 2.9	61.4 ± 1.2
● P4	4.7 ± 0.0	159.4 ± 3.7	36.1 ± 0.4	1.9 ± 0.0	142.8 ± 0.9	59.5 ± 0.4

385 nm LED light source

For the measurements a 385 nm OmniCure® Max LED light source was used. The light intensity at the sample surface was set to 10 mW/cm^2. The complete results are summarized in Table 32.

Table 32: Results of photo-DSC measurements of formulations, consisting of 1 mol% photoinitiator in the monomer UDMA, under irradiation with a LED light source (385 nm) with an intensity of 10 mW/cm^2.

385 nm	t_{max} [s]	R_p [mmol*L^{-1}*s^{-1}]	$t_{95\%}$ [s]	Onset [s]	Area [J/g]	DBC [%]
TPO	5.5 ± 0.2	138.5 ± 1.5	32.2 ± 1.1	1.9 ± 0.0	138.3 ± 3.6	57.7 ± 1.5
TPO-L	6.1 ± 0.0	131.0 ± 4.2	35.2 ± 1.5	2.5 ± 0.1	134.9 ± 2.0	56.3 ± 0.8
◆ P1	5.6 ± 0.1	139.9 ± 2.4	31.5 ± 1.0	1.9 ± 0.0	134.4 ± 3.1	56.0 ± 1.3
▬ P2	5.4 ± 0.1	151.4 ± 2.1	30.4 ± 1.2	2.0 ± 0.0	140.1 ± 1.1	58.5 ± 0.5
✚ P3	6.1 ± 0.2	135.1 ± 4.4	31.7 ± 1.6	2.4 ± 0.1	135.3 ± 2.4	56.5 ± 1.0
● P4	6.6 ± 0.1	118.0 ± 1.5	35.2 ± 1.8	2.0 ± 0.0	130.8 ± 1.1	54.5 ± 0.4

400 nm LED light source

For the measurements a 400 nm OmniCure® Max LED light source was used. The light intensity at the sample surface was set to 10 mW/cm^2. The complete results are summarized in Table 33.

Table 33: Results of photo-DSC measurements of formulations, consisting of 1 mol% photoinitiator in the monomer **UDMA**, under irradiation with a LED light source (400 nm) with an intensity of 10 mW/cm^2.

400 nm	t_{max} [s]	R_p [mmol*L^{-1}*s^{-1}]	$t_{95\%}$ [s]	Onset [s]	Area [J/g]	DBC [%]
TPO	5.3 ± 0.1	156.8 ± 1.3	30.5 ± 0.3	2.1 ± 0.0	145.8 ± 0.8	60.8 ± 0.3
TPO-L	6.4 ± 0.0	134.9 ± 3.1	34.7 ± 1.5	2.7 ± 0.0	135.4 ± 2.2	56.5 ± 0.9
◆ P1	5.6 ± 0.1	150.6 ± 4.7	29.7 ± 1.3	2.1 ± 0.1	140.2 ± 2.0	58.5 ± 0.8
▬ P2	5.1 ± 0.3	159.1 ± 7.7	30.2 ± 2.0	2.0 ± 0.1	151.7 ± 4.7	63.3 ± 2.0
✚ P3	5.7 ± 0.2	145.1 ± 7.6	30.8 ± 1.3	2.3 ± 0.1	139.6 ± 1.0	58.3 ± 0.4
● P4	5.8 ± 0.2	136.5 ± 4.8	33.9 ± 1.6	2.1 ± 0.1	136.2 ± 0.9	56.7 ± 0.4

2.4 Phosphorus modified MAPOs with heteroatom substituents

2.4.1 Synthesis

2.4.1.1 Synthesis of 2,4,6-trimethylbenzoyl-ethoxy(2,4,6-timethylphenyl)-phosphine oxide (**PH1**)

2.4.1.1.1 <u>Pathway A) Synthesis of ethyl *P*-(2,4,6-trimethylphenyl)phosphinate (**EMP**)</u>
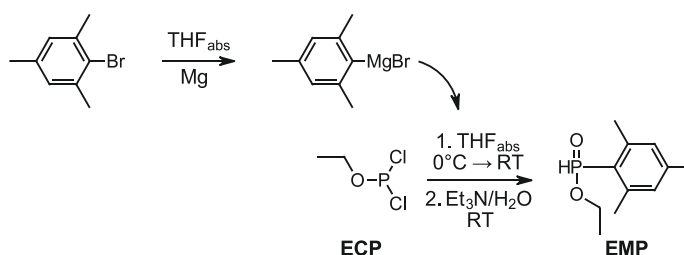
The reaction was performed in analogy to literature.[103] In inert gas atmosphere Mg-shavings (0.96 g, 39 mmol, 1.0 eq.) were suspended in 4 ml THF$_{abs}$. 5 drops of mesityl bromide were added to the stirring suspension and the Grignard reaction is started by the addition of one grain of iodine and heating until boiling. The remaining mesityl bromide (7.77 g, 39 mmol, 1.0 eq.) was diluted with 10 ml THF$_{abs}$ and slowly added to the reaction mixture. The reaction was stirred at ambient temperature for 3 h.

In a separate flask, under inert gas atmosphere, ethyldichlorophoshite (**ECP**, 5.72 g, 39 mmol, 1.0 eq.) was dissolved in 25 mL THF$_{abs}$ and cooled with an ice bath. The mesitylmagnesiumbromide solution was added dropwise with a transfer cannula while stirring. The ice bath was removed and after 2 h the reaction was quenched by the addition of a mixture of Et$_3$N (5.90 g, 58 mmol, 1.5 eq.), H$_2$O (1.05 g, 58 mmol, 1.5 eq.)

and THF (8 ml). The mixture was stirred for 1 h before being filtrated, dried with Na_2SO_4 and filtrated again. After evaporation of the solvent, a white solid crude product was obtained. UPLC-MS measurements showed that the reaction was successful, but yielded several by-products.

The crude product was attempted to be purified by column chromatography with solid loading and a mixture of PE and EE as eluent. Completely separated peaks could be observed by the UV detector. However, the respective fractions, contained mixed products, even after repeated column chromatography of the "pre-purified" products. Although, 2D-TLC did not indicate any degradation, it is assumed that the substance produced is not stable against silica under prolonged contact, resulting in degradation. An attempt to use the non-purified product for the follow-up reaction failed and no conversion was observed.

2.4.1.1.2 Pathway B) Synthesis of ethyl P-(2,4,6-trimethylphenyl)phosphinate (EMP)
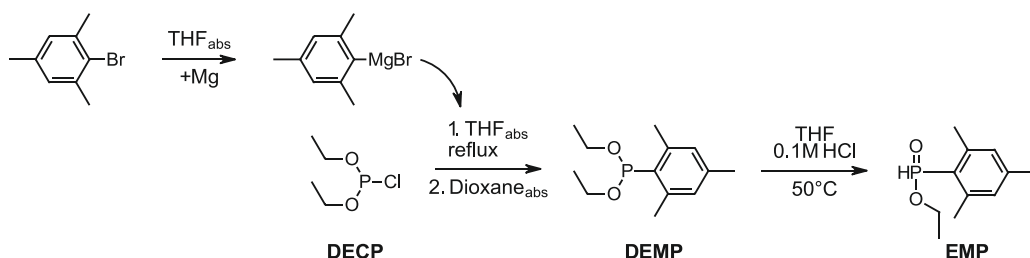
In the next step, an alternative synthesis route was performed in accordance with the literature, to produce the desired precursor **EMP**.[109] In inert gas atmosphere Mg-shavings (0.74 g, 30 mmol, 1.5 eq.) were suspended in 3 ml THF_{abs}. 2 drops of mesityl bromide were added to the stirring suspension and the Grignard reaction was started by heating until boiling. The remaining mesityl bromide (4.79 g, 24 mmol, 1.2 eq.) was diluted with 20 ml THF_{abs} and slowly added to the reaction mixture. The reaction was stirred at ambient temperature for 2 h.

In a separate flask, in inert gas atmosphere, diethyl P-(2,4,6-trimethylphenyl)phosphonite (**DECP**, 3.14 g, 20 mmol, 1.0 eq.) was dissolved in 30 mL THF_{abs}. The mesitylmagnesiumbromide solution was added dropwise, while stirring, to the DECP solution. The resulting yellow solution was refluxed for 2 h. After cooling to room temperature 43 ml $dioxane_{abs}$ were added. The resulting solids were removed in argon

atmosphere using a Schlenk frit. The solvents were removed and the yellow crude oil was purified by Kugelrohr distillation. **DEMP** was obtained as colorless oil in a quantity of 3.23 g (67% of the theory).

^{1}H-NMR (400 MHz, CDCl$_3$)	δ 6.83 (d, *J* = 2.3 Hz, 2H, C-**H**$_{Ar}$), 4.02 − 3.90 (m, 4H, O-C**H$_2$**-CH$_3$), 2.62 (s, 6H, C-C**H$_{3,Ar}$**), 2.28 (s, 3H, C-C**H$_{3,Ar}$**), 1.31 (t, *J* = 7.0 Hz, 6H, O-CH$_2$-C**H$_3$**). Corresponds to literature.[109]
^{31}P-NMR (162 MHz, CDCl$_3$)	δ 23.95. Corresponds to literature.[109]

In the second reaction step **DEMP** (3 g, 12 mmol) was dissolved in 13 mL THF. 30 ml 0.1M HCl were added, heated in an oil bath at 70°C and stirred for 2.5 h. The aqueous phase was extracted 4 times with 50 mL DCM. The organic phase was dried with Na$_2$SO$_4$, filtrated and the solvent was removed to yield the colorless oil **EMP** quantitatively.

^{1}H-NMR (400 MHz, CDCl$_3$)	δ 7.93 (d, *J* = 551.1 Hz, 1H, P-**H**), 6.87 (d, *J* = 4.6 Hz, 2H, C-**H**$_{Ar}$), 4.25 − 4.07 (m, 2H, -O-C**H$_2$**-CH$_3$), 2.55 (s, 6H, C$_{Ar}$-C**H$_3$**), 2.28 (s, 3H, C$_{Ar}$-C**H$_3$**), 1.38 (t, *J* = 7.1 Hz, 3H, -O-CH$_2$-C**H$_3$**). Corresponds to literature.[109]
^{31}P-NMR (162 MHz, CDCl$_3$)	δ 23.99. Corresponds to literature.[109]
UPLC-MS	1.51 min; [M+H]$^+$ 213.05

2.4.1.1.3 Pathway B) Synthesis of 2,4,6-trimethylbenzoyl-ethoxy(2,4,6-timethylphenyl)phosphine oxide (**PH1**)
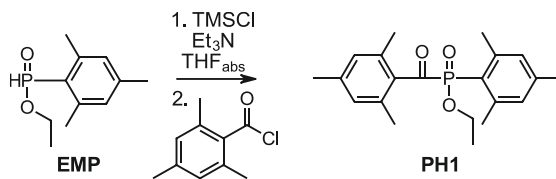
The reaction to produce the desired acylphosphine oxide **PH1** was carried out analogously to the literature.[99] Under argon atmosphere and light exclusion, **EMP** (2.83 g, 13 mmol, 1.0 eq.) was dissolved in THF$_{abs}$ (25 mL). Subsequently dry Et$_3$N (1.62 g, 16 mmol, 1.2 eq.) and distilled TMSCl (1.74 g, 16 mmol, 1.2 eq) were added to the stirring solution. White solid precipitated and the mixture was stirred for 68 h at room temperature. Afterwards, distilled 2,4,6-trimethylbenzoyl chloride (3.75 g, 20 mmol, 1.5 eq.) was added. After 48 h solids were removed by filtration and the solvent was evaporated. The crude product was purified by liquid loaded column chromatography with a mixture of PE and EE. This resulted in 2.53 g (53% of the theory) of a pale-yellow solid, which appears to be slightly impure based on the melting interval. For further purification 0.8 g of the pre-purified product were recrystallized from heptane, to yield 0.61 g (41% of the theory) of the pure pale-yellow solid product.

m.p.	85.3 – 88.8°C
¹H-NMR (400 MHz, CDCl$_3$)	δ 6.89 (d, J = 3.9 Hz, 2H, C-**H**$_{Ar}$), 6.80 (s, 2H, C-**H**$_{Ar}$), 4.37 – 4.09 (m, 2H, O-C**H$_2$**-CH$_3$), 2.49 (s, 6H, C-C**H$_3$**,$_{Ar}$), 2.29 (s, 3H, C-C**H$_3$**,$_{Ar}$), 2.27 (s, 3H, C-C**H$_3$**,$_{Ar}$), 2.10 (s, 6H, C-C**H$_3$**,$_{Ar}$), 1.37 (t, J = 7.1 Hz, 3H, O-CH$_2$-C**H$_3$**).
³¹P-NMR (162 MHz, CDCl$_3$)	δ 24.45.
¹³C-NMR (101 MHz, CDCl$_3$)	δ 215.72 (d, J = 106.7 Hz), 145.23 (d, J = 11.7 Hz), 143.26 (d, J = 2.9 Hz), 139.66, 137.02 (d, J = 46.9 Hz), 134.83, 131.10 (d, J = 13.3 Hz), 128.72, 121.20 (d, J = 118.6 Hz), 61.88 (d, J = 7.2 Hz), 23.53 (d, J = 2.3 Hz), 21.32, 21.28, 19.48, 16.58 (d, J = 6.2 Hz).
UPLC-MS	2.07 min.; [M+H]$^+$ 359.10
HRMS	Calculated: [M+Na]$^+$ 381.1589, Found: 381.1587

2.4.1.2 Synthesis of 2,4,6-trimethylbenzoyl-ethoxy(1-naphthyl)phosphine oxide (**PH2**)

2.4.1.2.1 Synthesis of ethyl *P*-1-naphthalenylphosphinate (**ENP**)
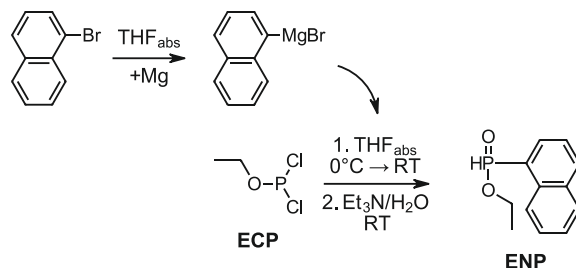
The reaction was carried out analogously to literature.[103] In a first step Mg-shavings (0.33 g, 13.6 mmol, 1.0 eq.) were suspended in 3 mL THF$_{abs}$ in argon atmosphere. 3 drops of 1-bromonaphthalene were added to the mixture and heated to boiling to start the conversion of the Grignard reagent. Subsequently, residual 1-bromonaphthalene (2.82 g, 13.6 mmol, 1.0 eq.) dissolved in 7 mL THF$_{abs}$ was added dropwise to the reaction and stirred for 90 min to yield an orange solution.

In a separate reaction apparatus, in argon atmosphere a solution of ethyl dichlorophosphite (2.00 g, 13.6 mmol, 1.0 eq.) in THF$_{abs}$ (10 mL) was stirred and cooled with an ice bath, before the freshly prepared Grignard reagent was added dropwise. The yellow reaction mixture was stirred for 3 h at room temperature and then quenched with a mixture of Et$_3$N (2.83 mL, 20.4 mmol, 1.5 eq.), H$_2$O (0.37 mL, 20.4 mmol, 1.5 eq.) and THF (2 mL). After 30 min the reaction mixture was filtrated, dried with Na$_2$SO$_4$ and the solvent was removed to yield a yellow high viscous crude product. In a first column chromatography with a solvent composition of DCM:MeOH (95:5) the product was not recovered. The product could be eluted only after washing the column with a more polar mixture. This eluted fraction was separated again by column chromatography with gradient elution with a solvent composition of DCM:MeOH (98:2 → 60:40). The product ENP was obtained as yellow oil, in a quantity of 0.29 g (10% of the theoretical yield).

¹H-NMR (400 MHz, CDCl₃) δ 8.44 (d, *J* = 8.4 Hz, 1H, C-C**H**$_{Ar}$), 8.08 (d, *J* = 7.2 Hz, 1H, C-C**H**$_{Ar}$), 7.94 (dt, 1H, C-C**H**$_{Ar}$), 7.93 (d, *J* = 563.2 Hz, 1H, P-**H**), 7.67 – 7.47 (m, 4H, C-C**H**$_{Ar}$), 4.30 – 4.10 (m, 2H, O-C**H₂**), 1.38 (t, *J* = 7.1 Hz, 3H, O-CH₂-C**H₃**).

³¹P-NMR (162 MHz, CDCl₃) δ 25.54.

2.4.1.2.2 Synthesis of 2,4,6-trimethylbenzoyl-ethoxy(1-naphthyl)phosphine oxide (**PH2**)
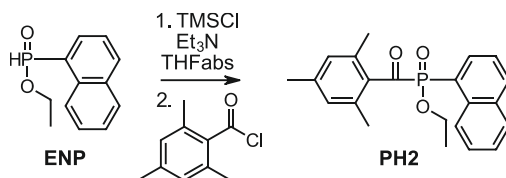
The reaction was carried out analogously to literature.[99] Under argon atmosphere and light exclusion, **ENP** (264 mg, 1.2 mmol, 1.0 eq) was dissolved in THF$_{abs}$ (5 mL). Subsequently, dry Et$_3$N (170 mg, 1.7 mmol, 1.4 eq.) and distilled TMSCl (179 mg, 1.7 mmol, 1.4 eq.) were added to the stirring solution. White solid precipitated and the mixture was stirred for 20 h at room temperature. Afterwards distilled 2,4,6-trimethylbenzoyl chloride (263 mg, 1.4 mmol, 1.2 eq.) was added. After 48 h solids were removed by filtration and the solvent was evaporated. The crude product was purified by liquid loaded column chromatography. The first attempt with a solvent composition of DCM:MeOH (99:1) was too polar and resulted in mixed fractions. The pre-purified mixed fractions were then subjected to further column chromatography with PE:EE (9:1) to yield the pure yellow liquid product in a quantity of 128 mg (29% of the theoretical yield).

^{1}H-NMR (400 MHz, CDCl$_3$)	δ 8.61 (dd, J = 7.0, 2.3 Hz, 1H, C-C**H**$_{Ar}$), 8.25 (ddd, J = 14.4, 7.1, 1.3 Hz, 1H, C-C**H**$_{Ar}$), 8.09 (d, J = 8.0 Hz, 1H, C-C**H**$_{Ar}$), 7.89 (dt, J = 6.3, 2.4 Hz, 1H, C-C**H**$_{Ar}$), 7.60 – 7.52 (m, 3H, C-C**H**$_{Ar}$), 6.77 (s, 2H, C-C**H**$_{Ar}$), 4.34 – 4.15 (m, 2H, -O-C**H$_2$**-CH$_3$), 2.25 (s, 3H, C$_{Ar}$-C**H$_3$**), 2.05 (s, 6H, C$_{Ar}$-C**H$_3$**), 1.39 (t, J = 7.1 Hz, 3H, -O-CH$_2$-C**H$_3$**).
^{31}P-NMR (162 MHz, CDCl$_3$)	δ 19.41.
^{13}C-NMR (101 MHz, CDCl$_3$)	δ 215.07 (d, J = 112.0 Hz), 139.99, 135.91 (d, J = 8.5 Hz), 134.81, 133.74 (d, J = 3.2 Hz), 133.63 (d, J = 2.8 Hz), 128.95 (d, J = 1.8 Hz), 128.78, 128.51, 127.88, 126.84 (d, J = 2.8 Hz), 126.71, 124.90 (d, J = 13.8 Hz), 123.65, 62.67 (d, J = 7.4 Hz), 21.29, 19.60, 16.66 (d, J = 6.4 Hz).
UPLC-MS	1.96 min.; [M+H]$^+$ 367.10
HRMS	Calculated: [M+H]$^+$ 367.1457; Found: 367.1454

2.4.1.3 Synthesis of *P*-2,4,6-trimethylbenzoyl-*P*-phenylphosphinic acid 1-adamantyl ester (**PH3**)

2.4.1.3.1 Pathway A) Synthesis of 1-adamantanyl *P*-phenylphosphinate (**AdPO**)
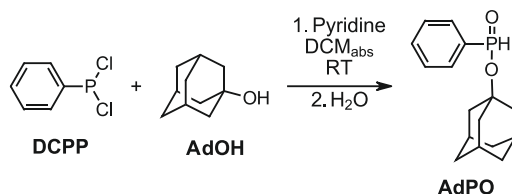
In the first step, the precursor **AdPO** was prepared analogously to the literature.[110] In inert gas atmosphere adamantanol (**AdOH**, 1.65 g, 10.86 mmol, 1.0 eq.) was dissolved in 25 mL DCM$_{abs}$, before pyridine (0.87 g, 10.86 mmol, 1.0 eq.) has been added. This solution was then added dropwise to an ice-cooled stirring solution of dichlorophenylphosphine (**DCPP**, 2.08 g, 11.62 mmol) in 5 mL DCM$_{abs}$. The reaction mixture was then stirred for 19 h at room temperature. After cooling in an ice bath, 8 mL of distilled water were added and the mixture stirred for another 23 h at room temperature. The workup was carried out without inert gas atmosphere. The organic phase was separated and the aqueous phase was extracted three times with 10 mL hexane each. The combined organic phases were washed with 20 mL saturated NaHCO$_3$ solution and dried with Na$_2$SO$_4$. The solvent was removed to yield a relatively pure white crystalline crude product (2.60 g, 87% of the theory).

Attempts of purification by recrystallization from EtOH, ethyl acetate and hexane failed, which is why the crude product was used for the subsequent reaction without further purification.

m.p.	51.5 – 58.1 °C
^{1}H-NMR (400 MHz, CDCl$_3$)	δ 7.79 (d, J = 553.3, 1H, P-**H**), 7.81-7.73 (m, 2H, C-**H**$_{Ar}$), 7.59-7.52 (m, 1H, C-**H**$_{Ar}$), 7.51- 7.45 (m, 2H, C-**H**$_{Ar}$), 2.22 (bs, 3H, C**H**-(CH$_2$)$_3$), 2.14 (d, J = 2.8 Hz, 6H, C-C**H$_2$**-CH), 1.66 (t, J = 3.1 Hz 6H, CH-C**H$_2$**-CH). Corresponds to literature.[110]
^{31}P-NMR (162 MHz, CDCl$_3$)	δ 14.17.

<div align="center">Corresponds to literature.[110]</div>

UPLC-MS   1.81 min. [M+H]$^+$ 277.05

2.4.1.3.2 Pathway A) Synthesis of *P*-2,4,6-trimethylbenzoyl-*P*-phenylphosphinic acid 1-adamantyl ester (**PH3**)
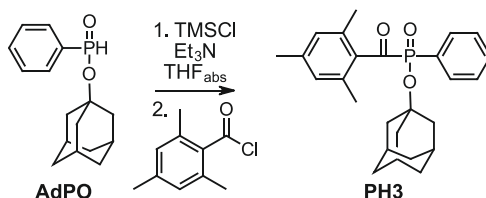
For this reaction the synthesis method described by Zhang et al. was used.[99] **AdPO** (1.00 g, 3.6 mmol, 1.0 eq.) were dissolved in 10 mL THF$_{abs}$. Et$_3$N (0.6 mL, 4.34 mmol, 1.2 eq.) and TMSCl (0.55 mL, 4.34 mmol, 1.2 eq.) were added and the mixture was stirred for 2 days at room temperature. After the addition of distilled 2,4,6-trimethylbenzoyl chloride (0.9 mL, 5.43 mmol, 1.5 eq.), stirring was continued for another 5 days at room temperature. The reaction was stopped, solids were removed by filtration and the solvent was evaporated. UPLC-MS measurements show that the desired product has been obtained with several by-products. Despite the fact that no decomposition could be detected using a 2D TLC control, the purification by conventional column chromatography failed. The product could not be recovered and most likely decomposed due to the conditions of the column chromatography.

Next, an attempt was made to separate the impurities using Kugelrohr distillation. At 140°C volatile impurities could be evaporated. The residue contained product of higher purity, but new contaminants previously not present were detected. Most probably, one component decomposed slowly at the high temperatures, resulting in new impurities, which is why this purification process was also not suitable. At this point, no further attempts were made to purify the product and another synthesis route was investigated.

2.4.1.3.3 Pathway B) Synthesis of phenyl(2,4,6-trimethylbenzoyl)phosphinic acid (**TPO-OH**)
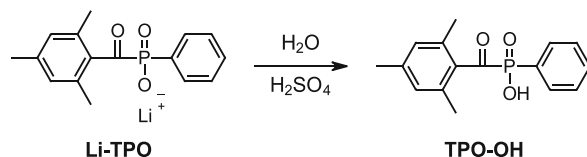
The preparation of **TPO-OH** was carried out analogously to the literature.[96, 111] This synthesis was performed in the absence of light. **Li-TPO** (3.92 g, 13.3 mmol, 1.0 eq.) was dissolved in 60 mL distilled water and converted by the dropwise addition of 0.5 M H_2SO_4 (13.3 mL) until a pH≈1 was reached. The resulting white precipitate was then dissolved by the addition of 130 mL ethyl acetate. The phases were separated and the aqueous phase was extracted two times with 30 mL ethyl acetate each. The combined organic phases were dried with Na_2SO_4, the solvent was removed and the product (3.67 g) was obtained as colorless crystalline solid in 96% yield of the theory. This product was used for subsequent reactions without further purification.

^{1}H-NMR (400 MHz, CDCl$_3$)	δ 12.09 (s, 1H, P-O**H**), 7.70 (ddd, J = 11.9, 8.2, 1.4 Hz, 2H, C-**H**$_{Ar}$), 7.54 (td, J = 7.4, 1.4 Hz, 1H, C-**H**$_{Ar}$), 7.38 (td, J = 7.7, 3.7 Hz, 2H, C-**H**$_{Ar}$), 6.72 (s, 2H, C-**H**$_{Ar}$), 2.23 (s, 3H, C-C**H$_{3,Ar}$**), 2.00 (s, 6H, C-C**H$_{3,Ar}$**).
	Corresponds to literature.[100]
^{31}P-NMR (162 MHz, CDCl$_3$)	δ 16.86.
UPLC-MS	1.92 – 2.13 min. (broad signal); [2M+H]$^+$ 577.15, [M-H]$^-$ 287.05; (λ$_{max}$: 378 nm)

2.4.1.3.4 Pathway B) Synthesis of 2,4,6-trimethylbenzoylphenylphosphinic acid chloride (**TPO-Cl**)
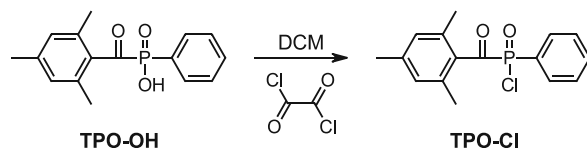
The preparation of **TPO-Cl** was carried out analogously to the literature.[100] This synthesis was carried out under inert gas atmosphere and exclusion of light. **TPO-OH** (1.84 g,

6.4 mmol, 1.0 eq.) was dissolved in 29 mL DCM$_{abs}$. Under stirring, oxalyl chloride (1 mL, 11.7 mmol, 1.8 eq.) was added slowly. The mixture was stirred for 24 h at room temperature and afterwards the solvent was evaporated maintaining the inert gas atmosphere. 20 mL toluene$_{abs}$ were added and evaporated again to yield a brown viscous oil. This substance was used for the subsequent reaction without further analysis and purification, whereby a complete conversion was assumed.

2.4.1.3.5 <u>Pathway B) Synthesis of *P*-2,4,6-trimethylbenzoyl-*P*-phenylphosphinic acid 1-adamantyl ester (**PH3**)</u>
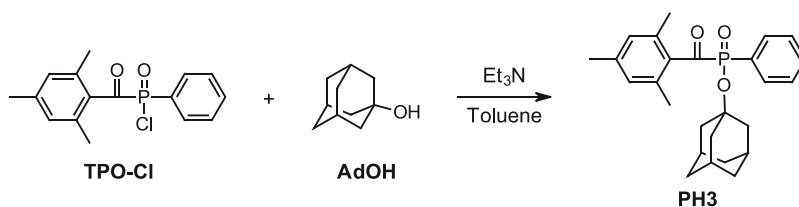
To produce the target structure **TPO-OAd**, the synthesis was performed based on the work of Roszkowski et al.[111] The synthesis was carried out under inert gas atmosphere and exclusion of light. Adamantanol (**AdOH**, 1.07 g, 7.0 mmol, 1.1 eq.) was dissolved in 30 mL toluene$_{abs}$, Et$_3$N (1.9 mL, 14.1 mmol, 2.2 eq.) was added and stirred for several minutes at room temperature. **TPO-Cl** (6.4 mmol, 1.0 eq.) was dissolved in 10 mL toluene$_{abs}$ and added dropwise and quantitatively to this stirring solution. The reaction mixture was stirred for 2 h at room temperature, before 30 mL distilled water were added. The layers were separated and the organic phase was washed three times with saturated Na$_2$CO$_3$ and one time with saturated NaCl solution. After drying with Na$_2$SO$_4$, the solvent was removed to yield a solid crude product. UPLC-MS analysis showed a mostly pure product where the main impurity is the excess of **AdOH**. In order to separate residual **AdOH**, attempts were made to extract the product by washing with refrigerated toluene. Although a higher purity of **PH3** could be achieved, **AdOH** could not be completely removed by this method, and a loss of yield resulted. This pre-purified product was then further purified by removing the remaining **AdOH** by means of Kugelrohr distillation at high vacuum and 85°C for about 10 min. **PH3** was thus obtained in good purity as highly viscous orange substance in 21% yield.

¹H-NMR (400 MHz, CDCl₃)	δ 7.85 (ddd, J = 11.5, 8.2, 1.3 Hz, 2H, C-**H**$_{Ar}$), 7.58 (td, J = 7.4, 1.4 Hz, 1H, C-**H**$_{Ar}$), 7.48 (td, J = 7.4, 3.6 Hz, 2H, C-**H**$_{Ar}$), 6.82 (s, 2H, C-**H**$_{Ar}$), 2.28 (s, 3H, C-**CH₃**$_{,Ar}$), 2.17 (s, 6H, C-**CH₃**$_{,Ar}$), 2.10 (bs, 3H, **CH**-(CH₂)₃), 2.00 (bs, 6H, C-**CH₂**-CH), 1.56 (t, J = 2.9 Hz, 6H, CH-**CH₂**-CH).
³¹P-NMR (162 MHz, CDCl₃)	δ 13.60.
¹³C-NMR (101 MHz, CDCl₃)	δ 216.21 (d, J = 120.0 Hz), 139.56, 134.61, 133.06 (d, J = 9.8 Hz), 132.83 (d, J = 3.0 Hz), 131.11, 129.88, 128.52, 128.49 (d, J = 12.8 Hz), 85.86 (d, J = 11.0 Hz), 44.67 (d, J = 3.7 Hz), 35.74, 31.44, 21.33, 19.69.
UPLC-MS	2.27 min.; [M+H]⁺ 423.15
HRMS	Calculated: [M + H]⁺ 423.2083; Found: 423.2078

2.4.1.4 Synthesis of *P*-2,4,6-trimethylbenzoyl-*P*-phenylphosphinic acid 2,6-bis(1,1-dimethylethyl)-4-methylphenyl ester (**PH4**)
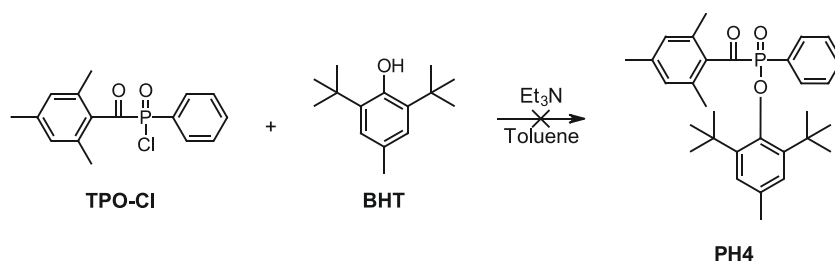
The synthesis was carried out under inert gas atmosphere and exclusion of light, analogously to the work of Roszkowski et al.[111] The precursor **TPO-Cl** was prepared as described in 2.4.1.3 B).

3,5-Di-*tert*-butyl-4-hydroxytoluol (**BHT**, 1.20 g, 5.4 mmol, 1.1 eq.) was diluted in 10 mL toluene$_{abs}$, Et₃N (1.5 mL, 10.9 mmol, 2.2 eq.) was added and stirred for 10 min. **TPO-Cl** (1.52 g, 5.0 mmol, 1.0 eq.) was dissolved in 14 mL toluene$_{abs}$ and added dropwise and to this stirring solution. The reaction mixture was stirred for 2 h at room temperature, before 15 mL water were added. The layers were separated and the organic phase was washed three times with 10 mL saturated Na₂CO₃ each and one time with 15 mL water. After drying with Na₂SO₄, filtration, and evaporation of the solvent no significant quantities were received. The analysis with UPLC-MS also showed only low-molecular substances. The

UPLC-MS analysis of the aqueous phase showed that obviously full conversion to **TPO-OH** was obtained.

UPLC-MS (aqueous phase)   Broad signal 1.92 – 2.26 min., $[2M+H]^+$ 577.10,

        $[M-H]^-$ 287.05; (λ_{max}: 378 nm)

2.4.1.5 Synthesis of 2,4,6-trimethylbenzoyl-(ethylthio)phenyl-phosphine oxide (**PH5**)

2.4.1.5.1 Pathway A) Synthesis of phenylphosphonochloridothious acid ethyl ester (**PCS**)
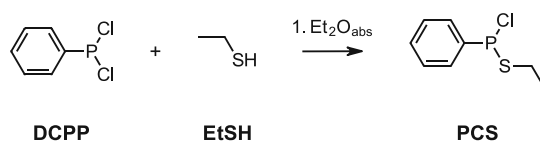
This reaction was prepared according to the patent literature of Ye et al.[112] In inert gas atmosphere dichlorophenylphosphine (**DCPP**, 2.88 g, 16.1 mmol, 1 eq.) was dissolved in 26 mL Et_2O_{abs} and cooled with an ice bath. While stirring ethanethiol (**EtSH**, 3.0 mL, 40.5 mmol, 2.5 eq.) were added dropwise. The reaction was stirred for 4 h at room temperature before volatile compounds were evaporated. The crude product was attempted to be purified by fractional distillation. However, the di-substituted side product, could not be completely separated. Therefore, the product obtained was contaminated with about 6.8% of this by-product. The yield of the liquid impure product amounted to 1.81 g (~51% of the theory).

¹H NMR (400 MHz, CDCl₃)   δ 7.85 – 7.80 (m, 2H, C-CH$_{Ar}$), 7.50 – 7.43 (m, 3H, C-CH$_{Ar}$), 3.08 – 2.86 (m, 2H, S-C**H₂**-CH₃), 1.45 (t, J = 7.4 Hz, 3H, S-CH₂-C**H₃**).

³¹P NMR (162 MHz, CDCl₃)   δ 141.25.

2.4.1.5.2 Pathway A) Synthesis of 2,4,6-trimethylbenzoyl-(ethylthio)phenyl-phosphine (**TPSEt**)

PCS **TPSEt**
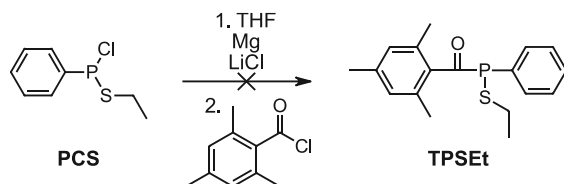
The reaction is not known from literature, but should be carried out analogously to 2.3.1.3 B), as described in the patent literature of Suzuki et al.[101] In inert gas atmosphere and with exclusion of light, metal Mg (0.38 g, 15.5 mmol, 1.75 eq.) and anhydrous LiCl (0.38 g, 8.8 mmol, 1.0 eq.) were suspended in 2 mL THF$_{abs}$. One drop of PCS was added to the stirring suspension to start the Grignard like reaction. The reaction mixture was cooled with an ice bath diluted and a solution of the residual **PCS** (1.81 g, 8.8 mmol, 1 eq.) in 8 mL THF$_{abs}$ was added slowly. The stirring was continued for 4 h on the ice bath, then the solution was filtrated to remove solid residues. The solution was cooled with an ice bath before distilled 2,4,6-trimethylbenzoyl chloride (1.61 g, 8.8 mmol, 1.0 eq.) was added dropwise. No obvious reaction could be observed during this addition. UPLC-MS reaction control after 3 h of stirring could not detect any conversion.

2.4.1.5.3 Pathway B) Synthesis of *S*-ethyl *P*-phenylphosphinothioate (**EtSPO**)

DCPP **EtSH** **EtSPO** **(EtS)₂PO**
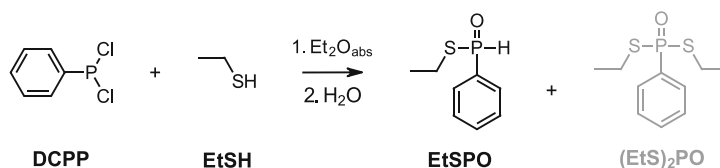
This reaction was prepared according to the patent literature of Ye et al., but with less excess of ethanethiol and with subsequent hydrolysis.[112] In inert gas atmosphere dichlorophenylphosphine (**DCPP**, 6.73 g, 37.6 mmol, 1 eq.) was dissolved in 60 mL Et$_2$O$_{abs}$ and cooled with an ice bath. Ethanethiol (**EtSH**, 3.3 mL, 45.1 mmol, 1.2 eq.) was added dropwise to the solution. The reaction was stirred for 3 h at room temperature. The reaction control with UPLC-MS showed both the desired product and the hydrolyzed educt **DCPP**, but no di-substituted side-product, which is why the reaction was stopped at this point. For this purpose, the reaction mixture was hydrolyzed by the addition of 15 mL H$_2$O and stirred for 10 min. The aqueous phase was extracted 3 times with 50 mL

hexane, the combined organic layers washed with 80 mL saturated NaHCO$_3$ solution, dried with Na$_2$SO$_4$ and filtrated. The solvents were evaporated to yield 0.43 g (6% of the theory) of a crude product. A UPLC-MS measurement of this crude product, indicated an approximately 60:40 mixture of the desired product **EtSPO** and a side-product, which regarding the mass indicates the disubstituted product **(EtS)$_2$PO**. The non-purified crude product was used for the subsequent reaction.

UPLC-MS   1.30 min.; [M+H]$^+$ 186.95; Area$_{254nm}$: 60%; EtSPO

1.69 min.; [M+H]$^+$ 246.95; Area$_{254nm}$: 40%; (EtS)$_2$PO

2.4.1.5.4 <u>Pathway B) Synthesis of 2,4,6-trimethylbenzoyl-(ethylthio)phenyl-phosphine oxide (**PH5**)</u>

EtSPO   **PH5**
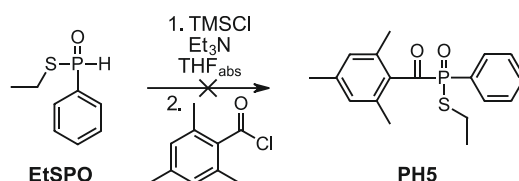
For this reaction the synthesis method described by Zhang et al. was used.[99] **EtSPO** (0.43 g, 2.3 mmol, 1.0 eq.) were dissolved in 6 mL THF$_{abs}$. Et$_3$N (0.38 mL, 2.7 mmol, 1.2 eq.) and TMSCl (0.35 mL, 2.7 mmol, 1.2 eq.) were added and the mixture was stirred for 2 days at room temperature. After the addition of distilled 2,4,6-trimethylbenzoyl chloride (0.56 mL, 3.4 mmol, 1.5 eq.), stirring was continued for another 3 days at room temperature. Control by UPLC-MS measurement shows no conversion to the desired product, therefore the reaction was aborted and discarded.

2.4.1.5.5 <u>Pathway C) Synthesis of 2,4,6-trimethylbenzoyl-(ethylthio)phenyl-phosphine oxide (**PH5**)</u>
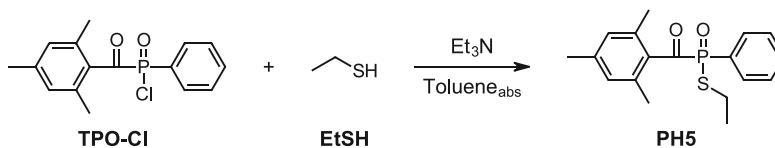
TPO-Cl   **EtSH**   **PH5**

The synthesis was carried out under inert gas atmosphere and exclusion of light, analogously to the work of Roszkowski et al.[111] The precursor **TPO-Cl** was prepared as described in 2.4.1.3 B).

Ethanethiol (**EtSH**, 0.51 mL, 6.83 mmol, 1.1 eq.) was diluted in 20 mL toluene$_{abs}$, Et$_3$N (1.9 mL, 13.66 mmol, 2.2 eq.) was added and stirred. **TPO-Cl** (1.90 g, 6.21 mmol, 1.0 eq.) was dissolved in 8 mL toluene$_{abs}$ and added dropwise and to this stirring solution. The reaction mixture was stirred for 1 h at room temperature, before 35 mL water were added. The layers were separated and the organic phase was washed three times with 30 mL saturated Na$_2$CO$_3$ each and one time with 30 mL saturated NaCl solution. After drying with Na$_2$SO$_4$ and filtration, the solvent and residual volatile reagents was evaporated.

An orange highly viscous and nearly pure product was obtained in a quantity of 1.86 g (95% of the theory).

¹H-NMR (400 MHz, CDCl$_3$)	δ 7.94 – 7.86 (m, 2H, C-C**H**$_{Ar}$), 7.57 (td, J = 7.3, 1.6 Hz, 1H, C-C**H**$_{Ar}$), 7.48 (td, J = 7.4, 3.7 Hz, 2H, C-C**H**$_{Ar}$), 6.81 (s, 2H, C-C**H**$_{Ar}$), 2.97 – 2.79 (m, 2H, S-C**H$_2$**-CH$_3$), 2.26 (s, 3H, C-C**H$_3$**$_{,Ar}$), 2.13 (s, 6H, C-C**H$_3$**$_{,Ar}$), 1.30 (t, J = 7.4 Hz, 3H, S-CH$_2$-C**H$_3$**).
³¹P-NMR (162 MHz, CDCl$_3$)	δ (ppm) 34.33.
¹³C-NMR (101 MHz, CDCl$_3$)	δ 214.55 (d, J = 74.0 Hz), 140.71, 135.03, 133.04 (d, J = 3.1 Hz), 132.44 (d, J = 9.7 Hz), 130.55, 129.66, 128.91, 128.82 (d, J = 12.4 Hz), 23.37 (d, J = 2.7 Hz), 21.35, 19.85, 16.58 (d, J = 4.6 Hz).
UPLC-MS	1.93 min.; [M+H]⁺ 333.00, [2M+H]⁺ 665.65
HRMS	Calculated: [M+Na]⁺ 355.0891; Found: 355.0900

2.4.1.6 Synthesis of 2,4,6-trimethylbenzoyl-(ethylsulfonyl)phenyl-phosphine oxide (**PH6**)

2.4.1.6.1 Pathway A) Synthesis of 2,4,6-trimethylbenzoyl-(ethylsulfonyl)phenyl-phosphine oxide (**PH6**)
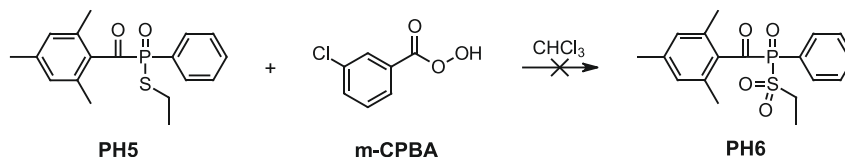
The reaction was carried out similarly to the work of Wu et al.[113] The photoinitiator **PH5** (13 mg, 0.04 mmol, 1.0 eq.) was dissolved in a small vial under exclusion of light. While stirring the oxidizing agent *m*-CPBA (77%, 14 mg, 0.06 mmol, 1.5 eq.) was added. After 4 min., 30 min. and 2 days stirring at room temperature, the mixture was evaluated using UPLC-MS measurements. The three measurements did not differ, and no mass indicating the product could be observed.

UPLC-MS   1.97 min.; [M+H]$^+$ 333.00, [2M+H]$^+$ 665.65; Area$_{254nm}$: 44%; PH5

2.03 – 2.30 min. (broad signal);   [2M+H]$^+$ 577.10, [M-H]$^-$ 287.00; Area$_{254nm}$: 36%; TPO-OH

In a second experiment the photoinitiator **PH5** (24 mg, 0.08 mmol, 1.0 eq.) was mixed directly with the oxidizing agent ***m*-CPBA** (77%, 69 mg, 0.31 mmol, 4 eq.) without any solvent. A distinct exothermic reaction was observed during the addition. A complete conversion of the educt **PH5** was observed in the UPLC-MS measurement of the sample. The desired target product was not obtained, but most likely **TPO-OH**.

UPLC-MS   Broad signal 1.90 – 2.10 min.; [2M+H]$^+$ 577.10, [M-H]$^-$ 287.00; TPO-OH

2.4.1.6.2 Pathway B) Synthesis of 2,4,6-trimethylbenzoyl-(ethylsulfonyl)phenyl-phosphine oxide (**PH6**)
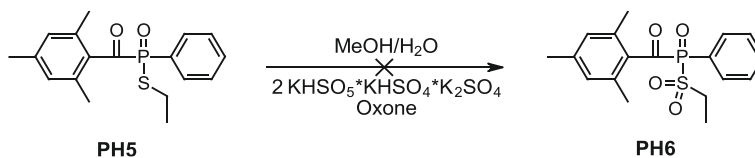
The reaction was carried out analogously to the literature, where thioanisol was oxidized to the corresponding sulfone.[114] The photoinitiator **PH5** (0.10 g, 0.32 mmol, 1 eq.) was dissolved in 3 mL of a 1:1 mixture of MeOH and H_2O. The oxidizing agent Oxone (0.12 g, 0.38 mmol, 1.2 eq.) was added in one portion to the stirring solution. UPLC-MS measurements were conducted after 1 h 45 min and 24 h stirring at room temperature. Increasing conversion of **PH5** was observed during this period, but the mass of the formed product does not correspond to that of the target product.

UPLC-MS (1 h 45 min.):   1.81 min. [303 (+)] (λ_{max}: 371 nm); $Area_{254\,nm}$: 7%; TPO-OMe

                                      1.97 min. [333 +] (λ_{max}: 378 nm); $Area_{254\,nm}$: 92%; PH5

                                      2.07 – 2.18 min. (broad signal), $[2M+H]^+$ 577.10, $[M-H]^-$ 287.00 $Area_{254\,nm}$: 1%, TPO-OH

UPLC-MS (24 h):   1.81 min. [303 (+)] (λ_{max}: 371 nm); $Area_{254\,nm}$: 17%; TPO-OMe

                                      1.97 min. [333 +] (λ_{max}: 378 nm); $Area_{254\,nm}$: 79%; PH5

                                      2.06 – 2.18 min. (broad signal); $[2M+H]^+$ 577.10, $[M-H]^-$ 287.00; $Area_{254\,nm}$: 4%; TPO-OH

2.4.1.7 Synthesis of (2,4,6-trimethylbenzoyl)diphenylphosphine selenid (**PH7**)

2.4.1.7.1 <u>Pathway A) Synthesis of (2,4,6-trimethylbenzoyl)diphenylphosphine selenid (**PH7**)</u>
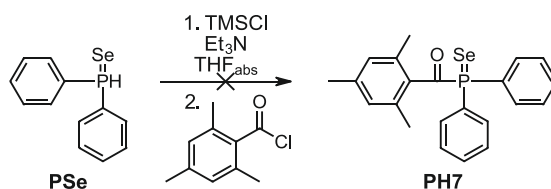
The reaction was carried out analogously to literature.[99] Under argon atmosphere and light exclusion, diphenylphosphine selenide (**PSe**, 0.64 g, 2.4 mmol, 1.0 eq.) was dissolved in THF_{abs} (10 mL). Subsequently dry Et_3N (0.4 mL, 2.9 mmol, 1.2 eq.) and distilled TMSCl (0.37 mL, 2.9 mmol, 1.2 eq.) were added to the stirring solution. White solid precipitated and the mixture was stirred for 2 days at room temperature. Afterwards distilled 2,4,6-trimethylbenzoyl chloride (0.61 mL, 3.6 mmol, 1.5 eq.) was added dropwise. The reaction mixture was stirred for a total of 5 days at room temperature and

reaction controls using UPLC-MS, ^{1}H-NMR and ^{31}P-NMR showed no evidence of a successful reaction, therefore the reaction was stopped and discarded.

2.4.1.7.2 Pathway B) Synthesis of (2,4,6-trimethylbenzoyl)diphenylphosphine (TP)

DPP   **TP**
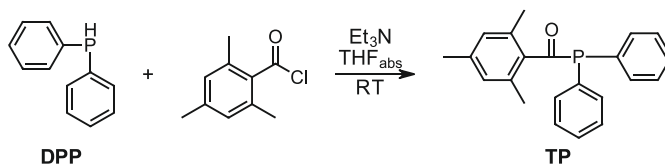
The reaction was carried out analogously to literature.[115] In inert gas atmosphere and with the exclusion of light, diphenylphosphine (**DPP**, 1.12 g, 6.0 mmol, 1.0 eq.) was dissolved in THF$_{abs}$ (10 mL). Dry Et$_3$N (1.0 mL, 7.2 mmol, 1.2 eq.) was added to the stirring solution before distilled 2,4,6-trimethylbenzoyl chloride (1.0 mL, 6.0 mmol, 1.0 eq.) had been added. After stirring for 24 h at room temperature, the reaction control with GCMS and ^{31}P-NMR showed full conversion of 2,4,6-trimethylbenzoyl chloride and some residual DPP. The mixture was filtrated under inert conditions through a bed of silica. The solvent was evaporated and residual DPP was removed at high vacuum by heating in an oil bath at 70°C. As a result, a solid was obtained which showed no more **DPP** peak in the ^{31}P-NMR, but some other side-products. When attempting to recrystallize the product from MeOH, as described in the literature, it did not precipitate on cooling. Therefore, the crude product was used for the subsequent reaction without further purification.

^{31}**P-NMR** (162 MHz, CDCl$_3$) δ 21.56.

2.4.1.7.3 Pathway B) Synthesis of (2,4,6-trimethylbenzoyl)diphenylphosphine selenid (PH7)

TP   **PH7**
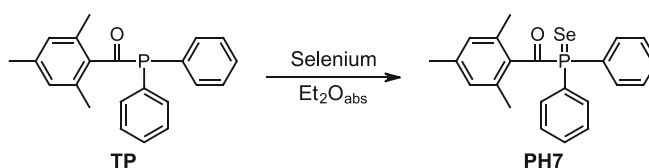
The reaction of **TP** with elemental selenium was carried out similarly as described in the literature.[116] The calculation was based on the theoretical yield of the previously produced **TP**. In argon atmosphere **TP** (2.00 g, 6.0 mmol, 1.0 eq) was dissolved in 50 mL Et$_2$O$_{abs}$

and mixed with elemental selenium (0.56 g, 7.1 mmol, 1.2 eq.). The mixture was stirred vigorously for 16 h at room temperature. The reaction control by NMR and UPLC-MS measurements indicated that the desired product was formed and the educt **TP** had been fully converted. Remaining selenium was filtered under inert conditions, the solvent was removed and the product was stored under inert conditions. After 3 days the product was analyzed by ^{31}P-NMR whereby the signal assigned to the product could no longer be observed. Also, the NMR sample of the reaction control was re-measured and the signal could no longer be observed here either.

^{31}P-NMR (162 MHz, CDCl$_3$)   δ 70.98 (t, J = 776.9 Hz).
UPLC-MS   2.26 min.

2.4.2 Characterization

2.4.2.2 Density functional theory (**DFT**) calculations of phosphanoyl radicals

The DFT calculations were performed at the TU Graz in the working group of Prof. Georg Gescheidt, using GAUSSIAN16. The geometries of the phosphanoyl radicals were optimized with the B3LYP functional and the 6-311++G** basis set. To further improve the result, Grimme's D3BJ dispersion correction was used.

2.4.2.3 Photo-DSC

The evaluation was performed analogous to the description in 2.2.2.2.

<u>320 – 500 nm broadband light source (OmniCure® S2000)</u>

For these measurements an OmniCure® S2000 high pressure mercury vapor light source equipped with a 320 – 500 nm filter was used as light source. The light intensity at the sample surface was set to 64 mW/cm^2. The results are summarized in Table 34.

Table 34: Results of photo-DSC measurements of formulations, consisting of 1 mol% photoinitiator in the monomer UDMA, under irradiation with a broadband light source (320-500 nm) with an intensity of 64 mW/cm².

320-500 nm	t_{max} [s]	R_p [mmol*L^{-1}*s^{-1}]	$t_{95\%}$ [s]	Onset [s]	Area [J/g]	DBC [%]
TPO	4.3 ± 0.2	176.0 ± 3.5	34.0 ± 1.6	1.7 ± 0.1	154.0 ± 0.2	64.2 ± 0.1
TPO-L	5.1 ± 0.3	147.8 ± 5.3	32.4 ± 1.5	2.1 ± 0.2	141.1 ± 1.3	58.9 ± 0.5
⬤ PH1	5.1 ± 0.1	147.6 ± 2.3	33.6 ± 0.9	2.2 ± 0.0	138.0 ± 2.3	57.6 ± 0.9
✕ PH2	6.3 ± 0.3	137.5 ± 1.6	35.9 ± 1.7	2.7 ± 0.2	139.2 ± 1.2	58.0 ± 0.5
⬟ PH3	5.6 ± 0.1	141.9 ± 0.7	32.7 ± 0.6	2.5 ± 0.1	137.0 ± 1.2	57.0 ± 0.5
▲ PH5	6.3 ± 0.2	121.8 ± 2.0	36.7 ± 0.9	2.6 ± 0.1	131.6 ± 2.3	54.9 ± 1.0

385 nm LED light source

For the measurements a 385 nm OmniCure® Max LED light source was used. The light intensity at the sample surface was set to 10 mW/cm². The results are summarized in Table 35.

Table 35: Results of photo-DSC measurements of formulations, consisting of 1 mol% photoinitiator in the monomer UDMA, under irradiation with a LED light source (385 nm) with an intensity of 10 mW/cm².

385 nm	t_{max} [s]	R_p [mmol*L^{-1}*s^{-1}]	$t_{95\%}$ [s]	Onset [s]	Area [J/g]	DBC [%]
TPO	5.5 ± 0.2	138.5 ± 1.5	32.2 ± 1.1	1.9 ± 0.0	138.3 ± 3.6	57.7 ± 1.5
TPO-L	6.1 ± 0.0	131.0 ± 4.2	35.2 ± 1.5	2.5 ± 0.1	134.9 ± 2.0	56.3 ± 0.8
⬤ PH1	6.2 ± 0.0	126.4 ± 1.8	35.5 ± 0.7	2.3 ± 0.1	131.5 ± 1.2	54.8 ± 0.5
✕ PH2	7.5 ± 0.1	108.8 ± 3.6	38.2 ± 1.7	3.0 ± 0.2	123.8 ± 1.7	51.6 ± 0.7
⬟ PH3	6.3 ± 0.3	124.8 ± 1.6	36.6 ± 0.7	2.6 ± 0.1	128.7 ± 1.5	53.6 ± 0.6
▲ PH5	7.8 ± 0.2	101.3 ± 1.5	38.7 ± 0.9	2.7 ± 0.0	121.7 ± 2.3	50.8 ± 0.9

400 nm LED light source

For the measurements a 400 nm OmniCure® Max LED light source was used. The light intensity at the sample surface was set to 10 mW/cm². The results are summarized in Table 36.

Experimental part

Table 36: Results of photo-DSC measurements of formulations, consisting of 1 mol% photoinitiator in the monomer UDMA, under irradiation with a LED light source (400 nm) with an intensity of 10 mW/cm².

400 nm	t_{max} [s]	R_p [mmol*L^{-1}*s^{-1}]	$t_{95\%}$ [s]	Onset [s]	Area [J/g]	DBC [%]
TPO	5.3 ± 0.1	156.8 ± 1.3	30.5 ± 0.3	2.1 ± 0.0	145.8 ± 0.8	60.8 ± 0.3
TPO-L	6.4 ± 0.0	134.9 ± 3.1	34.7 ± 1.5	2.7 ± 0.0	135.4 ± 2.2	56.5 ± 0.9
PH1	5.8 ± 0.0	129.6 ± 5.2	35.6 ± 0.2	2.2 ± 0.0	132.3 ± 2.2	55.2 ± 0.9
PH2	7.5 ± 0.4	113.8 ± 1.5	38.9 ± 1.6	3.3 ± 0.2	128.3 ± 1.7	53.5 ± 0.7
PH3	7.2 ± 0.2	114.5 ± 1.8	35.5 ± 1.3	3.2 ± 0.2	123.4 ± 2.4	51.4 ± 1.0
PH5	8.0 ± 0.1	104.8 ± 1.7	37.3 ± 0.0	3.3 ± 0.0	123.9 ± 1.7	51.7 ± 0.7

Materials and Methods

Chemicals

Chemical	Abbr.	Distributor
(±)-α-Tocopherol	TP	Sigma Aldrich
1,10-Decanediol dimethacrylate	D3MA	Ivoclar
1,2-Diphenylethan-1,2-dion / benzil		Acros
1,3,5-Trimethyl-2,4,6-tris(3,5-di-tert-butyl-4-hydroxybenzyl)benzene	TBM	TCI
1,6-Bis-[2-methacryloyloxyethoxycarbonylamino]-2,4,4-trimethylhexane (mixture of isomers)	UDMA	Ivoclar
1-Adamantanol	AdOH	TCI
1-Bromonaphthalene		Merck
1-Hydroxy-cyclohexyl-phenyl-ketone	I184	Ciba-Geigy
2,3,4,4'-Tetrahydoxybenzophenone	THBP	TCI
2,3,4-Trihydroxybenzaldehyde	4-APG	Sigma Aldrich
2,4,6-Triisopropylbenzoic acid		Alfa Aesar
2,4,6-Trimethoxybenzoic acid		ABCR
2,4,6-Trimethylbenzaldehyde (mesitaldehyde)		Sigma Aldrich
2,4,6-Trimethylbenzoyl chloride		TCI
2,4,6-Trimethylbenzoyldiphenyl phosphine oxide	TPO	Lambson
2,6-Dimethoxyphenol	DMP	Sigma Aldrich
2,6-Di-*tert*-butyl-4-methylphenol	BHT	Sigma Aldrich
2-Bromomesitylene		Aldrich
2-Hydroxy-1,2-diphenylethanon / benzoin		Merck
2-Hydroxy-2-methylpropiophenon	D1173	Merck
2-Hydroxy-4'-(2-hydroxyethoxy)-2-methylpropiophenon	I2959	Ciba
2-*tert*-Butylhydroquinone	TBHQ	Sigma Aldrich
3,4,5-Trihydroxybenzaldehyde	5-APG	TCI
4,4′-Dimethoxybenzil / *p*-anisil		Sigma Aldrich
4,4'-Dimethoxybenzoin / *p*-anisoin		Sigma Aldrich
4-Methoxyphenol	MeHQ	Fluka
4-Methylbenzaldehyde		ABCR
4-*tert*-Butylcatechin	BC	Merck
5-tert-Butylpyrogallol	BPG	Santa Cruz
Aluminium chloride (anhydrous)		Sigma Aldrich
Benzaldehyde		Carl Roth
Bis(2,4,6-trimethylbenzoyl)-phenylphosphineoxide	BAPO	BASF
Bis(4-methoxybenzoyl)diethylgermane / Ivocerin	Ivo	Ivoclar
Camphorquinine	CQ	Sigma Aldrich

Cumene hydroperoxide (80% solution in cumene)	CHP	Sigma Aldrich
Chemical	**Abbr.**	**Distributor**
Cyclohexyl bromide		Fluka
Diethyl chlorophosphite	DECP	Aldrich
Diphenylphosphine	DPP	Sigma Aldrich
Diphenylphosphine oxide	DPO	ABCR
Di-*tert*-butylchlorophosphine	(*t*-Bu)$_2$CP	Sigma Aldrich
Doverphos 11		Dover (ICC Industries)
Ethanthiol	EtSH	Merck
Ethyl (2,4,6-trimethylbenzoyl) phenyl phosphinate	TPO-L	BASF
Ethyl 3-benzoylacrylate	MC1	Alfa Aesar
Ethyl 4-(dimethylamino)benzoate	EDB	TCI
Ethyl dichlorophosphite	ECP	Lancaster
Lithium chloride	LiCl	Sigma Aldrich
Magnesium	Mg	Roth
Mesitylene	Mes	Acros
meta-Chloroperoxybenzoic acid	*m*-CPBA	Sigma Aldrich
Oxalyl chloride		TCI
Oxone		ABCR
P,*P*-Dichlorophenylphosphine	DCPP	Sigma Aldrich
Pentaerythritol tetrakis[3-(3,5-di-*tert*-butyl-4-hydroxyphenyl)propionate	PTP	TCI
Propyl gallate	PrG	Fluka
Pyrogallol	PyG	Merck
Rosmarinic acid	RA	ABCR
tert-Butylmagnesium chloride solution (1M in THF)	*t*-BuMgCl	Sigma Aldrich
Triethylamine	Et$_3$N	Sigma Aldrich
Trimethylsilyl chloride	TMSCl	ABCR
Tris(4-tert-butyl-3-hydroxy-2,6-dimethylbenzyl) Isocyanurate	TIC	Santa Cruz

Thin layer chromatography

TLC was carried out using TLC-aluminum foils, coated with silica gel 60 F254 from Merck.

Column chromatography

Column chromatography was performed with a Büchi MPLC-system equipped with the control unit C-620, fraction collector C-660 and an UV-photometer C-635. As stationary phase Merck silica gel 60 (0.040-0.063 mm) was used.

Orange light laboratory

Weighing, reactions and measurements of light-sensitive substances were carried out in an orange light laboratory, where the windows are laminated with Asmetec metolight SF-UV foils (type ASR-SF-LY5) and all lamps are of the type Osram lumix with chip controlled light color 62.

Melting points

The melting points were determined using an Optimelt MPA100 automated melting point apparatus.

NMR-spectroscopy

The ^{1}H-, ^{13}C- and ^{31}P-NMR spectra were recorded on a BRUKER Avance 400, or a BRUKER Ascend 600 spectrometer. The used frequencies are indicated in the respective experiments. The samples were dissolved in $CDCl_3$ (deuteration > 99.5%). The solvent signal was used as internal reference. The analysis of the spectra was performed with MestReNova version 14.3.3-33362.

GC-MS

The measurements were carried out on a Thermo Fisher Scientific ITQ 1100 equipped with a Fused Silica capillary column (30m x 0.25mm).

Ultra-high pressure liquid chromatography – mass spectroscopy (UPLC-MS)

A Nexera X2® UHPLC system (Shimadzu®) consisting of LC-30AD pumps, SIL-30AC autosampler, CTO-20AC column oven and DGU-20A5/3 degasser module was used in combination with an SPD-M20A photo diode array detector, an RF-20Axs fluorescence detector, an ELS-2041 evaporative light scattering detector (JASCO®) and a LC-MS-2020 mass spectrometer (ESI/APCI). All separations were performed using a Waters® XSelect® CSHTM C18 2,5 µm (3.0 x 50 mm) column XP at 40 °C, and a flowrate of 1.7 mL/min with water/acetonitrile + 0.1% formic acid gradient elution.

High-resolution mass spectrometry (HRMS)

The measurements were performed from acetonitrile solutions (concentration: 10 µM) using an HTC PAL system autosampler (CTC Analytics AG, Zwingen, Switzerland), an Agilent 1100/1200 HPLC with binary pumps, degasser, and column thermostat (Agilent Technologies, Waldbronn, Germany), and an Agilent 6230 AJS ESI-TOF mass spectrometer (Agilent Technologies, Palo Alto, CA).

Light sources

Depending on the experiment, different light sources were used, which are indicated in the respective section.

- OmniCure® S2000 spot UV curing system with a high-pressure mercury lamp equipped with a 320 – 500 nm or a 400 – 500 nm bandpass filter
- Omnicure® Max LED head 385 nm together with an OmniCure® LX 500 UV LED Spot Curing System
- Omnicure® Max LED head 400 nm together with an OmniCure® LX 500 UV LED Spot Curing System
- Ivoclar PrograPrint® Cure device (405 nm / 460 nm; Program: "Model"; 270 mW/cm²)
- Uvitron IntelliRay 600 UV flood curing system (broadband, 15 min., UV-A: 125 mW/cm², Vis: 125 mW/cm²)

Light intensity calibration

For photo-DSC measurements with the OmniCure® S2000 light source the light intensity was calibrated externally using an OmniCure® R2000 radiometer.

Apart from that, the light intensity was determined using an OceanOptics 2000+ USB device together with the software SpectraSuit.

UV-Vis spectroscopy

For the UV-Vis experiments the samples were dissolved in acetonitrile (HPLC grade: ≥99.9%) in the stated concentration. The solutions were placed into quartz cuvettes with an optical path length of d = 10 mm. The UV-Vis measurements were performed on a Thermo Scientific NanoDrop One/OneC Microvolume UV-Vis spectrophotometer. The spectra were recorded from 250 nm – 850 nm and baseline corrections were carried out at 750 nm.

The measurements of thin film samples were carried out in the same way, but the properly cut samples were measured without solvent, standing upright in the cuvette.

Photo-DSC

The photo-DSC measurements were conducted on a Photo-DSC 204 F1 from Netzsch, equipped with glassfiber filled double-core lightguide (3 mm fiber diameter). The samples (11 ± 1 mg) were measured in 15 µL aluminum pans and irradiated twice with the stated light source for 300 s. All measurements were conducted under constant nitrogen flow (20 mL/min). The heat flow of the polymerization reaction was recorded as a function of time. All measurements were performed in triplicates. For the evaluation Proteus - Thermal Analysis (V5.2.1) from Netzsch was used.

For samples irradiated with a 320 – 500 nm broadband light source, an OmniCure® S2000 high pressure mercury vapor light source equipped with a 320 – 500 nm filter was used. The light intensity was set to 1.0 W/cm² at the tip of the light guide with an OmniCure® R2000 radiometer. This corresponds to a light intensity of to 64 mW/cm² at the surface of the sample.

For samples irradiated with a 385 nm or a 400 nm LED light source, the corresponding OmniCure® Max LED head was used in combination with a LX500 trigger unit. The LED

     Materials and Methods

head was coupled with the light guide of the Photo-DSC and the light intensity at the sample surface was set to 10 mW/cm^2.

For the measurements with a 400 nm light source the corresponding OmniCure$^®$ Max LED head was used in combination with a LX500 trigger unit. The LED head was coupled with the light guide of the Photo-DSC and the light intensity at the sample surface was calibrated to 10 mW/cm^2 using an Ocean Optics 2000+ USB device together with the software SpectraSuit.

Thin film sample preparation / Photorheometer

The thin film samples for color evaluation with the UV-Vis spectroscopy method were prepared on an Anton Paar MCR 302 WESP rheometer, equipped with a P-PTD 200/GL Peltier glass plate and a PP25 measuring system. The glass plate was covered with PE tape so that the samples could be easily removed from the surface. The light source used for curing and the light intensity are indicated in 1.2.1.

Writing tools

Throughout the preparation of this work, ChatGPT-3.5 and DeepL were utilized to facilitate copyediting and rephrasing of text passages, to enhance the readability of the document. Subsequently, the content was thoroughly reviewed and revised as required.

Abbreviations

a(P)	Phosphorous hyperfine coupling constant
a*	Green-red error
b*	Blue-yellow error
BAPO	Bisacylphosphine oxide
CoI	Coinitiator
CTC	Charge transfer complex
DBC	Double bond conversion
DFT	Density functional theory
DLP	Digital light processing
EPR	Electron paramagnetic resonance
HOMO	Highest occupied molecular orbital
IC	Internal conversion
ISC	Intersystem crossing
L*	Lightness
LUMO	Lowest unoccupied molecular orbital
MAPO	Monoacylphosphine oxide
MC	Model compound
MO	Molecular orbital
PDA	Photo diode array
PI	Photoinitiator
R_p	Rate of polymerization
SLA	Stereolithography
$t_{95\%}$	Time until 95% of total heat flow
t_{max}	Time until peak maximum
VR	Vibrational relaxation
ΔAbs	Change in absorbance
ΔE	Total color change
ε	Molar absorption coefficient
λ_{max}	Wavelength of absorption maximum
Φ	Quantum yield

References

(1) Albert, P.; Dermann, K.; Rentsch, H. Amalgam und die Alternativen. *Chemie in unserer Zeit* 2000, *34* (5), 300-305. DOI: https://doi.org/10.1002/1521-3781(200010)34:5<300::AID-CIUZ300>3.0.CO;2-0.

(2) Anusavice, K. J.; Shen, C.; Rawls, H. R. Phillips' science of dental materials. 2013.

(3) Jirau-Colón, H.; González-Parrilla, L.; Martinez-Jiménez, J.; Adam, W.; Jiménez-Velez, B. Rethinking the Dental Amalgam Dilemma: An Integrated Toxicological Approach. In *International Journal of Environmental Research and Public Health*, 2019; Vol. 16.

(4) AlJehani, Y.; Baskaradoss, J.; Geevarghese, A.; Alshehry, M. Current Trends in Aesthetic Dentistry. *Health* 2014, *06*, 1941-1949. DOI: http://dx.doi.org/10.4236/health.2014.615227.

(5) Ferracane, J. L. Current Trends in Dental Composites. *Critical Reviews in Oral Biology & Medicine* 1995, *6* (4), 302-318. DOI: 10.1177/10454411950060040301.

(6) Habib, E.; Wang, R.; Wang, Y.; Zhu, M.; Zhu, X. X. Inorganic Fillers for Dental Resin Composites: Present and Future. *ACS Biomaterials Science & Engineering* 2016, *2* (1), 1-11. DOI: 10.1021/acsbiomaterials.5b00401.

(7) Moad, G.; Solomon, D. H. 2 - Radical Reactions. In *The Chemistry of Radical Polymerization (Second Edition)*, Moad, G., Solomon, D. H. Eds.; Elsevier Science Ltd, 2005; pp 11-48.

(8) Peutzfeldt, A. Resin composites in dentistry: the monomer systems. *European Journal of Oral Sciences* 1997, *105* (2), 97-116. DOI: https://doi.org/10.1111/j.1600-0722.1997.tb00188.x.

(9) Ruyter, I. E.; Øysæd, H. Composites for use in posterior teeth: Composition and conversion. *Journal of Biomedical Materials Research* 1987, *21* (1), 11-23. DOI: https://doi.org/10.1002/jbm.820210107.

(10) Fonseca, A. S. Q. S.; Labruna Moreira, A. D.; de Albuquerque, P. P. A. C.; de Menezes, L. R.; Pfeifer, C. S.; Schneider, L. F. J. Effect of monomer type on the CC degree of conversion, water sorption and solubility, and color stability of model dental composites. *Dental Materials* 2017, *33* (4), 394-401. DOI: https://doi.org/10.1016/j.dental.2017.01.010.

(11) Wardle, B. *Principles and Applications of Photochemistry*; John Wiley & Sons, 2009.

(12) Dietliker, K. *Chemistry & Technology of UV & EB Formulation for Coatings, Inks & Paints, Vol. 3: Photoinitiators for Free Radical and Cationic Polymerisation*; SITA Technology 1991.

(13) Fouassier, J.-P. *Photoinitiation, Photopolymerization, and Photocuring: Fundamentals and Applications.*; Hanser/Gardner Publications, 1995.

(14) Gruber, H. F. Photoinitiators for free radical polymerization. *Progress in Polymer Science* 1992, *17* (6), 953-1044. DOI: https://doi.org/10.1016/0079-6700(92)90006-K.

(15) Green, A. W. *Industrial Photoinitiators: A Technical Guide*; CRC Press, 2010.

(16) Allen, N. S. Photoinitiators for UV and visible curing of coatings: Mechanisms and properties. *Journal of Photochemistry and Photobiology A: Chemistry* 1996, *100* (1), 101-107. DOI: https://doi.org/10.1016/S1010-6030(96)04426-7.

(17) Kowalska, A.; Sokolowski, J.; Bociong, K. The Photoinitiators Used in Resin Based Dental Composite—A Review and Future Perspectives. In *Polymers*, 2021; Vol. 13.

(18) Ikemura, K.; Endo, T. A review of the development of radical photopolymerization initiators used for designing light-curing dental adhesives and resin composites. *Dental materials journal* 2010, *29*, 481-501. DOI: 10.4012/dmj.2009-137.

(19) Ikemura, K.; Ichizawa, K.; Jogetsu, Y.; Endo, T. Synthesis of a novel camphorquinone derivative having acylphosphine oxide group, characterization by UV-VIS spectroscopy and evaluation of photopolymerization performance. *Dental Materials Journal* 2010, *29* (2), 122-131. DOI: 10.4012/dmj.2009-026.

(20) Stansbury, J. W. Curing Dental Resins and Composites by Photopolymerization. *Journal of Esthetic and Restorative Dentistry* 2000, *12* (6), 300-308. DOI: https://doi.org/10.1111/j.1708-8240.2000.tb00239.x.

(21) Bowen, R. L.; Argentar, H. Amine Accelerators for Methacrylate Resin Systems. *Journal of Dental Research* 1971, *50* (4), 923-928. DOI: https://doi.org/10.1177/00220345710500042301.

(22) Schneider, L. F. J.; Cavalcante, L. M.; Consani, S.; Ferracane, J. L. Effect of co-initiator ratio on the polymer properties of experimental resin composites formulated with camphorquinone and phenyl-propanedione. *Dental Materials* 2009, *25* (3), 369-375. DOI: https://doi.org/10.1016/j.dental.2008.08.003.

(23) Fouassier, J. P.; Lalevée, J. *Photoinitiators: Structures, Reactivity and Applications in Polymerization*; 2021. DOI: 10.1002/9783527821297.

(24) Walling, C. *Free radicals in solution*; Wiley, 1957.

(25) Dietliker, K.; Jung, T.; Benkhoff, J.; Kura, H.; Matsumoto, A.; Oka, H.; Hristova, D.; Gescheidt, G.; Rist, G. New Developments in Photoinitiators. *Macromolecular Symposia* 2004, *217* (1), 77-98. DOI: https://doi.org/10.1002/masy.200451307.

(26) Berlin, K. D.; Taylor, H. A. The Reactions of Aroyl Halides with Phosphites. Esters of Aroylphosphonic Acids. *Journal of the American Chemical Society* 1964, *86* (18), 3862-3866. DOI: 10.1021/ja01072a053.

(27) Terauchi, K.-i.; Sakurai, H. Ultraviolet Spectral Studies in the Esters of Aroylphosphonic Acids. *Bulletin of the Chemical Society of Japan* 1969, *42* (3), 821-823. DOI: 10.1246/bcsj.42.821.

(28) Fouassier, J. P. Photopolymerization Reactions. In *Polymer Handbook*, 4th ed.; Brandrup, J., Immergut, E. H., Grulke, E. A., Abe, A., Bloch, D. R. Ed.; John Wiley & Sons, 1999.

(29) Albuquerque, P. P. A. C.; Moreira, A. D. L.; Moraes, R. R.; Cavalcante, L. M.; Schneider, L. F. J. Color stability, conversion, water sorption and solubility of dental composites formulated with different photoinitiator systems. *Journal of Dentistry* 2013, *41*, e67-e72. DOI: https://doi.org/10.1016/j.jdent.2012.11.020.

(30) Arikawa, H.; Takahashi, H.; Kanie, T.; Ban, S. Effect of various visible light photoinitiators on the polymerization and color of light-activated resins. *Dental Materials Journal* 2009, *28* (4), 454-460. DOI: 10.4012/dmj.28.454.

(31) Kim, G.-T.; Go, H.-B.; Yu, J.-H.; Yang, S.-Y.; Kim, K.-M.; Choi, S.-H.; Kwon, J.-S. Cytotoxicity, Colour Stability and Dimensional Accuracy of 3D Printing Resin with Three Different Photoinitiators. *Polymers* 2022, *14* (5), 979. DOI: https://doi.org/10.3390/polym14050979.

(32) Popal, M.; Volk, J.; Leyhausen, G.; Geurtsen, W. Cytotoxic and genotoxic potential of the type I photoinitiators BAPO and TPO on human oral keratinocytes and V79 fibroblasts. *Dental Materials* 2018, *34* (12), 1783-1796. DOI: https://doi.org/10.1016/j.dental.2018.09.015.

(33) Zeng, B.; Cai, Z.; Lalevée, J.; Yang, Q.; Lai, H.; Xiao, P.; Liu, J.; Xing, F. Cytotoxic and cytocompatible comparison among seven photoinitiators-triggered polymers in different tissue cells. *Toxicology in Vitro* 2021, *72*, 105103. DOI: https://doi.org/10.1016/j.tiv.2021.105103.

(34) Manojlovic, D.; Dramićanin, M. D.; Miletic, V.; Mitić-Ćulafić, D.; Jovanović, B.; Nikolić, B. Cytotoxicity and genotoxicity of a low-shrinkage monomer and monoacylphosphine oxide photoinitiator: Comparative analyses of individual toxicity and combination effects in mixtures. *Dental Materials* 2017, *33* (4), 454-466. DOI: https://doi.org/10.1016/j.dental.2017.02.002.

(35) European Parliament, C. o. t. E. U. Classification, labelling and packaging of substances and mixtures, amending and repealing. In *Regulation (EC) No 1272/2008* 16 December 2008.

(36) Schneider, L. F. J.; Cavalcante, L. M.; Prahl, S. A.; Pfeifer, C. S.; Ferracane, J. L. Curing efficiency of dental resin composites formulated with camphorquinone or trimethylbenzoyl-diphenyl-phosphine oxide. *Dental Materials* 2012, *28* (4), 392-397. DOI: https://doi.org/10.1016/j.dental.2011.11.014.

(37) Palin, W. M.; Hadis, M. A.; Leprince, J. G.; Leloup, G.; Boland, L.; Fleming, G. J. P.; Krastl, G.; Watts, D. C. Reduced polymerization stress of MAPO-containing resin composites with increased curing speed,

degree of conversion and mechanical properties. *Dental Materials* 2014, *30* (5), 507-516. DOI: https://doi.org/10.1016/j.dental.2014.02.003.

(38) Randolph, L. D.; Palin, W. M.; Bebelman, S.; Devaux, J.; Gallez, B.; Leloup, G.; Leprince, J. G. Ultra-fast light-curing resin composite with increased conversion and reduced monomer elution. *Dental Materials* 2014, *30* (5), 594-604. DOI: https://doi.org/10.1016/j.dental.2014.02.023.

(39) de Castro, E. F.; Nima, G.; Rueggeberg, F. A.; Araújo-Neto, V. G.; Faraoni, J. J.; Palma-Dibb, R. G.; Giannini, M. Effect of build orientation in gloss, roughness and color of 3D-printed resins for provisional indirect restorations. *Dental Materials* 2023, *39* (7), e1-e11. DOI: https://doi.org/10.1016/j.dental.2023.05.002.

(40) Kessler, A.; Hickel, R.; Reymus, M. 3D Printing in Dentistry—State of the Art. *Operative Dentistry* 2020, *45* (1), 30-40. DOI: https://doi.org/10.2341/18-229-l.

(41) Sitzmann, E. V.; Peter, W.; Bramer, D.; Jankauskas, J.; Losapio, G.; Wolf, J.-P.; Huguenard, S. Low color liquid acylphosphine oxide photoinitiators blends for UV coating applications. In *Radtech UV & EB Technical Conference Proceedings*, 2004.

(42) Tahayeri, A.; Morgan, M.; Fugolin, A. P.; Bompolaki, D.; Athirasala, A.; Pfeifer, C. S.; Ferracane, J. L.; Bertassoni, L. E. 3D printed versus conventionally cured provisional crown and bridge dental materials. *Dental Materials* 2018, *34* (2), 192-200. DOI: https://doi.org/10.1016/j.dental.2017.10.003.

(43) Abdullah, A. O.; Tsitrou, E. A.; Pollington, S. Comparative in vitro evaluation of CAD/CAM vs conventional provisional crowns. *J Appl Oral Sci* 2016, *24* (3), 258-263. DOI: https://doi.org/10.1590/1678-775720150451.

(44) Li, X.; Xie, B.; Jin, J.; Chai, Y.; Chen, Y. 3D Printing Temporary Crown and Bridge by Temperature Controlled Mask Image Projection Stereolithography. *Procedia Manufacturing* 2018, *26*, 1023-1033. DOI: https://doi.org/10.1016/j.promfg.2018.07.134.

(45) Berman, B. 3-D printing: The new industrial revolution. *Business Horizons* 2012, *55* (2), 155-162. DOI: https://doi.org/10.1016/j.bushor.2011.11.003.

(46) Revilla-León, M.; Özcan, M. Additive Manufacturing Technologies Used for Processing Polymers: Current Status and Potential Application in Prosthetic Dentistry. *Journal of Prosthodontics* 2019, *28* (2), 146-158. DOI: https://doi.org/10.1111/jopr.12801.

(47) Abduo, J.; Lyons, K.; Bennamoun, M. Trends in Computer-Aided Manufacturing in Prosthodontics: A Review of the Available Streams. *International Journal of Dentistry* 2014, *2014*, 783948. DOI: https://doi.org/10.1155/2014/783948.

(48) van Noort, R. The future of dental devices is digital. *Dental Materials* 2012, *28* (1), 3-12. DOI: https://doi.org/10.1016/j.dental.2011.10.014.

(49) Dawood, A.; Marti, B. M.; Sauret-Jackson, V.; Darwood, A. 3D printing in dentistry. *British Dental Journal* 2015, *219* (11), 521-529. DOI: https://doi.org/10.1038/sj.bdj.2015.914.

(50) Nayar, S.; Bhuminathan, S.; Bhat, W. M. Rapid prototyping and stereolithography in dentistry. *Journal of Pharmacy and Bioallied Sciences* 2015, *7*, S216-S219. DOI: https://doi.org/10.4103/0975-7406.155913.

(51) Tzeng, J.-J.; Yang, T.-S.; Lee, W.-F.; Chen, H.; Chang, H.-M. Mechanical Properties and Biocompatibility of Urethane Acrylate-Based 3D-Printed Denture Base Resin. *Polymers* 2021, *13* (5), 822. DOI: https://doi.org/10.3390/polym13050822.

(52) Amini, A.; Guijt, R. M.; Themelis, T.; De Vos, J.; Eeltink, S. Recent developments in digital light processing 3D-printing techniques for microfluidic analytical devices. *Journal of Chromatography A* 2023, *1692*. DOI: https://doi.org/10.1016/j.chroma.2023.463842.

(53) Bagheri, A.; Jin, J. Photopolymerization in 3D Printing. *ACS Applied Polymer Materials* 2019, *1* (4), 593-611. DOI: https://doi.org/10.1021/acsapm.8b00165.

(54) Scotti, C. K.; Velo, M. M. d. A. C.; Rizzante, F. A. P.; Nascimento, T. R. d. L.; Mondelli, R. F. L.; Bombonatti, J. F. S. Physical and surface properties of a 3D-printed composite resin for a digital workflow. *The Journal*

of Prosthetic Dentistry 2020, *124* (5), 614.e611-614.e615. DOI: https://doi.org/10.1016/j.prosdent.2020.03.029.

(55) Shin, J.-W.; Kim, J.-E.; Choi, Y.-J.; Shin, S.-H.; Nam, N.-E.; Shim, J.-S.; Lee, K.-W. Evaluation of the Color Stability of 3D-Printed Crown and Bridge Materials against Various Sources of Discoloration: An In Vitro Study. In *Materials*, 2020; Vol. 13.

(56) Gruber, S.; Kamnoedboon, P.; Özcan, M.; Srinivasan, M. CAD/CAM Complete Denture Resins: An In Vitro Evaluation of Color Stability. *Journal of Prosthodontics* 2021, *30* (5), 430-439. DOI: https://doi.org/10.1111/jopr.13246.

(57) Azzopardi, N.; Moharamzadeh, K.; Wood, D. J.; Martin, N.; van Noort, R. Effect of resin matrix composition on the translucency of experimental dental composite resins. *Dental Materials* 2009, *25* (12), 1564-1568. DOI: https://doi.org/10.1016/j.dental.2009.07.011.

(58) Ferracane, J. L.; Moser, J. B.; Greener, E. H. Ultraviolet light-induced yellowing of dental restorative resins. *The Journal of Prosthetic Dentistry* 1985, *54* (4), 483-487. DOI: https://doi.org/10.1016/0022-3913(85)90418-4.

(59) Rosentritt, M.; Huber, C.; Strasser, T.; Schmid, A. Investigating the mechanical and optical properties of novel Urethandimethacrylate (UDMA) and Urethanmethacrylate (UMA) based rapid prototyping materials. *Dental Materials* 2021, *37* (10), 1584-1591. DOI: https://doi.org/10.1016/j.dental.2021.08.009.

(60) Manojlovic, D.; Dramićanin, M. D.; Lezaja, M.; Pongprueksa, P.; Van Meerbeek, B.; Miletic, V. Effect of resin and photoinitiator on color, translucency and color stability of conventional and low-shrinkage model composites. *Dental Materials* 2016, *32* (2), 183-191. DOI: https://doi.org/10.1016/j.dental.2015.11.027.

(61) de Oliveira, D. C. R. S.; Rocha, M. G.; Gatti, A.; Correr, A. B.; Ferracane, J. L.; Sinhoret, M. A. C. Effect of different photoinitiators and reducing agents on cure efficiency and color stability of resin-based composites using different LED wavelengths. *Journal of Dentistry* 2015, *43* (12), 1565-1572. DOI: https://doi.org/10.1016/j.jdent.2015.08.015.

(62) Hadis, M. A.; Shortall, A. C.; Palin, W. M. Competitive light absorbers in photoactive dental resin-based materials. *Dental Materials* 2012, *28* (8), 831-841. DOI: https://doi.org/10.1016/j.dental.2012.04.029.

(63) Schneider, L. F. J.; Pfeifer, C. S. C.; Consani, S.; Prahl, S. A.; Ferracane, J. L. Influence of photoinitiator type on the rate of polymerization, degree of conversion, hardness and yellowing of dental resin composites. *Dental Materials* 2008, *24* (9), 1169-1177. DOI: https://doi.org/10.1016/j.dental.2008.01.007.

(64) Shin, D.-H.; Rawls, H. Degree of conversion and colorstability of the light curing resin with new photoinitiator systems. *Dental materials : official publication of the Academy of Dental Materials* 2009, *25*, 1030-1038. DOI: https://doi.org/10.1016/j.dental.2009.03.004.

(65) Segurola, J.; Allen, N. S.; Edge, M.; McMahon, A.; Wilson, S. Photoyellowing and discolouration of UV cured acrylated clear coatings systems: influence of photoinitiator type. *Polymer Degradation and Stability* 1999, *64* (1), 39-48. DOI: https://doi.org/10.1016/S0141-3910(98)00169-4.

(66) Kirchmayr, R.; Berner, G.; Huesler, R.; Rist, G. Nonyellowing photoinitiators. *Farbe Lack* 1982, *88*, 910-916.

(67) Barnes, C. E.; Elofson, R. M.; Jones, G. D. Role of Oxygen in Vinyl Polymerization. II. Isolation and Structure of the Peroxides of Vinyl Compounds. *Journal of the American Chemical Society* 1950, *72* (1), 210-215. DOI: https://doi.org/10.1021/ja01157a059.

(68) Imazato, S.; Tarumi, H.; Kobayashi, K.; Hiraguri, H.; Oda, K.; Tsuchitani, Y. Relationship Between the Degree of Conversion and Internal Discoloration of Light-activated Composite. *Dental Materials Journal* 1995, *14* (1), 23-30,101. DOI: 10.4012/dmj.14.23.

(69) Asmussen, E. Factors affecting the color stability of restorative resins. *Acta Odontol Scand* 1983, *41* (1), 11-18. DOI: 10.3109/00016358309162298.

(70) Bowen, R. L.; Argentar, H. Diminishing Discoloration in Methacrylate Accelerator Systems. *The Journal of the American Dental Association* 1967, *75* (4), 918-923. DOI: https://doi.org/10.14219/jada.archive.1967.0294.

(71) Pospíšil, J. Mechanistic action of phenolic antioxidants in polymers—A review. *Polymer Degradation and Stability* 1988, *20* (3), 181-202. DOI: https://doi.org/10.1016/0141-3910(88)90069-9.

(72) Pospíšil, J.; Habicher, W. D.; Pilař, J.; Nešpůrek, S.; Kuthan, J.; Piringer, G. O.; Zweifel, H. Discoloration of polymers by phenolic antioxidants. *Polymer Degradation and Stability* 2002, *77* (3), 531-538. DOI: https://doi.org/10.1016/S0141-3910(02)00112-X.

(73) Alariqi, S. A. S.; Pratheep Kumar, A.; Rao, B. S. M.; Tevtia, A. K.; Singh, R. P. Stabilization of γ-sterilized biomedical polyolefins by synergistic mixtures of oligomeric stabilizers. *Polymer Degradation and Stability* 2006, *91* (10), 2451-2464. DOI: https://doi.org/10.1016/j.polymdegradstab.2006.03.010.

(74) Janda, R.; Roulet, J.-F.; Kaminsky, M.; Steffin, G.; Latta, M. Color stability of resin matrix restorative materials as a function of the method of light activation. *European Journal of Oral Sciences* 2004, *112* (3), 280-285. DOI: https://doi.org/10.1111/j.1600-0722.2004.00125.x.

(75) Rueggeberg, F. A.; Ergle, J. W.; Lockwood, P. E. Effect of photoinitiator level on properties of a light-cured and post-cure heated model resin system. *Dental Materials* 1997, *13* (5), 360-364. DOI: https://doi.org/10.1016/S0109-5641(97)80107-8.

(76) Fischer, H.; Baer, R.; Hany, R.; Verhoolen, I.; Walbiner, M. 2,2-Dimethoxy-2-phenylacetophenone: photochemistry and free radical photofragmentation. *Journal of the Chemical Society, Perkin Transactions 2* 1990, (5), 787-798, 10.1039/P29900000787. DOI: 10.1039/P29900000787.

(77) Griesser, M.; Neshchadin, D.; Dietliker, K.; Moszner, N.; Liska, R.; Gescheidt, G. Decisive Reaction Steps at Initial Stages of Photoinitiated Radical Polymerizations. *Angewandte Chemie (International ed. in English)* 2009, *48*, 9359-9361. DOI: https://doi.org/10.1002/anie.200904473.

(78) Gorsche, C.; Harikrishna, R.; Baudis, S.; Knaack, P.; Husar, B.; Laeuger, J.; Hoffmann, H.; Liska, R. Real Time-NIR/MIR-Photorheology: A Versatile Tool for the in Situ Characterization of Photopolymerization Reactions. *Analytical Chemistry* 2017, *89* (9), 4958-4968. DOI: https://doi.org/10.1021/acs.analchem.7b00272.

(79) Islam, H. *Defining and Communicating Color: The CIELAB System*. Textile Research and Development, https://textilernd.com/defining-and-communicating-color-the-cielab-system/ (accessed 06.07.2024).

(80) Wolf, T. J. A.; Voll, D.; Barner-Kowollik, C.; Unterreiner, A.-N. Elucidating the Early Steps in Photoinitiated Radical Polymerization via Femtosecond Pump–Probe Experiments and DFT Calculations. *Macromolecules* 2012, *45* (5), 2257-2266. DOI: https://doi.org/10.1021/ma202673q.

(81) Michel, R. E.; Chapman, F. W.; Mao, T. J. Electron Spin Resonance Studies of Photodegradation in Poly(Methylmethacrylate). *The Journal of Chemical Physics* 1966, *45* (12), 4604-4611. DOI: 10.1063/1.1727543.

(82) Lin, Y.-S.; Lee, S.; Lin, B. C.; Cheng, C. P. EPR studies of high dose gamma-irradiated poly(methyl methacrylate). *Materials Chemistry and Physics* 2003, *78* (3), 847-851. DOI: https://doi.org/10.1016/S0254-0584(02)00450-9.

(83) Dietlin, C.; Trinh, T. T.; Schweizer, S.; Graff, B.; Morlet-Savary, F.; Noirot, P.-A.; Lalevée, J. Rational Design of Acyldiphenylphosphine Oxides as Photoinitiators of Radical Polymerization. *Macromolecules* 2019, *52* (20), 7886-7893. DOI: https://doi.org/10.1021/acs.macromol.9b01724.

(84) Bendich, A.; Machlin, L. J.; Scandurra, O.; Burton, G. W.; Wayner, D. D. M. The antioxidant role of vitamin C. *Advances in Free Radical Biology & Medicine* 1986, *2* (2), 419-444. DOI: https://doi.org/10.1016/S8755-9668(86)80021-7.

(85) Gijsman, P. 18 - Polymer Stabilization. In *Applied Plastics Engineering Handbook (Second Edition)*, Kutz, M. Ed.; William Andrew Publishing, 2017; pp 395-421.

(86) Soucek, M. D.; Khattab, T.; Wu, J. Review of autoxidation and driers. *Progress in Organic Coatings* 2012, *73* (4), 435-454. DOI: https://doi.org/10.1016/j.porgcoat.2011.08.021.

(87) Jockusch, S.; Turro, N. J. Phosphinoyl Radicals: Structure and Reactivity. A Laser Flash Photolysis and Time-Resolved ESR Investigation. *Journal of the American Chemical Society* 1998, *120* (45), 11773-11777. DOI: 10.1021/ja982463z.

(88) Gatlik, I.; Rzadek, P.; Gescheidt, G.; Rist, G.; Hellrung, B.; Wirz, J.; Dietliker, K.; Hug, G.; Kunz, M.; Wolf, J.-P. Structure–Reactivity Relationships in Radical Reactions: A Novel Method for the Simultaneous Determination of Absolute Rate Constants and Structural Features. *Journal of the American Chemical Society* 1999, *121* (36), 8332-8336. DOI: 10.1021/ja991008f.

(89) Dursun, C.; Degirmenci, M.; Yagci, Y.; Jockusch, S.; Turro, N. J. Free radical promoted cationic polymerization by using bisacylphosphine oxide photoinitiators: substituent effect on the reactivity of phosphinoyl radicals. *Polymer* 2003, *44* (24), 7389-7396. DOI: https://doi.org/10.1016/j.polymer.2003.09.020.

(90) Spichty, M.; Turro, N. J.; Rist, G.; Birbaum, J.-L.; Dietliker, K.; Wolf, J.-P.; Gescheidt, G. Bond cleavage in the excited state of acyl phosphene oxides: Insight on the role of conformation by model calculations: a concept. *Journal of Photochemistry and Photobiology A: Chemistry* 2001, *142* (2), 209-213. DOI: https://doi.org/10.1016/S1010-6030(01)00515-9.

(91) Sumiyoshi, T.; Schnabel, W.; Henne, A. Photolysis of acylphosphine oxides II: The influence of methyl substitution in benzoyldiphenylphosphine oxides. *Journal of Photochemistry* 1986, *32* (1), 119-129. DOI: https://doi.org/10.1016/0047-2670(86)85012-2.

(92) Xie, C.; Wang, Z.; Liu, Y.; Song, L.; Liu, L.; Wang, Z.; Yu, Q. A novel acyl phosphine compound as difunctional photoinitiator for free radical polymerization. *Progress in Organic Coatings* 2019, *135*, 34-40. DOI: https://doi.org/10.1016/j.porgcoat.2019.05.021.

(93) Liu, Y.; Wang, T.; Xie, C.; Tian, X.; Song, L.; Liu, L.; Wang, Z.; Yu, Q. Naphthyl-based acylphosphine oxide photoinitiators with high effiency and low migration. *Progress in Organic Coatings* 2020, *142*, 105603. DOI: https://doi.org/10.1016/j.porgcoat.2020.105603.

(94) Wu, Y.; Li, R.; Huang, C.; Wu, J.; Sun, X.; Situ, Y.; Huang, H. New acyl phosphine oxides as high-performance and low migration type I photoinitiators of radical polymerization. *Progress in Organic Coatings* 2022, *168*, 106876. DOI: https://doi.org/10.1016/j.porgcoat.2022.106876.

(95) Baxter, J. E.; Stephen Davidson, R.; Hageman, H. J. Acylphosphine oxides as photoinitiators for acrylate and unsaturated polyester resins. *European Polymer Journal* 1988, *24* (5), 419-424. DOI: https://doi.org/10.1016/0014-3057(88)90077-8.

(96) Oesterreicher, A.; Roth, M.; Hennen, D.; Mostegel, F. H.; Edler, M.; Kappaun, S.; Griesser, T. Low migration type I photoinitiators for biocompatible thiol-ene formulations. *European Polymer Journal* 2017, *88*, 393-402. DOI: https://doi.org/10.1016/j.eurpolymj.2016.10.040.

(97) Duan, H.; Leng, K.; Xu, X.; Li, Q.; Liu, D.; Han, Y.; Gao, J.; Yu, Q.; Wang, Z. Monoacylphosphine oxides with substituents in the phosphonyl moiety as Norrish I photoinitiators: Synthesis, photoinitiattion properties and mechanism. *Journal of Photochemistry and Photobiology A: Chemistry* 2021, *421*, 113517. DOI: https://doi.org/10.1016/j.jphotochem.2021.113517.

(98) Majima, T.; Schnabel, W. On the reactivity of phosphinoyl and thiophosphinoyl radicals: Flash photolysis studies. *Journal of Photochemistry and Photobiology A: Chemistry* 1989, *50* (1), 31-39. DOI: https://doi.org/10.1016/1010-6030(89)80018-8.

(99) Zhang, J.-Q.; Han, L.-B. Chlorosilane-Catalyzed Coupling of Hydrogen Phosphine Oxides with Acyl Chlorides Generating Acylphosphine Oxides. *Organic Letters* 2020, *22* (12), 4633-4637. DOI: 10.1021/acs.orglett.0c01384.

(100) Nazir, R.; Danilevicius, P.; Gray, D.; Farsari, M.; Gryko, D. T. Push–Pull Acylo-Phosphine Oxides for Two-Photon-Induced Polymerization. *Macromolecules* 2013, *46* (18), 7239-7244. DOI: 10.1021/ma4010988.

(101) Suzuki, K.; Kumamoto, N.; Ito, N.; Hatae, S.; Suzuki, H. Organic magnesium phosphide and method for producing same, organic magnesium phosphide complex and method for producing same, and method for producing organic phosphorus-containing compound using said phosphide. WO2018008510, 2018.

(102) Ullrich, G.; Ganster, B.; Salz, U.; Moszner, N.; Liska, R. Photoinitiators with functional groups. IX. Hydrophilic bisacylphosphine oxides for acidic aqueous formulations. *Journal of Polymer Science Part A: Polymer Chemistry* 2006, *44* (5), 1686-1700. DOI: https://doi.org/10.1002/pola.21276.

(103) Zhang, Q.; Liu, X.-T.; Wu, Y.; Zhang, Q.-W. Ni-Catalyzed Enantioselective Allylic Alkylation of H-Phosphinates. *Organic Letters* 2021, *23* (22), 8683-8687. DOI: 10.1021/acs.orglett.1c02986.

(104) Beaud, R.; Phipps, R. J.; Gaunt, M. J. Enantioselective Cu-Catalyzed Arylation of Secondary Phosphine Oxides with Diaryliodonium Salts toward the Synthesis of P-Chiral Phosphines. *Journal of the American Chemical Society* 2016, *138* (40), 13183-13186. DOI: 10.1021/jacs.6b09334.

(105) Holt, J.; Maj, A. M.; Schudde, E. P.; Pietrusiewicz, K. M.; Sieroń, L.; Wieczorek, W.; Jerphagnon, T.; Arends, I. W. C. E.; Hanefeld, U.; Minnaard, A. J. On the Resolution of Secondary Phosphine Oxides via Diastereomeric Complex Formation: The Case of tert-Butylphenylphosphine Oxide. *Synthesis* 2009, *2009* (12), 2061-2065.

(106) Mangin, L. P.; Michaud, G.; Zargarian, D. A Wacker-Type Strategy for the Synthesis of Unsymmetrical POCsp3E-Nickel Pincer Complexes. *Organometallics* 2020, *39* (22), 4006-4018. DOI: 10.1021/acs.organomet.0c00590.

(107) Duan, H.; Xu, X.; Leng, K.; Guo, G.; Yu, Q.; Li, X.; Han, Y.; Gao, J.; Wang, Z. AlCl3-catalyzed C-H p hosphination of benzene: A mechanistic study. *Applied Catalysis A: General* 2021, *611*, 117943. DOI: https://doi.org/10.1016/j.apcata.2020.117943.

(108) Stadler, E.; Eibel, A.; Fast, D.; Freißmuth, H.; Holly, C.; Wiech, M.; Moszner, N.; Gescheidt, G. A versatile method for the determination of photochemical quantum yields via online UV-Vis spectroscopy. *Photochemical & Photobiological Sciences* 2018, *17* (5), 660-669, 10.1039/C7PP00401J. DOI: 10.1039/C7PP00401J.

(109) Schuman, M.; Lopez, X.; Karplus, M.; Gouverneur, V. Synthesis of a novel diarylphosphinic acid: a distorted ground state mimic and transition state analogue for amide hydrolysis. *Tetrahedron* 2001, *57* (52), 10299-10307. DOI: https://doi.org/10.1016/S0040-4020(01)01048-1.

(110) Gatineau, D.; Nguyen, D. H.; Hérault, D.; Vanthuyne, N.; Leclaire, J.; Giordano, L.; Buono, G. H-Adamantylphosphinates as Universal Precursors of P-Stereogenic Compounds. *The Journal of Organic Chemistry* 2015, *80* (8), 4132-4141. DOI: 10.1021/acs.joc.5b00548.

(111) Roszkowski, P.; Sahin, M.; Ayalur-Karunakaran, S.; Gammer, C.; Schlögl, S.; Kern, W.; Krawczyk, K. K. Synthesis and evaluation of new radical photoinitiators bearing trialkoxysilyl groups for surface immobilization. *Polymer* 2017, *129*, 207-220. DOI: https://doi.org/10.1016/j.polymer.2017.09.054.

(112) Ye, Z.; Fan, Y.; Gu, Y. Photoinitiator suitable for light-emitting diode (LED) curing, and its preparation method and application. CN107033185, 2017.

(113) Wu, S. Y.; Toia, R. F.; Casida, J. E. Phosphorothiolate sulfoxides and sulfones: NMR characteristics and reactivity. *Journal of Agricultural and Food Chemistry* 1992, *40* (8), 1425-1431. DOI: 10.1021/jf00020a028.

(114) Travis, Benjamin R.; Ciaramitaro, Benjamin P.; Borhan, B. Preparation of Purified KHSO5·H2O and nBu4NHSO5 from Oxone by Simple and Efficient Methods. *European Journal of Organic Chemistry* 2002, *2002* (20), 3429-3434. DOI: https://doi.org/10.1002/1099-0690(200210)2002:20<3429::AID-EJOC3429>3.0.CO;2-D.

(115) Yu, R.; Chen, X.; Martin, S. F.; Wang, Z. Differentially Substituted Phosphines via Decarbonylation of Acylphosphines. *Organic Letters* 2017, *19* (7), 1808-1811. DOI: 10.1021/acs.orglett.7b00579.

(116) Kumar, P.; Siddiqui, M. M.; Reddi, Y.; Mague, J. T.; Sunoj, R. B.; Balakrishna, M. S. New bisphosphomide ligands, 1,3-phenylenebis((diphenylphosphino)methanone) and (2-bromo-1,3-phenylene)bis((diphenylphosphino)methanone): synthesis, coordination behavior, DFT calculations and

catalytic studies. *Dalton Transactions* 2013, *42* (32), 11385-11399, 10.1039/C3DT51046H. DOI: 10.1039/C3DT51046H.

(117) Guo, W.; Cheng, H.-G.; Chen, L.-Y.; Xuan, J.; Feng, Z.-J.; Chen, J.-R.; Lu, L.-Q.; Xiao, W.-J. De Novo Synthesis of γ,γ-Disubstituted Butyrolactones through a Visible Light Photocatalytic Arylation–Lactonization Sequence. *Advanced Synthesis & Catalysis* 2014, *356* (13), 2787-2793. DOI: https://doi.org/10.1002/adsc.201400041.

(118) Gao, P.-S.; Zhang, K.; Yang, M.-M.; Xu, S.; Sun, H.-M.; Zhang, J.-L.; Gao, Z.-W.; Zhang, W.-Q.; Xu, L.-W. A robust multifunctional ligand-controlled palladium-catalyzed carbonylation reaction in water. *Chemical Communications* 2018, *54* (40), 5074-5077, 10.1039/C8CC00324F. DOI: 10.1039/C8CC00324F.

(119) Bonete, P.; Najera, C. Lithium 3-Lithio-3-tosylalkanoates: .beta.-Acylvinyl Anion Equivalents of .beta.-Lithiated .alpha.,.beta.-Unsaturated Carboxylic Acids. *The Journal of Organic Chemistry* 1994, *59* (11), 3202-3209. DOI: 10.1021/jo00090a043.

(120) Kang, P.; Foote, C. S. Photosensitized Oxidation of 13C,15N-Labeled Imidazole Derivatives. *Journal of the American Chemical Society* 2002, *124* (32), 9629-9638. DOI: 10.1021/ja012253d.

(121) Thévenin, M.; Thoret, S.; Grellier, P.; Dubois, J. Synthesis of polysubstituted benzofuran derivatives as novel inhibitors of parasitic growth. *Bioorganic & Medicinal Chemistry* 2013, *21* (17), 4885-4892. DOI: https://doi.org/10.1016/j.bmc.2013.07.002.

(122) Kaduk, C.; Wenschuh, H.; Beyermann, M.; Forner, K.; Carpino, L. A.; Bienert, M. Synthesis of Fmoc-amino acid fluorides via DAST, an alternative fluorinating agent. *Letters in Peptide Science* 1996, *2* (5), 285-288. DOI: 10.1007/bf00142240.

(123) Leonard, J. Heats and Entropies of Polymerization, Ceiling Temperatures, Equilibrium Monomer Concentrations, and Polymerizability of Heterocyclic Compounds. In *Polymer Handbook*, 4th ed.; Brandrup, J., Immergut, E. H., Grulke, E. A., Abe, A., Bloch, D. R. Ed.; John Wiley & Sons, 1999.

(124) Peer, G.; Dorfinger, P.; Koch, T.; Stampfl, J.; Gorsche, C.; Liska, R. Photopolymerization of Cyclopolymerizable Monomers and Their Application in Hot Lithography. *Macromolecules* 2018, *51* (22), 9344-9353. DOI: 10.1021/acs.macromol.8b01991.

(125) Haynes, R. K.; Freeman, R. N.; Mitchell, C. R.; Vonwiller, S. C. Preparation of Enantiomerically Pure Tertiary Phosphine Oxides from, and Assay of Enantiomeric Purity with, (Rp)- and (Sp)-tert-Butylphenylphosphinothioic Acids. *The Journal of Organic Chemistry* 1994, *59* (11), 2919-2921. DOI: 10.1021/jo00090a003.

(126) Smoll, K. A.; Kaminsky, W.; Goldberg, K. I. Photolysis of Pincer-Ligated PdII–Me Complexes in the Presence of Molecular Oxygen. *Organometallics* 2017, *36* (7), 1213-1216. DOI: 10.1021/acs.organomet.7b00020.
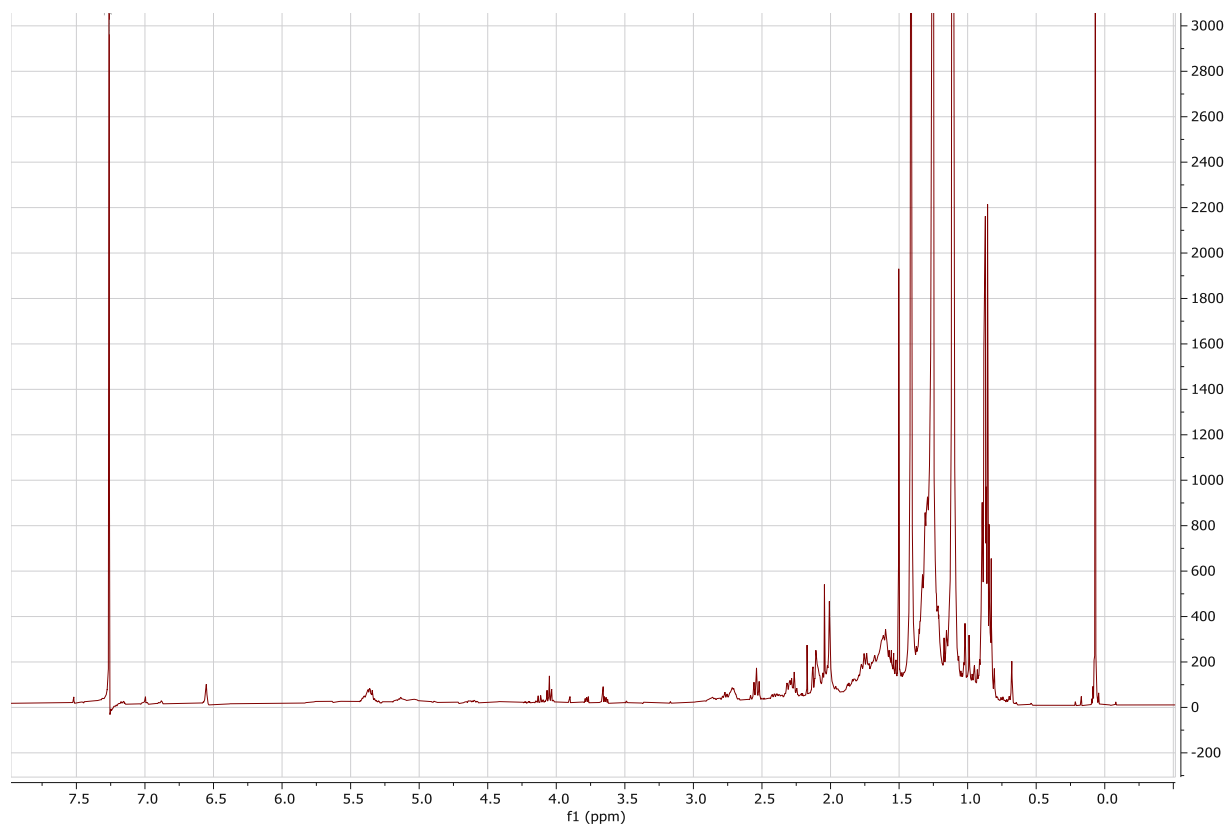
Figure 110: ¹H-NMR experiment of the yellow fraction of the 6th attempt of "1.3.6 Leaching tests" in deuterated chloroform.

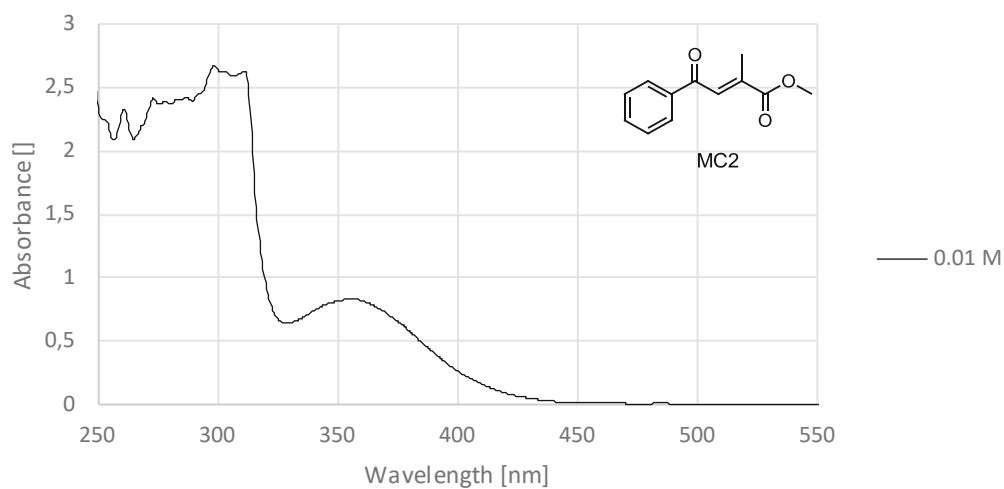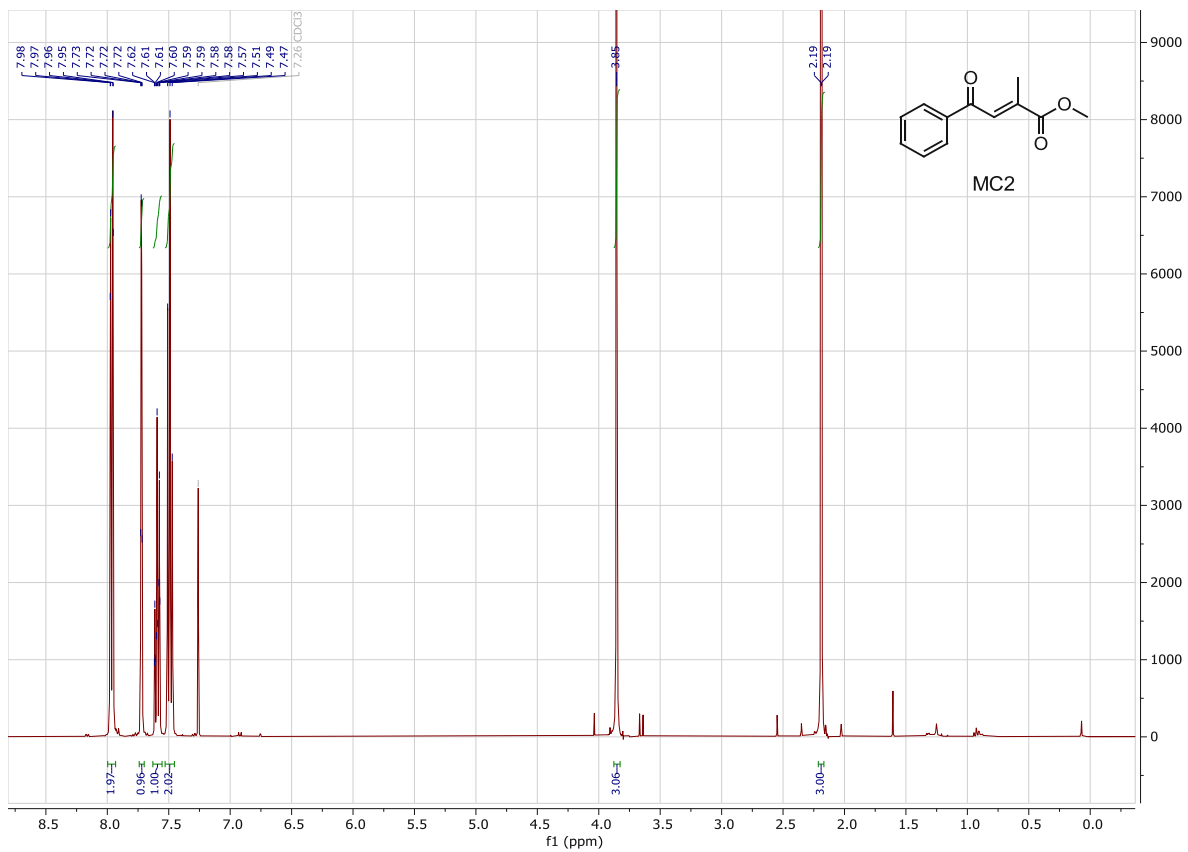*Figure 111: UV-Vis absorption spectra of MC2 (0.01M) in acetonitrile.*

Figure 112: ^{1}H-NMR (400 MHz) spectrum of MC2 in CDCl$_3$.

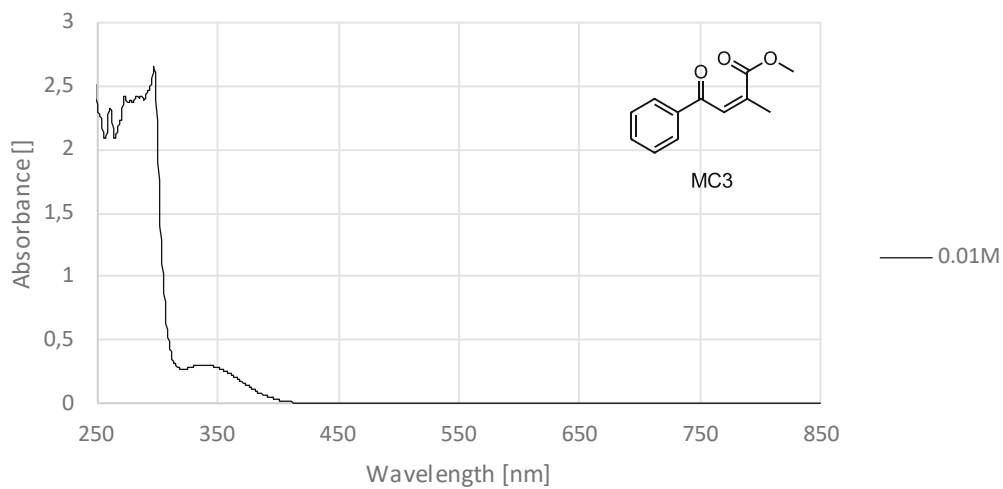*Figure 113: UV-Vis absorption spectra of MC3 (0.01M) in acetonitrile*

Appendix

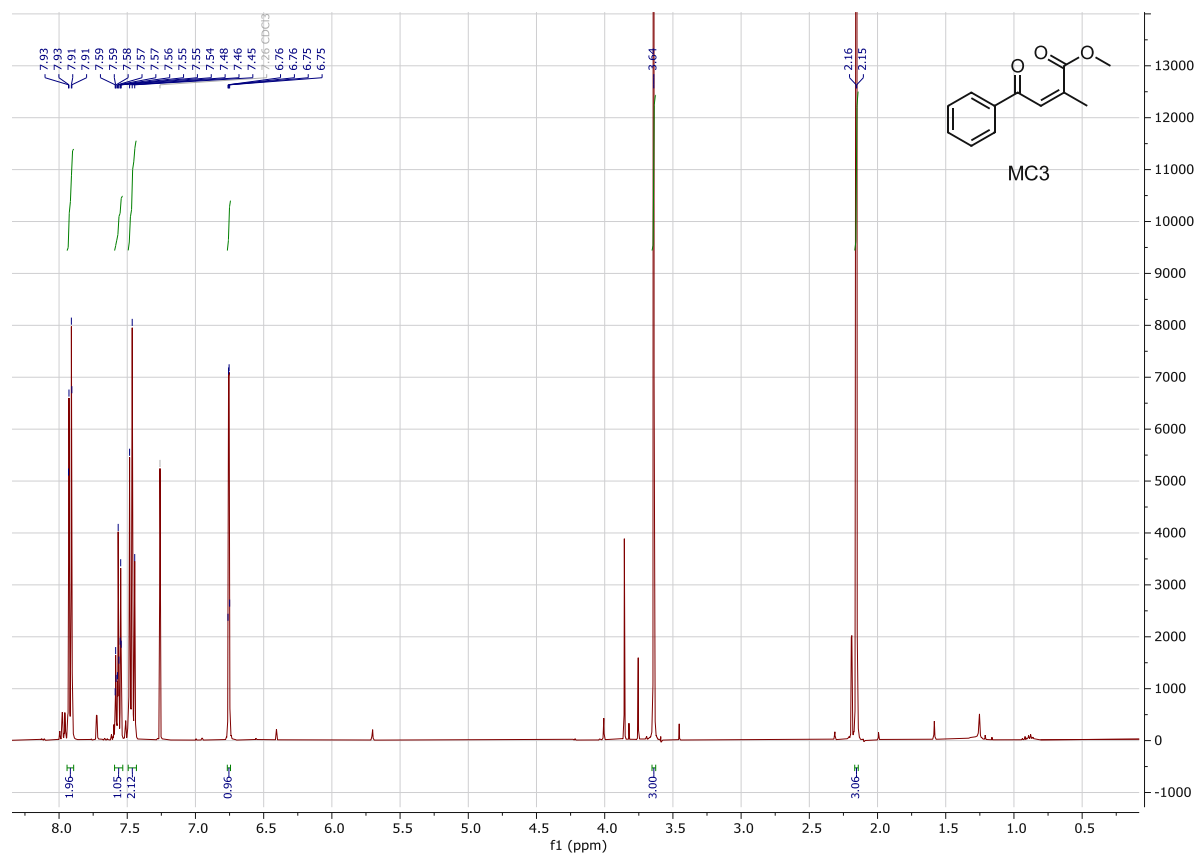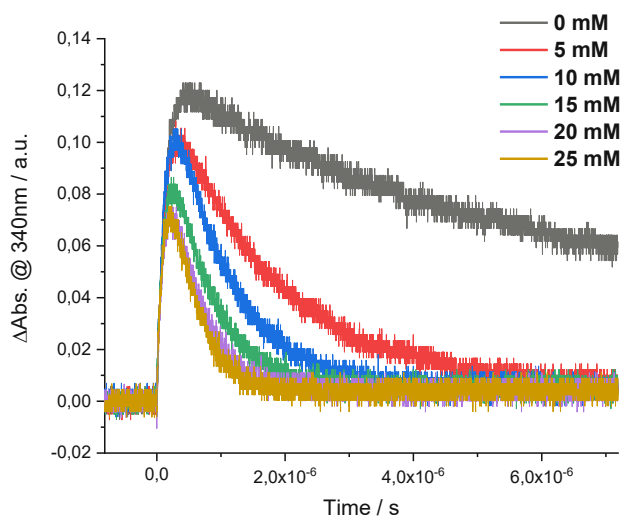*Figure 114: ^{1}H-NMR (400 MHz) spectrum of MC3 in CDCl$_3$.*

Figure 115: Time traces of the signal intensities (absorption at 340 nm) for LFP of TPO in presence of butyl methacrylate in different concentrations.
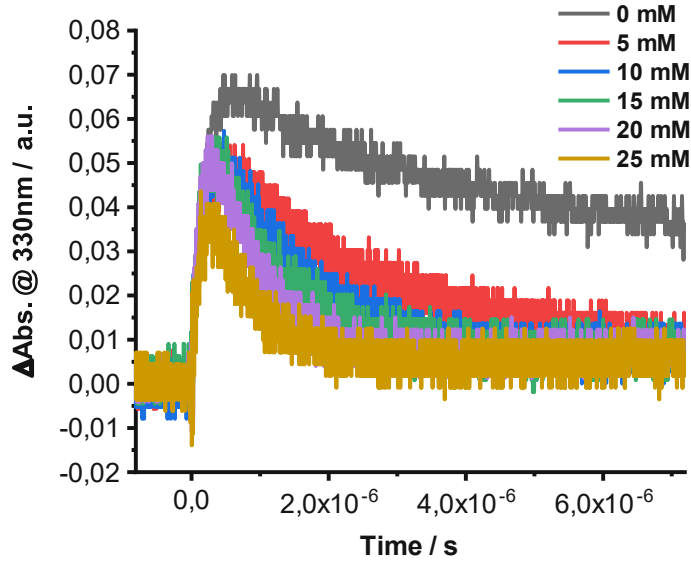
Figure 116: Time traces of the signal intensities (absorption at 330 nm) for LFP of P1 in presence of butyl methacrylate in different concentrations.
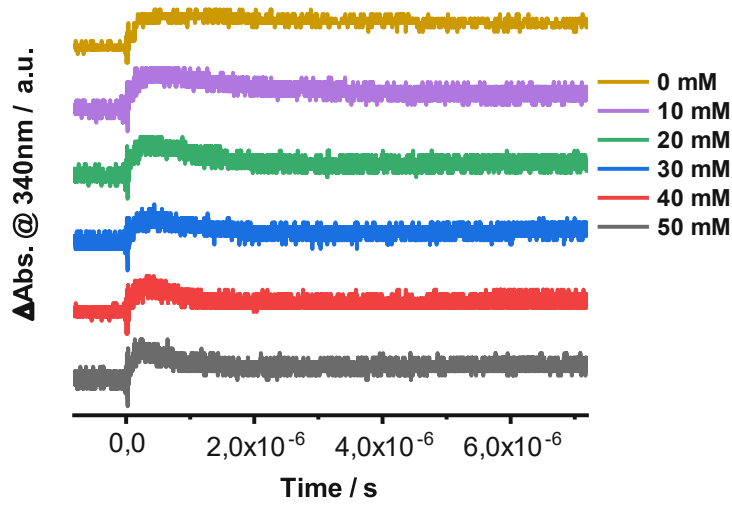

Figure 117: Time traces of the signal intensities (absorption at 340 nm) for LFP of P2 in presence of butyl methacrylate in different concentrations.

Appendix

Table 37. List of the fitted pseudo-first order decay constants and their absolute fitting errors.

TPO

c(Butyl methacrylate) / molL^{-1}	fitted k / s^{-1}	absolute fitting error / s^{-1}
0	207680	2219
0.005	599400	1728
0.01	1128770	3308
0.015	1577191	6866
0.02	2061705	11097

P1

c(Butyl methacrylate) / molL^{-1}	fitted k / s^{-1}	absolute fitting error / s^{-1}
0	116598	716
0.005	444141	3620
0.01	779656	5116
0.015	1110858	7114
0.02	1442203	9339

P2

c(Butyl methacrylate) / molL^{-1}	fitted k / s^{-1}	absolute fitting error / s^{-1}
0	112791	4540
0.01	607267	14906
0.02	1227803	30474
0.03	1861516	72056
0.04	2410722	153614